The Nucleus

An Open Access International Scientific Journal

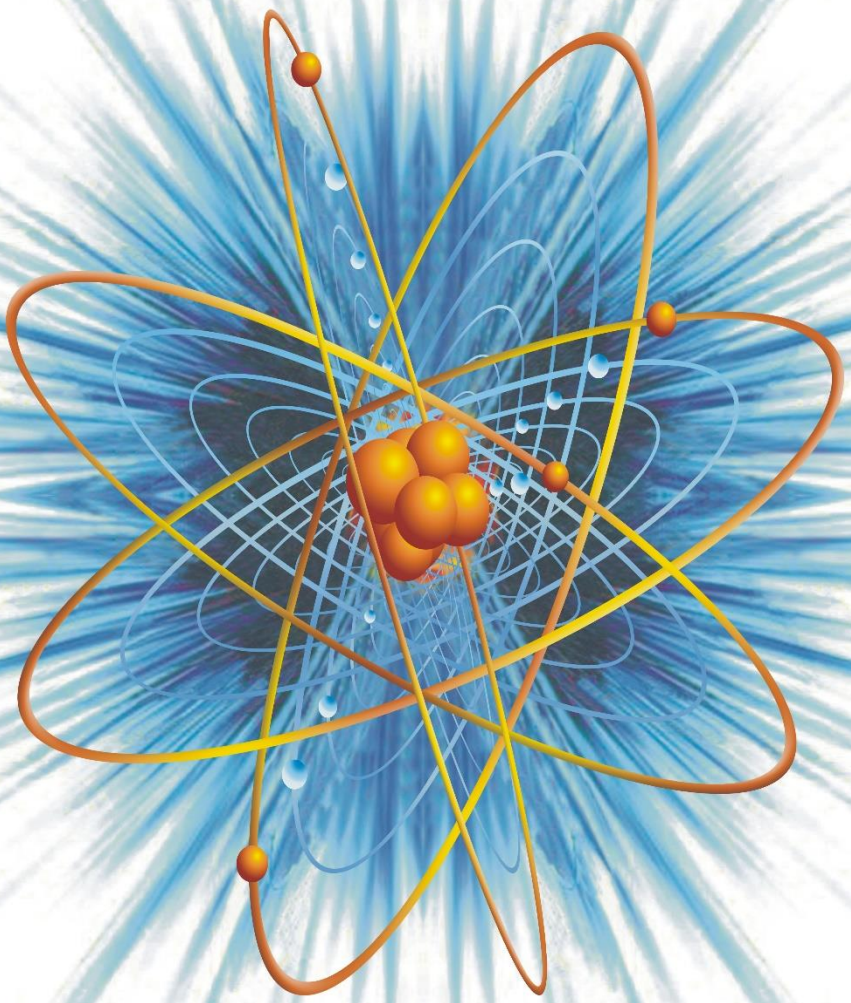

Vol. 60, No. 1, 2023

ISSN 0029-5698 (Print)

eISSN 2306-6539 (Online)

The Nucleus

An international journal devoted to all branches of natural and applied sciences

Website: *www.thenucleuspak.org.pk* **E-mail:** *editorialoffice@thenucleuspak.org.pk*
Phone: +*92-51-9248429* **Fax: +***92-51-9248808*

Editorial Office, The Nucleus

PINSTECH, Nilore, 45650, Islamabad, Pakistan

Printed at

PINSTECH Printing Press

The Nucleus

Aims and Scope: The Nucleus is an open access multidisciplinary peer-reviewed academic journal. It offers a platform for the scientists and engineers to publish their recent research of high scientific values in all areas of natural, applied and management sciences at international level. The journal is being published electronically as well as in paper version. It is easily accessible, free of charge and is being distributed widely.

Abstracting and Indexing: The journal is being abstracted and indexed by Chemical Abstracts, Citefactor, Biological Abstracts, INIS Atom Index, Bibliography of Agriculture (USA), The Institution of Electrical Engineers Publication, Virology Abstracts (England) and Pakistan Science Abstracts. The journal is recognized by the Higher Education Commission of Pakistan (Category Y).

ISSN and eISSN: The international standard serial numbers (ISSN) for The Nucleus are [0029-5698 (Print) and 2306-6539 (Online)].

The Nucleus is published at Pakistan Institute of Nuclear Science & Technology, Islamabad, on behalf of the Pakistan Atomic Energy Commission.

Published since 1964

The Nucleus
ISSN 0029-5698 (Print)
ISSN 2306-6539 (Online)

CONTENTS

Deployment of a Smart Trading System for Intelligent Stock Trading 1
I. Ali, S.Z. Mahfooz, N.Q. Mehmood, M.N. Mehmood

Reliance of the Strength of a Sandstone on Petrographic Attributes: A Preliminary Study 9
M. Yar, A. Meraj, A. Basit, F. Naseem, M.A. Khan

Spatio-Temporal Analysis of Land Use Change and Its Driving Factors in Layyah, Punjab, Pakistan 15
M. Sajid, M. Mohsin, M. Mobeen, A. Rehman, A. Rafique, M. Rauf, G. Ali

Review of Different Models of Coastdown Transient in Pressurized Water Reactor 24
I. Ahmad and S. Ahmad

Some Historical Briefs and Outlooks of the Chemical and Biological Acid Leaching of Uranium Ores 28
T.M. Bhatti and O.H. Tuovinen

Performance Evaluation of Various Algorithms for Cluster Head Selection in WSNs 35
H. Afzal, S. Kanwal, M. Zulfiqar, H.B. Gill, M.R. Mufti

Mechanical Design Verification of Chasnupp Bottom Nozzle 45
M. Waseem, A. Anwer, A.A. Siddiqui

Value Addition in Gemstones by Nuclear Techniques 51
W.A. Butt and F. Mohyuddin

Quenching of Fluorescent ADS560HO molecule with Eco-Friendly Synthesized Silver Nanoparticles 56
V.B Tangod

Thorium Based Indian Nuclear Program 60
W. Hussain, K.M. Ahmed, A. Azam and S. Rehman

Continuous Heating and Cyclic Heating for Composite Materials Containing PA2200 and One of Ceramic Additives (Al2O3, MgO and Nanoclay) Monitoring System 64
Md M. Danish

Amkhoi Geopark: Geotourism and Socio-economic Development of the Rural Areas of Chaupahari Forest and Adjoining Area, Birbhum, West Bengal, India 71
B. Saha

Insight into the Local Atomic Structure Order and Luminescence of Rare Earths 78
L.U. Khan, Z.U. Khan, M.A. Umer

Role of In-Service Inspections in the Nuclear Power Plants (Npps) 86
M. Khan, M.U.F. Awan, K. Lal, M. Gulab, S. Ahmed, Z. Ahmed

Organophosphate pesticides use and contamination in groundwater of Pakistan: A review 98
M. Sadia, M. Mohsin, M. S. Rehman, Z. Iqbal, A. Rehman, N. Naheed

A Comprehensive Review of the Impact of Thermal Radiations on Energy Exchange Systems 108
M. Ashraf

The Nucleus ***60****, No. 1 (2023) 1-8*

www.thenucleuspak.org.pk

The Nucleus

ISSN 0029-5698 (Print)
ISSN 2306-6539 (Online)

Deployment of a Smart Trading System for Intelligent Stock Trading

Iftikhar Ali[1], Syed Zeeshan Mahfooz[2*], Nadeem Qaisar Mehmood[3], Mirza Nasir Mehmood[4]

[1]*Department of Mathematics, University of Hafr Al-Batin, 31991, Saudi Arabia*

[2]*Department of Computer Sc. & Eng., University of Hafr Al-Batin, 31991, Saudi Arabia*

[3]*Department of Computer Science & Information Technology, University of Lahore, Chenab Campus, Pakistan*

[4]*GIFT Business School, GIFT University, Gujranwala, Pakistan*

ABSTRACT

In this article we evaluate the deployment of a smart trading system that exploits the features of different technical indicators for intelligent stock trading. Depending on their behaviors, these indicators help in trading under various market conditions. Our smart trading system uses a unified trading strategy that selects five indicators from three well-known categories referred as leading, lagging, and volatility indicators. The trading system looks for common trend signals from at least three indicators within a certain period of time. Collectively generated signals from the technical indicators are used to train a neural network model. The trained neural network model is then used to produce buy and sell signals for trading in stocks. The system is efficient and convenient to use for both individual traders and fund managers. We tested the model on actual data collected from Saudi Stock Exchange and New York Stock Exchange. The performance of the model was checked in terms of percentage returns. The results of the proposed trading model were compared with the benchmark trading strategy. The deployed smart trading system is efficient to produce significant returns over the longer and shorter timeframes.

Keywords: *Stock market forecasting, Time series data, Smart trading, Trend indicators, Artificial neural network*

1. Introduction

Trading stocks is very intricate profession that requires an efficient trading system and careful planning with persistent hard work and reliable strategy [1]. Many traders seek help of the professionals to get guidance which is normally costly. Others use different software without any prior experience and knowledge. Furthermore, there are investors who are unfamiliar with the use of technology, and they often fell into vicious market cycles [2, 3]. Before investing, a trader must acquire the knowledge of the company, its business operations and financial statements [2]. Moreover, the purpose of a trading model is to help traders to make right decisions at the right time and to avoid any trading decision which is based on emotions or random news. Professional trading models aim to setup rules of taking trades, and they wait for the good opportunities to invest the capital [4].

The use of Technical Indicators (TIs) for stock trading helps in chart analysis and to look for new patterns available in data values. Based on the nature of a technical indicator, it may be a leading, lagging, or volatile indicator. Leading TIs like Relative Strength Index (RSI) and Triple Exponential Average (TRIX) predict trends based on rate of change of stock prices and they are also called momentum-based indicators [5, 6]. To measure volatility level of stock prices, we use volatile technical indicators. One of the examples of volatile TIs is the Average Directional Index (ADX) [7]. The lagging technical indicators are used to quantify the strength of a trend. Exponential Moving Averages (EMA) and Moving Average Convergence Divergence (MACD) are among some well-known lagging indicators [5, 8]. They are called lagging indicators because of their delayed feedback after a large shift has occured.

The traditional algorithms used to implement technical indicators are slow and computationally costly. Artificial Intelligence (AI) with its application in various fields serves as compact and efficient solution for the real world problems. The field of Artificial Neural Network (ANN) as an extension of AI is quite advanced now. Neural networks mimic the working of the human brain, and they provide solutions for the AI and machine learning related problems. Since last few decades, automated trading based on neural networks and technical indicators is used for forecasting in financial markets [9, 10].

Recurrent Neural Network (RNN) is normally considered to deal with the sequential data problems. Long Short-Term Memory (LSTM) as a variant of RNN is capable of learning from historical time-series data and predicts the future values. Stock market data is an example of time-series data, and it is very suitable to train an LSTM neural network for predictions. Many studies show the effectiveness of LSTM neural network for predicting the future prices after they are trained on historic stock prices [11]. These models are limited and may not provide information about the consistent changes of the price values [12]. Our proposed trading system model is designed differently, and it is capable to learn the behavior of technical indicators. Instead of predicting the future price values, it predicts trends, and generates buy/sell signals accordingly.

Our smart trading model can efficiently respond to a set of data values for predicting new up or down trends and it helps in profitable trading by generating buy and sell signals. We compare the performance of this model with the performance of a benchmark trading strategy called Buy & Hold (B&H) and the results show that the proposed smart trading model is efficient, and it produces significant returns over the longer and shorter timeframes.

*Corresponding author:zeexhan@hotmail.com

2. Literature Review

Several types of trading strategies are developed to analyze the market conditions and the future price levels. Trading strategies systemize the process of taking trades and they help to set the rules for productive trading. Trading systems implement predictive models to help the traders. In all the models, the basic goal is to construct a strategy based on price movement or the market volatility and to give recommendations for taking trades [13]. Some well-known strategies are used to develop new trading models [14]. A smart trading model helps to automate the trading process by employing some probabilistic reasoning on price values and volume information [15, 16].

Researcher have used Open, High, Low, Close (OHLC) values of stock data along with the business news, social media, and market sentiment analysis to predict future prices [17, 18]. Widely available trading systems use various technical indicators, such as ADX, TRIX, RSI, MACD etc., and the performance of the system is optimized by using smart techniques, like swarm optimization method or artificial neural networks [19-21]. In most cases, the aim is to find patterns in the past prices of a stock and then use statistical and analytical methods to predict future price values [22, 23].

Unified Trading Strategy benefits from the features of multiple indicators and it helps to automate stock trading by providing potential opportunities of buying and selling shares in stock market [24]. Five different technical indicators, including EMA, ADX, MACD, RSI, and TRIX are simultaneously applied on the stock data and if three or more technical indicators are able to mark a potential trend, UTS generate buy/sell signals accordingly. The marked up/down trends and corresponding buy/sell signals are generated under the combined influence of collaborated technical indicators [24].

Machine learning helps to solve the problems of algorithmic trading. With the help of forecasting by machine learning methods, we can avail particular opportunities for useful trading [25]. LSTM works effectively with time series data like stock price values. It has been used extensively to investigate prediction for stocks, econometrics, and financial markets [26-28]. The features of LSTM are added with other methods for better predictions [29].

Our smart trading system do not train an LSTM model on regular stock price values. We adopt the data values which are marked by UTS as a part of up/down trend. The expected result of trained model is to efficiently predict the future movements of market by establishing a correlation of data patterns and market trends. In this supervised machine learning process, the trend data is considered as input and the output is a binary signal of value zero or one. The output is zero, if the set of input price values form a down-trend, and it is one, if these values are a part of up-trend. Such kind of trained neural network models are able to replace the traditional trading by searching for potential buy/sell opportunities. This solution provides reusability with effective and efficient operation.

3. Methodology

UTS generates highly accurate buy and sell signals to enter and exit a trade. Some popular technical indicators like MACD, ADX, EMA, RSI, and TRIX form the base of UTS. The selection of these technical indicators is from three broad categories such as leading, lagging and volatility indicators. The technical indicators are applied on the historical data of stock prices and the corresponding trends are marked and stored. To mark a valid trend, it must be commonly declared by at least three of total five indicators (Fig. 1). Later, the data from these confirmed trends is used to train a neural network. In the following subsection, we briefly describe these indicators and their usage.

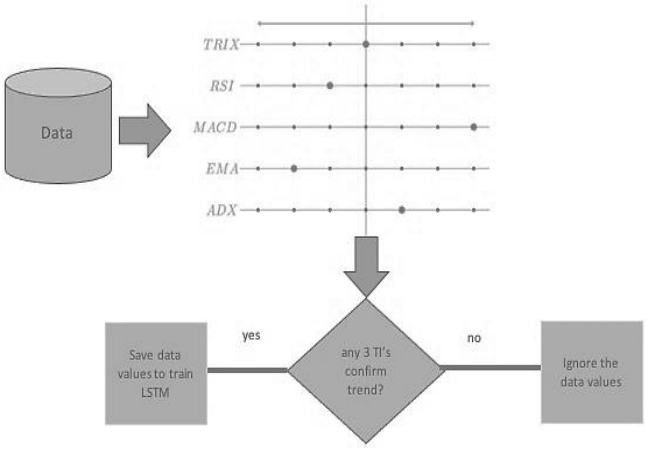

Fig. 1: Searching and saving common trends data marked by different indicators

3.1. Technical Indicators and their Interpretation

In this section, we provide definitions of technical indicators that are used by the trading model along with their interpretations.

Let C_t represent the closing price of a stock on a particular trading day, where the subscript t stands for time and it starts from 1 and ends at some value T, i.e., $1 \leq t \leq T$. Similarly, H_t, L_t, and O_t denote the high, low, and open prices of a stock.

Define an index set for a period of p number of trading days as follows, $I_{t,\,p} = \{i\colon t - (p - 1) \leq i \leq t\}$, where $p \leq t \leq T$. For example, if $p = 10$ and $t = 10$ then $I_{10,10} = \{i\colon 1 \leq i \leq 10\}$.

3.1.1 Simple Moving Average (SMA)

Given a sequence of closing prices $\{C_t\}_{t=1}^{N}$ for N days, simple moving average (SMA) for the period p is defined by taking the arithmetic mean of subsequences of p terms, that is,

$$s_t = \frac{1}{p}\sum C_i \tag{1}$$

Here, simple moving average is represented by s. It yields a new sequence $S_p = \{s_t\}_{t=p}^{N}$. The simple moving averages are used to measure the direction of the trend whether it is upward or downward.

3.1.2 Exponential Moving Average (EMA)

Exponential Moving Average (EMA) works like a filter that applies weights to older values in a time series that keep decreasing exponentially. Given a sequence of closing prices $\{C_t\}_{t=1}^{N}$, EWMA for the period *p* is defined as follows:

$$E_t = wC_t + (1-w)E_{t-1} \qquad t \geqslant 2 \tag{2}$$

where *E* represents the exponentially weighted moving average, *w* is a smoothing constant and it is calculated by the formula $w = \frac{2}{p+1}$. The values of *w* lie between 0 and 1. The first EWMA E_1 is set in different ways, for example, $E_1 = C_1$, or E_1= mean of the first *p* values. It yields a new sequence $\{E_t\}_{t=1}^{T}$. Some authors prefer to take $\{E_t\}_{t=p}^{T}$ .The exponential weighted moving averages are used to measure the direction of the trend whether it is upward or downward. The difference between SMA and EMA is that EMA gives higher weights to the recent prices of a stock.

3.1.3 Triple Exponential Moving Average (TRIX)

It is considered as a momentum indicator that follows the trend. It shows the percentage change in the EMA of closing prices that has been smoothed three times. It is given as:

$$E_t^1 = E_t(C_t)$$
$$E_t^2 = E_t(E_t^1)$$
$$E_t^3 = E_t(E_t^2)$$
$$TRIX_t = \frac{E_t^3 - E_{t-1}^3}{E_{t-1}^3} \tag{3}$$

TRIX is plotted against time *t* on the *xy*-plane. The TRIX-curve keep oscillating around a zero-line.

Rule: A buy signal is generated whenever the TRIX-curve crosses the 0-line from bottom and a sell signal vice versa. But most of the time, the use of TRIX is augmented with other indicators or the candlestick chart.

3.1.4 Moving Average Convergence Divergence (MACD)

It is a difference of short EMA and long EMA, given as follows:

$$\mathrm{M_t} = \mathrm{E^{short}} - \mathrm{E_t^{long}} \tag{4}$$

This yields a sequence of MACD, $\{M_t\}_{t=1}^{N}$.The most used short and long EMAs are 12-day and 26-day EMAs. MACD is used in diverse ways, we will describe the two rules below.

Rule 1:

The values of MACD can be positive, negative or zero, and when these values are plotted against time on the *xy*-plane, they oscillate around the 0-line (the *x*-axis). When the MACD curve crosses the 0-line from the lower half plane to upper half plane, then a buy-signal is generated, and when it crosses the 0-line from upper half plane to lower half plane, then a sell-signal is generated. Mathematically, it is defined as follows:

Buy: $M_{t-1} < 0$ and $M_t > 0$
Sell: $M_{t-1} > 0$ and $M_t < 0$

Rule 2:

Given a sequence of MACD, $\{M_t\}_{t=1}^{N}$,first calculate the 9-day EWMA of MACD sequence. It yields a new sequence which is denoted by $\{E_t^M\}_{t=1}^{N}$.The values of the new sequence can be positive, negative or zero, and these are plotted against time on the *xy*-plane, along with the MACD sequence. The MACD curve is called the momentum curve and the 9-day EWMA of MACD is called the signal curve. A buy signal is marked for MACD curve crossing the signal line from bottom and when it crosses the signal line from top, we take it as sell signal. It is expressed as follows:

Buy: $M_{t-1} < E_{t-1}^M$ and $M_t > E_t^M$
Sell: $M_{t-1} > E_{t-1}^M$ and $M_t < E_t^M$

3.1.5 Relative Strength Index (RSI)

It is a powerful indicator to determine the strength of the trend. It is defined in the following way. First, we define two sequences named as upper (U_t) and lower sequences (L_t) for time period of N days i.e., *t=1 to N* as follows:

$$U_t = \begin{cases} C_t - C_{t-1} & \text{if} \quad C_t > C_{t-1} \\ 0 & \text{otherwise} \end{cases}$$

$$L_t = \begin{cases} C_{t-1} - C_t & \text{if} \quad C_{t-1} > C_t \\ 0 & \text{otherwise} \end{cases}$$

Both the sequences $\{U_t\}_{t=1}^{N}$ and $\{L_t\}_{t=1}^{N}$ are nonnegative sequences. Next, we take simple moving averages for the period *p* of these sequences.

$$\overline{U_t} = \frac{1}{p} \sum_{i=t-(p-1)}^{t} U_i,$$

and

$$\overline{L_t} = \frac{1}{p} \sum_{i=t-(p-1)}^{t} L_i$$

It yields two new sequences $\{\overline{U}_t\}_{t=p}^{N}$ and $\{\overline{L}_t\}_{t=p}^{N}$. By using these sequences, we define another sequence by taking their ratio. It is named as the sequence of relative strengths and is defined by

$$\mathrm{RS_t} = \frac{\overline{\mathrm{U}}_\mathrm{t}}{\overline{\mathrm{L}}_\mathrm{t}} \tag{5}$$

It produces the sequence $\{RS_t\}_{t=p}^{T}$. Next, we define the relative strength index as follows:

$$RSI_t = 100 - \frac{100}{RS_t}.$$

It generates the sequence of relative strengths, that is, $\{RSI_t\}_{t=p}^{T}$. RSI value remains between 0 and 100. If the value of RSI is close to zero, it shows a downward trend and if the value of RSI is close to one hundred it shows an upward trend.

Rules:

RSI can be used in diverse ways to determine the strength of the trend. RSI is plotted against time on the *xy*-plane with the horizontal lines at *RSI* = 30, 50 and 70. The region below the line *RSI* = 30 is considered as the oversold region, and the region above the line *RSI* = 70 is considered as the overbought region. If the *RSI* curve crosses the line *RSI = 30* from below,

and it is also increasing, then an upward trend is depicted and similarly if the *RSI* curve crosses the line *RSI* = 70 from above and it is also decreasing, then a downward trend is depicted. Most of the authors also consider the middle line *RSI* = 50 as a reference. For instance, a buy signal is generated if $RSI_t > 50$ and $RSI_{t-1} < 50$, and similarly a sell signal is generated if $RSI_t < 50$ and $RSI_{t-1} > 50$.

3.1.6 Directional Indicators

Directional indicators (*DI*) were developed by Wilder (1978) and are used to enter and exit a trade. The *DI* are constructed by using not only closing price of a stock but also the information about the intraday high and low prices of a stock. To define (DI), first we define two sequences named as upper move (UM_t) and lower move (LM_t) sequences as follows:

$$UM_t = \begin{cases} H_t - H_{t-1} & \text{if} \quad H_t > H_{t-1} \\ 0 & \text{otherwise} \end{cases}$$

$$LM_t = \begin{cases} L_{t-1} - L_t & \text{if} \quad L_{t-1} > L_t \\ 0 & \text{otherwise} \end{cases}$$

Both the sequences $\{UM_t\}_{t=1}^{N}$ and $\{LM_t\}_{t=1}^{N}$ are nonnegative sequences.

Positive Directional Movement (DM $^+$)

$$DM_t^+ = \begin{cases} UM_t & \text{if} \quad UM_t > 0 \quad \text{and} \quad UM_t > LM_t \\ 0 & \text{otherwise} \end{cases}$$

Negative Directional Movement (DM $^-$)

$$DM_t^- = \begin{cases} LM_t & \text{if} \quad LM_t > 0 \quad \text{and} \quad LM_t > UM_t \\ 0 & \text{otherwise} \end{cases}$$

Note that both $\{DM_t^+\}_{t=1}^{N}$ and $\{DM_t^-\}_{t=1}^{N}$ form sequences of nonnegative numbers and at least one of them must be zero at any given value of *t.*

True range is a term used to provide the price range of day-to-day trading, and it is defined as follows:

$$TR_t = \max\{H_t - L_t, \quad H_t - C_{t-1}, C_{t-1} - L_t\}$$

Where, TR_t represents true range on a particular trading day.

Next, we define the positive directional indicators DI_t^+, and negative directional indicators DI_t^- with the help of *DM* and *TR* for a period of *p* number of days.

Positive Directional Indicator (DI $^+$)

$$DI_t^+ = \frac{\sum_{i=t-(p-1)}^{t} DM_i^+}{\sum_{i=t-(p-1)}^{t} TR_i}$$

Negative Directional Indicator (DI $^-$)

$$DI_t^- = \frac{\sum_{i=t-(p-1)}^{t} DM_i^-}{\sum_{i=t-(p-1)}^{t} TR_i}$$

These indicators measure the upward and downward price movements as the fraction of trading range over a period of *p* number of days. Moreover, they are inversely proportional to each other, that is, if one of them increases the other decreases and vice versa.

Directional movement index is defined as the hundred times the ratio of the absolute values of the difference between the positive and negative directional indicators and the sum of the positive and negative directional indicators, that is,

$$DX_t = \left| \frac{DI_t^+ - DI_t^-}{DI_t^+ + DI_t^-} \right|$$

The values of *DX* lie between 0 and 100. It yields a sequence $\{DX_t\}_{t=1}^{T}$

3.1.6.1 Average Directional Movement Index (ADX)

The average directional movement index is obtained by taking the simple moving average of the sequence $\{DX_t\}_{t=1}^{T}$ for the period of *p* number of days, that is,

$$\mathrm{ADX_t} = \frac{1}{\mathrm{p}} \sum_{\mathrm{i=t-(p-1)}}^{\mathrm{t}} \mathrm{DX_i} \qquad (6)$$

The range of *ADX* values is from 0 to 100. It is a powerful indicator to determine the strength of the trend.

Trading Rules: *ADX* is plotted against time *t* on the *xy*-plane. Two horizontal lines at *ADX* = 20 and *ADX* = 40 are drawn which are used to generate the signals. If *ADX* is greater than twenty and increasing, then the trend's strength is increasing, and if *ADX* is smaller than forty and decreasing, then the trend's strength is decreasing.

3.2 Smart Trading Strategy

The use of technical indicators without a strategy does not assure profits. Moreover, dependence on any single indicator is risky, and often multiple indicators are combined to determine the strength of the trend and momentum.

The goal of the deployed model is to develop a strategy which uses the most popular technical indicators. The idea is to use three or more indicators that generate buy and the sell signals within a predefined range. The potential signals are used to train a neural network model that learns the nature of the data that comprise signals. Later, the same neural network model works as stand-alone system to predict buy and sell signals. We adopt the default configuration of the neural network model [24]. The overall strategy is depicted through Fig. 2.

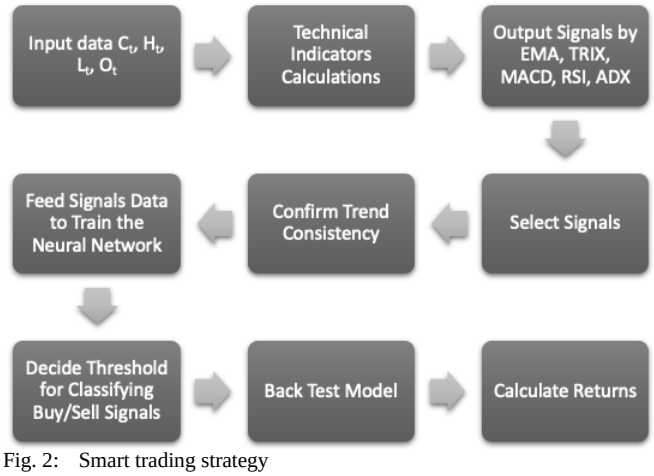

Fig. 2: Smart trading strategy

Here, we outline the composition of the strategy.

1. Apply the technical indicators, *ADX*, *EMA*, *MACD*, *RSI*, and *TRIX*.
2. Mark the initial signals by each indicator (may not be common).

3. Mark trend days based on the output of each indicator.
4. Define the search range to locate the same indexes in other indicators.
5. Define sensitivity i.e., at least how many indicators must confirm a signal.
6. Data comprising potential signals is used to train a neural network model.
7. Trained model is used to generate buy/sell signals depending on threshold values.
8. Smart trading is performed accordingly, and returns are calculated.

4. Simulations and Results

In this section we will apply the above strategy to show its effectiveness through backward and forward testing.

4.1 Data Collection

We have obtained the historical data of the companies from the online resources. For example, the stock data for Apple Inc., a US technology company is obtained from Yahoo Finance [30], and the data for the Saudi Cement Company (SCC) is obtained from Tadawul [31]. The data is collected for a period of ten years, from Jan 01, 2010, to Dec 31, 2019.

4.2 Backward Testing

Backward testing is a process to determine how well the new strategy will perform if it is applied on the historical data of the stock prices. In the first case we have applied the trading model on the stock prices of Saudi Cement Company and obtained the buy and sell signals. We will describe this in the form of an investment scenario. In the first problem, we consider an investment in the Saudi Stock Exchange, and in the second problem we consider an investment in the New York Stock Exchange.

Problem Statement 1:

Mr. Ali wants to invest SAR 10,000 for a tenure of 10 years. Suppose, he purchases the stocks of SCC. His risk tolerance level is 5% and he intends to achieve a return of 10% annually over his investments. Use the trading model defined in this paper to determine the entry and exit points, and also determine the success rate of this strategy.

1. Initial capital = 10,000 SAR
2. Investment time frame = 10 years
3. Risk tolerance = 5% of initial capital
4. Profit target = 10% annually
5. Entry point = buy signal
6. Exit point = sell signal
7. Assume no fees, no taxes, no cost
8. Determine the profit or loss

We collect the data of SCC from Jan 01, 2010, to Dec 31, 2019, and apply the above strategy to get the buy and the sell signals. We enter the first trade when we obtain the buy signal and exit the trade when we obtain the sell signal. We buy the shares so that the cost is less than the initial capital and the left-over amount remains in the account as a cash. We sell the shares when a sell signal is obtained, and the amount received is kept as a cash until the next buy signal is obtained. We repeat the process for the tenure of ten years. The results are shown in Table 1. The above strategy yields tremendous results. The initial capital SAR 10000 is turned into an amount of SAR 303497.45 which is a return of 3000%.

Table 1: Backward Testing Results for Problem Statement 1

	Buy					Sell					
No. of Trades	Date	Price	No	Cost	Cash	Date	Price	No	Cost	Cash (new)	Return (%)
1	2/16/2010	40	250	10000	0	5/17/2010	49	250	12250	12250	22.5
2	7/5/2010	45	272	12240	10	7/9/2011	62	272	16864	16874	37.77
3	8/22/2011	58	290	16820	54	3/12/2012	92	290	26680	26734	58.62
4	4/14/2012	88.25	302	26652	82.5	5/5/2012	93.25	302	28162	28244	5.66
5	6/12/2012	90.75	311	28223	20.75	11/4/2012	88.25	311	27446	27466.5	-2.75
6	12/3/2012	90	305	27450	16.5	2/17/2013	97.25	305	29661	29677.75	8.05
7	4/24/2013	95.75	309	29587	91	12/2/2013	107	309	33063	33154	11.74
8	1/9/2014	102.25	324	33129	25	3/17/2014	114.5	324	37098	37123	11.98
9	4/23/2014	107.75	344	37066	57	9/22/2014	121.16	344	41679	41736.04	12.44
10	4/15/2015	91.82	454	41686	49.76	6/9/2015	95.91	454	43543	43592.9	4.45
11	11/19/2015	65.75	663	43592	0.65	12/7/2015	69	663	45747	45747.65	4.94
12	1/28/2016	50.41	907	45722	25.78	3/24/2016	67.16	907	60914	60939.9	33.22
13	5/26/2016	64.45	945	60905	34.65	6/16/2016	66.54	945	62880	62914.95	3.24
14	11/7/2016	52.93	1188	62881	34.11	1/5/2017	71.51	1188	84954	84987.99	35.1
15	5/17/2017	52.52	1618	84977	10.63	6/5/2017	53.23	1618	86126	86136.77	1.35
16	11/30/2017	38.59	2232	86133	3.89	3/29/2018	56.13	2232	125282	125286.05	45.45
17	9/20/2018	40	3132	125280	6.05	10/10/2018	43.1	3132	134989	134995.25	7.75
18	10/30/2018	38.3	3524	134969	26.05	7/23/2019	77	3524	271348	271374.05	101.04
19	9/19/2019	62.5	4341	271313	61.55	1/2/2020	69.9	4341	303436	303497.45	11.84

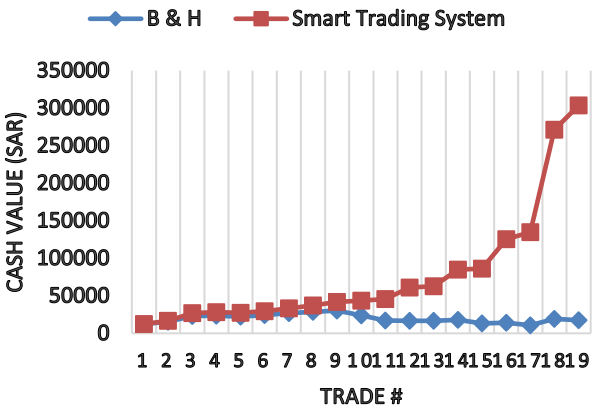

Fig. 3: The comparison of smart trading system with B&H (Problem-I)

As noticed in Fig. 3, the profits gained by smart trading system are higher in each trade than the profits by benchmark strategy i.e., Buy and Hold (B&H).

Problem Statement 2:

Mr. Neil wants to invest US$ 10,000 for a tenure of 10 years. Suppose he purchases the stocks of Apple Inc. His risk tolerance level is 5% and he intends to achieve a return of 10% annually over his investments. Use the strategy define in this paper to determine the entry and exit points, and also determine the success rate of this strategy.

1. Initial capital = $ 10000
2. Investment time frame = 10 years
3. Risk tolerance = 5% of initial capital
4. Profit target = 10% annually
5. Entry point = buy signal
6. Exit point = sell signal
7. Assume no fees, no taxes, no cost
8. Determine the profit or loss

We collect the data of Apple Inc. from Jan 01, 2010, to Dec 31, 2019, and apply the above strategy to get the buy and the sell signals. We enter the first trade when we obtain the buy signal and exit the trade when we obtain the sell signal. We buy the shares so that the cost is less than the initial capital and the left-over amount remains in the account as a cash. We sell the shares when a sell signal is obtained, and the amount received is kept as a cash until the next buy signal is obtained. We repeat the process for the tenure of ten years. The results are shown in Table 2. The above strategy yields tremendous results. The initial capital 10000$ is turned into an amount of 301834.2$ which is a return of almost 3000%.

Table 2: Back Testing Results for Problem Statement 2

	Buy					Sell					
No. of Trades	Date	Price	No	Cost	Cash	Date	Price	No	Cost	Cash (new)	Return(%)
1	2/26/2010	29.23	342	9997.14	2.85	5/20/2010	33.96	342	11616.27	11619.12	16.19
2	8/31/2010	34.72	334	11599.34	19.78	3/16/2011	47.14	334	15746.19	15765.97	35.75
3	7/1/2011	49.03	321	15740.92	25.05	10/3/2011	53.51	321	17178.08	17203.13	9.13
4	12/20/2011	56.56	304	17195.54	7.59	5/1/2012	83.16	304	25281.07	25288.66	47.02
5	7/2/2012	84.64	298	25224.42	64.24	10/5/2012	93.22	298	27781.68	27845.93	10.13
6	3/14/2013	61.78	450	27803.57	42.36	3/27/2013	64.58	450	29062.28	29104.64	4.52
7	4/26/2013	59.59	488	29084.79	19.84	6/12/2013	61.74	488	30129.81	30149.66	3.59
8	7/16/2013	61.45	490	30113.99	35.66	9/11/2013	66.81	490	32739.69	32775.36	8.71
9	10/7/2013	69.67	470	32748.92	26.43	1/6/2014	77.7	470	36521.01	36547.44	11.51
10	4/24/2014	81.11	450	36499.5	47.94	12/9/2014	114.1	450	51354	51401.95	40.69
11	1/26/2015	113.1	454	51347.39	54.55	6/8/2015	127.8	454	58021.2	58075.75	12.99
12	10/21/2015	113.8	510	58017.6	58.15	12/10/2015	116.2	510	59246.69	59304.85	2.11
13	3/2/2016	100.8	588	59241	63.85	4/15/2016	109.8	588	64591.79	64655.64	9.03
14	5/20/2016	95.22	679	64654.38	1.26	10/28/2016	113.7	679	77215.88	77217.14	19.42
15	12/9/2016	113.9	677	77144.14	73	6/9/2017	149	677	100859.5	100932.5	30.74
16	7/13/2017	147.8	683	100926.9	5.54	1/26/2018	171.5	683	117141.3	117146.9	16.06
17	2/14/2018	167.4	699	116991.6	155.2	4/20/2018	165.7	699	115838.3	115993.5	-0.98
18	5/1/2018	169.1	685	115833.5	160	10/23/2018	222.7	685	152570	152730.1	31.71
19	1/30/2019	165.3	924	152691	39.07	5/8/2019	202.9	924	187479.6	187518.7	22.78
20	6/6/2019	185.2	1012	187442.6	76.02	2/24/2020	298.2	1012	301758.2	301834.2	60.98

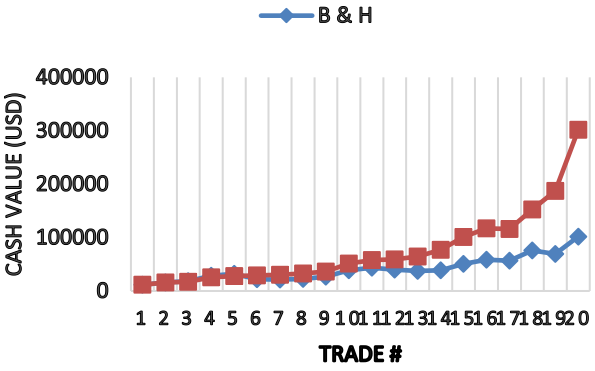

Fig. 4: The comparison of smart trading system with B&H (Problem-II)

As shown in Fig. 4, the profits gained by both the smart trading system and B&H are almost same for the first five trades. The profits of smart trading system are higher in each trade after the fifth trade. Our results show that the model is efficient to perform well during all market cycles like upward, downward, or sideways. As the model is trained on the confirmed buy and sell signals generated by different indicators, it is able to mark the relevant patterns in any sequence, and forecast the future trends.

5. Conclusions

We evaluated a smart trading model that uses a blend of different indicators taken from three well-known classes of technical indicators. The model is effective to exploit the patterns of price values, and it performs automated trading by generating buy/sell signals for positive returns. Our smart trading model utilizes distinguished features of LSTM neural network model. We trained LSTM model on the confirmed buy and sell signals generated by different technical indicators. We adopted unified trading strategy that helps to unify indicators and it can be customized according to the needs and preferences of the traders. The model was back-tested by feeding the historical data from the international stock markets and the buy and sell signal were obtained. These signals were used to enter or exit a trade according to the designed methodology. The performance of the model was compared with the performance of buy and hold benchmark strategy. The results show that the model outperforms under various market conditions, and it is able to gain outstanding profits.

References

[1] A.W. Lo, H. Mamaysky, and J. Wang, "Foundations of Technical Analysis: Computational Algorithms, Statistical Inference, and empirical implementation," The Journal of Finance, vol. 55, no. 4, pp. 1705–1765, Aug., 2000.

[2] L. Koskinen, "Statistical models and methods for Financial Markets by Tze Leung Lai, Haipeng Xing," International Statistical Review, vol. 77, no. 1, pp. 154–155, Apr., 2009.

[3] Y. Chen and X. Wang, "A hybrid stock trading system using genetic network programming and mean conditional value-at-risk," European Journal of Operational Research, vol. 240, no. 3, pp. 861–871, Feb., 2015.

[4] B.I. Jacobs, K.N. Levy, and H.M. Markowitz, "Financial market simulation," The Journal of Portfolio Management, vol. 30, no. 5, pp. 142–152, Jan., 2004.

[5] V. Tanoe, "Stocks trading using relative strength index, moving average and Reinforcement Learning Techniques: A case study of apple stock index," SSRN Electronic Journal, Dec., 2019. https://dx.doi.org/10.2139/ssrn.3497805

[6] J.K. Hutson, "TRIX-triple exponential smoothing oscillator," Technical Analysis of Stocks and Commodities, pp.105-108, Jul., 1983.

[7] J.W. Wilder, New Concepts in Technical Trading Systems. Winston-Salem, NC: Hunter Pub., 1978.

[8] A. Antonio Agudelo Aguirre, R. Alfredo Rojas Medina, and N. Darío Duque Méndez, "Machine learning applied in the stock market through the moving average convergence divergence (MACD) indicator," Investment Management and Financial Innovations, vol. 17, no. 4, pp. 44–60, Dec., 2020.

[9] D. Bao and Z. Yang, "Intelligent stock trading system by turning point confirming and probabilistic reasoning," Expert Systems with Applications, vol. 34, no. 1, pp. 620–627, Jan., 2008.

[10] J.L. Wu, L.C. Yu, and P.C. Chang, "An intelligent stock trading system using comprehensive features," Applied Soft Computing, vol. 23, pp. 39–50, Oct., 2014.

[11] S. Banik, N. Sharma, M. Mangla, S.N. Mohanty, and S.S., "LSTM based decision support system for Swing Trading in Stock Market," Knowledge-Based Systems, vol. 239, p. 107994, Mar., 2022.

[12] S. Argade, P. Chothe, A. Gawande, S. Joshi, and A. Birajdar, "Machine learning in stock market prediction: A Review," Available at SSRN Electronic Journal 4128716, Jun., 2022. https://dx.doi.org/10.2139/ssrn.4128716

[13] W. Wang and K.K. Mishra, "A novel stock trading prediction and recommendation system," Multimedia Tools and Applications, vol. 77, no. 4, pp. 4203–4215, 2017.

[14] G.S. Atsalakis and K.P. Valavanis, "Surveying stock market forecasting techniques – part II: Soft computing methods," Expert Systems with Applications, vol. 36, no. 3, pp. 5932–5941, 2009.

[15] T. Chavarnakul, D. Enke, "A hybrid stock trading system for intelligent technical analysis-based equivolume charting," Neurocomputing, vol. 72, no. 16-18, pp. 3517-3528, 2009.

[16] X. Lin, Z. Yang, and Y. Song, "Intelligent stock trading system based on improved technical analysis and Echo State Network," Expert Systems with Applications, vol. 38, no. 9, pp. 11347–11354, 2011.

[17] S. Duz Tan and O. Tas, "Social media sentiment in international stock returns and trading activity," Journal of Behavioral Finance, vol. 22, no. 2, pp. 221–234, 2020.

[18] D. Shah, H. Isah, and F. Zulkernine, "Predicting the effects of news sentiments on the stock market," 2018 IEEE International Conference on Big Data (Big Data), pp. 4705-4708, Dec., 2018.

[19] S.M. Huang, Y.C. Hung, and D.C. Yen, "A study on decision factors in adopting an online stock trading system by brokers in Taiwan," Decision Support Systems, vol. 40, no. 2, pp. 315–328, 2005.

[20] A.C. Briza and P.C. Naval, "Stock trading system based on the multi-objective particle swarm optimization of technical indicators on end-of-day market data," Applied Soft Computing, vol. 11, no. 1, pp. 1191–1201, 2011.

[21] O.B. Sezer, A.M. Ozbayoglu, and E. Dogdu, "An artificial neural network-based stock trading system using technical analysis and Big Data Framework," Proceedings of the SouthEast Conference, 2017.

[22] T. Han, Q. Peng, Z. Zhu, Y. Shen, H. Huang, and N.N. Abid, "A pattern representation of stock time series based on DTW," Physica A: Statistical Mechanics and its Applications, vol. 550, p. 124161, 2020.

[23] M. Vogl, P.G. Rötzel, "Chaoticity versus stochasticity in financial markets: Are daily S&P 500 return dynamics chaotic?". Communications in Nonlinear Science and Numerical Simulation, vol. 108, 106218, May., 2022. https://doi.org/10.1016/j.cnsns.2021.106218

[24] S.Z. Mahfooz, I. Ali, and M.N. Khan, "Improving stock trend prediction using LSTM neural network trained on a complex trading strategy,"

International Journal for Research in Applied Science and Engineering Technology, vol. 10, no. 7, pp. 4361–4371, 2022.

[25] M. Obthong, N. Tantisantiwong, W. Jeamwatthanachai, and G. Wills, "A survey on machine learning for stock price prediction: Algorithms and techniques," Proceedings of the 2nd International Conference on Finance, Economics, Management and IT Business, pp. 63-71, May., 2020.

[26] A.S. Girsang, F. Lioexander, D. Tanjung, "Stock price prediction using lstm and search economics optimization," IAENG International Journal of Computer Science, 47(4), 758-764, 2020.

[27] A. Moghar and M. Hamiche, "Stock market prediction using LSTM recurrent neural network," Procedia Computer Science, vol. 170, pp. 1168–1173, 2020.

[28] X. Yan, W. Wang, M. Chang. "Research on financial assets transaction prediction model based on LSTM neural network," Neural Computing and Applications, vol. 33, no. 1, pp. 257-270, 2021.

[29] S. Dami and M. Esterabi, "Predicting stock returns of Tehran Exchange using LSTM neural network and feature engineering technique," Multimedia Tools and Applications, vol. 80, no. 13, pp. 19947–19970, 2021.

[30] Yahoo Finance [Online]. Available: https://finance.yahoo.com.

[31] Saudi Exchange [Online]. Available: https://www.tadawul.com.sa

The Nucleus ***60***, *No. 1 (2023) 9-14*

www.thenucleuspak.org.pk

The Nucleus
ISSN 0029-5698 (Print)
ISSN 2306-6539 (Online)

Reliance of the Strength of a Sandstone on Petrographic Attributes: A Preliminary Study

Mustafa Yar[1], Asad Meraj[2], Abdul Basit[2], Fawad Naseem[2], Mumtaz Ali Khan[2*]

[1]*Department of Geology, FATA University, Akhurwal, Darra Adam Khel, F.R. Kohat, Pakistan*

[2]*Department of Earth and Environmental Sciences, Bahria University, H-11, Islamabad, Pakistan*

ABSTRACT

For the present preliminary geotechnical investigation, sandstone from Dandot Formation of Permian age has been selected with eighteen samples that were collected for detailed petrographic analysis while three bulk samples were collected for geotechnical analysis. On the basis of grain size sandstone of Dandot Formation was divided into three parts. The lower part was mostly very fine, middle part was generally fine and upper part was of medium grain. Texturally and mineralogically the sandstone was sub-mature. Framework grains in the studied samples essentially consisted of variable amount of quartz (62 to 73%), feldspar (10 to 19%), and rock fragments (3 to 6%). Accessory minerals include muscovite, biotite, iron ore minerals, zircon and glauconite. The cement type in the samples was clayey ferruginous. The modal composition of the sandstone falls in the category of Arkose. The strength test including unconfined compressive strength, unconfined tensile strength, shear strength, specific gravity, and water absorption tests were employed on the rock samples to assess their geotechnical utilities. After evaluating these properties, the acquired test results indicated that the sandstone is very weak and hence cannot be used for construction purposes.

Keywords: *Petrography, Sandstone, Mechanical properties, Dandot formation, Salt range*

1. Introduction

Sandstone has been widely used in architecture works not only restricted to Pakistan but all over the world. Architectural works include both interior and exterior usage. Interior uses of sandstone include countertops, decorative aggregate whereas exterior uses consist of building stone, facing stone, blocks, slabs, tiles and bricks generally used for building walls. Sandstone having good compressive strength and low absorption values are extensively used in foundation for residential and commercial buildings.

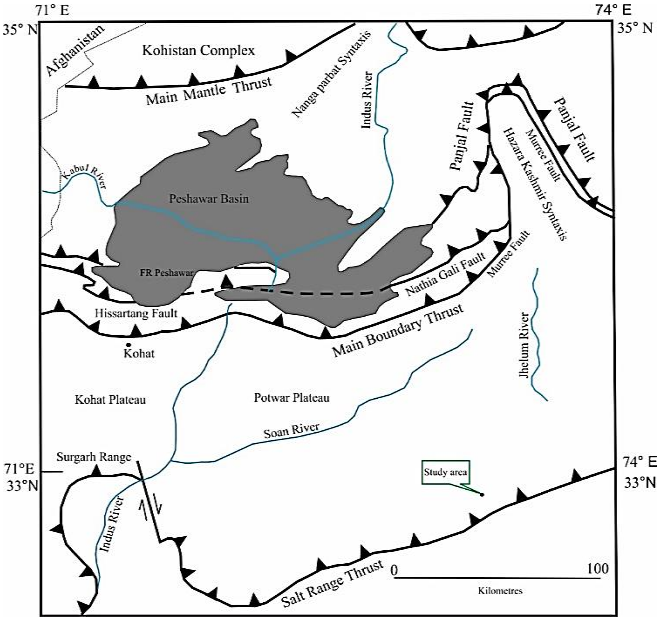

Fig. 1: Tectonic map of North Pakistan. The box demarcates the location of study area [1].

Study area lies at the Choa-Saidan Shah to Khewra road section, Pidh Village, Eastern Salt Range, Upper Indus basin, Pakistan. Dandot Formation is a part of Nilawahan Group of Permian age (Fig. 1). Nilawahan Group consists of four formations (see Table 1).

Dandot Formation comprises of sandstone with shale interbeds. This Sandstone is the main focus of the present study. Sedimentological and Paleontological studies of sandstone from Dandot Formation have been done by various researchers [2-4] while the geotechnical investigation has been carried out for the first time, in order to know whether it is feasible for construction purposes. The current research is of preliminary nature and aimed to know the dependence of strength of sandstone on certain petrographic parameters.

Table 1: Formations detail of Nilawahan Group

	Formations	Lithologies	
Nilawahan Group	Sardhai formation	Clays, shales (variegated colors reddish, greyish, greenish)	Permian Age
	Warchha sandstone	Sandstone containing pebbles of granite (Reddish in color)	
	Dandot formation	Sandstone and shale interbeds (brownish to yellowish)	
	Tobra formation	conglomerates, sandy matrix (brownish in color)	

2. Materials and Methods

Field work was carried out to collect samples from sandstone unit of Dandot Formation for microscopic study. Different lithological characteristics were observed in Fig. 2. Three bulk samples were also collected for preliminary geotechnical examination.

*Corresponding author: mumtazkhan@bui.edu.pk

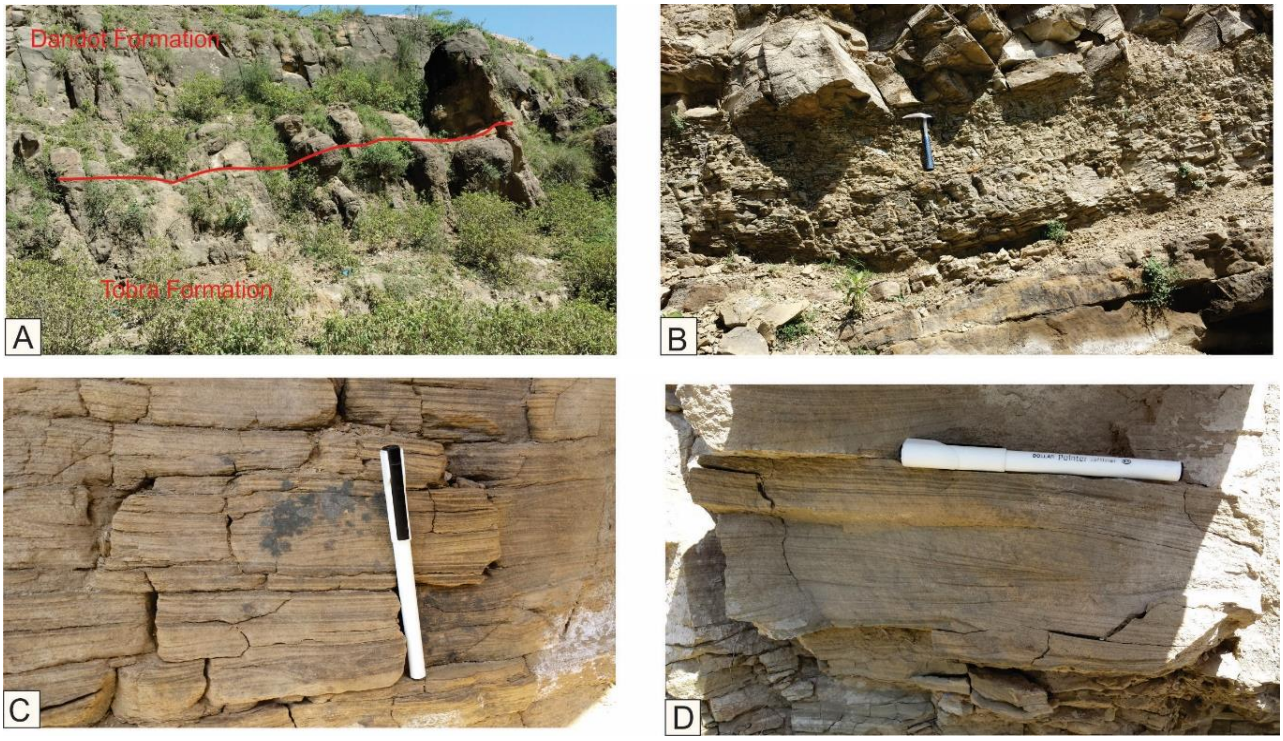

Fig. 2: Field photographs showing contact between Dandot and Tobra Formation (A), interbeds of shale in sandstone (B), Sandstone showing parallel laminations (C), Depicting cross laminations within sandstone unit (D)

Eighteen samples were made into thin sections for petrographic analysis. Among these only nine are selected for microscopic study.

According to the ASTM specifications [5], three cylindrical and three disc-shaped cores for determining Uniaxial Compressive Strength (UCS) and Uniaxial Tensile Strength (UTS) respectively, were drilled from each of the collected block samples. The UCS test was performed directly on these cores. During the present examination the indirect tensile method or Brazilian method [5] was used as it is much simpler and inexpensive [6-10]. Shear strength parameters were determined indirectly in the current study due to its simplicity as stated above in case of UTS. Mohr circles were drawn for the resulting values of UCS and UTS. UCS and UTS readings of the respective sandstone were taken on the positive and negative x-axis respectively. A common tangent to both the Mohr circles was drawn and Cohesion (C) and angle of internal friction (Φ) were determined. The angle of the tangent with the horizontal axis gives the value of Φ while the distance between the x-axis and the points at which the tangent cuts the y-axis gives the value of cohesion (Fig. 3).

The specific gravity and water absorption competence of rock samples were determined and their related information regarding definition and geotechnical importance of the inspected properties, procedure for sample preparation and methods used for their determination are given elsewhere [9-11].

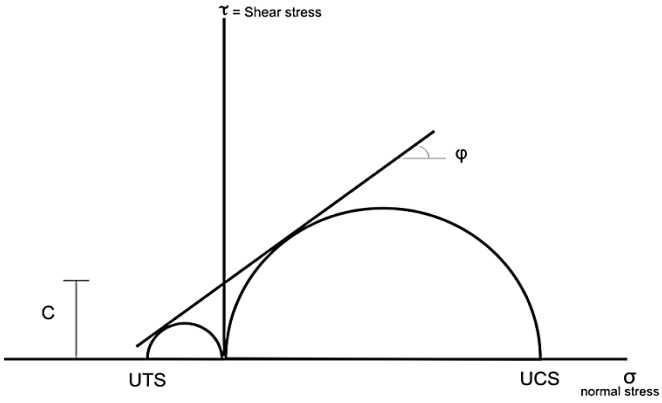

Fig. 3: Represents the indirect measurement of shear strength parameters.

3. Petrography

The petrographic study of sandstone unit of Dandot Formation exposed in Pidh village, Eastern Salt Range is based on the nine (9) representative thin-sections from the selected stratigraphic levels across the formation, where lithologic variations occurred. The data obtained from this petrographic study provides information about textural properties, modal mineralogy and diagenetic changes of the Dandot Sandstone. During present study the framework grains, matrix and cement were identified and relative abundance of each was determined in comparison with visual estimation charts given by [12].

Table 2: Showing textural details of Dandot sandstone

Formation	S. No	Grain size	Roundness	Sorting
Lower Part	D St – 1	Very fine	Angular to sub-rounded	Well
	D St – 2	Very fine	Angular to sub-rounded	Moderate
	D St – 3	Very fine	Sub-rounded	Moderate
Middle Part	D St – 4	Fine	Angular to sub-rounded	Well
	D St -5	Fine	Sub-angular to sub-rounded	Moderate
	D St -6	Fine	Angular to sub-rounded	Moderately well sorted
Upper Part	D St – 7	Medium	Sub-angular to Sub-rounded	Moderate
	D St -8	Medium	Sub-Angular to sub-rounded	Moderately well sorted
	D St - 9	Medium	Angular to sub-rounded	Moderate to well

3.1. Texture details

Textural details such as grain size, roundness and sorting are shown in Table 2. On the basis of grain size sandstone unit is divided into three parts. Lower part is very fine grained, middle part is fine grained (Fig. 4A) and upper part is medium grain. Overall the sandstone is moderately to well sorted and grains are angular to sub-angular to sub-rounded (Fig. 4B). In the studied thin-sections tangential and long contacts are common between the grains. The fabric is grain supported.

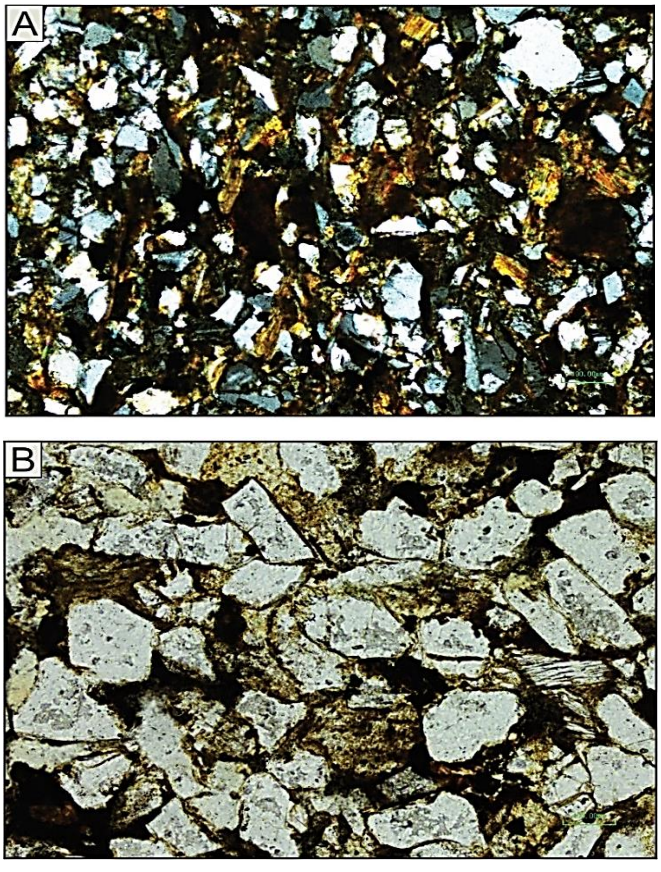

Fig. 4: Photomicrographs (A) indicates very fine to fine grain size PPL whereas (B) shows moderate to well sorting XPL.

3.2. Modal Composition

The detailed thin sections study reveals quartz, feldspars, and lithics as framework grains. Micas (muscovite and biotite), zircon, glauconite and opaque minerals are present as accessory minerals. The detailed description of minerals is as follows;

Quartz is present as dominant framework grains in the sandstone of Dandot Formation. The percentage of the quartz ranges from 62 to 73 percent (Table 3). Quartz is present both in monocrystalline and polycrystalline forms. Monocrystalline quartz are the most dominant framework grains in the Dandot Sandstone (Fig. 5A). Mostly monocrystalline quartz grains are unstrained with non-undulatory extinction, but few are present with undulatory extinction commonly known as strained quartz. Microfractures are dominant features noted in quartz grains.

Feldspars are the second most abundant constituent of sandstone. The overall percentage of feldspar (Fig. 5B), including plagioclase and K-feldspars, ranges from 19 to 54 percent (Table 3). Plagioclase is more dominant than K-feldspars. Mostly plagioclase shows albite polysynthetic twinning (Fig. 5C). Majority of the feldspar grains show alteration and fracturing.

Lithics are present in a small proportion as compared to other framework grains. The percentage of lithics ranges from 3 to 19 percent (Table 3). Chert is dominant lithic present in the sandstone of Dandot Formation (Fig. 5D). Among accessory minerals micas are most dominant in the studied sandstone and these are present as detrital constituents. Micas present include muscovite and biotite, muscovite is more abundant than biotite. Muscovite flakes show bending due to compaction (Fig. 5E). Opaque minerals include magnetite and hematite. Apart from these a few grains of glauconite are present (Fig. 5F).

Table 3: Normalized values of framework grains in sandstone of Dandot Formation

S.No	Quartz (%)	Feldspar (%)	Lithics (%)
01	69	27	04
02	67	30	03
03	71	25	04
04	62	19	19
05	65	29	06
06	38	54	08
07	71	23	06
08	73	23	04
09	65	24	11

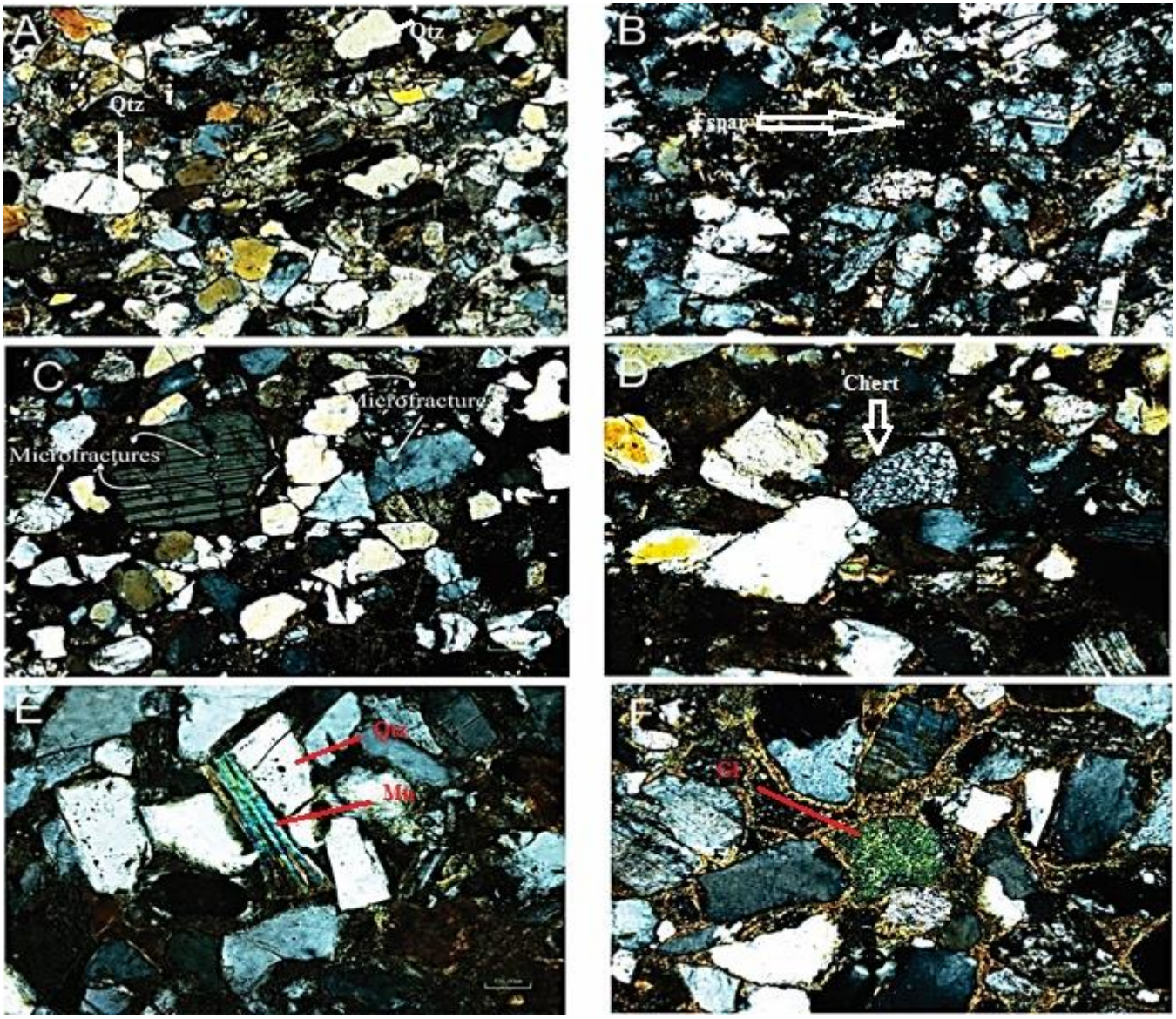

Fig. 5: Photomicrograph A) showing quartz (Qtz) grains, (B) showing highly altered feldspar (Fspar), (C) showing a grain of plagioclase and microfractures in grains (D) chert grain, (E) grain of a Muscovite (green) and a fractured quartz grain to the right of Muscovite (Mu), (F) grain of glauconite (Gl) (green) and ferruginous cementing material between the grains. All photomicrographs are in XPL.

3.3. Sandstone Classification

There are several triangular classification schemes exist with end members of quartz (Q), feldspar (F) and rock-fragments (RF). However, [13] classification was followed. The triangular classification indicates that the sandstone of Dandot Formation is arkose (Fig. 6).

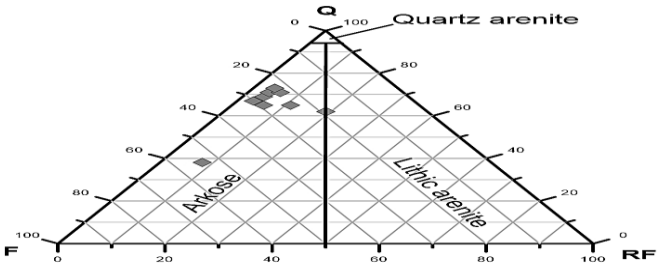

Fig. 6: Classification of studied sandstone samples following [13].

4. Mechanical Properties

4.1. Results and discussion

The most important and vital scope in rock mechanics is measuring and determination of rock properties and behavior by using the suggested testing methods, procedures and specifications. The engineering characteristics of rocks include such as its strength, mode of deformation and failure and modulus of elasticity. UCS is considered as the most striking property among all the mechanical properties. Three to five UCS determinations are recommended to achieve statistical significance of the results [14]. As discussed earlier three core samples of sandstone of Dandot Formation were obtained through drilling of bulk samples. UCS and UTS tests were performed on these samples and the resulting values are given in Table 4 and 5 respectively.

Table 4: Details of UCS test results of the studied samples.

Sample		Core (length)			Core (Diameter)			Area	Load	Strength
S.No	Type	mm	m	Inches	mm	m	Inches	m^2	KN	MPa
01	S1	304.8	0.304	12	152.4	0.152	6	0.0232	304	12.91
02	S2	304.8	0.304	12	152.4	0.152	6	0.0232	300	12.48
03	S3	304.8	0.304	12	152.4	0.152	6	0.0232	290	13.09

Table 5: Details of UTS test results of the studied samples.

Sample		Cube (Thickness)			Disc (Diameter)			Load	Strength
S.No	Type	mm	m	Inches	mm	m	Inches	KN	MPa
01	S1	25.4	0.0254	1	50.8	0.0508	2	5	3.87
02	S2	25.4	0.0254	1	50.8	0.0508	2	4	3.10
03	S3	25.4	0.0254	1	50.8	0.0508	2	3	2.32

Table 6: Material grading based on Unconfined Compressive Strength [8].

Geological Society (Anon, 1977)		IAEG (Anon, 1979)		ISRM (Anon,1981)	
Term	UCS (MPa)	Term	UCS (MPa)	Term	UCS (MPa)
Very Weak	<1.25	Weak	<15	Very low	< 6
Weak	1.25-5.00	Moderately Strong	15 - 50	Low	6 – 10
Moderately Weak	5.00-12.50	Strong	50 – 120	Moderate	20 - 60
Moderately Strong	12.50-50	Very Strong	120 – 230	High	60 – 200
Strong	50-100	Extremely Strong	Over 230	Very High	Over 200
Very Strong	100-200				
Extremely Strong	Over 200				

According to [15], UCS of rocks is eight times their UTS. Nevertheless, [16] suggested the ratio between UCS and UTS to be 10:1. But this is not the case in the present study. The UCS is 4 to 6 times greater than UTS. Similar results have also been obtained by [9, 17]. According to them the lower value of UCS to UTS ratio could be either of two reasons (i) the value of UCS is underestimated or (ii) UTS value is overestimated. In Table 6 the materials/rocks are specified according to their UCS values (see for detail) [8].

In the present research UCS values of the sandstone samples reveals that these rocks lie in the category of very weak to weak following [18] and Anon [19] respectively. The average values of cohesion and angle of internal friction of the Sandstone from Dandot Formation are 6.4MPa and 38º respectively. Specific gravity and water absorption are also calculated for the respective sandstone unit. Values are given in the following Table 7.

Table 7: Comparison of UCS, Specific gravity and Water Absorption.

Sample	UCS (MPa)	Specific Gravity	Water Absorption (%)
S1	12.91	2.02	11.91
S2	12.48	2.11	14.43
S3	13.09	1.81	9.25

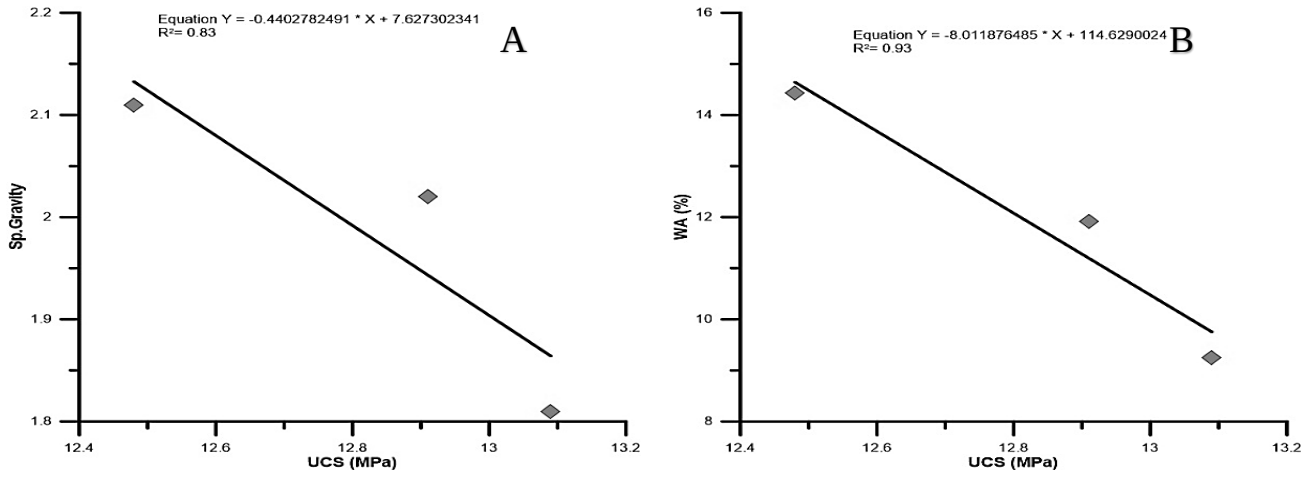

Fig. 7: A and B Showing Inverse relation of Specific gravity and water absorption with UCS.

UCS value is very low and reasons are i) the type and most importantly the amount of cementing material (see for detail) [8] and ii) most of the feldspar grains show alteration to sericite and kaolinite. Rocks having silica as cementing material are the strongest followed by calcite and ferruginous and with clayey binding material are the weakest [20]. On the other hand, a positive relationship has been observed between uniaxial compressive strength and percent cement/ matrix [21, 22]. In the current investigation the low amount of cement (less than 15%) and type of cement i-e ferruginous and presence of sericite and kaolinite (clay minerals are highly porous) shows high water absorption leads to the reduction in strength of sandstone of Dandot Formation. Apart from this, microfracturing in grains and nature of contacts of grains (long and tangential) also play a vital role in decreasing the UCS of the respective sandstone. Microfracturing results due to proximity of study area to the Salt Range Thrust. In [23] Blyth and DeFreitas proposed that rocks with specific gravity $\geq$ 2.55 are appropriate for heavy construction works. In the present case it is low and show inverse relation with UCS (Fig. 7A). On the other hand, water absorption values are also very high and depicts negative relation with the UCS (Fig. 7B).

5. Conclusions

Following are the main conclusions of this work.

i. Sandstone unit from Dandot Formation is classified as Arkose and is regarded as sub-mature both mineralogically and texturally.

ii. Grains of sandstone of Dandot Formation ranges from very fine to medium size and moderate to well sorted.

iii. The nature of grains contacts are tangential and long while, Ferruginous material acting as cement.

iv. Due to very low UCS values, low specific gravity and high water absorption values it is concluded that sandstone of the respective formation is not even suitable for small construction purposes rather than being used in heavy construction works.

References

[1] S.M.I. Shah, Stratigraphy of Pakistan, Geological Survey of Pakistan Memoir, 12, 1977.

[2] A.H. Kazmi and R.A. Rana, "Tectonic map of Pakistan", Geological Survey of Pakistan, Quetta, 1982.

[3] S. Ghazi, N.P. Mountney, A.A. Butt and S. Sharif, "Stratigraphic and palaeoenvironmental framework of the Early Permian sequence in the Salt Range, Pakistan", Journal of Earth System Science, vol. 121(5), pp.1239-1255, 2012.

[4] I.U. Jan, A. Shah, M.H. Stephenson, S. Iqbal, M. Hanif, M. Wagreich and H.S. Hussain, "The sedimentology of the lower Permian Dandot Formation: a component of the Gondwana deglaciation sequence of the Salt Range, Pakistan", Rivista Italiana di Paleontologia e Stratigrafia, vol. 122(1), pp. 75-90, 2016.

[5] ASTM D-3976, "Standard test method for splitting tensile strength of intact rock core", American society for testing material, Philadelphia, Pennsylvania, U.S.A. 1986.

[6] M. Arif, A. Mulk, M.T. Mehmood and M.H. Shah, "Petrography and mechanical properties of the Mansehra granite, Hazara, Pakistan", Geological Bulletin University of Peshawar, vol. 32, pp. 41–49, 1999.

[7] M. Arif, W.H. Bukhari, N. Muhammad and M. Sajid, "Petrography and physicomechanical properties of rocks from the Ambelagranitic complex, NW Pakistan", The Scientific World Journal, Article ID 349381, 8 pages, 2013.

[8] F.G. Bell, Engineering Geology, 2nd edition. United Kingdom: Butterworth-Heinemann: Animprint of Elsevier, 2007.

[9] M. Sajid, M. Arif and N. Muhammad, "Petrographic characteristics and mechanical properties of rocks from Khagram-Razagram area, Lower Dir, NWFP, Pakistan", Journal of Himalayan Earth Sciences, vol. 42, pp. 25-36, 2009.

[10] M. Yar, M. Arif, A.K. Afridi, M. Saeed, M. Ziad and A. Ali, "Petrographic and mechanical characteristics of sandstone from Murree Formation, Jena Kor area, Peshawar Basin", A case study. Pakistan Journal of Engineering and Applied Sciences, vol. 20, pp. 69–78, 2017.

[11] Y.S. Khalil, M. Arif, H.A. Bangash, M. Sajid and N. Muhammad, "Petrographic and structural controls on geotechnical feasibility of dam sites: implications from investigation at Sher Dara area (Swabi), north-western Pakistan", Arabian Journal of Geosciences, vol. 8, pp. 5067-5079, 2015.

[12] L. Baccelle and A. Bosellini, "Diagrammi per la stima visiva della composizione Percentuale Nelle Rocce Sedimentarie", Annuali Dell'Universita Di Ferrara, vol. 9, pp. 59–62, 1965.

[13] F.J. Pettijohn, P.E. Potter and R. Siever, Sand and sandstone, 2nd edition, New York, Springer-Verlag, pp. 618, 1987.

[14] ASTM D-2938, "Standard test method for unconfined compressive strength of intact rock core specimens", American society for testing material, Philadelphia, Pennsylvania, U.S.A. 1971.

[15] B.H.G. Brady and E.T. Brown, "Rock mechanics for underground Mining, 3rd edition, Kluwer, Academic Publishers, 2004.

[16] I.W. Farmer, Engineering behavior of rocks, Chapman and Hall, London. 1983.

[17] M. Sajid and M. Arif, "Reliance of physico-mechanical properties on petrographic characteristics: consequences from the study of Utla granites, north-west Pakistan", Bulletin of Engineering Geology and Environment, vol. 74, pp. 1321-1330, 2014.

[18] Anon, "The description of rock masses for engineering purposes", Quarterly Journal of Engineering Geology, vol. 10, pp. 355-388, 1977.

[19] Anon, "Classification of rocks and soils for engineering geological mapping. Part 1- Rock and soil materials", Bulletin of the International Association of Engineering Geology, vol. 19, pp. 364-371, 1979.

[20] V.S. Vutukuri, R.D. Lama and S.S. Saluja, Handbook on Mechanical properties of Rock, Testing Technique and Results, Vol. 1. Clausthal, Germany, Trans Technical Publications, 1974.

[21] M.P. Fahy and M.J. Guccione, "Estimating the strength of sandstone using petrographic thin section data", Bulletin of the Association of the Engineering Geologists, vol. 16, pp. 467-485, 1979.

[22] A. Shakoor and R.E. Bonelli, "Relationship between petrographic characteristics, engineering index properties and mechanical properties of selected sandstone", Bulletin of the Association of Engineering Geologists, vol. 28, pp. 55-71, 1991.

[23] F.G. Blyth, M.H. DeFreitas, A geology of engineers, London, ELBS and Edward Arnold, pp. 514, 1974.

The Nucleus ***60***, *No. 1 (2023) 15-23*

www.thenucleuspak.org.pk

The Nucleus

ISSN 0029-5698 (Print)
ISSN 2306-6539 (Online)

Spatio-Temporal Analysis of Land Use Change and Its Driving Factors in Layyah, Punjab, Pakistan

Muhammad Sajid[1], Muhammad Mohsin[2], Muhammad Mobeen[3], Abder Rehman[3*], Anum Rafique[4], Muhammad Rauf[3], Ghulam Ali[5]

[1]*Department of Geography, Govt. Graduate College, Chowk Azam, Layyah, Punjab, Pakistan*

[2]*Department of Geography, Govt. Sadiq Egerton Graduate College, Bahawalpur, Punjab, Pakistan*

[3]*Department of Earth Sciences, University of Sargodha, Punjab, Pakistan*

[4]*Department of Geography, Govt. Associate College for Women, Mela Mandi, Sargodha, Pakistan*

[5]*Department of Political Science, Govt. Graduate College, Chowk Azam, Layyah, Punjab, Pakistan*

ABSTRACT

Specific objective of this study was to find out the distribution of various land use changes in District Layyah from 2000 to 2020 using geographic information system (GIS) and remote sensing (RS) techniques, and the forces or factors that lead to land use change. District Layyah has experienced remarkable land use and land cover (LULC) changes for the past three decades. Three Landsat satellite images i.e. thematic mapper (TM), Landsat enhanced thematic mapper plus (ETM+) and operational land imager (OLI)/ TIRS for the years 2000, 2010 and 2020 were acquired from USGS website in order to detect the land use changes. By using ERDAS Imagine software, the maximum likelihood classification was employed in order to classify the images. The spatial and spectral distribution of five land use types was made including i.e. Water, Built-up, Vegetation, Desert, Bare and Sparse land. Ground Truth points were noted and these points were used for the validation and classification of the images. This accuracy showed an overall accuracy rate of 85% with a Kappa coefficient of 0.9 which demonstrated the basic classification method because the images used in the research were highly good. Results showed that the rise was revealed in Vegetation, Built-up and Water land uses from the year 2000 to 2020. On the other side, the decrease in Bare and Sparse land and Desert land use was calculated. The main driving factors behind these LULC changes were found the growth in population, agro-technological advancement and various physical factors (e.g. availability of water and so on), resulting an increase in built-up area. Present research will be beneficial in understanding the most important land use changes to estimate the future change trends in various land use classes for policy making and land use management.

Keywords: *Land Use Change, Driving Factors, RS, GIS, Layyah*

1. Introduction

Land use is can be defined as the manner in which biophysical resources of land are being used for various purposes like built-up, industrial and vegetation use and so on [1]. Land use changes perform an important role at the local and global levels [2]. Increased and unchecked population growth besides the industrial and economic growth particularly in the emerging countries in the late 21st century, have accelerated the pace of land use change. Therefore, the Land use changes have been witnessing greatly throughout the world during the few past years especially in the developing countries with growing population growth and the increasing urbanization [3, 4]. Land use change is one of the main environmental issues globally, which is responsible for climbing of the land values and conversion of the farmlands to numerous urban and miscellaneous uses and degradation of land beside fall in ecosystem services [5-7]. Principal driving forces responsible for land use change are political and socioeconomic decisions which are regarded as the key factors in this sense [8]. Moreover, any changes in the land use and land cover (LULC) can be the result of alteration in the intensity of the present LULC types because of man-made activities and the natural factors [9]. It has been noticed from the previous researches that the land use change is possess the potential to have an important ecological impacts [10]. Various researches have also been confirmed the impacts of land use changes on agricultural production and on environment [11-13]. Despite the impacts of the human actions on land use changes, changing in the climate, environmental factors, conditions of soil and landscape features have also been regarded as land use changes. Besides the human variables for example, the environment and government decisions [14]. LULC has a direct link with the change in climates of the cities as well [15]. Therefore, recently, the LULC changes and their environmental impacts have attained a prompt attention globally [16, 17].

Satellite remote sensing spatial data is considered tremendously useful to map out the discrete land use classes [18]. It concentrated the world wide change significant problems on the global, local and at the regional levels [19]. Furthermore, in year 2000, Council of the Europe implemented the Convention on European landscape because of increased changes in land use which adversely influenced the surface of the earth [20]. The Landsat images were initially administered in the ERDAS Imagine Software according to the need of the study area and selected land use classes i.e. agricultural land use and barren land classes were mapped to know the potential impact on the land use [21, 22]. Change detection techniques have been distributed into three stages mainly based on the pixels [23].

The land use change researches provide us very much useful information towards improved information of the past practices, present land use change patterns and the future land use trends as crucial for policy makers and land use management [24-26]. Many studies have been conducted in various areas of Pakistan to determine the land use and it's causing factors and impacts. Like a study conducted in Quetta, Balochistan using satellite imageries found increase in built-up area and decrease in open spaces [27]. Similarly, another

*Corresponding author: abdurrehmanuospk@gmail.com

study conducted in Quetta to monitor the urban sprawl and urban land use change found the substantial increase in built-up area (52.33%) and a great loss of vegetation up to 60% [28]. Similarly, the extensive urban sprawl and resultant land use changes are monitored in different parts of the Karachi, the biggest city of Pakistan by using the remote sensing and geographic information systems [29]. Therefore, the present research aimed at accomplishing the comparative analysis of LULC of District Layyah, Punjab, Pakistan by using tools of Remote Sensing data and Geographic Information System. The district has high agricultural potential but facing notable changes in its land use over the past years which are needed to highlight for better planning and management of land use. Therefore, the objectives of the present study were; First, to identify and detect various categories of LULC and the changing pattern in land use in District Layyah from 2000 to 2020 by using the Remote Sensing data and Geographic Information System to disseminate the various changes in study area and second, to evaluate the main driving factors or forces keeping in view the extent and role of the LULC change.

2. Materials and Methods

2.1 Description of Study Area

District Layyah lies in southern Punjab and it is bounded by district Jhang on its East, Dera Ghazi Khan on its West, Bakkar on its North and district Muzaffargarh on its South. Layyah has three tehsils (sub-divisions) namely Layyah, Chaubara and Karor Lal Esan. The population of the district was about 1.82 million according to the 2017 National Census of Pakistan as compared to the 1.12 million in 1998 with a growth rate of 2.59 [30, 31]. District Layyah is located at 30° 45′ to 31° 24′ North latitudes and 70° 30′ to 71° 47′ East longitudes (Fig. 1).

Its height is 500 feet from sea level. The area eastern part of the district comprised sandy desert. So, the area under study region is famous for its sand storms due to extraordinary temperatures throughout the summer season. A very little annual rainfall pours in Layyah in two seasons of the year. Relief features of the study area include rich and fertile fields, citrus gardens, grams and historical places. The area possesses rich agricultural lands and access to an extensive canal system, harvests many crops and being most popular for the production of grams [32].

2.2 Data Acquisition and Collection

In order to meet the objective of the study, the satellite images for the years 2000, 2010 and 2020 were acquired from the website of USGS to examine the spatio-temporal land use changes of the District Layyah, study area. The characteristics of these downloaded satellites images have been shown in the table 1. The field work was performed to collect the Ground Control Points (GCPs). Maps and preprocessed images were validated.

2.3 Image Pre-processing

Radiometric, geometric correction and layer stacking correction techniques are regarded as preprocessing methods prior to the extraction of information from the images. Landsat TM of years 2000, 2010 and 2020 were acquired. The various bands of the tiff image were converted in the image format via layer stacking technique in the ERDAS IMAGINE 8.0 software to generate the False Color Composite (FCC) image. Then all the images were geometrically exported to the ArcGIS software and then to the Universal Transverse Mercator (UTM). The district Boundary of the study area was extracted via Software ArcGIS 10.2 through masking tool. Images of the various acquired years were independently classified using supervised classification. The spectral signature for all land use classes were created through pixel analysis of the image. The study area images were broadly classified into five major land use classes such as Barren, Vegetation, Desert, Water and Built-up land use class.

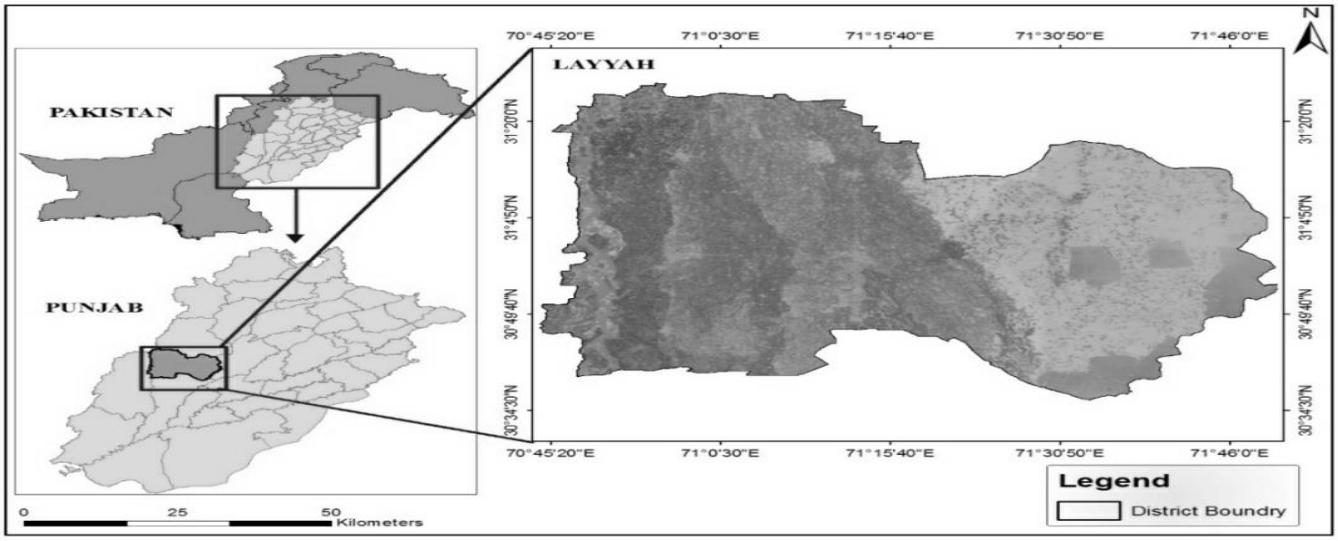

Fig. 1: Map of the Study Area

Table 1. Features of the Acquired Remote Sensing Images

Year	Satellite	Sensor	Band	Pixel	Season	Source
2000	Landsat 5	Thematic Mapper(TM)	7	30m	Dry	http://glovis.usgs.gov/
2010	Landsat 7	ETM+	7	30m	Dry	http://glovis.usgs.gov/
2020	Landsat 8	Operational Land Imager (OLI/TIRS)	9	30m	Dry	http://glovis.usgs.gov/

The images which were classified revealed the common ground features of the District Layyah, study area and gave the required information to understand the changes in land use patterns of the study area. After, the images were processed and the land use classes were extracted. These images data were acquired from the Landsat 5 Thematic Mapper (TM) for 2000, Landsat 7 Enhanced Thematic Mapper Plus (ETM+) for 2010 and Landsat 8 Operational Land Imager (OLI)/ TIRS for 2020 respectively of study area, District Layyah. These satellite images were downloaded from the website of the United States Geological Survey (USGS) (Earth Explorer). These satellite images were acquired in the form of geo-tiff with various spatio-spectral bands in the distinct files. The ancillary spatial data comprised on the earth reference data (most occasionally it is regarded as the data on ground truth) acquired through the real surveys of the ground which was obtained individually. The Global Positioning System (GPS) was utilized to validate the data related to the ground truth while accomplishing field work. Water, Built-up, Vegetation, Desert, Bare and Sparse land classes were included in the present study and the images acquisition dates were July 21, 2000, July 22, 2010 and July 23, 2020 respectively.

2.4 Image Classification and Accuracy Assessment

Supervised classification technique was used for classifying the images. Sample's training was created by using the training sample manager, visual explanation of the acquired satellite images in Google Earth Software and in the ground truth data. Each land use category's training samples were merged then. Training sample's signature file was generated. Maximum likelihood classification was used in order to classify the images. Image accuracy had been performed from ground truth data by producing the random points and then comparing these points to the map which has been classified by creating the confusion matrix. Producer accuracy, User accuracy and Overall accuracy were also performed by using the following Equation. Overall accuracy ¼ number of the sampling classes was classified correctly with number of the reference sampling classes (1).

Equation 1: Image Accuracy Assessment Types

$$User\ Accuracy = \frac{Number\ of\ Correctly\ Classified\ Pixels\ in\ a\ class}{Total\ Number\ of\ Pixels\ in\ a\ Class}$$

$$Producer\ Accuracy = \frac{Number\ of\ Correctly\ Classified\ Pixels\ in\ a\ class}{Total\ Number\ of\ Pixels\ in\ all\ Classes}$$

$$Overall\ Accuracy = \frac{Total\ Number\ of\ All\ Correctly\ Classified\ Pixels}{Total\ Number\ of\ Pixels\ in\ all\ Classes}$$

The values of Kappa (K) measures show how well the Remote Sensing classification approves or are correct with reference data [33]. The Overall accuracy was 87.81%, 93.3% and 95.4% for the images classified for the year 2000, 2010 and 2020 respectively which is indicative that classification is good and acceptable.

Table 2. Land-use Classification System and Type Description.

Land Use/Cover Types	National Land Cover Description
Built Up Area	Land that includes a settlement
Vegetation	Land exclusively utilized for growing the agricultural crops
Desert	Land which receives annual rainfall less than 10 inches
Bare and Sparse Land	Land which includes, bare land, rock and sand
Water	Comprises the water of inland and the River Water

Source: [34]

2.5 Land use Change Analysis

The internal trading for the land use classes were assessed using the vector datasets for the 20 years. These image datasets were intersected with the help of the intersect tool available in the ArcMap 10.2. These datasets were acquired in this manner and were then transferred to MS Excel. Land use change matrix was also created with the help of the pivot table. The resulting datasets were then noted in stable or in the converted land areas.

2.6 Image Enhancement

Image enhancement is basically a process of presenting an image more interpretable for a specific application. The basic purpose of image enhancement is to make the raw image or the remote sensing data more un-testable for the human eye. Enhancement procedures are most commonly used instead of the classification techniques in order to extract the features, locating and studying various areas, some objects on ground and to derive the meaningful information from these images. Usually, the enhanced images are used only for visual analysis, besides the actual images are used for specific automated analysis [35]. Geographic Information System and Remote Sensing define the changes in the land use types [36, 37]. LULC based on the visual understanding and satellite images was verified from the inspection of the field also.

3. Data Analysis

3.1 Overall Accuracy and Kappa Index

The Kappa statistics and overall classification accuracy (in percentages) was used to assess the classification accuracies [34]. To investigate the classification accuracy result of the images, the Kappa index or Kappa Coefficient (K) was calculated for all the maps classified. So, the overall classification accuracies for the year 2000, 2010 and 2020 were 87.6%, 85.65% and 89.2% respectively and the statistics

of the Kappa for the images of 2000, 2010 and 2020 were 84.2%, 81.9% and 91.2% respectively.

Table 3. Land-use Classification and the Techniques used to Study.

Application	Techniques Used to Study
Land use/Land cover change	Differencing of Image, Image rationing, PCA, Chi-square, Post-classification, Detecting hybrid change and GIS
Vegetation	Differencing of Image and Post-classification
Urban change	Differencing of Image, Post-classification, Hybrid change detection, PCA & GIS
Landscape change	Post-classification and GIS
Deforestation	Post-classification, Differencing of Image and PCA

Source: [34]

3.2 Land Use Change Detection

Post classification change detection method in ArcGIS 10.2 was used in the present study. This classification technique is most commonly utilized by many researchers in the urban environments because of its accuracy and efficacy to detect the location, rate and nature of the change.

3.3 Principle Component Analysis (PCA)

Eigenvector transformation is also known as the Principal Component Analysis (PCA). During the process of change detection, two mechanisms/techniques can be applied for PCA. The very first technique can be applied by addition of the two images with different dates in one file. The other way is to subtract the second satellite image from the concerning image for first day or date after executing the Principal Component Analysis (PCA) distinctly. Thus, Standardized PCA, the first technique is considered most suitable than un-standardized PCA for change detection process while detecting land use change [38, 39].

3.4 Post-Classification Comparison

It is a very helpful method to extract the land use data. Supervised classification was basically the technique in which the analyst itself picks a number of the area of an image, then recognizes the kind of the task on the screen of the computer. According to this process as recognized by analyst, the system recognizes an attribute of the data which includes every kind. It classifies nearly all the similar image pixels remaining. Geographic Information System (GIS) and Remote Sensing (RS) are the vital tools for detection of the land use changes [40] important in investigating and assessing the land use changes [41, 42]. Spatial data and remote sensing possess the ability to identify the synoptic land use changes data over the particular time period with respect to location [43-45]. Land use change analysis was performed using co-relation analysis [46]. Kappa Coefficient (K) and Overall Accuracy (OA) were used for the evaluation of the accuracy from error matrix. The Producer's Accuracy (PA) 87.1% and User's Accuracy (UA) 88.3% were also assessed for the selected classes of land use.

4. Results and Discussion

4.1 Land Use Change Detection for the Year 2000

Table 4 and Fig. 2 and 6 showed the different land use classes in 2000. Water land use class was covered the land area of 200.2 km^2, Built-up land use covered just 88.7 km^2, Vegetation land use covered the biggest share of 2,330.3 km^2, Desert land use covered 1,602.3 km^2, while the Bare and sparse land use covered the land use of 2,159.3 km^2.

4.2 Land Use Change Detection for the Year 2010

Table 5 and Fig. 3 and 7 showed the different land use classes and their change detection in 2010. Water land use class was increased to 243.6 km^2, Built-up land use also enhanced the land area and reached 165.2 km^2, Vegetation land use also shown the increase and reached to 2,965.3 km^2, whereas the Desert land use shown a decrease and reduced to 1,194.4 km^2, while the Bare and sparse land use also declined to 1,811.7 km^2. These results demonstrated the notable variations in the land use of the district Layyah from 2000 to 2010.

4.3 Land Use Change Detection for the Year 2020

Table 6 and Fig. 4 and 8 showed the different land use classes and their change detection in 2020. Water land use class was again slightly increased to 251.9 km^2, Built-up land use also considerably augmented the land area and reached 237.2 km^2, Vegetation land use also exhibited the slight increase and reached to 3,054.0 km^2, whereas the Desert land use shown an unexpected increase in land area to 1,506.7 km^2, while the Bare and sparse land use again declined to 1,598.6 km^2. These results proved the important variations in the land use of the district Layyah from 2010 to 2020.

4.4 Accuracy Assessment of Classified Map of Past 20 Years (2000-2020)

The analysis results of the remote sensing imageries from 2000-2020 showed that District Layyah has undergone many changes in the land use patterns (Table 7 and Fig. 5 and 11). Firstly, the area of Vegetation land use class, which is the biggest portion of the land use class, encompassing miscellaneous crops and vegetation. During the last 20 years, Vegetation land has been considerably increased from 2,330 km^2 in 2000 to 3,054 km^2 in 2020. Secondly, the area of Water considerably increased from 200.2 km^2 in 2000 to 251.9 km^2 in 2020. Thirdly, the Bare and sparse land area was decreased from 2,159 km^2 in 2000 to 1,598 km^2 in 2020. Besides, the area of Built-up land was considerably increased from 88.7 km^2 in 2000 to 237.2 km^2 in 2020 was also classified, as study area is covered with the settlements mixed with the farm areas having low density. These results verified in various researches as a recent study conducted in Bahawalpur city by employing satellite remote sensing, machine learning and geographic information modelling found the massive increase in urban built-up area 4,768 acres

(90.08%) from 1990 to 2020 and in contrast, the decrease in vegetation and barren classes at the rates of 2,116.55 acres (6.61%) and 2,785.47 acres (32.11%) [47]. Another study undertaken in Tehsil Shorkot, District Jhang to assess the impact of changing land use on agricultural production from 2010 to 2020 using RS and GIS data revealed the noteworthy increase in built-up land class (16.6 km^2 in 2010 to 26.8 km^2 in 2020) and decrease in forest land class (90.8 km^2 in 2010 to 61.84 km^2 in 2020) and barren land class (528.54 km^2 in 2010 to 333.1 km^2 in 2020) [48]. Similarly, a study conducted in Dong Trieu district, Vietnam with utilizing Remote Sensing data from 2000 to 2019 to assess land use and its driving forces concludes a net decreasing tendency in major land use classes i.e. Cropland (1,852 acres), Forest (882.6 acres), Water body (2,836 acres) and Barren land (8,837.7 acres) [49].

4.5 The Land Use Transition Matrix from 2000 to 2020

The land use change detection matrix for the period among 2000, 2010 and 2020 was created with the help of pixel-by-pixel process to examine the land use change detection in District Layyah. It was examined the variable pattern of the land use types. Over the past 20 years it was revealed a substantive rise in the vegetation land use class at the place of other land use types. This land use increased greatly. Bare soil demonstrated a decreasing tendency during the year of 2000 to 2020. While the change in the built-up area slightly increased, and this revealed a prompt increase in the population. Desert land use area decreased and water land use class also increased progressively.

Table 4. Land-use Change detection for the year 2000

Name of land use class	Area (km^2)
Water	200.2
Built-up	88.7
Vegetation	2,330.3
Desert	1,602.2
Bare and Sparse land	2,159.3

Table 5. Land-use Change detection for the year 2010

Name of land use class	Area (km^2)
Water	243.6
Built-up	165.2
Vegetation	2,965.9
Desert	1,194.4
Bare and Sparse land	1,811.7

Table 6: Land-use Change detection for the year 2020

Name of land use class	Area (km^2)
Water	251.9
Built-up	237.2
Vegetation	3,054.0
Desert	1,506.7
Bare and Sparse land	1,598.6

Table 7. Land use Change matrix (2000-2020)

Class	Year 2000	Year 2010	Year 2020
Water	200.2 km^2	243.6 km^2	251.9 km^2
Built-up	88.7 km^2	165.2 km^2	237.2 km^2
Vegetation	2,330.3 km^2	2,965.9 km^2	3,054.0 km^2
Desert	1,602.2 km^2	1,194.4 km^2	1,506.7 km^2
Bare and Sparse land	2,159.3 km^2	1,811.7 km^2	1,598.6 km^2

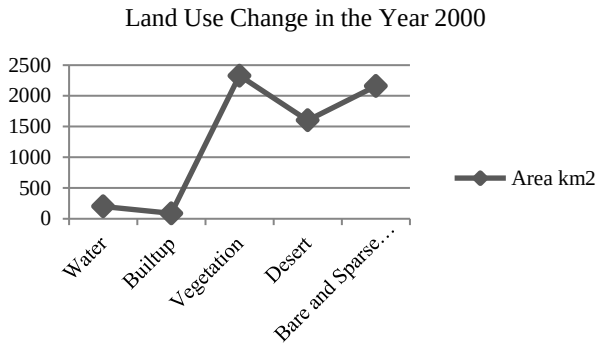

Fig. 3: Land-use Change Detection in 2000 in District Layyah

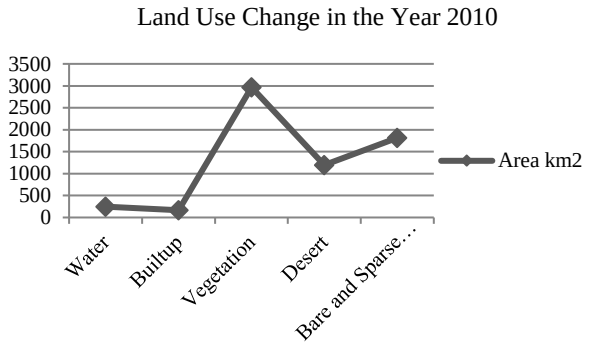

Fig. 3: Land-use Change Detection in 2010 in District Layyah

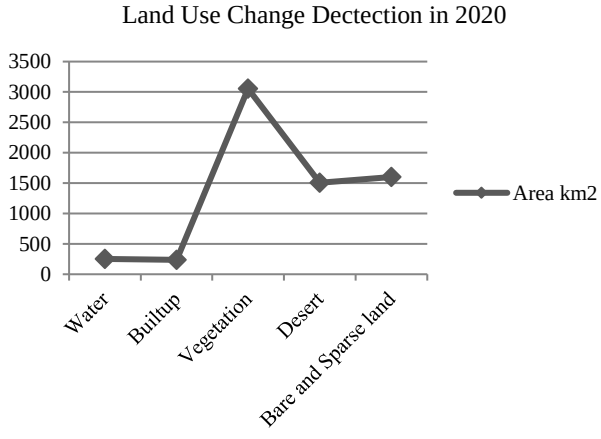

Fig. 4: Land-use Change Detection in 2020 in District Layyah

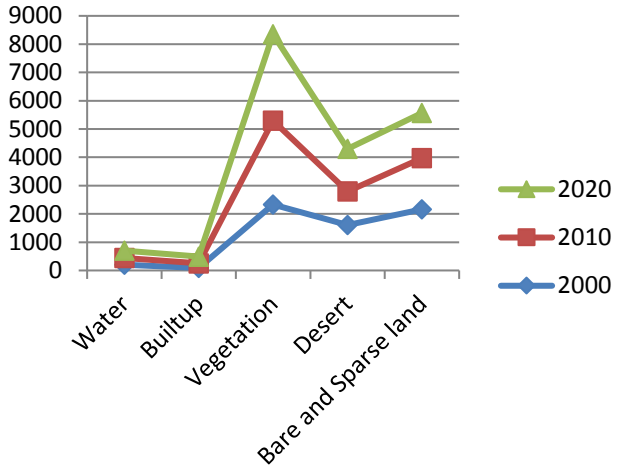

Fig. 5: Land use Changes in different classes from 2000-2020 in District Layyah

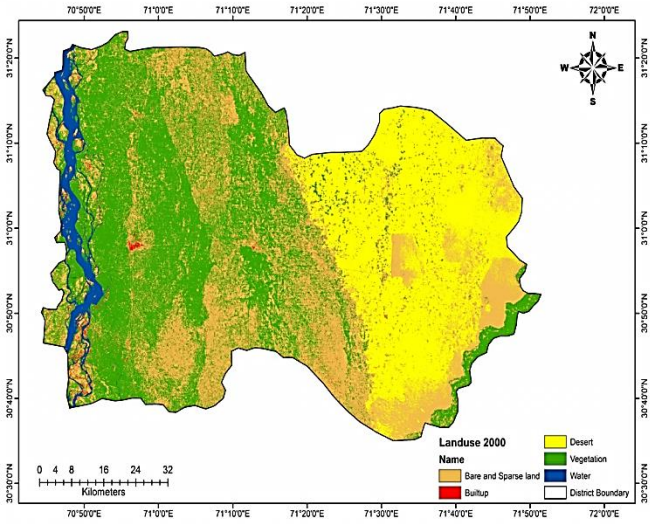

Fig. 6: Land-use Change for the year 2000 in District Layyah

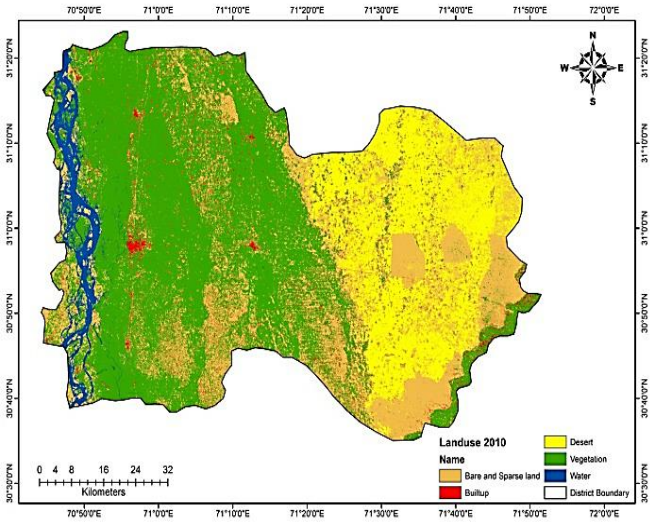

Fig. 7: Land-use Change for the year 2010 in District Layyah

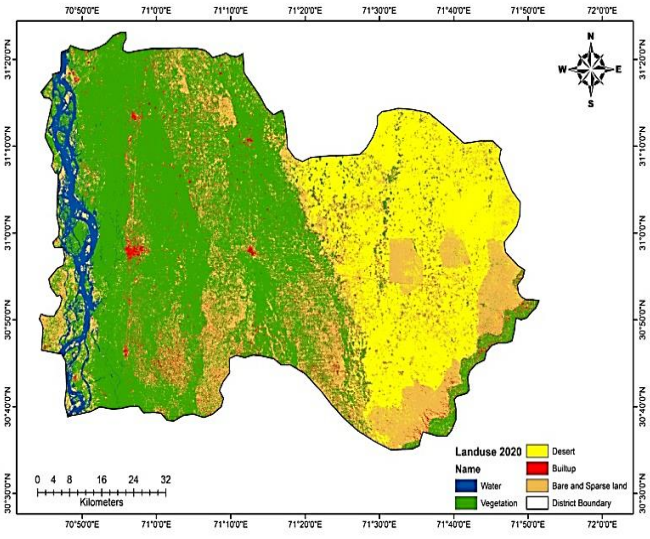

Fig. 8: Land-use Change for the year 2020 in District Layyah

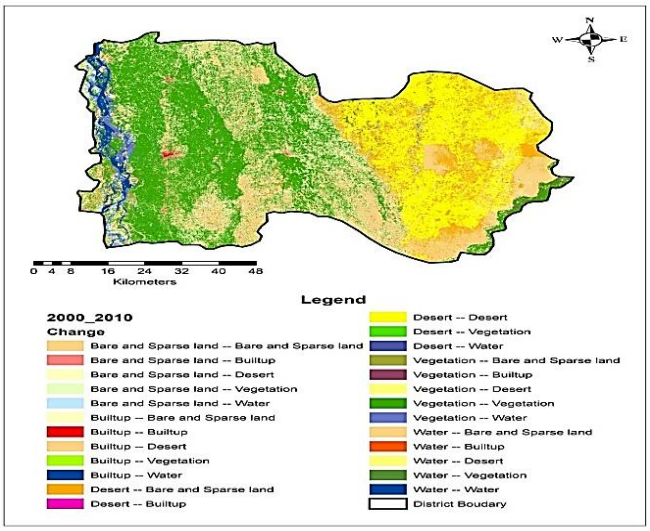

Fig. 9: Land-use Change from 2000-2010 in District Layyah

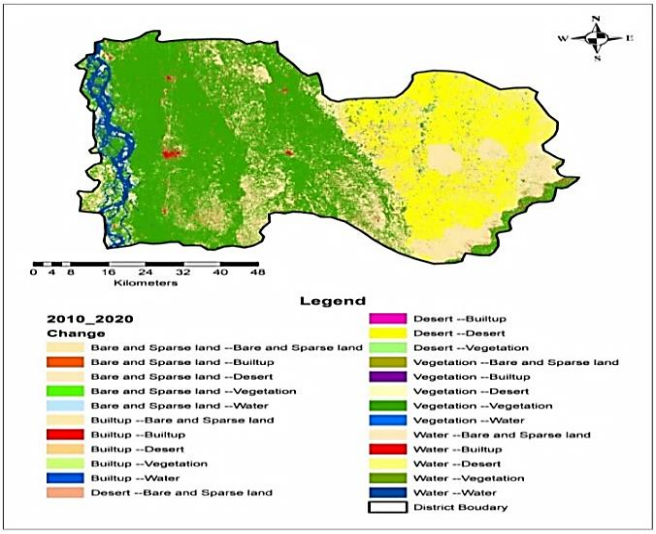

Fig. 10: Land use Change from 2010-2020 in District Layyah

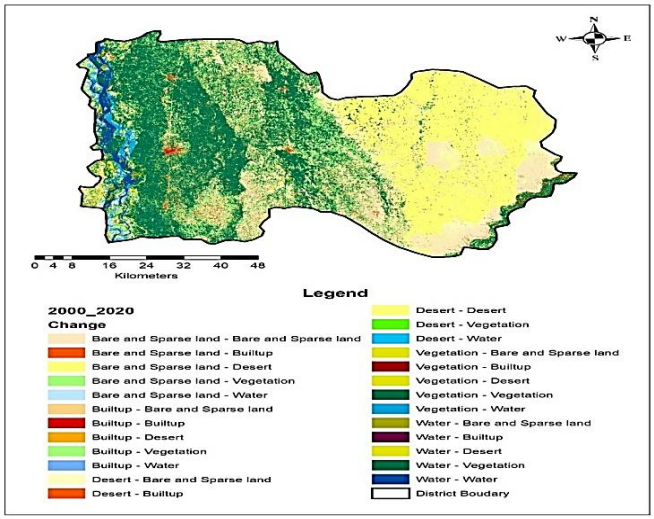

Fig. 11: Land-use Change from 2000 to 2020 in District Layyah

4.3 Proximate Drivers of Land Use Change

The amalgamation of the human activities which aims at seeking to certify the supply of the food and to make better the incomes of growing families or population were the main driving factors or force behind the land use change. It was observed through the field observations that the human activities had an adverse effect which became a reason of the land use changes of the area under study.

4.4 Primary Land Use Change Drivers

It is found that the accelerated consumption patterns which are needed to fulfill the hiking food requirements were among the major causes of land use change. Furthermore, the information derived from the natives of the study area through the interviews that improved infrastructure and ameliorated roads had increased the expansion in agricultural activities when compared with the other land use activities.

4.4.1 Population Growth

Growth in the population had been increasing gradually in the study area since 2000 to 2020 as it was 1.12 million in 1998 and climbed to 1.82 million in 2017 [31]. Moreover, Migration of the individuals from rural to urban places was very much common. It is believed that if the population density is high, there will be more built-up land use. The growth of population and urbanization also brought changes in land use i.e. as these are witnessed in case of many Pakistani cities (e.g. Quetta, Bahawalpur and others) [27, 50].

4.4.2 Agro-technological Advancement

Advancement in agriculture in the study area comprises excessive use of the spray, pesticides and fertilizers along with heavy machinery in order to prepare the land ready for the extensive agriculture. It means that the agricultural expansion takes place at the place of the other kinds of the land use of the study area. Though, urban land use planning has got due attention in many researches but agricultural land use planning turned little focus in many studies [51]. According to a study in the District Layyah, the study area, the rise in the use of pesticides and using the desert and barren land for agriculture and for residential purposes had influenced the land use changes in the area under study [32].

4.4.3 Physical Factors

Various physical factors are also responsible for the rapid changes in land use of many areas. For instance, the availability of water responsible for conversion of desert and barren land use class into vegetation land use class. Past studies focused on the land use changes especially centered at its various patterns [52]. During the 20th century, due to fast increase in the population, the available resources of land has been depleted rapidly, which has drawn the attention of various countries of the world more on the current status of the land use [53, 54], impacts on the land use and environment [55-57], vigorous simulation and forecast [58, 59] at various spatiotemporal epochs. It is widely believed that the chief driving forces analysis and spatiotemporal dynamics estimation for land use in future may assist ascertain the emerging trends and extent of the particular changes in land use. These changes are very serious for justifiable land use and reduction of the global environmental issues regarding land use. Many studies have also proved the impact of land use change impact on agricultural production around the globe [60, 61].

5. Conclusion

The present study aims at investigating the land use changes in District Layyah and its driving forces. For examining the land use changes dynamics, the explanation of the multi temporal satellite images has been concluded to be very useful technique. Results revealed that a constant reduction was recorded in Desert and Bare land use classes, whereas the Water, Built-up and vegetation land use class areas were increased drastically during the year 2000 to 2020. In present research, the assessment of land use and its changes detection was performed by using digital image processing methods. The findings revealed that the important reason for conversion of Barren and Desert land into agriculture land was to fulfill the requirements of the food and alteration in the land use. During this period, the human population increase led to increased desire in the vegetation production. The high-quality LULC maps can produce essential base for fruitful policies of planning and land management [34]. The land use change researches provide us very much useful information towards improved information of the past practices, present land use change patterns and the future land use trends as crucial for policy makers and land use management. Hence, this study could be assisting in future research on land use and land cover and their causing factors on local and regional levels. The study suggests that land use change detection is vital for land use management so that it should be deployed in policy formulation and decision making. The district Layyah has possessed good fertile agricultural land therefore the haphazard population growth dangerous for the agricultural land base and as well as for surrounding land uses transformations. Therefore, it should be regularly monitored

and land use policies should be formulated according to the ground realities to make the land use efficient and sustainable.

Reference

[1] T.M. Lillesand and R.W. Kiefer, "Remote Sensing and Image Analysis", John Wiley and Sons: New York, NY, USA, Vol. 46, p. 736, 2000.

[2] M. Sahana, R. Ahmed and H. Sajjad, "Analyzing land surface temperature distribution in response to land use/land cover change using split window algorithm and spectral radiance model in Sundarban Biosphere Reserve, India", Modeling Earth Systems and Environment, 2(2), p. 1-11, 2016.

[3] W. T. Dibaba, T.A. Demissie and K. Miegel, "Drivers and implications of land use/land cover dynamics in Finchaa catchment, northwestern Ethiopia", Land, 9(4), p. 113-133, 2020.

[4] Z.M. Fan and S.B. Li, "Change pattern of land cover and its driving force since 2001 in the New Eurasian Continental Bridge Economic Corridor", Acta Ecol. Sin, 39, p. 5015-5027, 2019.

[5] M. Mohsin, "Urban growth and conversion of farmland in Bahawalpur City, Pakistan: Causes, Rates and Remedies", LAP LAMBERT Academic Publishing: Saarbrücken, Germany, 2014.

[6] M. Mohsin, M.M. Anwar, M. Dawood, M.A.A. Shah, F. Jamal and M. Basit, "Impact of land use change on land values: A case of Jhangiwala, Bahawalpur City, Pakistan", Journal of Biodiversity and Environmental Sciences, 14(6), p. 152-160, 2019.

[7] R. Hoyer and H. Chang, "Assessment of freshwater ecosystem services in the Tualatin and Yamhill basins under climate change and urbanization", Applied Geography, 53, p. 402-416, 2014.

[8] S. Hishe, W. Bewket, J. Nyssen and J. Lyimo, "Analysing past land use land cover change and CA-Markov-based future modelling in the Middle Suluh Valley, Northern Ethiopia", Geocarto International, 35(3), p. 225-255, 2020.

[9] H.J. Geist and E.F. Lambin, "Proximate causes and underlying driving forces of Tropical deforestation", Bio Science, 52(2), p. 143-150, 2002.

[10] J. Zheng, X. Chen, Y. Du, X. Li and J. Zhang, "Short text sentiment analysis of micro-blog based on bert", In: Advanced Multimedia and Ubiquitous Engineering (pp. 390-396). Springer: Singapore, 2019.

[11] S. Das and R. Sarkar, "Predicting the land use and land cover change using Markov model: A catchment level analysis of the Bhagirathi-Hugli River", Spatial Information Research, 27(4), p. 439-452, 2019.

[12] J. Tan, D. Yu, Q. Li, X. Tan and W. Zhou, "Spatial relationship between land-use/land-cover change and land surface temperature in the Dongting Lake area, China", Scientific Reports, 10(1), p. 1-9, 2020.

[13] B.J. Zoungrana, C. Conrad, L.K. Amekudzi, M. Thiel, E.D. Da, G. Forkuor and F. Löw, "Multi-temporal landsat images and ancillary data for land use/cover change (LULCC) detection in the Southwest of Burkina Faso, West Africa", Remote Sensing, 7(9), p. 12076-12102, 2015.

[14] A.M.A. Athick and K. Shankar, "Data on land use and land cover changes in Adama Wereda, Ethiopia, on ETM+, TM and OLI-TIRS Landsat sensor using PCC and CDM techniques", Data in Brief, 24, 2019.

[15] Z. Szantoi, G.N. Geller, N.E. Tsendbazar, L. See, P. Griffiths, S. Fritz, P. Gong, M. Herold, B. Mora and A. Obregón, "Addressing the need for improved land cover map products for policy support", Environmental Science & Policy, 112, p. 28-35, 2020.

[16] S. Twisa and M.F.J.L. Buchroithner, "Land-use and land-cover (LULC) change detection in Wami river basin, Tanzania", Land, 8(9), p. 136, 2019.

[17] S. Nunez, J. Verboom and R. Alkemade, "Assessing land-based mitigation implications for biodiversity", Environmental Science & Policy, 106, p. 68-76, 2020.

[18] N.T. Huyen, L.H. Tu, N.D. Liem, V.N.Q. Tram, D.N. Minh and N.K. Loi, "Assessing impacts of land use and climate change on soil and water resources in the Srepok watershed, Central Highland of Vietnam", Policy Brief Series, p. 1-4, 2016.

[19] B.L. Turner II, W.B. Meyer and D.L. Skole, "Global Land use/Land-cover Change: Towards an Integrated Study", Ambio, 23, p. 91-95, 1994.

[20] P. Krajewski, I. Solecka and K. Mrozik, "Forest landscape change and preliminary study on its driving forces in Ślęża Landscape Park (Southwestern Poland) in 1883–2013", Sustainability, 10(12), p. 1-21, 2018.

[21] M.T.U. Rahman, F. Tabassum, M. Rasheduzzaman, H. Saba, L. Sarkar, J. Ferdous and A.Z. Islam, "Temporal dynamics of land use/land cover change and its prediction using CA-ANN model for southwestern coastal Bangladesh", Environmental Monitoring and Assessment, 189(11), p. 1-18, 2017.

[22] M. Rani, P. Kumar, P.C. Pandey, P.K. Srivastava, B.S. Chaudhary, V. Tomar and V.P. Mandal, "Multi-temporal NDVI and surface temperature analysis for Urban Heat Island inbuilt surrounding of sub-humid region: A case study of two geographical regions", Remote Sensing Applications: Society and Environment, 10, p. 163-172, 2018.

[23] M.J. Khan, M.M. Zeeshan and S.S. Ali, "GIS-based change detection of coastal features along Karachi coast Pakistan", Pakistan Journal of Science, 72(2), p. 124-133, 2020.

[24] M. Almazroui, A. Mashat, M.E. Assiri and M.J. Butt, "Application of Landsat data for urban growth monitoring in Jeddah", Earth Systems and Environment, 1(2), p. 1-11, 2017.

[25] R. Bhagyanagar, B.M. Kawal, G.S. Dwarakish, and S. Surathkal, "Land use/land cover change and urban expansion during 1983-2008 in the coastal area of Dakshina Kannada district, South India", Journal of Applied Remote Sensing, 6(1), p. 063576, 2012.

[26] Z. Zhang, S. Liu, J. Wei, J. Xu, W. Guo, W. Bao and Z. Jiang, "Mass change of glaciers in Muztag Ata–Kongur Tagh, Eastern Pamir, China from 1971/76 to 2013/14 as derived from remote sensing data", PloS One, 11(1), p. e0147327, 2016.

[27] Z. Khan, A. Saeed and M.H. Bazai, "Land use/land cover change detection and prediction using the CA-Markov model: A case study of Quetta city, Pakistan", Journal of Geography and Social Sciences, 2(2), p. 164-182, 2020.

[28] M.H. Bazai and S. Panezai, "Assessment of urban sprawl and land use change dynamics through GIS and remote sensing in Quetta, Balochistan, Pakistan", Journal of Geography and Social Sciences, 2(1), p. 31-50, 2020.

[29] M.A. Mahboob, I. Atif and J. Iqbal, "Remote sensing and GIS applications for assessment of urban sprawl in Karachi, Pakistan", Science Technology and Development, 34(3), p. 179-188, 2017.

[30] GOP, "District Layyah", Government of the Punjab, 2023, Available from: http://www.punjab.gov.pk/layyah (9 January, 2023).

[31] GOP, "District Census Report Layyah", 2017, Government of the Punjab, Available from: http://www.pbs.gov.pk/census-2017-district-wise/results/069 (9 January, 2023).

[32] M.S. Sajid, Z. Iqbal, M.N. Khan, G. Muhammad, G. Needham and M.K. Khan. "Prevalence, associated determinants, and in vivo chemotherapeutic control of hard ticks (Acari: Ixodidae) infesting domestic goats (Capra hircus) of lower Punjab, Pakistan", Parasitological Research, 108, p. 601-609, 2011.

[33] Q. Safder and U. Babar, "Assessment of Urbanization and Urban Sprawl Analysis through Remote Sensing and GIS: A Case Study of Faisalabad, Punjab Pakistan", International Journal of Academic Research in Business and Social Sciences, 9(4), p. 16-36, 2019.

[34] S. Talukdar, P. Singha, S. Mahato, Shahfahad, S. Pal, Y. Liou, and A. Rahman. "Land-Use Land-Cover Classification by Machine Learning Classifiers for Satellite Observations-A Review", Remote Sensing, 12, p. 1135, 2020.

[35] B. Kumari, M. Tayyab, H.T. Hang, M.F. Khan and A. Rahman, "Assessment of public open spaces (POS) and landscape quality based on per capita POS index in Delhi, India", SN Applied Sciences, 1(4), p. 1-13, 2019.

[36] R. Kharazmi, A. Tavili, M.R. Rahdari, L. Chaban, E. Panidi and J. Rodrigo-Comino, "Monitoring and assessment of seasonal land cover changes using remote sensing: A 30-year (1987–2016) case study of Hamoun Wetland, Iran", Environmental Monitoring and Assessment, 190(6), p. 1-23, 2018.

[37] M. Romaguera, R.G. Vaughan, J. Ettema, E. Izquierdo-Verdiguier, C.A. Hecker and F.D. Van der Meer, "Detecting geothermal anomalies and evaluating LST geothermal component by combining thermal remote sensing time series and land surface model data", Remote Sensing of Environment, 204, p. 534-552, 2018.

[38] Y. Liu, "Analysis of Four Change Detection Algorithms in Bi-Temporal Space with a Case Study", International Journal of Remote Sensing, 25(11), p. 2121-2139, 2004.

[39] D. Ameta, "Integration of Remote Sensing Data with Geographic Information System (GIS): Applications and Change Detection Techniques", International Journal of Managing Public Sector Information and Communication Technologies, 6(4), p. 15-24, 2015.

[40] A. Harris, A.S. Carr, and J. Dash, "Remote sensing of vegetation cover dynamics and resilience across southern Africa", International Journal of Applied Earth Observation and Geoinformation, 28, p. 131-139, 2014.

[41] G.T. Ayele, A.K. Tebeje, S.S. Demissie, M.A. Belete, M.A. Jemberrie, W.M. Teshome and E. Teshale, "Time series land cover mapping and change detection analysis using geographic information system and remote sensing, Northern Ethiopia", Air, Soil and Water Research, 11, p. 1178622117751603, 2018.

[42] C. Chew, R. Shah, C. Zuffada, G. Hajj, D. Masters and A.J. Mannucci, "Demonstrating soil moisture remote sensing with observations from the UK Tech DemoSat-1 satellite mission", Geophysical Research Letters, 43(7), p. 3317-3324, 2016.

[43] M.S. Saleem, S.R. Ahmad and M.A. Javed, "Impact assessment of urban development patterns on land surface temperature by using remote sensing techniques: a case study of Lahore, Faisalabad and Multan district", Environmental Science and Pollution Research, 27(32), p. 39865-39878, 2020.

[44] M. Aboelnour and B.A. Engel, "Application of remote sensing techniques and geographic information systems to analyze land surface temperature in response to land use/land cover change in Greater Cairo Region, Egypt", Journal of Geographic Information System, 10(1), p. 57-88, 2018.

[45] S.M. Malik, S. Arshad, A. Khan and O. Bilal, "Monitoring urban growth and land use changes using GIS and remote sensing: A case study of Tehsil Burewala", Journal of Himalayan Earth Sciences, 53(1), p. 140-152, 2020.

[46] A. Rehman, M. Mobeen, S. Bashir, M. Rauf, F. Ullaha, A. Aziz, T. Aziz and O. Riaz, "Impact of land use change on water quality of Jhang District", Journal of Biodiversity and Environmental Sciences, 13(6), p. 174-182, 2018.

[47] M. Waleed, M. Sajjad, A.O. Acheampong, and M.T. Alam, "Towards Sustainable and Livable Cities: Leveraging Remote Sensing, Machine Learning and Geo-Information Modelling to Explore and Predict Thermal Field Variance in Response to Urban Growth", Sustainability, 15, p. 1416, 2023.

[48] M. Sajid, M. Mohsin, T. Jamal, M. Mobeen, A. Rehman and A. Rafique, "Impact of Land-use Change on Agricultural Production & Accuracy Assessment through Confusion Matrix", International Journal of Innovations in Science & Technology, 04(01), p. 233-245, 2022.

[49] T.T. Vu and Y. Shen, "Land-Use and Land-Cover Changes in Dong Trieu District, Vietnam, during Past Two Decades and their Driving Forces", Land, 10, p. 798, 2021.

[50] A.A. Khan, S. Arshad and M. Mohsin, "Population Growth and Its Impact on Urban Expansion: A Case Study of Bahawalpur, Pakistan", Universal Journal of Geoscience, 2(8), p. 229-241, 2014.

[51] Y. Xie, M. Batty, and K. Zhao, "Simulating Emergent Urban Form Using Agent-Based Modeling: Desakota in the Suzhou-Wuxian Region in China", Annals of the Association of American Geographers, 97(3), p. 477-495, 2007.

[52] C. Homer, J. Dewitz, S. Jin, G. Xian, C. Costello, P. Danielson and K. Riitters, "Conterminous United States land cover change patterns 2001–2016 from the 2016 national land cover database", ISPRS Journal of Photogrammetry and Remote Sensing, 162, p. 184-199, 2020.

[53] S. Tiwari, C. Singh, S. Boudh, P.K. Rai, V.K. Gupta, and J.S. Singh, "Land use change: A key ecological disturbance declines soil microbial biomass in dry tropical uplands", Journal of Environmental Management, 242, p. 1-10, 2019.

[54] H. Long and Y. Qu, "Land use transitions and land management: A mutual feedback perspective", Land Use Policy, 74, p. 111-120, 2018.

[55] J. Cao, X. Zhang, R. Deo, Y. Gong and Q. Feng, "Influence of stand type and stand age on soil carbon storage in China's arid and semi-arid regions", Land Use Policy, 78, p. 258-265, 2018.

[56] D. Yan, R.L. Scott, D.J.P. Moore, J.A. Biederman and W.K. Smith, "Understanding the relationship between vegetation greenness and productivity across dryland ecosystems through the integration of PhenoCam, satellite, and eddy covariance data", Remote Sensing of Environment, 223, p. 50-62, 2019.

[57] A. Veldkamp and E.F. Lambin, "Predicting land-use change", Agriculture, Ecosystems and Environment, 85, p. 1-6, 2001.

[58] X. Fu, X. Wang and Y.J. Yang, "Deriving suitability factors for CA-Markov land use simulation model based on local historical data", Journal of Environmental Management, 206, p. 10-19, 2018.

[59] M. Jiao, M. Hu and B. Xia, "Spatiotemporal dynamic simulation of land-use and landscape-pattern in the Pearl River Delta, China", Sustainable Cities and Society, 49, 101581, p. 1-35, 2019.

[60] D. Choudhury, K. Das and A. Das, "Assessment of land use land cover changes and its impact on variations of land surface temperature in Asansol-Durgapur Development Region", The Egyptian Journal of Remote Sensing and Space Science, 22(2), p. 203-218, 2019.

[61] R.J. Corner, A.M. Dewan and S. Chakma, "Monitoring and prediction of land-use and land-cover (LULC) change", In: Dhaka Megacity, A. Dewan, and R. Corner (Eds.), pp. 75-97, Springer, Dordrecht, The Netherlands, DOI: 10.1007/978-94-007-6735-5_5, 2014.

The Nucleus ***60****, No. 1 (2023) 24-27*

www.thenucleuspak.org.pk

The Nucleus
ISSN 0029-5698 (Print)
ISSN 2306-6539 (Online)

Review of Different Models of Coastdown Transient in Pressurized Water Reactor

Idrees Ahmad, Shakeel Ahmad

Pakistan Institute of Engineering and Applied Sciences (PIEAS), P.O. Nilore, Islamabad, Pakistan

ABSTRACT

Problems related to the loss of coolant flow in nuclear reactor may initiate fuel meltdown and fuel-cladding interaction (FCI) due to the overheating of fuel and are therefore of great concern in power reactor safety. Therefore, licensee must provide evidence through rigorous analyses of all conceivable flow problems that plant's engineered safety systems (EES) have the capability to maintain fuel and cladding temperatures well below the melting point. Among the loss of flow events the flow coastdown transient is also a critical issue considered for the safety analysis of Pressurized Water Reactor (PWR), which is characterized by a sudden loss of power to the main reactor coolant pump (RCP). There has been a provision in RCP to maintain flow through reactor core for some time, immediately after the loss of power to pump, like in case of Station Blackout (SBO) due to the flywheel mechanism of RCP. However, that is inadequate for the extended times following the SBO and RCP must be powered by emergency diesel generators (EDGs) to maintain flow through the reactor core to remove heat from the fuel without any break. After the event of Fukushima, a lot of progress has been made to analyze situations, where the EDGs become inundated or unavailable. Analytical and empirical models have continuously been evolved to simulate the characteristics of pumps in such a crucial event to guide accident prevention and mitigation strategies. These models are divided into two broad categories like the short models and detailed models. The short models take into account the inertia of the flywheel, pump speed and the flow rate in core. The detail models also consider the pump characteristic curve on which homologous curves are derived and help to establish head and flow rate third degree polynomial. It has been observed that the detail models predict more accurate results in comparison with the experimental data. It has also been observed that the accuracy of the simulated results also relies on the inclusion of the pump mechanical friction losses in the model. Moreover, an attempt has been made to extend the coastdown transient analysis to predict the core outlet temperature during the course of the accident which requires an efficient solution strategy for solving models for the pump, coolant half time and the core time constant. In this article, evolution of different models has been discussed in detail.

Keywords: *Coastdown, Energy Ratio, Inertia flywheel, Transient Flow*

1. Review of Different Models

The coastdown transient is a highly sensitive issue as the pump head is no longer available owing to the loss of the off-site power. As a result, the reactor is scrammed, nevertheless, the heat generation in fuel continues due to decaying fission products. Additionally, a serious setback can be faced in case the diesel generators are unable to restore the power supply for keeping the coolant pumps in operation. Quantitatively, the decay heat piles up and approximately within one hour and reaches to 1.5% of the steady state power before its shutdown. Eventually, the fuel assemblies may disintegrate or at least experience bowing, cladding ballooning, etc. which cannot be ignored from safety perspective. So, the safety analysis of the nuclear reactor imposes the stringent requirement of having enough cooling ability to keep the fuel temperature below the specified limit. So, a lot of effort has been made for studying the coastdown transient because the fate of the core depends upon the inertia of the flywheel of the pump. Basically, coastdown transient models can be classified in two main categories, termed as the short models and detailed models. The simulation with the short models needs only design head, rated flow and moment of inertia. While the detail models consider the pump characteristic curve upon homologous curves are drawn and pump head and flow rate were calculated by fitting the third order polynomial to these homologous curves.

Analytical methods were the first to be developed for the establishing the characteristics of pump during operational transients. In these methods, mathematical models of varying complexity considering characteristics of energy, torques, friction of pump and associated components in the flow loops were suggested. First analytical method to study the behavior of pump during operational transients utilized the model for hydraulic characteristics of machine and pipeline and projected them on a single diagram[1]. The model was generalized to incorporate start-up transients as well as valves opening and closing by improving energy conservation considerations [2]. They also linked the accuracy of their method to the availability of components' steady state input data for the flow prediction[2]. Then, a dynamic model by combining the pump rotary parts and fluid in the connecting pipes for the coastdown event originating from the failure of the power appeared, in which the resulting equations were solved analytically for the rigid fluid columns and the elastic fluid columns. Also, the technique was extendable to simulate other abnormalities in the system[3]. The calculation of An analytical method to determine velocity of flow during a coastdown transient in a loop without the use of pump characteristic curves the for single-suction and double-suction centrifugal pumps was suggested [4]. While comparing the predictions of analytical method and experimental characteristics' curves, it was found that the effect of a mechanical friction loss on the flow rate was very small in the early stage of pump failure transient, and the time of two-third decay of the flow was not affected very much by the friction loss. However, this effect is larger in the later stage of the flow decay. Therefore, the time when the flow rate becomes zero, depends very much on the estimation of this loss [5].

With respect to nuclear power plant, a model considering the torque speed dependence to electric torque to predict primary coolant flow rate and the primary pump rotation speed for different transients was suggested [6]. The method

*Corresponding author: idrees@pieas.edu.pk

was applicable to simulate various scenarios like station blackout, pump startup and the valve opening installed on the pump discharge line.

Following the improving trend of envisioning of the accident scenario, a pragmatic model relying on the motor and the revolving parts of the pump was established [7]. However, model did not consider the electrical energy and therefore, no longer suitable for coastdown transient analysis. While analyzing the test data for the PWR at the Shipping port (Pa.) Power Station. (NSA 22: 33101), kinetic energy in pump rotor was found to be a significant parameter in determining the rate of flow during coastdown. Therefore, an empirical method for treating the transfer of energy from the pump rotor to the fluid was developed [8].

Another experimental validation study of a thermal-hydraulic model[9] revealed that in first half the simulated results were of higher side while the converse behavior was observed in the second half of the time-line of the coast down event. For having deep insight on the pump start-up related issues, the torque equation was solved adopting the detailed characteristic data of the pump[10]. A theoretical model [11] was developed by investigating the pump characteristic like flow rate, pump speed and rotational speed in a stopping period of the centrifugal pump experimentally. It was explored that, initially, the pressure rise coefficient is higher than the quasi-steady state coefficient and at the later stage the converse situation was observed. The main finding of this study was that the impulsive pressure and the lag in circulation formation around impeller vanes play predominant roles in the difference between dynamic and quasi-steady characteristics of turbo pumps. To address the safety related issues of nuclear power plant a simple method utilizing steady state governing equations of centrifugal pump characteristics was developed with the hypothesis that pump head is changing proportional to the square of the pump speed [12]. Despite the simplicity of his method, he successfully handled the highly fast startup issue of the pump and expanded its application to the pump stopping case. The method was successful as no big anomalies were reported in comparison with the experimental trends. Another experimental and theoretical study [13] on the stopping and starting periods of a centrifugal pump on a set-up having a small pipeline connected to discharge flange of the pump revealed that unsteady pump dynamic's characteristics considerably deviates from steady-state characteristics. The researchers also solved their numerical model by the method of characteristics.

In another study, dedicated to characterize the experimental facility ATLAS (Advanced Thermal–hydraulic test Loop for Accident Simulation)with reference to scaling and behavior of the pumps in single and two phase flow cases came up with the homologous curves in single phase in all quadrants [14]. While characterizing KALIMER-600 against coastdown accident, various influential factors such as the size of the flywheels, initiation of decay heat and peak temperature were considered to optimize the design with a coastdown time of 25 s for the safe end of the accident [15]. Furthermore, the investigation of the coastdown transient for a pool type Material Test Reactor (MTR) was carried out employing a mathematical model for kinetic energy of pump and in the piping system [16]. The results predicted by simulation have shown an excellent agreement to that of the experiments results. The worthwhile effort regarding coastdown transient has been made for Dayawan nuclear reactor which was a three loops nuclear power plant, where a simplified mathematical model was developed for solving flow rate transient and pump speed transient during flow coastdown period [17]. The quadruplicate polynomial curve equation was found to adequately simulate the flow-rate, rotate speed along with time for the analysis of station blackout accident at nuclear main pump [18]. The simulated strategy depends upon the total pressure drop relation, balanced momentum equation of the primary coolant, coolant pump momentum balance relation, pump half time, coolant half time and the energy ratio. The energy ratio which was foundation stone of their study depends upon pump half time and coolant half time and directly affect all pump parameters, such as the speed, non-dimensional flow rate, torque and head of the pump. They solved the resulting equations analytically for finding the transient flow rate and pump speed. From the comparison to the experimental data, it can be inferred that the calculated flow rate values agree well with the experimental values in the first half of the flow coastdown process. In the later-half of the experiment, the calculated values were over-estimated in comparison with the experimental data. The well-known reason is that of ignoring the mechanical friction loss of the coolant pump as the mechanical friction loss becomes dominate when the pump speed approaches to zero.

Similarly, a mathematical model of core thermal-hydraulics for the flow of coastdown transient has been developed for power as well as in the research reactor and compared results to the experimental results[19]. They also simulated the core temperature with simple heat transfer relation instead of solving the complex equations as programmed in popular transient simulating code (RELAP). The solution technique of their model incorporates parameters like, pump half time, the loop half time and the core time constant. The excellent agreement between experimental and simulated core temperature has been observed. Recall that such simulation methods are only suitable for case when there is no boiling in the core. Initially, the matching trend between experimental and the simulated results was better and after that the trend becomes wider that might be due to ignoring the mechanical friction in pump. The other reason might be the complete stoppage of the one coolant pump during the course of the accident.

The parameters of the primary coolant pump in the Jordan Research and Training Reactor (JRTR)were studied by using a software package, Modular Modeling System (MMS) and characteristics have been developed [20]. The loop coolant inertia effect was found to be small in the JRTR PCS loop, i.e., about one second increases in a coastdown half time required to halve the coolant flow rate. The coastdown half

time was found to linearly increase with the flywheel inertia, however remained within the safe limits of fuel integrity [21]. While studying the coastdown transient in the generation IV reactors ESPR–sodium cooled fast reactor, it was found that the Generation IV reactors have more safety as compared to their predecessors, as a tertiary loop has been added [22]. Briefly, the ESPR is as industrial type reactor having three cooling systems- primary secondary and tertiary systems. The primary system is composed of three primary coolant pumps, six decay heat removals, six intermediate heat exchanger. The secondary system has six intermediate loops comprised of one intermediate heat exchanger and six sodium/water heat exchangers. Then, the tertiary loops thirty-six separate loops. For simulation the coastdown transient, they used well known TRACE code and observed some discrepancy in their results and lack of inclusion of pump mechanical friction loss responsible for it.

The coastdown transient model in research and power reactors was extended to simulate the other core parameters such as the flow rate, temperature, pressure and departure from nucleate boiling ratio [23]. It is worth mentioning that no complicated equation like RELAP is solved and whole scenario is based upon the pressure drop relation and pump moment balance equation. It can be seen that with increasing time these parameters getting departure in comparison with experimental data. The reason might be the ignoring the pump mechanical friction loss like other models discussed earlier in the article. Then the coastdown transient was analyzed for a floating nuclear power plant by solving the complete pump speed modeling equation. A first-degree polynomial was fitted to measure the pump's internal part friction factor. The results for different energy ratios were presented for the flow rate and the speed of the pump [24]. It was suggested to include the a model for frictional torque in governing equations for minimizing discrepancies [12, 14, 16, 17, 19, 22, 23]. A quasi-steady state approach was introduced to simulate other parameters such pressure, temperature and DNBR and an excellent agreement with the experimental data was obtained. To qualify safety features of Super-Fast Reactors (Super FR), accident and transient's analyses were performed using validated computer codes SPRAT and SCRELA. For the partial loss of feed water, one of the reactor-coolant pumps trips with a coastdown time of 5 s, which leads to a decrease in the feed water flow rate by 50%. Signal of low flow rate (90%) is detected at the beginning, which leads to scram actuation. For the total loss of feed water flow accident, the scram signal is released at 0.5 s and the power rapidly decreases to the decay heat level in about 1 s. Scram actuation and/or auxiliary feed system actuation have been found effective to mitigate all abnormal transients in the Super FR [25, 27].

Additionally, a pump model for Sodium cooled fast reactor was solved using the TRACE code and argued to incorporate the friction factor in the model equations as well[22]. So, a novel method for the coastdown event by exploiting the pressure drop relation and pump movement balance equations was articulated [28]. In this approach the primary coolant flow and the pump speed governing equations were derived with the inclusion of frictional torque caused by the pump revolving part. Remember that the complete pump modeling equation was solved has the following form:

$$I\frac{d\omega}{dt} = \mathrm{M}_{em}(\omega) - \mathrm{M}_{h}(\omega) - \mathrm{M}_{f}(\omega)$$

where Mem(ω) stands for the electromagnetic torque and, $M_h(\omega)$ represents the hydraulic torque and $M_f(\omega)$ is for the friction torque. Moreover, $I\frac{d\omega}{dt}$represents the inertial torque of a rotor, I stands for the moment of inertia of the reactor coolant pump, ω is the angular velocity of the motor of the coolant pump respectively. It is worth mentioning that in the most of the previous studied the frictional torque of the pump is ignored which has shown a major flaw in the results of the previous studies, usually, in the latter half of the accident. But, in the study [28], the complete pump modeling equation is solved and the friction factor in the frictional torque is estimated with the second order polynomial and is derived using the concept of pump characteristics [29]. Resultantly, the key parameter, the effective energy ratio which interlinks the kinetic energies of the pump and of the primary coolant flow has become variable as the accident proceeds. The resulting method is applied to the Pakistan research reactor (PARR-1) and the Chashma-2 nuclear power plant (CHASNUPP-2) and plausible matching are found between experimental and theoretical results over longer time.

It is clear from [28] that the simulated results for the two pumps are showing off trend; the reason is that one pump has stopped during the course of the transients. Surprisingly, the results are for better that [12, 14, 16,17] because the visible off trend can be felt in latter half of the accident. Recall that the detail model is used for the present simulation.Similarly, the experimental study [30] to explore characteristics of coastdown transient following the loss of off-site power revealed that inertia of coolant pump should be high so that the speed of the pump and flow rate degrades slowly. This conclusion has been drawn by changing the inertia of the pump and seeing its effects of pump rotatory speed and the flow rate. In another study, a mathematical model of idling speed and flow characteristic curve of reactor coolant pump under the power failure condition was suggested and orthogonal optimization schemes was used with hydraulic modeling database of different vane structure parameters. The predictions from multiple linear regressions were compared with the experimental data [31].

Conclusion

Summarizing, the different simulated models can be divided into two types- the detail models and the short models. The detail models take into account all the pump parameters like pump speed modeling equation the pump characteristic curves and has the ability to predict results closer to the experimental data in comparison with short models. The close observation of the results of the different models has revealed that the Inertia of the Flywheel must be enough that the coolant pumps have ability to flood the core for the enough

period until the Generator System becomes in the full operation. Also, it has been observed that the most models ignore the friction torque and consequently that results are comparable to experimental data for the longer time. Additionally, some discrepancy in the results can be observed at the initial stage of the accident [12, 14, 16, 17, 19, 22, 23]. So the inclusion of the frictional torque and homologous curves are must for predicting the correctness of experimental data, [28]. Also, some of the coastdown transient models has the capacity to predict the core decay heat to the coolant [19, 23]. These models take into account the simple equations and utilize the different parameters like the pump half time, the core time constant, the coolant half time, surprisingly, simulated the core outlet temperature comparable to the experimental data.

References

[1] R.T. Knapp, "Complete characteristics of centrifugal pumps and their use in the prediction of transient behavior," Trans. ASME, pp. 683–689, 1937.

[2] A.J. Arker and D.G. Lewis, "Rapid flow transients in closed loops," in Reactor Heat Transfer Conference of 1956, pp. 33–47,1956.

[3] C.P. Kittredge and N.J. Princeton, "Hydraulic transients in centrifugal pump systems," Trans. ASME, vol. 78, no. 6, pp. 1307–1321, 1956.

[4] D. Burgreen, "Flow coastdown in a loop after pumping power cutoff," Nucl. Sci. Eng., vol. 6, no. 4, pp. 306–312, 1959.

[5] B.S. Givi, "A Model for Analyzing Flow Transients in a Single Closed Loop," in Fluids Engineering Division Summer Meeting, vol. 48401, pp. 591–597, 2008.

[6] G.M. Boyd Jr, R.M. Rosser, and B.B. Cardwell Jr, "Transient flow performance in a multiloop nuclear reactor system," Nucl. Sci. Eng., vol. 9, no. 4, pp. 442–454, 1961.

[7] T. Yokomura, "Flow coastdown in centrifugal pump systems," Nucl. Eng. Des., vol. 10, no. 2, pp. 250–258, 1969.

[8] G.M. Fuls, "FLOT-1: flow transient analysis of a pressurized water reactor during flow coastdown (LWBR Development Program)," Pittsburgh, 1968. [Online]. Available: https://www.osti.gov/biblio/6741552.

[9] Y. Takada, T. Yokomura, and A. Kurosawa, "Thermo-hydraulic model test of the first nuclear ship reactor in Japan," Nucl. Eng. Des., vol. 10, no. 2, pp. 126–147, 1969.

[10] R.B. Grover and S.M. Koranne, "Analysis of pump start-up transients," Nucl. Eng. Des., vol. 67, no. 1, pp. 137–141, 1981.

[11] H. Tsukamoto, S. Matsunaga, H. Yoneda, and S. Hata, "Transient characteristics of a centrifugal pump during stopping period," 1986.

[12] Rizwanuddin, "Steady-state characteristics based model for centrifugal pump transient analysis," Ann. Nucl. Energy, vol. 21, no. 5, pp. 321–324, 1994.

[13] P. Thanapandi and R. Prasad, "Centrifugal pump transient characteristics and analysis using the method of characteristics," Int. J. Mech. Sci., vol. 37, no. 1, pp. 77–89, 1995.

[14] K.Y. Choi, Y.S. Kim, S.J. Yi, and W.P. Baek, "Development of a pump performance model for an integral effect test facility," Nucl. Eng. Des., vol. 238, no. 10, pp. 2614–2623, 2008.

[15] J.W. Han, T.H. Lee, J.H. Eoh, and S.O. Kim, "Investigation into the effects of a coastdown flow on the characteristics of early stage cooling of the reactor pool in KALIMER-600," Ann. Nucl. Energy, vol. 36, no. 9, pp. 1325–1332, 2009.

[16] K. Farhadi, "Analysis of flow coastdown for an MTR-pool type research reactor," Prog. Nucl. Energy, vol. 52, no. 6, pp. 573–579, 2010.

[17] H. Gao, F. Gao, X. Zhao, J. Chen, and X. Cao, "Transient flow analysis in reactor coolant pump systems during flow coastdown period," Nucl. Eng. Des., vol. 241, no. 2, pp. 509–514, 2011.

[18] L. Xiajie, W. Dezhong, Z. Jige, L. Junsheng, and Y. Zhe, "Test study on safety features of station blackout accident for nuclear main pump," At. Energy Sci. Technol., vol. 43, 2009.

[19] I. Ahmad, M. Ilyas, and Z. Akram, "Pressurized water reactor core thermal-hydraulics model for flow coastdown transient," Proc. Inst. Mech. Eng. Part A J. Power Energy, vol. 228, no. 5, pp. 592–599, 2014.

[20] Y. Alatrash, H. Kang, H. Yoon, K. Seo, D.Y. Chi, and J. Yoon, "Experimental and analytical investigations of primary coolant pump coastdown phenomena for the Jordan Research and Training Reactor," Nucl. Eng. Des., vol. 286, pp. 60–66, 2015.

[21] Y.M. Alatrash, H. Kang, H. Yoon, S. Zhang, and J. Yoon, "Analyses for primary coolant pump coastdown phenomena for Jordan Research and Training Reactor," in International Conference on Nuclear Thermal Hydraulics and Safety, pp. 27–28, 2014.

[22] J.O. Ródenas, A.L. Chueca, and S.M. Alsina, "Pumps modelling of a sodium fast reactor design and analysis of hydrodynamic behavior," EPJ Nucl. Sci. and Technol., vol. 2, p. 38, 2016.

[23] I. Ahmad, S. Arshad, S. Tahir, Q. Nadeem, and A. Samee, "An improved core thermal-hydraulic model for coastdown transient in pressurized water reactor," Proc. Inst. Mech. Eng. Part A J. Power Energy, vol. 232, no. 4, pp. 416–424, 2018.

[24] W. Li, L. Yu, and T. Yuan, "Modeling Study on the Centrifugal Pump for a Floating Nuclear Power Plant," in IOP Conference Series: Earth and Environmental Science, vol. 252, no. 3, pp. 32215, 2019.

[25] S. Sutanto and Y. Oka, "Safety Analysis of a Super-Fast Reactor with Single Flow Pass Core," Transactions, vol. 109, no. 1, pp. 1092–1094, 2013.

[26] Y. Oka et al., "Accidents and transients analyses of a super-fast reactor with single flow pass core," Nucl. Eng. Des., vol. 273, pp. 165–174, 2014.

[27] H. Li, Y. Oka, and Y. Ishiwatari, "Safety analysis of a supercritical water cooled fast reactor with all-upward two-pass flow," Ann. Nucl. Energy, vol. 59, pp. 1–9, 2013.

[28] S. Khalid, I. Ahmad, and A. Zahur, "Highly Accurate Method for the Solution of Flow Coastdown in Pressurized Water Reactor," Nucl. Technol., 2019.

[29] E.E. Lewis, Nuclear power reactor safety. New York: John Wiley & Sons. Inc., 1977.

[30] W. Xiuli, X. Wei, W. Hongliang, Z.R. Sheng, Z.Y. Yuan, and Z.H. Zhou, "An Experimental Study on Transient Characteristics of a Nuclear Reactor Coolant Pump in Coast-Down Process Under Power Failure Condition," Front. Energy Res., vol. 8, pp. 234, 2020, doi: 10.3389/fenrg.2020.579291.

[31] X. Wang et al., "Mathematical Modelling Forecast on the Idling Transient Characteristic of Reactor Coolant Pump," Processes, vol. 7, no.7, pp. 452, 2019.

The Nucleus ***60***, *No. 1 (2023) 28-34*

www.thenucleuspak.org.pk

The Nucleus

ISSN 0029-5698 (Print)
ISSN 2306-6539 (Online)

Some Historical Briefs and Outlooks of the Chemical and Biological Acid Leaching of Uranium Ores

Tariq M. Bhatti*, Olli H. Tuovinen

Department of Microbiology, Ohio State University, Columbus, OH 43210, U.S.A

ABSTRACT

The purpose of this paper is to briefly review early developments in the chemical and biological acid leaching of uranium ores in Portugal, Canada, Sweden, Finland, Estonia, and Pakistan. Uranium exists in tetravalent (U(IV)) and hexavalent (U(VI)) oxidation states in igneous, metamorphic, and sedimentary mineral deposits. Acidic ferric sulfate is a chemical oxidant of tetravalent uranium and is reqenerated from ferrous iron in the leachate and produced also from pyrite (FeS_2, cubic), marcasite (FeS_2, orthorhombic), greigite (Fe_3S_4) and pyrrhotite ($Fe_{1-x}S$) by acidophilic Fe- and S-oxidizing bacteria and archaea. The hexavalent uranium is soluble in sulfuric acid solution (lixiviant) and is recovered in downstream hydrometallurgical processing to produce a concentrate (yellowcake). The acid bioleaching reactions are optimal at pH 1.5-3 as the low pH facilitates proton attack on minerals and alleviates the precipitation of metals in the leachate and on mineral surfaces. Uranium is extracted from ores on a commercial scale using heap, dump, and stope leaching processes. In some operations other metals can also be recovered as byproducts in the process.

Keywords: *Acid leaching, Acidophilic Microbes, Bioleaching, Pyrite Oxidation, Uranium Leaching*

1. Introduction

Uranium deposits occur in igneous, metamorphic and sedimentary rock types are widespread, with the largest deposits found in Australia, Kazakhstan and Canada [1-3]. To date, the largest high-grade uranium deposits containing 13.88%-15.92% U_3O_8 occur in the Athabasca Basin of northern Saskatchewan, Canada (Cigar Lake) [4, 5]. Uranium ore deposits are generally classified into 15 main categories of deposit types, each with multiple subtypes, according to their geological setting and genesis of mineralization and arranged by to their approximate economic significance [6]. About 40% of the uranium reserves are in sandstone type uranium ore deposits [7]. Almost 300 uranium minerals have been identified in the form of halides, oxides, carbonates, sulfates, phosphates, arsenates, vanadates, and silicates [8, 9]. Uranium also exists in organic complexes such as thucholite and uranyl oxalate minerals uroxcite and metauroxcite [10]. Some major and minor uranium-producing countries are presently Australia, Canada, China, India, Kazakhstan, Namibia, Nigeria, Pakistan, Russia, South Africa, Ukraine, United States and Uzbekistan [1]. According to the World Nuclear Association, the top four uranium producers in the world in 2021 ranked Kazakhstan, Namibia, Canada, and Australia.

Uranium can be extracted from ores with sulfuric acid (H_2SO_4) or carbonate solution ($NaHCO_3$, Na_2CO_3, NH_4HCO_3, $(NH_4)_2CO_3$, K_2CO_3, $KHCO_3$). Biological leach solutions with acidophilic iron- and sulfur-oxidizing autotrophs can also be used for the extraction of uranium from ores. In the leaching process, uranyl ion (UO_2^{2+}) forms soluble sulfate ($UO_2(SO_4)_3^{4-}$) or carbonate ($UO_2(CO_3)_3^{4-}$) complexes. The role of acidophilic iron- and sulfur-oxidizing mesophiles and thermophiles, archaea, and iron-oxidizing heterotrophs in the bioleaching of uranium ores is well documented and reviewed in the literature [11-15]. In the bioleaching process, dilute sulfuric acid is the leach solution promoting proton attack and ferric iron is the oxidizing agent. If uranium is initially present in the insoluble tetravalent state (U(IV)) in the ore, Fe^{3+} in sulfuric acid solution oxidizes it to U(VI), dissolving it as soluble UO_2^{2+}. Fe^{3+} is reduced to Fe^{2+} in this redox reaction and is re-oxidized by iron- and sulfur-oxidizing acidophilic bacteria and archaea [16-18]. An example of a flow sheet diagram of the bioleaching of uranium is shown in Fig. 1.

Depending on the specific grade and mineralogy of the ore body, the use of acidophilic iron- and sulfur-oxidizing bacteria in the industrial-scale extraction of uranium from ores containing pyrite and/or other sulfide minerals may be a feasible, alternative approach to the chemical hydrometallurgical process technology. Heap and dump leaching processes are technically feasible for bioleach operations, whereas the bioleaching of uranium is not practiced in stirred tank processes in commercial scale. The technology is particularly applicable to low-grade uranium ores (≤0.042% U), which contain pyrite or other sulfide minerals. The leaching process may be amended with pyrite or sulfur for the acidophilic iron- and sulfur-oxidizing bacteria to provide for oxidation and acid capacity of the leach solution [19, 20].

Many countries have had research groups working on uranium bioleaching projects using bench-scale, pilot-scale, and commercial-scale techniques with varying successes. These projects were primarily evaluating uranium leaching yields with changes in physical and chemical experimental conditions. The underlying microbiology of the leaching process was relatively poorly understood in the 1950's-1960's. Key enzymes, taxonomic and phylogenetic diversity, and molecular biological analysis of microbial cultures were practically unknown in the first 15-20 years of the emerging bioleaching technology. The domain Archaea was not discovered until 1977 [21]. The fundamental discovery and

*Corresponding author: tariqbcgp@gmail.com

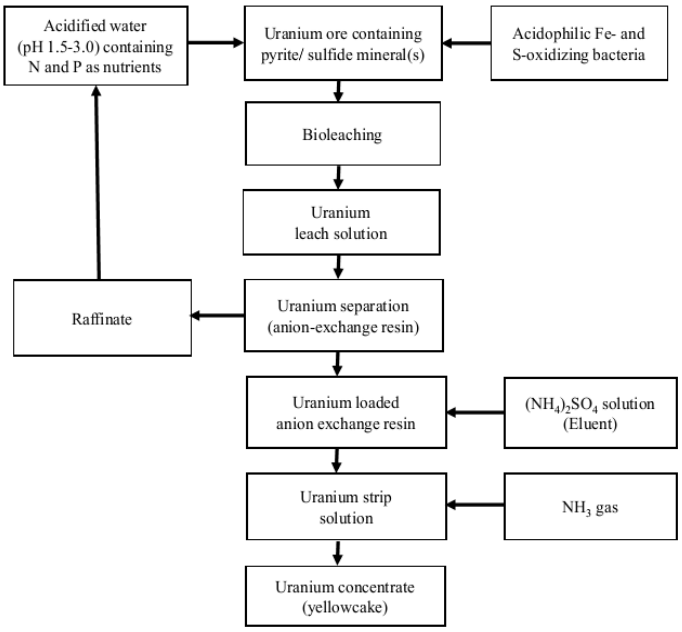

Fig. 1: An example of a flow sheet diagram showing bioleaching of uranium from ore to produce uranium concentrate (yellowcake).

emergence of molecular biology and omics have led in subsequent years to information on acidophilic thermophiles that are potentially useful in bioleaching processes at elevated temperatures.

The purpose of this paper is to review brief historical aspects, starting in the 1950's, of the chemical and biological leaching of uranium from ores in several countries including Pakistan. The history of the acid bioleaching of uranium coincides with R&D in the bioleaching of sulfidic ores for the extraction of copper, which was subsequently expanded to nickel, cobalt, and zinc. One driving force in boosting uranium extraction from ores in the 1950's-1960's especially and gradually ebbing through 1990, was the Cold War and stockpiling of nuclear weapons for nuclear deterrence. Uranium is now mostly used as fuel for nuclear power plants and nuclear reactors in naval vessels and as a source of isotopes in medicine, many industrial processes, and military purposes. The non-fissile U-238 isotope with a >99% relative abundance is the most common in nature.

Portugal

Early advances in the bioleaching of uranium ores date back to the 1950's. It was reported that the Urgeiriça uranium ore-processing plant in Portugal was not achieving the expected yield of uranium from the ore stockpiles [22]. The discrepancy in terms of the loss of uranium was eventually attributed to substantial leaching of uranium caused by rainwater. Subsequently, it was discovered that uranium dissolution from the ore was catalyzed by acidophilic Fe- and S-oxidizing autotrophs [23]. The Urgeiriça uranium ore contained, on average, 5% pyrite, which was oxidized by bacteria to acidic ferric sulfate lixiviant. In the 1950's, some studies on uranium bioleaching processes were initially directed towards preventing dissolution of uranium from ore, but it soon became apparent that this process could be applied to extract uranium from low-grade ores. In 1952-1953, a heap leaching process was started for the recovery of uranium on commercial scale at the Urgeiriça plant site. The Urgeiriça is one of the early milestones in the bioleaching of uranium ores [24]. Multiple small mines were active in mining uranium ores through 1962. In subsequent years, uranium mining did not employ specifically designed bioleaching processes with native bacteria, but heap leaching was practiced for low-grade ores [24]. Uranium mining in Portugal ceased in 2001.

Canada

In the 1960's, bioleaching processes were applied for commercial scale uranium extraction by heap, dump, and stope-leaching of mine waste rocks and worked-out stopes in uranium mines in the Elliot Lake area, Ontario, Canada [25-27]. The uranium mine waters containing acidic ferric sulfate were circulated through surface heaps and underground-stopes [28, 29]. Some mines leached uranium by hosing down roofs, walls, and floors of mine stopes at intervals of several months, because supporting underground structures could not be safely mined via conventional processing. Other left-behind uranium ore materials and waste piles were also treated with mine waters at acidic pH 2-3, yielding dissolved uranium at concentrations that were economically recoverable by using a strong basic anion ion-exchange resin [Amberlite IRA-400 (OH^-)].

The Agnew Lake Mine (Ontario) was the first operation where uranium bioleaching process was applied to a virgin orebody. Full-scale operation at the Agnew Lake Mine was launched in 1976 [30]. In the first year of stope leaching operations, the mine shafts and chambers were fill with the leachate. The underground and stope leaching works were discontinued in 1980 as fractures in the orebody failed to prevent the loss of leach solution. The surface heap bioleaching continued until 1985 [31]. Tailings in some

uranium mines contain light and heavy rare earth elements in addition to other metals. In recent years, this has prompted interest in recovering rare earth elements from tailings by acid and bacterial leaching in abandoned or inactive uranium mines [32, 33]. In some mines, for example, yttrium could also be recovered as by-product from the raffinate solutions, which further improves the overall process economics.

Sweden

In Sweden, the alum-shale fields in the southern part are among the largest uranium-containing shale deposits in the world. Uranium ore from the alum-shale orebody was processed in the Ranstad mine during 1965-1969 [34]. The process was based on the leaching of uranium with sulfuric acid, yielding about 182 t U [35]. Weathering of the ore outdoors for weeks before the leaching process decreased the pyrite content and increased the subsequent yield of uranium by about 10%, but addition of bacteria was not tested in the process. Bacterial leaching of uranium from the alum-shale was tentatively tested in a laboratory-scale [36], but the research did not proceed to further experiments or optimization. After the mine closure, the site was eventually reclaimed, but analyses of drainage from pyritic materials at the site have shown acidic, sulfate-rich drainage, Fe(III) precipitation, and dissolved metals [37].

Bhatti [38] reported that 68-76% yield of U was obtained in stirred tank leaching of samples of black shale from the Kyrk Tåsjö deposit in central Sweden using mixed cultures of Fe- and S-oxidizing bacteria with 15-20 days of contact time. Uranium is also associated with the organic-rich fraction of the shale. Kalinowsky et al. [39] showed that uranium is dissolved from alum shale in *Pseudomonas* cultures. This was attributed to uranium sequestration with pyoverdine (a *Pseudomonas* protein) as well as microbial decomposition of the organic fraction of the shale, thus causing uranium dissolution.

In 1976, the Swedish government announced that uranium mining and production in large-scale were not compatible with Sweden's nuclear policy, thus causing major shifts in uranium exploration and processing. Uranium mining in Sweden was banned in August 2018, with consequent financial losses of pending and planned uranium mining projects. There has been continuing commercial interest in exploring Swedish uranium-containing shale deposits [40], presumably for metals such as nickel and rare earth elements for which there is a high global demand. Uranium-rich alum shales (0.005-0.04% U) occur in Skåne, Västergötland, Östergötland, Öland, Närke and along the Swedish mountain range [41, 42]. In Häggån, for example, the large black shale uranium field in central Sweden is claimed to be the second largest undeveloped uranium resource in the world, also containing Mo, Ni, V and Zn [43, 44].

Finland

In Finland, uranium was produced in 1958-1961 in pilot-scale in the Paukkajanvaara mine (North Karelia) using sulfuric acid as the lixiviant [45]. A total of 40,000 t ore was excavated yielding about 30 t U before the uranium rich section was depleted. The process was not designed for native bacteria to accelerate the leaching. Thirty years later, the mine site was reclaimed, and field research revealed typical acid mine drainage at the mine site, evidence for microbial oxidation of residual Fe-sulfides exposed to humidity, rainwater, and air and the site has an established microbial community [46]. Reconnaissance and environmental sampling have been implemented to monitor the release of radionuclides and base metals from the mine site [47-49].

In 2007, the Terrafame Ltd. (called Talvivaara Ltd. at that time) mining company started a bioheap leaching process to recover Ni, Co, Cu, and Zn from a black schist ore in the Kainuu region [50-53]. Since then, in the intervening years, the company secured a permit to also recover uranium from the leach solution cycle. Terrafame Ltd. is now in the process of optimizing uranium recovery for full-scale operation (200 t U/year) in 2024 from the leach solution cycle at the mine site (www.terrafame.com). Uranium recovery is additional to the Ni, Zn, Cu, and Co concentrates already produced in the bioheap leaching operation. The plan is to initiate uranium production alongside the production of other metals throughout the operating period, which covers at least the next 30 years. The black schist mineralization contains about 0.0017% U, some of it as thucholite. The grade is not sufficient to be classified as uranium ore, nor could it economically support uranium mining as the sole product. The bioheap plant is in the boreal climate with snow cover during the winter, but the winter and snow have little effect on the microbial activity in the interior zones of the heaps due to intense exothermic oxidation of sulfide minerals.

Estonia

In Estonia, the Sillamäe metallurgical plant processed uranium ores for the Soviet nuclear program, starting in the mid-1940's. Sillamäe is on the southern coast of the Gulf of Finland, at the mouth of the Sõtke River. The history of the uranium plant processing graptolite-argillite ore has been reviewed by Lippmaa and Maremäe [54-56] and Hade and Soesoo [57]. The plant also processed uranium ores shipped from eastern and central European countries until 1977. In 1960-1963 the Sillamäe plant tested the bacterial leaching of uranium from graptolite-argillite ore in open air heaps and a large outdoor 2,000-ton concrete percolator reactor as well as in wooden percolators with shelves over 23 months. The yields of uranium leaching decreased with increasing particle size: 55% U with 25 mm and 33% with 50 mm material. For reference, 1% leaching of uranium was noted with 100-200 mm lumps over 18 months [54, 58, 59]. No follow-up test work on the bacterial leaching was announced. The plant subsequently tested the pressure leaching of uranium, but the results did not justify uranium processing in commercial scale and the funding was finally discontinued in 1973. The graptolite-argillite mineralization in northern Estonia is a potential resource of many metals in addition to uranium [60, 61]. Anaerobic decomposition of organometallic complexes can also release some metals in the solution phase [62, 63].

The metals in the shales are, however, of low grades and commercial processing with conventional hydrometallurgy or bioleaching is presently not economically feasible.

Pakistan

In Pakistan, polymetallic black shale deposits represent potential uranium reserves. For example, uranium deposits in Pakistan have been summarized by Butt [64], Mansoor [65] and Akhtar et al. [66]. Shake flasks bioleaching experiments with a mixed culture of Fe- and S-oxidizing bacteria performed at 50% pulp density of a black shale sample containing 0.0042% U solubilized 76-80% U in 30 days of contact time [67]. Uranium dissolution from the shale was mainly attributed to Fe^{3+}, >500 mV redox potential, and low pH 1.5-1.9 in the leach solution. Uranium from the Baghalchur low-grade sandstone ore (0.023% U) amended with elemental sulfur and/or sulfur mud was leached by acidophilic autotrophs in shake flasks, columns, and small pilot-scale bioheap studies [68, 69]. Bacterial oxidation of sulfur generated sulfuric acid as lixiviant for uranium solubilization from the sandstone ore.

Reddish-brown Fe(III)-precipitates collected from the water channels of the bed-rock seepage in the black shale formation of Chamiari (Ghazi Tarbela) and Kala Katha area of District Haripur, Khyber Pakhtunkhwa (Pakistan) are shown in Fig. 2. Such precipitates are attributed to the microbiological iron and pyrite oxidation in black shales, with subsequent ferric iron precipitation as Fe(III)-hydroxysulfates. The precipitates are mixed jarosite types (solid solutions of jarosite) and schwertmannite. Fe(III)-precipitates sequester and retain dissolved uranium from mine drainage, shown as an example in the chemical analysis in Table 1. The mechanism of uranium sorption by iron precipitates is not clear.

Table 1: Uranium content of iron precipitates collected from the seepage channels of black shale bedrock in Chamiari (Ghazi, Tarbela), Khyber Pakhtunkhwa (Pakistan). All samples were reddish-brown Fe(III)-hydroxysulfate precipitates (unpublished data, T.M. Bhatti).

Sample No.	Description of sample	U content (ppm)
SW-1	Water channel	13
SW-2	Seepage of shale bed rock	109
CHW-2	Seepage of shale bed rock	9
CHW-3	Seepage of shale bed rock	46

Pakistan has reserves of uranium mineral resources locked up in black shales and sandstone type deposits. Uraniferous black shales are widely distributed in the Precambrian sediments in Khyber Pakhtunkhwa Province and adjoining areas of Azad Jammu and Kashmir [70-72]. The black shales contain abundant organic matter (kerogen), disseminated fresh, tiny, and large crystals of pyrite (7-10%) and U, Ni, V, Zn, and rare earth elements. The black shales in the Manki Formation, Ghandgarh Range, near Ghazi-Tarbela (Khyber Pakhtunkhwa) contain on average 0.0042-0.006% U [73].

Fig. 2: Acid mine drainage representing bacterial oxidation of pyrite and sulfide minerals in the black shale formation of Chamiari (Ghazi Tarbela) and Kala Katha, Khyber Pakhtunkhwa (Pakistan). The arrows point at the formation of red-brownish Fe(III)-precipitation in the mine drainage.

In general, shale deposits are considered as polymetallic with variable content of pyrite and other sulfide minerals, sometimes also carbonate nodules or layers. Some mineralizations are enriched in Ag, Mo, Zn, Ni, Cu, Cr, V and less commonly Co, Se, and U [41, 43, 44, 74]. The weathering causes changes in the elemental and mineralogical composition in black shale deposits and leads to elevated concentrations of metals and sulfates in surface water and stream sediments. Metal-bearing minerals and metals are interspersed in the organic fraction in the shale-matrix. Based on the weathered bedrock/soil profiles, disintegration is initiated with the oxidation of pyrite and organic matter, which increase the overall porosity and water penetration. Prolonged exposure of black shales and coal-seams to rainwater, humidity, and air promotes the oxidation of pyrite and other Fe-sulfides to elemental S, thiosulfate, polythionates and sulfates, typically mediated by native acidophilic iron- and sulfur-oxidizing bacteria in sulfidic mine sites.

Conclusion

Since the initial uranium bioleaching studies in the early 1950's, applications of acidophilic microbes for recovering uranium from various minerals, ores and rocks have been tested in several countries. Historically, the Cold War boosted the uranium production often without regard to environmental safeguards, and the environmental and human health legacies of this era are still apparent in many inactive and abandoned mine sites worldwide. Major advances have been made in the understanding of the kinetics of bacterial activities and leaching reactions as well as electrochemical basis of mineral dissolution. Indigenous bacteria and their communities in uranium mine sites have been characterized and new species have been discovered. The flux of molecular and genetic knowledge of microbial biochemistry and physiology has discovered insights on microbe-mineral interactions and regulatory mechanisms underlying microbial responses for example to dissolved metals and other stress and inhibitory factors, permissive temperature ranges, substrates, nutrients, and microbial population dynamics. Such biological parameters affect bacterial efficacy in the leaching process and are targets for optimization with fine tuning for specific ore or rock types. Mineral composition and galvanic coupling, particle size distribution, pulp density, aeration, and ore/rock permeability are some examples of the physical parameters that must be considered for engineering design in the leaching process. The bioleaching-based technology is particularly suited for low-grade uranium ores, which are economically marginal or otherwise difficult to process by conventional hydrometallurgy. Scientific discoveries, R&D priorities, collaborations, and economic incentives to further the biotechnology of mineral processing are regularly discussed in the biennial International Biohydrometallurgy Symposium (IBS) series. This is an international forum and meeting place for scientists and other specialists as well as the industry representatives with wide backgrounds to address critical issues in the mineral biotechnology. Similarly, the European Union has sponsored international programs such as BIOSHALE, BIOMINE, and BIOMOre, which have promoted collaborative problem-solving, troubleshooting, and research efforts. Bioleaching technology requires inputs from many disciplines, requiring cooperation, training, and funding as well as skilled scientists and engineers collaborating with the mining industry.

References

[1] Hore-Lacy, I. (Ed.), "Uranium for Nuclear Power: Resources, Mining and Transformation to Fuel," Elsevier, Amsterdam, 2006.

[2] F.J. Dahlkamp, "Uranium Ore Deposits," First Edition, Springer-Verlag, Berlin Heidelberg, New York, 1993.

[3] International Atomic Energy Agency, "Geological Classification of Uranium Deposits and Description of Selected Examples," IAEA-TECDOC-1842, Vienna, Austria, 2018.

[4] P. Bruneton, "Geological environment of the Cigar Lake uranium deposit," Canadian Journal of Earth Sciences, vol. 30, no. 1, pp. 653-673, 1993.

[5] M. Fayek, J. Janeczek, and R.C. Ewing, "Mineral chemistry and oxygen isotopic analyses of uraninite, pitchblende and uranium alteration minerals from the Cigar Lake deposit, Saskatchewan, Canada," Applied Geochemistry, vol. 12, no. 5, pp. 549-565, 1997.

[6] P. Bruneton, and M. Cuney, "Geology of uranium deposits," In: Hore-Lacy, I. (ed.), Uranium for Nuclear Power: Resources, Mining and Transformation to Fuel, Elsevier, Amsterdam, pp. 11-52, 2006.

[7] W.A. Gow, "Recent advances in uranium ore processing," In: Advances in Uranium Ore Processing and Recovery from Non-Conventional Resources, Proceedings of a Technical Committee Meeting, Vienna, 26-29 September 1983", IAEA-TC-491/1, 3-12, 1985.

[8] International Atomic Energy Agency, "Descriptive Uranium Deposit and Mineral System Models," IAEAL 20-01322 Vienna, Austria, 2020.

[9] R.G. Skirrow, S. Jaireth, D.L. Huston, E.N. Bastrakov, A. Schofield, S.E. van der Wielen, and A.C. Barnicoat, "Uranium Mineral Systems: Processes, exploration criteria and a new deposit framework," GeoCat # 69124, Record 2009/20, Geoscience Australia, Australian Government, 2009.

[10] A.R. Kampf, J. Plášil, B.P. Nash, I. Němec, and J. Mart, "Uroxite and metauroxite, the first two uranyl-oxalate minerals," Mineralogical Magazine, vol. 84, no. 1, pp. 131-141, 2020.

[11] A.H. Kaksonen, A.M. Lakaniemi, and O.H. Tuovinen,"Acid and ferric sulfate bioleaching of uranium ores: a review," Journal of Cleaner Production, vol. 264, 121586, 2020.

[12] Q. Li, Y. Yang, J. Ma, J. Sun, G. Li, R. Zhang, Z. Cui, T. Li, and X. Liu, "Sulfur enhancement effects for uranium bioleaching in column reactors from a refractory uranium ore," Frontiers in Microbiology, vol. 14, 110764, 2023

[13] N. Reynier, R. Gagné-Turcotte, L. Coudert, S. Costis, R. Cameron, and J.F. Blais, "Bioleaching of uranium tailings as secondary sources for rare earth elements production," Minerals, vol. 11, 302, 2021.

[14] X. Wang, Y. Liu, Z. Sun, J. Li, L. Chai, X. Min, Y. Guo, P. Li, and Z. Zhou, "Heap bioleaching of uranium from low-grade granite-type ore by mixed acidophilic microbes," Journal of Radioanalytical and Nuclear Chemistry, vol. 314, pp. 251-258, 2017.

[15] Abhilash, and B.D. Pandey, "Microbially assisted leaching of uranium - a review," Mineral Processing and Extractive Metallurgical Review, vol. 34, no. 2, pp. 81-113, 2013.

[16] A. Mahmoud, P. Cézac, A.F.A. Hoadley, F. Contamine, and P. D'Hugues, "A review of sulfide minerals microbially assisted leaching in stirred tank reactors," International Biodeterioration and Biodegradation, vol. 119, pp. 118-146, 2017.

[17] Abhilash, K.D. Mehta, V. Kumar, B.D. Pandey, and P.K. Tamrakar, "Bioleaching - an alternate uranium ore processing technology for India," Energy Procedia, vol. 7, pp. 158-162, 2011.

[18] O.H. Tuovinen, and T.M. Bhatti, "Microbiological leaching of uranium ores," Minerals and Metallurgical Processing, vol. 16, no. 4, pp. 51-60, 1999.

[19] H. Hamidian, "Microbial leaching of uranium ore," In: Tsvetkov, P. (Ed.), Nuclear Power – Deployment, Operation and Sustainability, InTech, Rijeka, Croatia, pp. 291-304, 2012.

[20] Abhilash, and B.D. Pandey, "Microbiological extraction of uranium from ores," In: Abhilash, Pandey, B.D., and Natarajan, K.A. (eds.), Microbiology for Minerals, Metals, Materials and the Environment, CRC Press, Boca Raton, pp. 59-98, 2015.

[21] C.R. Woese, and G.E. Fox, "Phylogenetic structure of the prokaryotic domain: The primary kingdoms," Proceedings of National Academy of Sciences of the United States of America, vol. 74, no. 11, pp. 5088-5090, 1977.

[22] J. Cameron, "Natural leaching of uranium ores," Transactions of the Institution of Mining and Metallurgy, vol. 72, No. 7, pp. 513-515, 1963.

[23] R.T. Lowson, "Bacterial leaching of uranium ores – a review," Technical Report No. AAEC/E356, Australian Atomic Energy Commission, Lucas Heights, NSW, Australia, 1975.

[24] R. Pereira, S. Barbosa, and F.P. Carval, "Uranium mining in Portugal: a review of the environmental legacies of the largest mines and environmental and human health impacts," Environmental Geochemistry and Health, vol. 36, pp. 285-301, 2014.

[25] R.A. MacGregor, "Recovery of U_3O_8 by underground leaching," Canadian Institute of Mining Bulletin, vol. 59, no. 649, pp. 583-587, 1966.

[26] D. Wadden, and A. Gallant, "The in-place leaching of uranium at Denison Mines," Canadian Metallurgy Quarterly, vol. 24, pp. 127-134, 1985.

[27] A. Marchbank, "Update on uranium leaching at Denison mines," In: McCready, R.G.L. (ed.), Proceedings of the 4th Annual General Meeting of CANMET, CANMET Special Publication No. SP87-10, Canadian Government Publication Centre, Ottawa, pp. 3-18, 1987.

[28] J.R. Fisher, "Bacterial leaching of Elliot Lake uranium ore," Canadian Mining and Metallurgical Bulletin, vol. 59, pp. 588-592, 1966.

[29] V.F. Harrison, W.A. Gow, and K.C. Ivarson, "Leaching of uranium from Elliot Lake ore in the presence of bacteria," Canadian Mining Journal, vol. 87, pp. 64-67, 1966.

[30] R.A. Thomas, "Agnew Lake Mines: Taking giant steps in solution mining," Engineering and Mining Journal, vol. 179, no. 11, pp. 58-161, 1978.

[31] Anonymous, "Agnew Lake Mines encounters problems in leaching uranium ore," Engineering and Mining Journal, vol. 179, no. 6, p. 43, 1978.

[32] J.R. Goode, "Thorium and rare earth recovery in Canada: the first 30 years," Canadian Metallurgical Quarterly, vol. 52, pp. 234-242, 2003.

[33] N. Reynier, R. Gagné-Turcotte, L. Coudert, S. Costis, R. Cameron, and J.-F. Blais, "Bioleaching of uranium tailings as secondary sources for rare earth elements production," Minerals, vol. 11, 302, 2021.

[34] Å. Hultgren, and G. Olsson, "Uranium Recovery in Sweden. History and Perspective," SKB Arbetsrapport 93-42. Svensk Kärnbränslehantering Aktiebolag, Solna, Sweden, 1993.

[35] A. Peterson, "Status report from Sweden," In: Processing of Low-grade Uranium Ores. Proceedings of Panel on Processing of Low-Grade Uranium Ores; 27 Jun - 1 Jul 1966, IAEA, Vienna, Austria, pp. 41-48, 1967.

[36] T. Björling, "Biogenic lakning av uranskiffer," KTH Royal Institute of Technology. Trita-Mel 08 Report 733312, 1973 [in Swedish].

[37] B.E. Kalinowski, A. Oskarsson, Y. Albinsson, J. Arlinger, A. Ödegaard-Jensen, T. Andlid, and K. Pedersen, "Microbial leaching of uranium and other trace elements from shale mine tailings at Ranstad," Geoderma, vol. 122, pp. 177-194, 2004.

[38] T.M. Bhatti, "Bioleaching of organic carbon rich polymetallic black shale," Hydrometallurgy, vol. 157, pp. 246-255, 2015.

[39] B.E. Kalinowski, A. Johnsson, J. Arlinger, K. Pedersen, A. Ödegaard-Jensen, and F. Edberg, "Microbial mobilization of uranium from shale mine waste," Geomicrobiology Journal, vol. 23, pp. 157-164, 2006.

[40] World Nuclear News, "Swedish resource world's second largest," https://www.world-nuclear-news.org/Articles/Swedish-resource-world-s-second-largest., 2012.

[41] A. Lecomte, M. Cathelineau, R. Michels, C. Peiffert, and M. Brouand, "Uranium mineralization in the Alum Shale Formation (Sweden): Evolution of a U-rich marine black shale from sedimentation to metamorphism**,"** Ore Geology Reviews, vol. 88, pp. 71-98, 2017.

[42] A. Parviainen, and K. Loukola-Ruskeeniemi, "Environmental impact of mineralised black shales," Earth-Science Reviews, vol. 192, pp. 65-90, 2019.

[43] N.H. Schovsbo, "Uranium enrichment shorewards in black shales: A case study from the Scandinavian Alum Shale," GFF, vol. 124, no. 2, pp. 107-115, 2002.

[44] D. Guy-Ohlson, and B. Lindqvist, "Palynomorph content of the uraniferous alum shales of Cambrian-Ordovician age in Sweden," Ore Geology Reviews, vol. 5, no. 5-6, pp. 525-536, 2017.

[45] A. Colpaert, "The forgotten uranium mine of Paukkajanvaara, North Karelia, Finland," Nordia Geographical Publications, vol. 35, No. 2, pp. 31-38, 2006.

[46] M. Lusa, J. Knuutinen, M. Lindgren, J. Virkanen, and M. Bomberg,"Microbial communities in a former pilot-scale uranium mine in Eastern Finland – association with radium immobilization," Science of the Total Environment, vol. 686, pp. 619-640, 2019.

[47] H. Tuovinen, E. Pohjolainen, D. Vesterbacka, K. Kaksonen, J. Virkanen, D. Solatie, J. Lehto, and D. Read," Release of radionuclides from waste rock and tailings at a former pilot uranium mine in eastern Finland," Boreal Environment Research, vol. 21, no. 5-6, 471-480, 2016.

[48] H. Tuovinen, D. Vesterbacka, K. Kaksonen, J. Virkanen, D. Read, D. Solatie, and J. Lehto, "Release of base and potentially harmful metals from waste deposits at a former uranium mine in Eastern Finland," International Journal of Environmental Monitoring and Analysis, vol. 7, no. 4, pp. 85-92, 2019.

[49] S. Majlesi, J. Akkanen, P. Roivainen, T.S. Tuovinen, J. Sorvari, J. Naarala, and J. Juutilainen, "Transfer of elements relevant to radioactive waste into chironomids and fish in boreal freshwater bodies," Science of the Total Environment, vol. 791, 148218, 2021.

[50] M. Riekkola-Vanhanen, "Talvivaara Sotkamo mine – bioleaching of a polymetallic nickel ore in subarctic climate," Nova Biotechnologica, vol. 10, no. 1, pp. 7-14, 2010.

[51] J.A. Puhakka, A.H. Kaksonen, and M. Riekkola-Vanhanen," Heap leaching of black schist," In: Rawlings, F.D.E., and Johnson, D.B. (eds.), Biomining, Springer, Heidelberg, pp. 139-151, 2007.

[52] A. Hubau, A.-G. Guezenneca, C. Joulian, C. Falagán, D. Dew, and K.A. Hudson-Edwards, "Bioleaching to reprocess sulfidic polymetallic primary mining residues: determination of metal leaching mechanisms," Hydrometallurgy, vol. 197, 105484, 2020.

[53] M. Gericke, J.W. Neale, and P. Määttä, "Biomining in Finland: commercial application of heap and tank bioleaching," In: Johnson, D.B., Bryan, C.G., Schlömann, M., and Roberto, F.F. (eds.), Biomining Technologies: Extracting and Recovering Metals from Ores and Waste, Springer Nature, Cham, Switzerland, pp. 209-228, 2023.

[54] E. Lippmaa, and E. Maremäe, "Dictyonema shale and uranium processing at Sillamäe," Oil Shale, vol. 16, no. 4, pp. 291-301, 1999.

[55] E. Lippmaa, and E. Maremäe, "Uranium production from the local Dictyonema shale in North-East Estonia," Oil Shale, vol. 17, no. 4, pp. 387-394, 2000.

[56] E. Lippmaa, and E. Maremäe, "The beginnings of uranium production in Estonia," Oil Shale, vol. 20, no. 2, pp. 167-174, 2003.

[57] S. Hade, and R. Soesoo, "Estonian graptolite argillites revisited: a future resource?" Oil Shale, vol. 31, no. 1, pp. 4-18, 2014.

[58] E. Maremäe, "A problem of complex processing of Estonia alum shale as a raw material metallurgy," Oil Shale, vol. 6, no. 1, pp. 28-36, 1989.

[59] E. Maremäe, H. Tankler, H. Putnik, and I. Maalmann, "Historical survey of nuclear non-proliferation in Estonia, 1946-1995," Tallin: Estonian Radiation Protection Centre, 2003.

[60] A. Soesoo, J. Vind, and S. Hade, "Uranium and thorium resources of Estonia," Minerals, vol. 10, no. 9, 798, 2020.

[61] J. Vind, and K. Tamm, "Review of the extraction of key metallic values from black shales in relation to their geological and mineralogical properties," Minerals Engineering, vol. 174, 107271, 2021.

[62] A. Menert, M. Kivisaar, S. Sippkulli, A. Heinaru, and T. Maidre, "Method for decomposition of the metallorganic matter of graptolite-argillite by microbial consortium," U.S. Patent. US 2020/0157577 A1, 2020.

[63] A. Menert, T. Korb, K. Orupõld, A. Teemusk, H. Sepp, Ü. Mander, T. Ilmjärv, J. Truu, P. Paiste, K. Kirsimäe, T. Menert, I. Kamenev, E. Heinaru, A. Heinaru, S.S. Kulli, and M. Kivisaar, "Methanogenesis and metal leaching on anaerobic decomposition of graptolite argillite," Environmental Technology and Innovation, vol. 31, 103139, 2023.

[64] K.A. Butt, "Uranium occurrences in magmatic and metamorphic rocks of Northern Pakistan," In: Uranium Deposits in Magmatic and Metamorphic Rocks, Proceedings of a Technical Committee Meeting on Uranium Deposits in Magmatic and Metamorphic Rocks. International Atomic Energy Agency, Salamanca, IAEA-TC-571/9, September 29-October 3, 1986.

[65] M. Mansoor, "Nuclear minerals in Pakistan," Nucleus, vol. 42, no. 1-2, pp. 73-83, 2005.

[66] S. Akhtar, X.Y. Yang, and F.Y Wang, "Uranium deposits and resources potential in Pakistan: a review," Science International, vol. 27, no. 2, pp. 1293-1296, 2015.

[67] T.M. Bhatti, and K.A. Butt, "Bioleaching of uranium from Chamiari low-grade black shale," Technical Report No. DGNFC-AEMC-1/2007, Islamabad, Pakistan, 2007.

[68] T.M. Bhatti, K.A. Malik, and A.M. Khalid, "Microbial leaching of low-grade sandstone uranium ores: column leaching studies," In: Malik, K.A., Naqvi, M.H., and Aleem, M.I.H. (eds.), Proceedings of the International Symposium on Biotechnology for Energy December 16-21, 1989, NIAB/ NIBGE, Faisalabad, Pakistan, pp. 329-340, 1991.

[69] T. Mahmood, "Bacterial heap leaching studies of low-grade uranium ores from Siwalik sandstone ore deposits, Suleiman Range, Pakistan," Ph.D. Thesis, University of the Punjab, Lahore, Pakistan, 1994.

[70] K.A. Butt, and N.A. Qamar, "Leaching and possible enrichment of uranium in graphitic schists in Balakot area – a working hypothesis," AEMC Technical Report No. AEMC/Geo-10, 1977.

[71] K.A. Butt, and N.A. Qamar, "Radiometric survey of graphitic schist zones of Salkhala Series, Kaghan Valley, District Mansehra," AEMC Technical Report No. AEMC/Geo-20, 1978.

[72] N.A. Qamar, and M.A.S. Baig, "A report on radiometric traverses in Allai and Chor Valleys and results of preliminary evaluation of graphitic schist zones of Salkhala Series discovered in Chor Valley," AEMC Technical Report No. AEMC/Geo-24, 1980.

[73] J. Ahmad, A. Khaliq, A. Qadir, and S. Iqbal, "Uranium potential of graphitic metapelites of Gandghar Range, N.W. Pakistan," In: Ashraf, M., Hussain, S.H., and Dawood, H. (eds.), Contribution to Geology of Pakistan, Proceedings of the 5th Pakistan Geological Congress 2004, National Geological Society of Pakistan, Islamabad, pp. 119-140, 2007.

[74] L. Bian, N.H. Schovsbo, A. Chappaz, and X. Zheng, "Molybdenum-uranium-vanadium geochemistry in the lower Paleozoic alum shale of Scandinavia: Implications for vanadium exploration," International Journal of Coal Geology, vol. 239, no. 1, 103730, 2021.

The Nucleus ***60***, *No. 1 (2023) 35-44*

www.thenucleuspak.org.pk

The Nucleus

ISSN 0029-5698 (Print)
ISSN 2306-6539 (Online)

Performance Evaluation of Various Algorithms for Cluster Head Selection in WSNs

Humaira Afzal[1], Saba Kanwal[1], Muhammad Zulfiqar[2], Humera Batool Gill[3], Muhammad Rafiq Mufti[4*]

[1]*Department of Computer Science, Bahauddin Zakariya University, Multan, Pakistan*

[2]*Department of Telecom System, Bahauddin Zakariya University, Multan, Pakistan*

[3]*Department of CS&IT, The Women University Multan, Pakistan*

[4]*Department of Computer Science, COMSATS University Islamabad, Vehari Campus Vehari, Pakistan*

ABSTRACT

With the huge growth of wireless sensor networks (WSNs) and massive rise in upcoming electronic devices, network management becomes difficult as it affects the overall performance of the wireless networks. Earlier, in WSN, simple clustering was employed to cover this limitation but over the time, it became evident that without an effective mechanism of the cluster formation and cluster head (CH) selection, effective WSN performance cannot be achieved. As CH selection is one of the important phases of wireless communication, that is why, it becomes essential to enhance this phase. This enhancement reflects the great improvement in the overall performance of WSNs. Different types of methodologies have been introduced in the last 10 years for cluster formation and especially for CH selection. In this article, we investigate some important methodologies such as A-LEACH, MWCSGA, DEEC-Gauss, and eeTMFO/GA of cluster formation and CH selection. From the analysis, significant results such as the energy consumption, reliability, number of alive nodes, the lifetime and throughput of network are computed that can be further utilized in selection of the best algorithm for CH selection.

Keywords: *Networks, Sensors, Algorithms, WSNs, Reliability, Nodes, Cluster head, Energy consumption*

1. Introduction

WSNs are a branch of the basic ad-hoc technology consisting of numerous sensor nodes distributed in a given area. In these types of networks, sensor nodes are interconnected and communicated wirelessly to gather data from the surrounding. These nodes are usually low-powered devices organized in an ad-hoc manner. Due to its huge rate of growth, WSNs have become a matter of concern for all researchers. Initially, these were used for monitoring different kinds of systems of military applications [1]. Now, these are being implemented in several types of scenarios like health monitoring, reducing pollution in the atmosphere, ecosystem observation, physical hazards inhibition, fire detection in forests and daily activity monitoring. With the immense growth and demand of these sensor nodes, it has become difficult to manage wireless environment. So, there is a need of controlling this situation by making the structures of WSNs flexible and adaptable to any environment.

The structure of WSN is illustrated in Fig. 1. The wireless devices also called sensors sense the environment to acquire useful information like state, values, etc. and transfer them to other sensors. In WSN, a sensor is termed as a node and the blue node indicates the member node, whereas, the red node indicates the head node also called cluster head (CH). Clustering is an important technique for increasing and extending the lifetime of WSNs because in general, WSNs have a limited lifetime.

If each node directly communicates with other nodes then the structure of WSN becomes easy but on the other hand, it will not be very efficient. The nodes which are far apart from each other cannot communicate because of signal loss. Due to this, a node that is selected or fixed as a CH of the cluster so that other nodes can communicate through it other than communicating directly with each other. Member nodes can send/receive data only through CHs. Being an integral part of all clusters, the base station (BS) controls the whole transmissions in the network. Since CHs act as a bridge between member nodes and BS, therefore, CH selection plays a vital role in WSN. In case, if this bridge is not efficient then the successful communication will not take place.

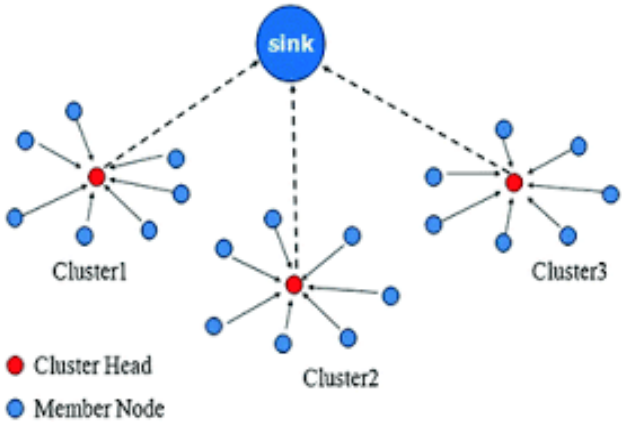

Fig.1: The general architecture of clustered WSN.

Due to the proliferation of nodes and to improve the data transmission in WSNs, the researchers are motivated towards the effective management methods of sensor nodes. The factors which are involved in the development and enhancement of WSNs depends upon the limitations on many issues particularly in the designing phase, energy consumption, reliability, network lifetime, scalability, cost, topology, etc. These limitations can be reduced by the use of clusters.

Different techniques have been reported in literature for the cluster formation. One is Low-energy adaptive clustering

*Corresponding author: rafiq_mufti@ciitvehari.edu.pk

hierarchy (LEACH) that is basically used to decrease the energy consumption. Further, many advanced versions of LEACH such as I-LEACH, T-LEACH, HLEACH and LEACH-II have been developed and the idea of CH selection is introduced. Particle swarm optimization (PSO) with bio-inspired aging model is developed for CH selection. Some other algorithms like gravitational search algorithm (GSA), genetic algorithm (GA) and multi-objective evolutionary algorithm (MOEA) have been designed for CH selection. These algorithms provide the optimal solutions [2]. Moreover, some hybrid techniques such as PSO with GSA, GA with MOEA, etc., are introduced for better optimal results.

In dynamic optimization of a sensor node, CHs selection is accomplished by GA. MOEA is multi-objective nature used GA and PSO for CHs selection. A fuzzy-based CH selection scheme is also described in [3, 4]. This scheme utilizes an eligibility index computed for each sensor node and then an optimal solution for CH selection is derived. In this paper, various algorithms and techniques for clustering and the CH selection are discussed comprehensively. Based on different parameters, the best algorithm is evaluated.

An algorithm using unique neighbor node approach was proposed in [5], where selection of CH took place based on connectivity to at least one neighbor node that is unique. In case if cluster had no unique neighbor node, then CH selection was carried out on the basis of maximum residual energy and the number of other neighbor nodes. This algorithm ensured the connectivity of the overall network. A mechanism for selecting dynamic CH was suggested in [6, 7] by introducing the first kind of CH, second kind of CH, and so on. The Voronoi diagram was incorporated for cluster formation in the monitoring area and due to redundant nodes death priority and network coverage performance, the first kind of CH was employed and when it became dead, then second kind of CH was selected on the basis of the average energy of the network nodes and the residual energy. In [3], a fuzzy-based balance cost CH selection technique (FBECS) was introduced by using an eligible index for each sensor node of each cluster, which was computed and the optimal value of the index was then chosen. A similar scheme for CH selection and clustering was also presented in [8] for enhancing the lifetime of the WSNs but these methodologies depending on one level head selection were not so efficient in the multi-hop systems. Therefore, there was a need for another algorithm that exploits two-level fuzzy CH selection. An energy-efficient dynamic scenario (EEDS) was reported in [9] which introduced a new mechanism of selection of CH based on network traffic and the node localization. The multi-hop decision-making technique named Fuzzy-Topsis for CH selection was also introduced in [10] using distances between neighbor nodes, the distance from the BS and the remaining energy of the nodes, as parameters. A high-quality and high-power clustering algorithm (HQCA) was incorporated in [11], where selection of CH was carried out based on energy that is remaining in the sensor nodes, the mean distance of sensors in the cluster and lowest distances of the sensors from the BS.

In [12], an energy-efficient CH selection technique was proposed describing the energy dissipation based on locations depending upon the residual energy. For this scheme, the radio energy model was employed for CH selection by measuring the distance from the sink, so increasing the lifetime of WSN. The rotating role is one of the approaches used for CH selection and the role of the head is rotated among all of the sensor nodes in a given cluster. In [13], the k-mean algorithm was suggested for finding the centroid node of the cluster and then adopted it initially as a head node. A Fault-tolerant head selection method was then proposed to compute the fitness function of the head node for initializing and updating CH, whenever the initial CH had a low fitness function and less residual energy. To improve this algorithm, another approach by combining the k-mean algorithm and Huffman coding algorithm was incorporated in [14]. Huffman's coding algorithm is efficient in terms of energy consumption but has a problem with respect to node residual energy and its communication distance. This problem can be resolved by using a gradient descent algorithm that reflects its effects in the form of an enhanced lifetime, latency, energy consumption and delivery rates.

The flower pollination algorithm (FPA) is one of the famous bio-inspired algorithms consisting of two components: 1) self-pollination and 2) cross-pollination, where self-pollination performs local pollination search and cross-pollination is for global pollination search exploring. In [15], FPA was proposed for CH selection by doing a local search and then global search exploring. In [16], an improved flower pollination algorithm (IFPA) was designed to enhance traditional FPA in terms of capacity, energy and lifetime. In this technique, groups of parallel operation-based pollination were developed to follow the strategy of enhanced communication depending upon the replacement of old pollen by new high-quality pollen. The functional fitness of each group was then evaluated. In [17], the chicken swarm optimization (CSO) technique was discussed for selecting CHs based on the fitness function of all the type (roosters, chicks and the hens) together. However, the fitness function calculation requires more space and cost.

2. Selected Algorithms for Performance Analysis

2.1 Multi Weight Chicken Swarm based Genetic Algorithm (MWCSGA)

Multi weight chicken swarm-based genetic algorithm (MWCSGA) expresses the reflective view of bio-inspired GA and uses the clustering CSO method for CH selection [18]. Clustering is performed through GA and the head is selected through swarm optimization technique. In this strategy, the multi-weight clustering method is first constructed for cluster formation and a head for communication is then selected. This strategy comprising of two levels derives the individual's best fitness functions whose values are used for CH selection. The process is performed for three groups (indicate as rooster, hens and chicks by employing fitness value, swarm updating frequency, Energy, CHs count, mutation and the crossover, as a parameter. Based on efficient fitness function values for

individual chicks (nodes), CH is selected and transferred to consequent generation. The consumed energy (E) of CH in this strategy is given as:

$$E = \left[L\left(\frac{N}{A} - 1\right) \times E_d + \frac{N}{A} E_{com}\right] + \psi(E_R, E_T)$$

where

$$\psi(E_R, E_T) = E_R(L, d) + E_T(L, d_{BS}),$$

Where L is the amount of data transferred by the transmitting node to the CH; N is the number of alive nodes; A is the number of clusters in the network; E_d is dissipated energy; d_BS is the distance from BS to CH; E_T and E_R is energy consumption of transmitter and receiver respectively. Here, fitness function value calculation is carried out through a new mechanism because the old CSO is not so efficient in terms of cost and speed.

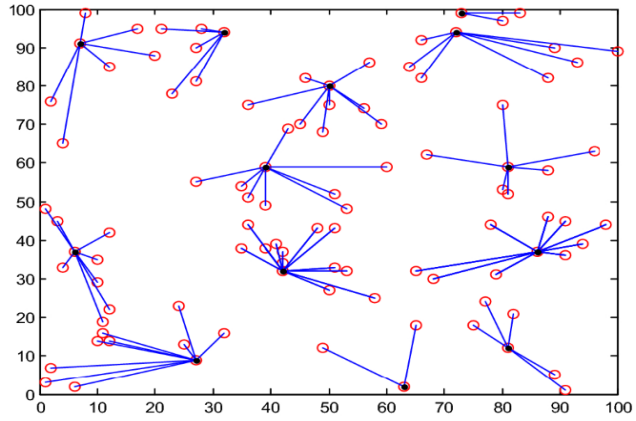

Fig. 2: Structure of cluster eeTMFO/GA.

2.2 *Energy-efficient Trusted Moth Flame Optimization and Genetic Algorithm-based Clustering Algorithm (eeTMFO/GA)*

The eeTMFO/GA introduced in [19] is an optimal selection algorithm for cluster formation to enhance network performance. Structure of a cluster eeTMFO/GA is shown in Fig. 2. Due to its GA feature, it has the ability for selecting the cluster head with minimum energy consumption. Fitness function is evaluated by using residual energy of elected node, connected node density, packet forwarding progress, the average delay of transmission and average cluster distance as parameters.

2.3 *Advanced LEACH (A-LEACH)*

LEACH was the first algorithm designed for WSN for the formation of clusters, CHs, measuring network lifetime, throughput and reliability. It uses simple and traditional parameters such as residual energy and distance from BS in the selection of CH. In [20], CH selection is carried out based on the distance between BS and the CH. The cluster is divided into semi-clusters and threshold is given as:

$$T_r = P_G + P_C$$

where

$$P_G = \frac{\kappa}{\eta - \kappa\left(\tau \, mod \frac{\eta}{\kappa}\right)}$$

$$P_C = \frac{E_{current}}{E_{initial}} \times \frac{\kappa}{\eta}$$

P_G denotes the general probability; P_C represents the current state probability; τ represents any round; κ shows the expected number of CHs in a round; η denotes the total number of sensor nodes in the network; $E_{current}$ is the current energy of the node relative to initial energy $E_{initial}$. A node having higher residual energy nearer to sink is to be selected as a CH. This technique is beneficial for energy-aware techniques and dissipates energy from clusters leading to improve overall network lifetime.

2.4 *Distributed Energy Efficient Clustering with Gaussian (DEEC-Gauss)*

Enhanced distributed energy-efficient clustering (E-DEEC) presented in [21] set a node as CH having higher remaining energy. DEEC used the probability of ratio of average energy and residual the energy. E-DEEC introduced the supernode to increase the heterogeneity and enhance the network lifetime. Using some additional parameters, an enhanced version of the E-DEEC algorithm was designed and combined with the Gaussian algorithm that filters out the best supernode (i.e. CH) of the cluster.

3. Comparative Studies

Tables of comparative studies are given in Appendix 1. The comparative analysis of existing techniques used in CH selection is discussed in Table 1. The methodologies along with its parameters such as fitness value, mutation, residual energy, sense power, node position, etc. are listed in the table. These parameters play an important role in performance evaluation. The research gaps are also identified in the given methodologies. From the parameters given in Table 1, five parameters are selected for Table 2 as a benchmark for performance evaluations. These parameters are the key points in our proposed work.

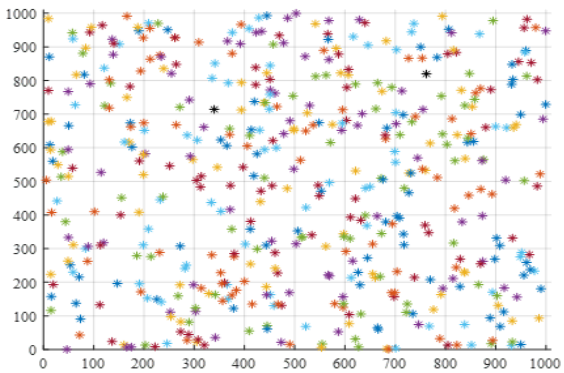

Fig. 3: Wireless sensor network.

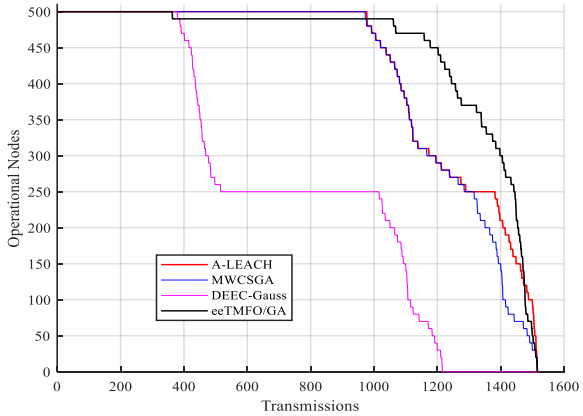

Fig. 4: Data transmissions.

4. Performance Evaluation

4.1 Simulation Procedure

The effectiveness of the algorithms discussed in Section 3 is evaluated based on alive node, energy consumption, time complexity and throughput. The simulation is done by using MATLAB/SIMULINK environment. The basic level parameters used for simulations are given in Table 3 (Appendix 1).

The experiments are performed with 500 operational nodes of WSN by setting the rounds as 50 and 100. Assume that, data length is 12000 bits and the transmission power is 0.0175 nJ/bit/m^2. The initial energy assigned to every node is 0.28 Joule. The model under consideration for WSN is illustrated in Fig. 3. The data transmission rates of A-LEACH, MWCSGA, DEEC-Gauss and eeTMFO/GA algorithms are represented in Fig. 4. The data transmission rates of MWCSGA and A-Leach are almost the same, whereas eeTMFO/GA has the highest data transmission rate for particular operational nodes.

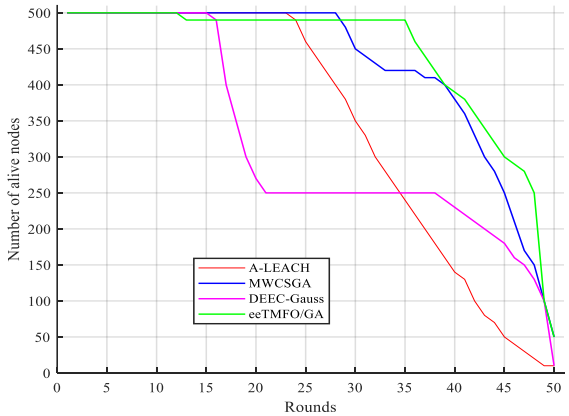

Fig. 5a: Number of alive nodes with 50 rounds.

4.2.1 Analysis of alive nodes

Alive nodes are used to send data to BS/sink immediately after successfully aggregated it. These nodes calculate the weights of randomly selected numbers dynamically. This concept of random number selection was first introduced in the LEACH protocol for CH selection. Fig. 5 depicts the number of alive nodes of each algorithm with 50 and 100 rounds. The increment of rounds affects the first node death (FND), half node death (HND) and last node death (LND) percentage of each algorithm.

In 50 rounds, the FND of MWCSGA is the highest and of eeTMFO/GA is the lowest but the HND and LND of eeTMFO/GA are larger that make the total percentage of alive nodes highest. On the other hand, in 100 rounds, the eeTMFO/GA has a high percentage in terms of FND, HND and LND. In general, the dimension of alive rate depends upon the number of nodes. As the number of nodes increases, the alive rate decreases, i.e., it almost goes to zero. It can be observed that the lowest possible alive rate of any node is approximately 0.00003s. From Fig. 5, it is clear that eeTMFO/GA algorithm has a large number of alive nodes as compared to other algorithms.

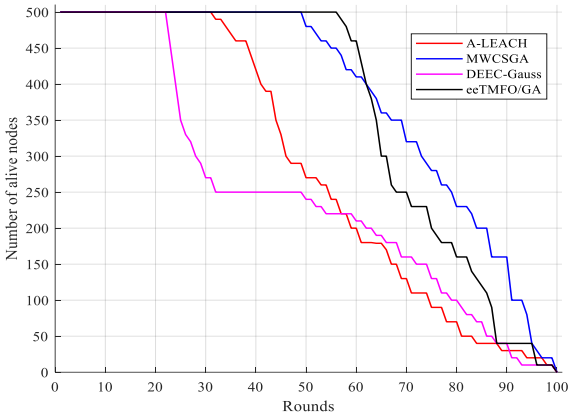

Fig. 5b: Number of alive nodes with 100 rounds.

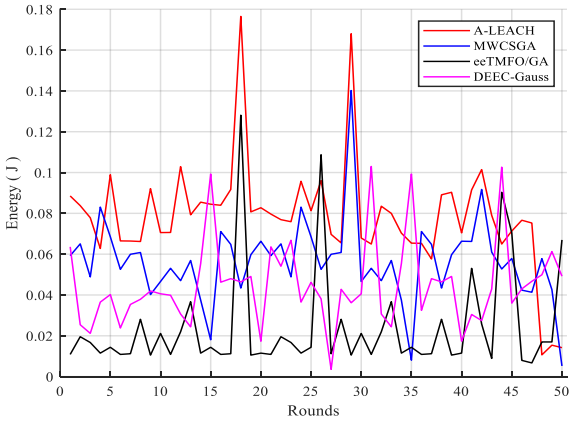

Fig. 6a: Energy with 50 rounds.

4.2.2 Analysis of Energy Consumption

Energy utilization is the main concern in WSNs, as it plays a vital role in the selection of CH. A node having minimum amount of energy consumption is to be selected as a CH in the cluster. Fig. 6 shows the flow of energy consumption in which the energy or power consumption of A-LEACH is high. This is due to its traditional structure and transmission. MWCSGA

and DEEC-Gauss have an average energy consumption but eeTMFO/GA consumes less energy as compared to others. From this figure, it can be observed that energy consumption is directly proportional to the number of rounds. The number of rounds increases with the increase of consumption.

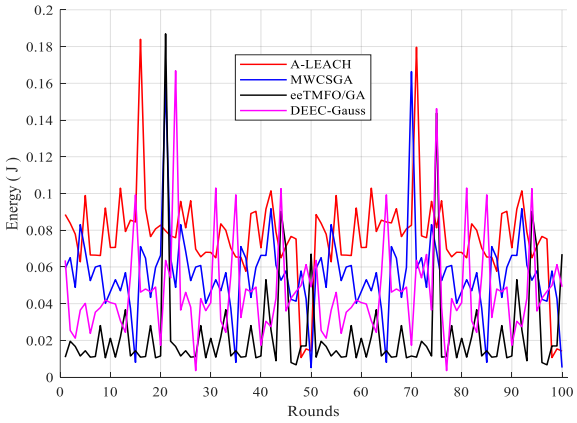

Fig. 6b: Energy with 100 rounds.

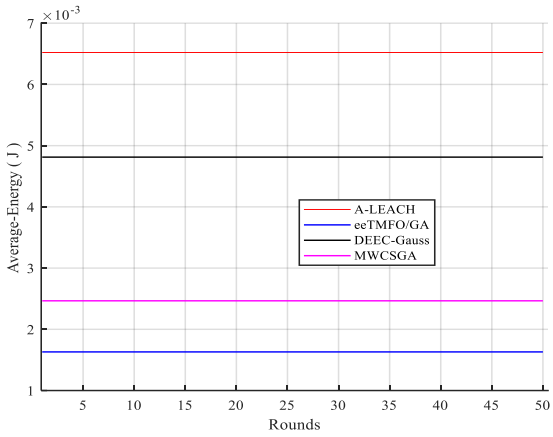

Fig. 7a: Average energy for 50 rounds.

Fig. 7 represents the average consumed energy at 50 and 100 rounds. MWCSGA and DEEC-Gauss have low average consumption whereas eeTMFO/GA has the lowest average energy consumption.

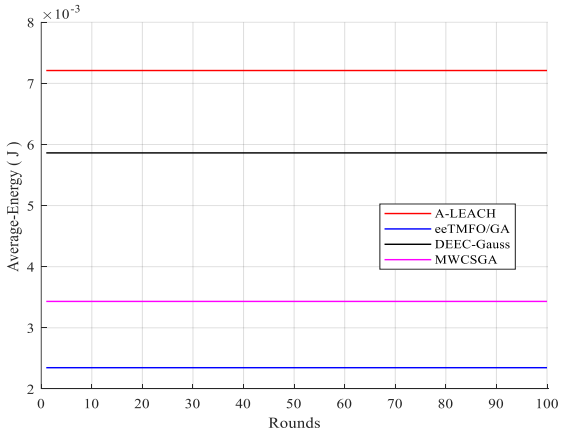

Fig. 7b: Average energy for 100 rounds.

Similarly, Fig. 8 shows the overall energy consumption of head selection. eeTMFO/GA has the lowest energy consumption as compared to other algorithms regarding CH selection.

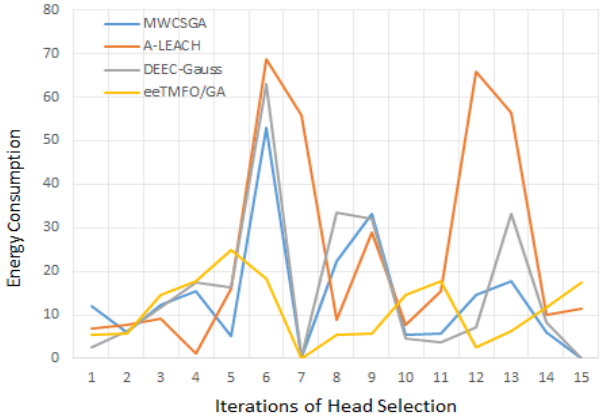

Fig. 8: Overall energy consumption.

4.2.3 *Cluster Head Selection Phases*

CH selection takes place in four phases. In the first phase, CH selection using residual energy and fitness factor provides the large number of nodes selected as CHs as shown in Fig. 9a. DEEC-Gauss provides the selection of CHs that is high at the beginning but low at the end, so this behavior is not acceptable. On the other hand, eeTMFO/GA and MWCSGA provide the average rate of CHs and the average ratio of eeTMFO/GA is higher than the average ratio of MWCSGA, so it implies that eeTMFO/GA provides the optimal and efficient CHs selection in the first phase.

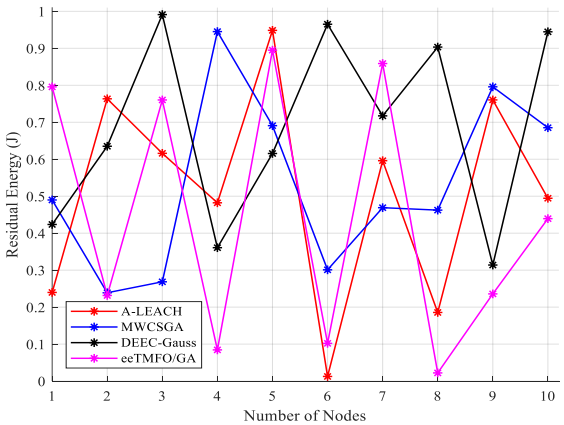

Fig. 9a: Head selection phase 1.

In the second phase as shown in Fig. 9b, CH selection takes place by using residual energy and node position for (x, y). MWCSGA provides the lowest selection rate and A-LEACH has either the same effect or higher selection rate. eeTMFO/GA and DEEC-Gauss have an average ratio of selection but the ratio of eeTMFO/GA remains higher than the ratio of DEEC-Gauss. In the third phase, A-LEACH and DEEC-Gauss have a larger selection ratio than MWCSGA.

eeTMFO/GA leads with their highest ratio in the average rate of selection and the same is the case in fourth phase.

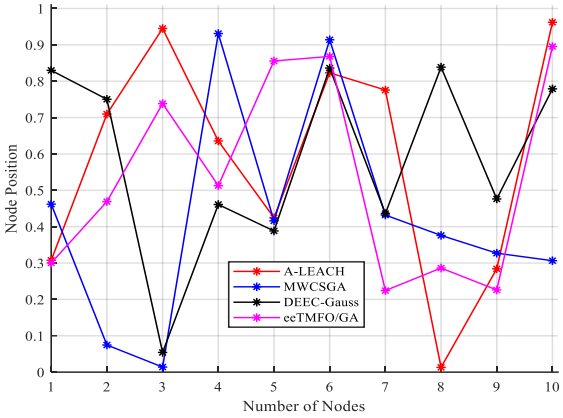

Figure 9b: Head selection phase 2.

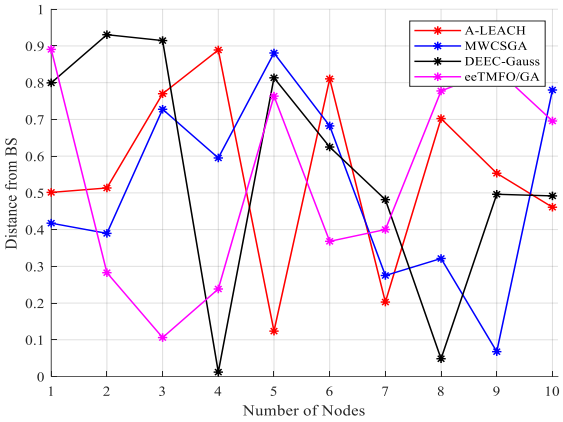

Fig. 9c: Head selection phase 3.

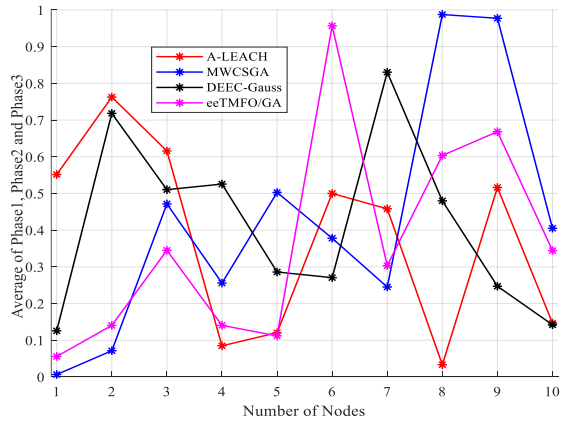

Fig. 9d: Head selection phase 4.

4.2.4 Analysis of Throughput

Throughput is mainly concerned with data transfer rate in unit time. The basic goal of WSN is to increase the network lifetime with enhanced reliability by improving the throughput. Residual energy is used as a primary aspect in the improvement of throughput. As energy resources increases and energy consumption decreases, then throughput increases. The performance analysis in terms of throughput is given in Table 4. It is obvious from Table 4a, eeTMFO/GA has the highest throughput as compared to other algorithms for all aspects. This enhancement is due to the involvement of certain factors such as death rate, transmission media, power consumption and scalability and their impacts are given in Table 4b.

Table 4a: Throughput performance of algorithms for various rounds.

Algorithm	With 50 Rounds	With 100 Rounds	Overall
MWCSGA	65%	56%	60%
eeTMFO/GA	68%	60%	64%
A-LEACH	55%	49%	52%
DEEC-Gauss	65%	53%	59%

Table 4b: Throughput enchantment factors.

Algorithm	Death Rate	Transmission media	Power consumption	Scalability
MWCSGA	Mediam	Stable	Low	High
eeTMFO/GA	High	Very Stable	Low	High
A-LEACH	Mediam	Not Stable	Large	Mediam
DEEC-Gauss	High	Sometime Stable Sometime not stable	Mediam	Mediam

Table 5. Overall analysis

	MWCSGA	eeTMFO/GA	A-LEACH	DEEC-Gauss
Average Consumed energy 50 With Rounds	2.34J	1.98J	6.4J	4.5J
Average Consumed energy 100 With Rounds	3.5J	2.48J	7.2J	5.9J
The difference with an increment of Rounds 50-100	1.16J	0.5J	0.8J	1.4J
First Node Death Percentage with 500 Nodes	60%	25%	61%	27%
Half Node Death Percentage with 500 Nodes	80%	71%	86%	32%
Last Node Death Percentage with 500 Nodes	76%	94%	94%	76%
Throughput	60%	65%	51%	59%

4.2.6 Time Complexity

Big-O is one of the common factors used to evaluate the complexity of any algorithm. It is the worst-case analysis to determine the execution time of an algorithm. The Big-O of algorithms is described in Table 6 which shows that A-LEACH consumes a lot of costs as compared to others, whereas eeTMFO/GA exhibits the lowest cost. The cost consumed in A-LEACH is n5 which is large enough to affect

the overall contributions of network reliability. DEEC-Gauss consumes the cost in factorial of iterations that reflect its drawback in terms of memory rudiments. Similarly, the cost utilized in MWCSGA is in binary form that gives a bit effect of high energy consumption in peak value. Overall, the efficiency of MWCSGA and eeTMFO/GA is significant in terms of throughput as compared to others.

Table 6: Big-O analysis.

Algorithm	Big-O
MWCSGA	$O(n(n-r)2^{n-1})$
eeTMFO/GA	$O\big(c(n^2+n)\big) = O(n^2)$
A-LEACH	$O\big(n^4(n-1)logn + n^2 + n^3(n-1)\big) = O(n^5)$
DEEC-Gauss	$O\big((n-1)n! + (n-1)(n+1)!\big) = O\big((n-1)(n+1)!\big)$

5. Conclusion

Cluster Head (CH) selection has become a matter of attention for researchers because of its contribution to the overall performance of WSNs. In this paper, the previous studies of CH selection have been discussed. The well-known techniques for CH selection such as A-LEACH, DEEC-Gauss, MWCSGA and eeTMFO/GA have been investigated and evaluated in terms of energy consumption, alive rate, lifetime and reliability. Based on performance, it can be concluded that eeTMFO/GA method perform better as compared to the traditional methods in terms of energy efficiency. Moreover, eeTMFO/GA has efficient energy consumption, a high network lifetime and a large rate of alive nodes. It provides 12%, 9% and 8% performance improvements in all aspects as compared to A-LEACH, DEEC-Gauss and MWCSGA respectively.

A low power and trust aware network has become one of the essential parameters of WSNs. Our future work is mainly focused on the design of an energy efficient algorithm which may be expected to have reliability and high network lifetime.

References

[1] M. Majid, S. Habib, A.R. Javed, M. Rizwan, G. Srivastava, T.R. Gadekallu and J.C.W. Lin, "Applications of wireless sensor networks and internet of things frameworks in the industry revolution 4.0: A systematic literature review", Sensors, vol. 22, no. 6, pp. 2087, 2022.

[2] R. Sinde, F. Begum, K. Njau and S. Kaijage, "Refining network lifetime of wireless sensor network using energy-efficient clustering and DRL-based sleep scheduling", Sensors, vol. 20, no. 5, pp.1540, 2020.

[3] P.S. Mehra, M.N. Doja and B. Alam, "Fuzzy based enhanced cluster head selection (FBECS) for WSN", J. King Saud Univ. Sci., vol. 32, no. 1, pp. 390-401, 2020.

[4] G.A. Safdar, T.S. Syed and M. Ur-Rehman, "Fuzzy Logic-Based Cluster Head Election-Led Energy Efficiency in History-Assisted Cognitive Radio Networks", IEEE Sens. J., vol. 22, no. 22, pp. 22117-22126, 2022.

[5] T.K. Jain, D.S. Saini and S.V. Bhooshan, "Cluster head selection in a homogeneous wireless sensor network ensuring full connectivity with minimum isolated nodes", J. Sens, vol. 2014, pp. 724219, 2014.

[6] D. Jia, H. Zhu, S. Zou and P. Hu, "Dynamic cluster head selection method for wireless sensor network", IEEE Sens. J., vol.16, no. 8, pp. 2746-2754, 2015.

[7] P.S. Mehra, M.N. Doja and B. Alam, "Fuzzy Based Enhanced Cluster Head Selection (FBECS) for WSN", J. King Saud Univ. Sci., vol. 32, no. 1, pp. 390-401, 2018.

[8] N. Shivappa and S.S. Manvi, "Fuzzy-based cluster head selection and cluster formation in wireless sensor networks", IET Netw., vol. 8, no. 6, pp. 390-397, 2019.

[9] P.K. Dutta, M.K. Naskar and O.P. Mishra, "Impact of two-level fuzzy cluster head selection model for wireless sensor network: An Energy efficient approach in remote monitoring scenarios", arXiv preprint arXiv:1308.0690, 2013.

[10] B.M. Khan, R. Bilal and R. Young, "Fuzzy-TOPSIS based cluster head selection in mobile wireless sensor networks", J. Electr. Eng. Technol, vol. 5, no. 3, pp. 928-943, 2018.

[11] A.A. Baradaran and K. Navi, "HQCA-WSN: High-quality clustering algorithm and optimal cluster head selection using fuzzy logic in wireless sensor networks", Fuzzy Sets Syst., vol. 389, pp. 114-144, 2020.

[12] M. Senthil, V. Rajamani and G.R. Kanagachidambaresan, "Energy-efficient cluster head selection for life time enhancement of wireless sensor networks", J. Inf. Technol., vol. 13, no. 4, pp. 676. 2014.

[13] A.F. Jemal, R.H. Hussen, D. Y.Kim, Z. Li, T. Pei and Y.J. Choi, "Energy-efficient selection of cluster headers in wireless sensor networks", Int. J. Distrib. Sens., vol. 14, no. 3, pp. 1550147718764642, 2018.

[14] G.P. Agbulu, G.J.R. Kumar and A.V. Juliet, "A lifetime-enhancing cooperative data gathering and relaying algorithm for cluster-based wireless sensor networks", Int. J. Distrib. Sens., vol. 16, no. 2, pp. 1550147719900111, 2020.

[15] X.S. Yang, "Flower pollination algorithm for global optimization", 11th Int. conf. unconv. Comput. Nat. computation, Orléan, France, September 3-7, 2012, pp. 240-249, Springer, Berlin, Heidelberg, 2012.

[16] T.K. Dao, T.T. Nguyen, J.S. Pan, Y. Qiao and Q.A. Lai, "Identification failure data for cluster heads aggregation in WSN based on improving classification of SVM", IEEE Access, vol. 8, pp. 61070-61084. 2020.

[17] W. Osamy, A.A. El-Sawy and A. Salim, "CSOCA: Chicken swarm optimization based clustering algorithm for wireless sensor networks", IEEE Access, vol. 8, pp. 60676-60688, 2020.

[18] N. Ajmi, A. Helali, P. Lorenz and R. Mghaieth, "MWCSGA—Multi Weight Chicken Swarm Based Genetic Algorithm for Energy Efficient Clustered Wireless Sensor Network", Sensors, vol. 21, no. 3, pp. 791, 2021.

[19] R. Sharma, V. Vashisht and U. Singh, "eeTMFO/GA: a secure and energy efficient cluster head selection in wireless sensor networks", Telecommun Syst., vol. 74, no. 3, pp. 253-268, 2020.

[20] A.O.A Salem and N. Shudifat, "Enhanced LEACH protocol for increasing a lifetime of WSNs", Pers Ubiquitous Comput., vol. 23, no. 5, pp. 901-907, 2019.

[21] P. Saini and A.K. Sharma, "E-DEEC-enhanced distributed energy efficient clustering scheme for heterogeneous WSN", 1st IEEE Int. conf. parallel, distrib. grid comput. (PDGC 2010), Solan, India, pp. 205-210, 2010,

[22] O.J. Aroba, N. Naicker and T. Adeliyi, "A Hyper-Heuristic Heterogeneous Multisensor Node Scheme for Energy Efficiency in Larger Wireless Sensor Networks Using DEEC-Gaussian Algorithm", Mob. Inf. Syst., vol. 2021, pp. 6658840, 2021.

[23] D.L. Reddy, C. Puttamadappa and H.N. Suresh, "Merged glowworm swarm with ant colony optimization for energy efficient clustering and routing in Wireless Sensor Network", Pervasive Mob Comput., vol. 71, pp. 101338, 2021.

[24] A. Rahiminasab, P. Tirandazi, M.J. Ebadi, A. Ahmadian and M. Salimi, "An energy-aware method for selecting cluster heads in wireless sensor networks", Appl. Sci., vol. 10, no. 21, pp. 7886, 2020.

[25] K.N. Qureshi, M.U. Bashir, , J. Lloret and A. Leon, "Optimized cluster-based dynamic energy-aware routing protocol for wireless sensor networks in agriculture precision", J. Sens., vol. 2020, pp. 1-19, 2020.

[26] S.J. Jassbi and E. Moridi, "Fault tolerance and energy efficient clustering algorithm in wireless sensor networks: FTEC", Wirel. Pers. Commun., vol. 107, no. 1, pp. 373-391. 2019.

[27] J.G. Lee, S. Chim and H.H. Park, "Energy-efficient cluster-head selection for wireless sensor networks using sampling-based spider monkey optimization", Sensors, vol. 19, no. 23, pp. 5281, 2019.

[28] L. Zhao, S. Qu and Y. Yi, "A modified cluster-head selection algorithm in wireless sensor networks based on LEACH", EURASIP J. Wirel. Commun. Netw, vol. 2018, no. 1, pp.1-8, 2018.

[29] T. Rahman, I. Ullah, A.U. Rehman and R.A. Naqvi, "Notice of violation of IEEE publication principles: Clustering Schemes in MANETs: Performance Evaluation, Open Challenges, and Proposed Solutions", IEEE Access, vol. 8, pp. 25135-25158, 2020.

[30] P.K. Batra and K. Kant, "LEACH-MAC: a new cluster head selection algorithm for Wireless Sensor Networks", Wirel. Netw, vol. 22, no. 1, pp. 49-60, 2016.

[31] S. Gajjar, M. Sarkar and K. Dasgupta, "Cluster head selection protocol using fuzzy logic for wireless sensor networks", Int. J. Comput. Appl., vol. 97, no. 7, 2014.

[32] C. So-In, K. Udompongsuk, C. Phudphut, K. Rujirakul and C. Khunboa, "Performance evaluation of LEACH on cluster head selection techniques in wireless sensor networks", 9th Int. Conf. Comput. Inf. Technol. (IC2IT2013), May 9-10, 2013, Springer, Berlin, Heidelberg, pp. 51-61.

[33] A.S. Toor and A.K. Jain, "Energy aware cluster based multi-hop energy efficient routing protocol using multiple mobile nodes (MEACBM) in wireless sensor networks", AEU - Int. J. Electron. Commun, vol. 102, pp. 41-53, 2019.

[34] G. Krishnasamy, "An Energy Aware Fuzzy Trust based Clustering with group key Management in MANET Multicasting" Proc. Int. Conf. Comput. Sci. Netw (ICTCS), pp. 1-5, 2019.

Appendix

Table 1: Comparative studies of existing approaches.

References	Parameter	Methodology	Limitations
Nader Ajmi et al. (2021) [18]	Fitness value, mutation, swarm updating frequency, crossover Energy, and the cluster heads count	CSO and GA work together, Selects the CH based on efficient fitness function values for individual chicks(nodes) and transfers it to consequent generation.	Fitness function calculation needs more space and cost
D. Laxma Reddy et al. (2021) [24]	Residual Energy, Sense power, Node Position, Fitness of nodes	Combination of ACI and GSO, selection based on local searching and global searching. Rapid discovery of solution by ACO and GSO based non-centralized control	More Cost required
Oluwasegun Julius Aroban et al. (2021) [22]	Communication range, data packet size, residual energy, distance with sink	An enhanced version of the E-DEEC algorithm that uses Gaussian formula that shows the efficient performance	The complex structure of Gaussian make cost higher
Atefeh Rahiminasab et al. (2020) [25]	Energy, effeicent use of the size od data queues, distance to the center, and the mobility.	Multi-factor decision-making, a combination of AHP and CSP.	Dead rate not enhanced
Ramadhani Sinde et al. (2020) [2]	Node degree, residual energy, and distance	Combine PSO with AP for selection. Selection is done with local and then global best solutions	AP exemplar selections are not effective after a little enhancement
eeTMFO/GA (2020) [19]	Density, Energy, Distance with packet forwarding progress, Transmission delay,	Combination of GA and MFO, Selects the optimal solution	This procedure has network delay
Thi-Kien Dao et al. (2020) [16]	Data aggregation, network status, Classification Support Vector Machine(SVM)	Decision function classification deployed the data aggregation. Improved flower pollination algorithm (IFPA) solves this problem by dividing the parallel operation into groups and then calculate the fitness function of each group. Replace the optimal solution with the original one.	The complexity of the overall algorithm is increased that reflects the problematic outcomes in terms of cost function calculations.
Kashif Naseer Qureshi et al. (2020) [25]	Gateway Node weight, centroid position, energy consumption model,	Gateway Energy-Efficient Centroid (GCEEC) routing protocol nature-inspired algorithm for agriculture. Selects the CH by calculating the centroid position of node and gateway node for transmission of data with BS.	Inter-cluster Multi-Hop communication needs more energy, also has network delay
G Pius Agbulu et al. (2020) [14]	Aggregation-energy, Network Traffic	A combination of K-mean and Huffman algorithms. K-mean calculates the nearest node and the Huffman algorithm is used to organize the nodes.	Huffman algorithm complexity affects the overall cost or complexity of cluster formation.
Pawan Singh Mehra et al. (2020) [3]	Nodes States(Show the current state of the node), RegionvBased probability	Enhanced Version Of BCSA algorithm. The density and power level of nodes is used to calculate the energy expenditure of selected CH.	Requires More Cost for Node Status Calculation
Amir Abbas Baradarana et al. (2019) [11]	Based on residual energy of node, all node distance with BS, amount of energy per cluster, and cluster density	Uses Fuzzy Decision Block (FDB) and checks the parameters. A node that has less distance from BS, has higher in remaining energy, enhanced cluster quality, and less mean distance is selected as CH.	Fuzzy logic in high vagueness
Amanjot Singh Toor et al. (2019) [34]	NetworkvStatus, Residual Energy, node location	Energy-Aware Cluster-Based Multi-hop (MEACBM), uses Subcluster formation and	The structure becomes complex and

		residual energy-based selection. Also Calculates efficient multi-hop routes for commination.	has network overhead due to sub-cluster formation processes
Somaye Jafarali Jassbi et al. (2019) [26]	Communication range, data packet size, residual energy, distance with sink	Backup Cluster Head (BCH) is selected after HEED CH selection based on minimum distance and maximum residual energy.	Overhead of HEED is deployed but not fully removed
Jin-Gu Lee et al. (2019) [27]	Objective Function, Homogeneous Energy, aggregation rate, Location	SSMOECHS protocol for CH selection based on sampling-based SMO by using the received information	Delay increases
Krishnasamy Gomathi (2019) [34]	The trust factor, Energy	Secure CH selection, fuzzy logic is used for selection of CH	More memory is required as you consider
Liang Zhao et al. (2018) [28]	ResidualvEnergy, Network Address	LEACH-M is an improved version of LEACH, a distributed approach used to find Optimal Solution	Delay increases
Adem Fanos Jemal et al. (2018) [13]	Energy and power consumption, and the packet loss	Uses k-mean to select initial cluster header and use Euclidean distance for CH selection	Network delay increases
Bilal Muhammad Khan et al. (2018) [10]	Data aggregation, member Nodes,	Selection is done by multi-conditional decision. Network robustness and effective network expectancy	Fuzzy logic in highly vagueness and sink mobility prediction is complex
Taj Rahman et al. (2020) [29]	Quality of Service (QoS)	Merge two ideas in MANET, first is cross-layer design and second is self-organization	The pre-specified version needs more memory
Payal Khurana Batra et al. (2016) [30]	Stability Period, Energy Consumption	Randomness is used in LEACH	Needs more cost function for prediction
Sachin Gajjar et al. (2014) [31]	Data aggregation, energy, BS location, Energy Consumption, reachability from its neighborhood,	CH selection protocol by using Fuzzy Logic (CHUFL), the selection is based on residual energy based on neighbor nodes.	Energy consumption is not so effective when the number of nodes increased
M. Senthil et al. (2014) [12]	The energy dissipated and the distance between the base station and the CH	Distance based CH selection between sink and CH. In this paper, cluster divides into semi-cluster that have less distance from the sink.	Network robustness effects
Tapan Kumar Jain et al. (2014) [5]	Residual Energy of neighbor nodes, unique nodes that connected to each node of the cluster	In this strategy, the CH is selected based on neighbor unique node connectivity. The selected CH fitness function is calculated. Then less distance with BS reflects the validity of CH.	This procedure has network delay
Chakchai So-In et al. (2013) [32]	Energy consumption, optimal weight	Uses moving energy window energy computation on previous LEACH algorithms and enhanced probability of CH.	Network robustness effects
P. K. Dutta et al. (2013) [9]	Network traffic, residual energy, remaining energy of node, the cost function for each node	Uses three parameters and select CH, initially CH is selected randomly, and then its remaining energy and cost fitness for CH is calculated. After that performance is measured by electing CH among these randomly selected CHs.	More memory is required for two way selection
Parul Saini et al. (2010) [21]	ResidualvEnergy, Distance With BS, Network Area	E-DEEC Algorithm uses for CH selection that is energy efficient and enhances the clustering	The death rate is very large

Table 2: Comparative study of parameters.

Reference	Reliability	Energy Consumption	Network Lifetime	Alive Node Per Round	Throughput
Pawan Singh Mehra et al. (2020) [3]	Dense	5J	✓	30%	✓
M. Senthil et al. (2014) [12]	Nearest Neighbor	1.6bJ	✓	7%	-
P.K. Dutta et al(2013) [9]	In terms of Cost Function	7J	✓	_-	✓
Tapan Kumar Jain et al. (2014) [5]	Stability	-	✓	48%	-
Amir Abbas Baradarana et al. (2019) [11]	Complexity	1.5J	✓	82%	✓
G Pius Agbulu et al. (2020) [14]	Latency	0.9bJ	✓	50%	✓
Thi-Kien Dao et al. (2020) [16]	Accuracy	4.7J	-	-	✓
Kashif Naseer Qureshi et al. (2020) [25]	Error Free	8.5J	✓	40%	✓

Amanjot Singh Toor et al. (2019) [33]	-	10J	✓	45%	✓
eeTMFO/GA (2020) [19]	effective and Secure	2.2J	✓	75%	✓
Sachin Gajjar et al. (2015) [31]	Latency	5J	✓	10%	✓
Somaye Jafarali Jassbi et al. (2019) [26]	Effective And Secure	4J	✓	38%	✓
Nader Ajmi et al. (2021) [18]	Efficiency	3J	✓	65%	✓
Ramadhani Sinde et al. (2020) [2]	Efficiency, Accuracy	11J	✓	17.50%	✓
Jin-Gu Lee et al. (2019) [27]	Accuracy	3J	✓	54%	✓
Bilal Muhammad Khan et al. (2018) [10]	latency, Mobility	0.08bJ	✓	_-	✓
D. Laxma Reddy et al. (2021) [23]	Scalable	12J	✓	56%	✓
Adem Fanos Jemal et al. (2018) [13]	Nearest Neighbor	3J	✓	34%	✓
Atefeh Rahiminasab et al. (2020) [24]	Mobility	2J	✓	65%	-
Payal Khurana Batra et al. (2016) [30]	-	5J	✓	54%	✓
Taj Rahman et al. (2017) [29]	Robust, Adaptive & Scalable	9J	✓	-	-
Krishnasamy Gomathi (2019) [34]	Secured	-	-	-	✓
Xin-She Yang et al. (2012) [15]	-	7J	✓	45%	_
Chakchai So-In et al. (2013) [32]	Adaptive	0-5% improved	✓	_	✓
Parul Saini et al. (2010) [21]	Energy	2J	-	25%	✓
Oluwasegun Julius Aroban et al. (2021) [23]	Energy	1.0891bJ	✓	70%	✓

Table 3: Simulation parameters.

Sr. No.	Parameters	Value
1	Number of Nodes	500
2	Sensed Area	500*500m^2
3	BS Coordinate	(250,250)
4	Initial Energy	0.28J
5	Length of data Packet	12000 bit
6	Elec(Elected Energy)	25nJ/bit/m^{-1}
7	efs (Free Space energy)	0.0013pJ/bit/m^4
8	emp()	20pJ/bit/m^{-2}
9	Number of Rounds1	20
10	Number of Rounds2	50
11	Number of Rounds3	100
12	Sense power	0.0175nJ/bit/m^2
13	Transmission power	0.744nJ/bit/m^2
14	Receiving Power	0.0648 nJ/bit/m^2

The Nucleus ***60***, *No. 1 (2023) 45-50*

www.thenucleuspak.org.pk

The Nucleus
ISSN 0029-5698 (Print)
ISSN 2306-6539 (Online)

Mechanical Design Verification of CHASNUPP Bottom Nozzle

Waseem*, Muhammad Arslan Anwer, Ashfaq Ahmad Siddiqui

Directorate General Nuclear Power Fuel, P.O Box No. 1847, Islamabad, Pakistan

ABSTRACT

The bottom nozzle is a critical component of the fuel assembly of 340 MWe PWR Nuclear Power Plant at Chashma site (CHASNUPP). It bears axial loads during fabrication, handling, transportation, and reactor operation. The perforated plate, containing flow-holes of complex orientation, is the main critical load bearing and supporting component of the bottom nozzle. Therefore, mechanical strength and stresses of the bottom nozzle need to be analyzed and tested under limiting load conditions, i.e., transportation load 6g. The present study is an attempt to develop the finite element (FE) methodology in order to assess the structural integrity and determine the maximum stress concentration area of the bottom nozzle at applied limiting load of 6g, at standard temperature and pressure (STP). The FE model of the bottom nozzle was produced by solid element (C3D8R) and solved by the static linear analysis using computer code ABAQUS/CAE 6.10-1. Final results acquired from the FE analysis are compared with the mechanical compression test results for mechanical design verification. The values of maximum stress calculated through FE analysis are much comparable with the stress values obtained from each strain gauge at similar locations, which confirmed the accuracy of the FE methodology. The value of the max. von-mises stress (Seqv.), obtained by the FE analysis, and max. value of the stress obtained through test, under applied load of 6g, are less than the design stress limit (yield strength) of bottom nozzle material, SS-321, thereby verifying its structural integrity as well as satisfying its mechanical design criteria under limiting load of 6g.

Keywords: *CHASNUPP, Bottom nozzle, Perforated plate, Finite element, Compression analysis, Stress measurement.*

1. Introduction

In Pressurized Water Reactor (PWR) the Fuel assembly bears a variety of loads, such as compressive, tensile, torsional impact and bending etc., Moreover, the other external load as shipping, handling and reactor operation. The buckling structural strength of the fuel assembly is provided by the fuel assembly skeleton [1]. Bottom nozzle is a square box like structure which serves as the bottom structural element of the CHASNUPP fuel assembly. It consists of a perforated plate, four enclosure plates, and four bearing pates as shown in Fig 1.

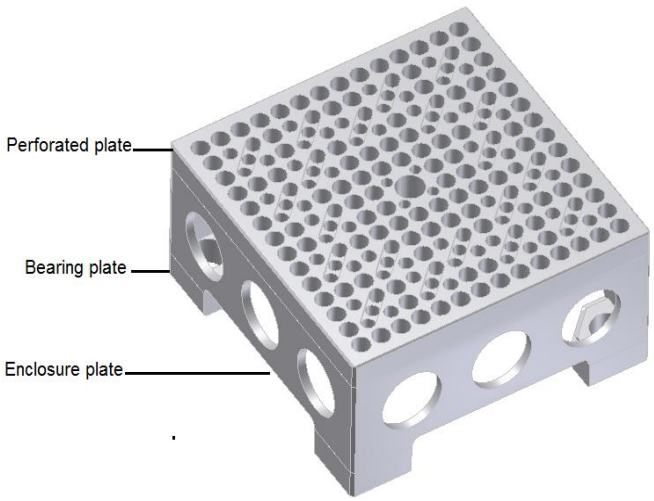

Fig. 1: Bottom nozzle of CHASNUPP fuel assembly.

The perforated plate has square cross-section, which is provided with number of holes to permit flow of coolant upward through the bottom nozzle, as well as provides connection to the bottom ends of the guide thimbles at respective hole positions through bolts.

Four enclosure plates are welded to the perforated plate to form a plenum. One bearing plate is welded at each corner of the plenum to form the bottom nozzle subassembly. Bearing plates act as supporting pads of the bottom nozzle. Each bearing plate has a hole that can mate with lower core plate pin for indexing and positioning of the fuel assembly.

During reactor normal operation entire weight of fuel assembly and associated core components passes to lower core plate through bottom nozzle. Moreover, the perforated plate has to bear axial loads during transportation and handling of fuel assembly. Among all axial loads, the load during transportation is considered as the limiting one [2]. Thus mechanical tests and finite element (FE) analysis for the CHASNUPP fuel assembly and components are needed for determination of structural integrity against such loads.

For this purpose, a FE model of bottom nozzle has been produced to evaluate the mechanical strength and stress concentration areas. Its static linear analysis has been performed using ABAQUS, CAE 6.10-1 software. The strength test of the bottom nozzle has also been conducted by SNERDI, China [3] to determine local stresses in the X and Y directions (axes in the plane of plate) at specified locations. The bottom nozzle test specimen was manufactured from stainless steel (SS-321). The details of material properties used for the test specimen and FE model are given in Table 1.

Table 1: Material properties of bottom nozzle at room temperature [4]

Material	Yield strength (MPa)	Tensile strength (MPa)	Modulus of elasticity (GPa)	Poisson's ratio (γ)
Bottom nozzle (SS 321)	≥ 205	≥ 515	200	0.3

*Corresponding author: wazim_me@hotmail.com

We have already made attempts towards research and design work of CHASNUPP fuel assembly. Our experience includes structural integrity assessment of the CHASNUPP fuel assembly and associated components, i.e. stiffness and stress measurement of the spacer grid support system using ANSYS Code [5], study of the buckling or deformation behavior as well as the stress has been determined across the fuel assembly at compression load using ANSYS Code [6], and study of the deformation behavior and the stress measurement of the skeleton of fuel assembly using ANSYS Code [1]. Moreover, Chen [7] had reviewed 300 MWe Qinshan fuel assembly and associated core components design and proposed some modification. Now, in the present study, we have performed FE analysis for CHASNUPP bottom nozzle using analytical code ABAQUS, CAE 6.10-1. The details of present analytical and experimental work along with the results are described in the subsequent sections.

2. FE model

The bottom nozzle of fuel assembly has symmetry in the cross section. The boundary conditions symmetry is true in geometry, loads, constraints and material properties. Therefore, the advantage of symmetry has been taken into account and only quarter part of the bottom nozzle has been simulated and analyzed. The solid model is illustrated in Fig. 2.

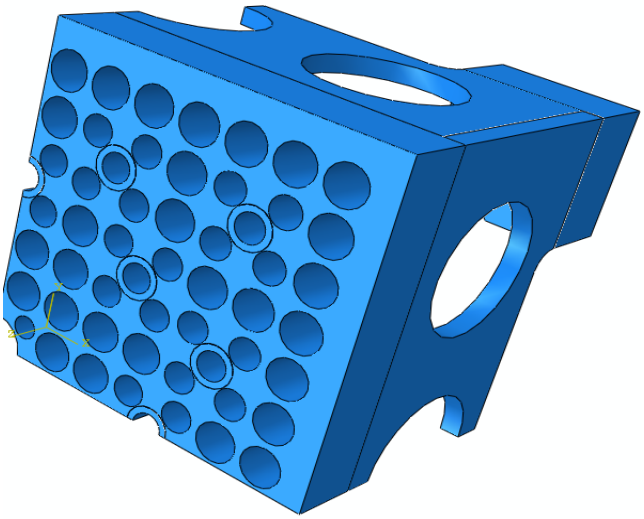

Fig. 2: Solid model (volume plot 3-D).

The FE model of the bottom nozzle has been developed using ABAQUS to simulate the applied boundary conditions, which prevail during transportation. The solid element C3D8R type is used to generate meshing of the geometry.

C3D8R is a 3D element having 8-nodes and reduced integration points (computationally inexpensive) with six degree of freedom at each node, well-suited for geometrically linear or non-linear, large strain, displacement and rotation problems.

The symmetry of the geometry has been applied at all nodes associated with inside edges of quarter portion of the bottom nozzle. To constraint the FE model nodes associated with bottom surface of the bearing plates are fixed. The load has been applied on the upper surface area associated with the guide thimbles. The weight of fuel assembly is 450 kg or ~4410 N. The load has been applied in step multiples of 1g. Maximum applied load equivalent to 6g (26460 N) is distributed uniformly on 20 holes for the guide thimbles. The FE model with all boundary conditions is shown in Fig. 3.

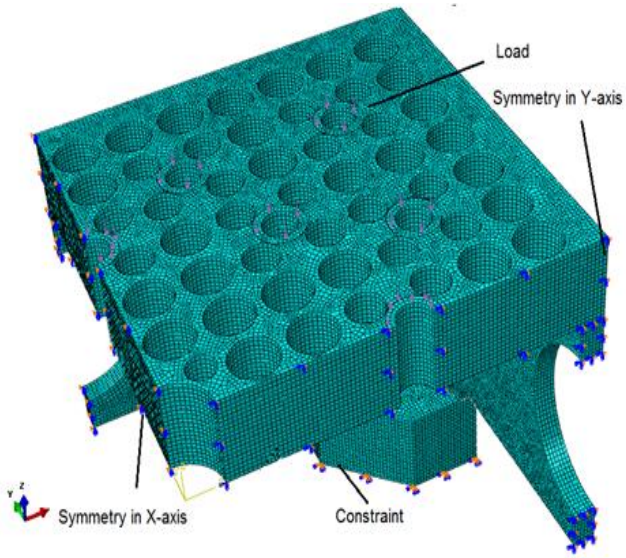

Fig. 3: Applied boundary conditions (element plot 3D).

3. Numerical results

1. A high mesh refinement level based on sensitivity analysis has been applied to final FE model at which results are converged.
2. The max. elemental Seqv, 128 MPa, is located at upper surface of the perforated plate, near the edge of the instrumentation tube flow hole, which is the stress concentration area, as shown in Fig. 4. The Seqv. value 128 MPa is less than the yield strength of the bottom nozzle material, 205 MPa [4], fulfilling the structural integrity criterion. The min. elemental Seqv, 0.03 MPa, is located at the corner of the bottom nozzle.
3. Maximum tensile stress at Y-direction, 84.39 MPa, is located at the bottom surface of the perforated plate and near the edge of the instrumentation tube flow hole as shown in Fig. 5.
4. The max. compressive stress in Y-direction, -88.4 MPa, is located near the joint of bearing plate and enclosure plate as illustrated in Fig. 6.

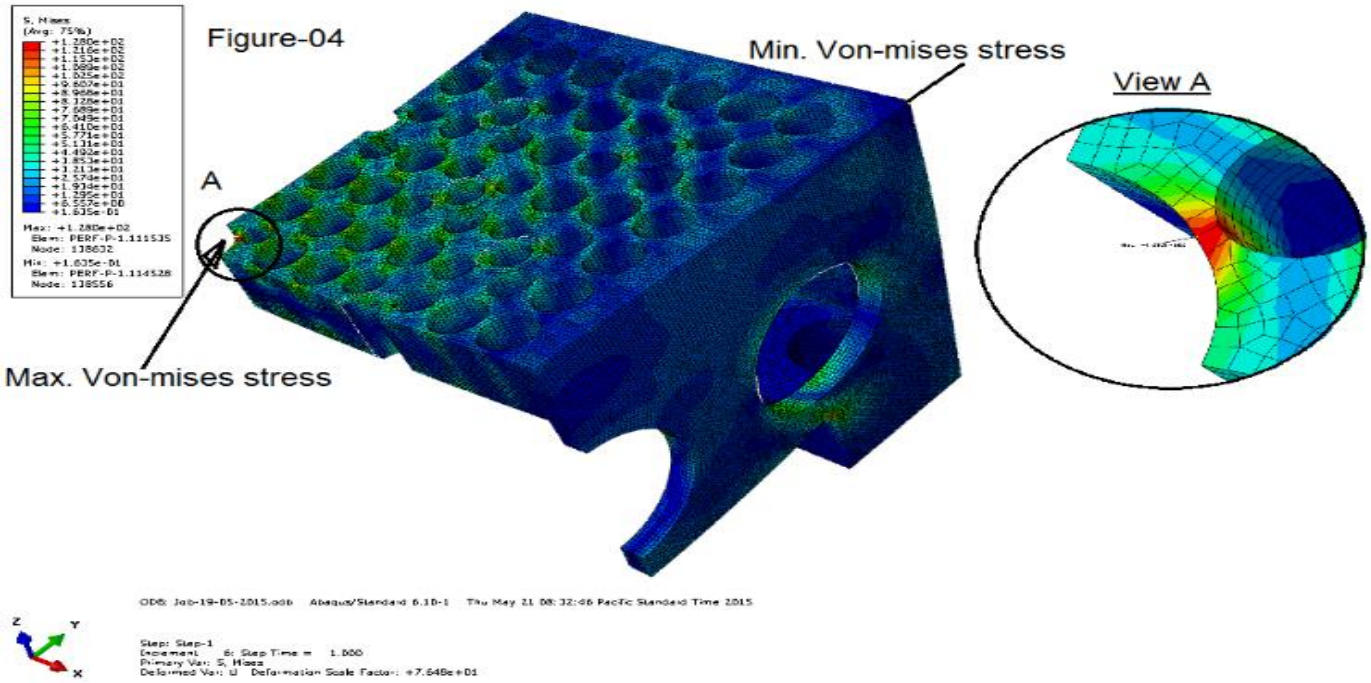

Fig. 4: Plot of elemental von-mises stress.

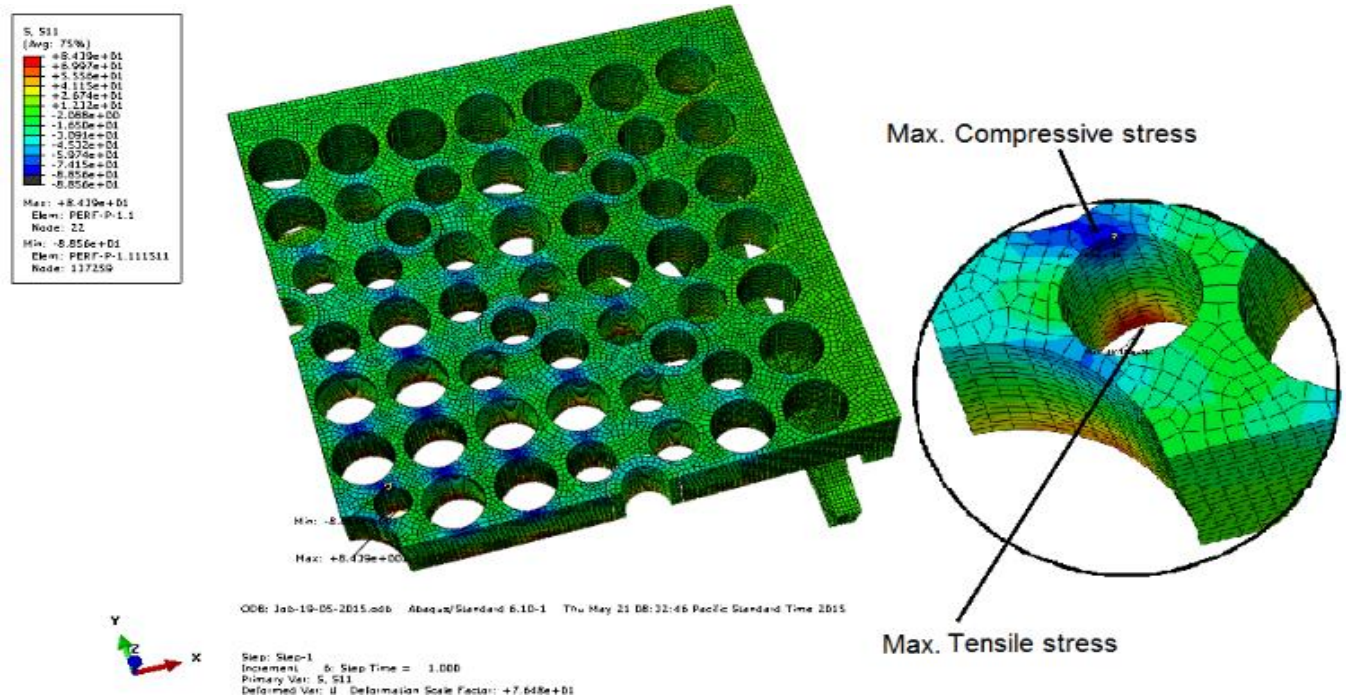

Fig. 5: Plot of elemental stress along x-direction.

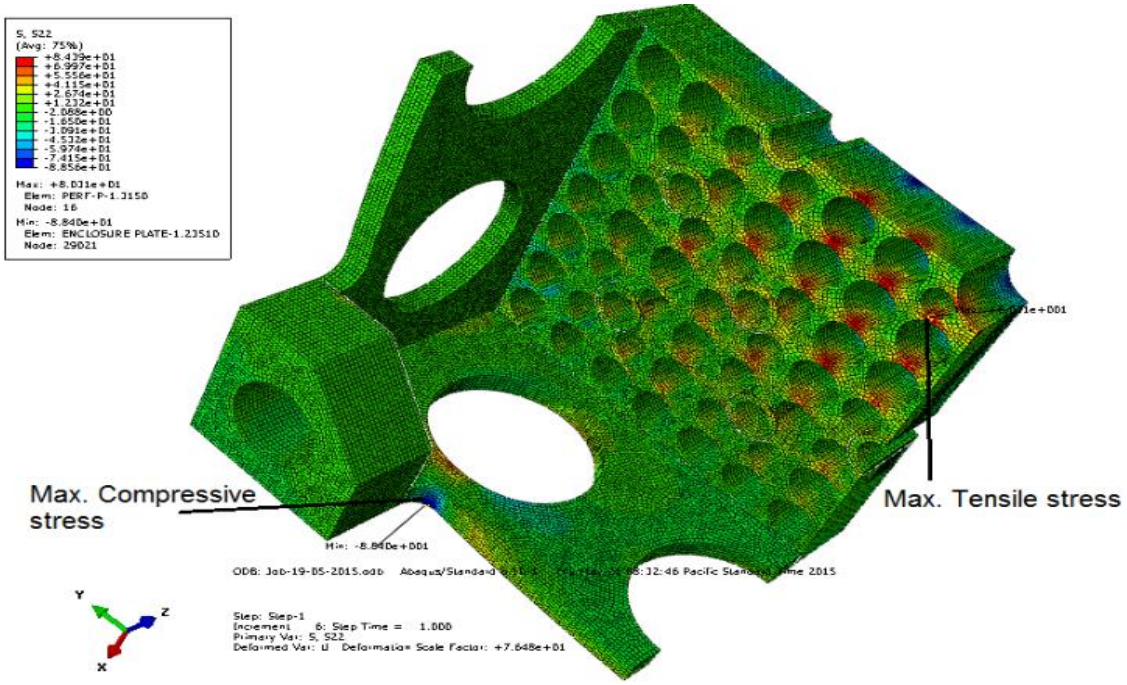

Fig. 6: Plot of elemental stress in y-direction.

4. Experimental work

The Mechanical (compression) test has been performed to measure the strength of bottom nozzle under the applied load of 6g (26460 N). This load is considered as the maximum limiting load on the CHASNUPP bottom nozzle. There is a symmetrical loading condition on the bottom nozzle in all respects. The structural design of the bottom nozzle is also symmetrical. Therefore, $1/8^{th}$ of the bottom nozzle is selected for the test measurements, to save the data analysis time and to facilitate the installation of strain gauges, as there is a space limitation for the gauge pasting and taking out the lead-wires safely.

5. Design and fabrication of test specimen

In order to perform test, the bottom nozzle test specimen has been designed considering as the structural part of a 15×15 CHASNUPP fuel assembly. For applying the load at the guide thimbles locations as per actual fuel assembly, 20 guide thimble tubes are connected with loading plate by using argon arc welding.

These guide thimbles along with the loading plate are tightened with perforated plate, using bolts after inserting through their respective holes and locations as per actual conditions. The bottom nozzle test specimen has been manufactured using the same material (SS 321) and dimensions as per actual fuel assembly. All of these parts are assembled to simulate actual bottom nozzle of CHASNUPP fuel assembly as shown in Fig. 7.

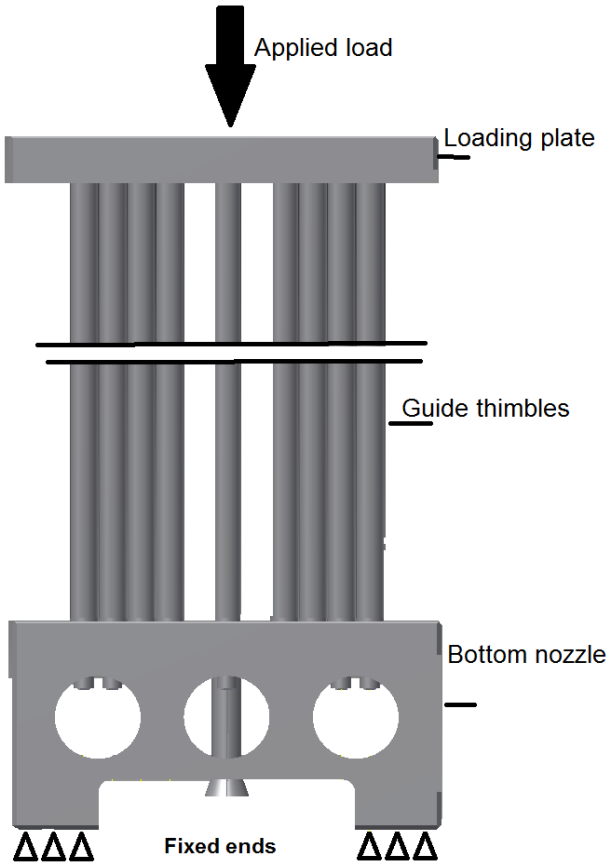

Fig. 7: Bottom nozzle test specimen.

Test Description

1. Mechanical (compression) test of the bottom nozzle has been performed at SNERDI, China [3]. The strain gauges of very small size of dimension 1mm × 1mm have been used for measurement of the strain during the test. These gauges are pasted on the 1/8th top surface of the perforated plate. The compression load is applied through a computerized Universal Testing Machine (UTM). Its calibration and verification has been performed as per ASTM Standard [8] and strain values on the bottom nozzle have been calculated from the strain data obtained from the Data Acquisition System.
2. Total 22 biaxial strain gauges have been used for the test of bottom nozzle to obtain strain data from 22 locations. All these gauges have been installed on the compression (upper) side of perforated plate. The critical 22 locations, where it is desired to measure the stress values, are shown in Fig. 8.

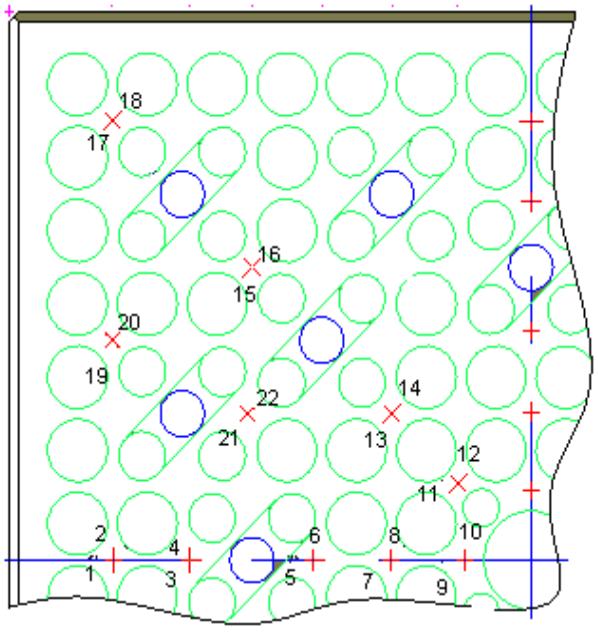

Fig. 8: Arrangement and orientation of the gauges on test specimen.

3. The bottom nozzle compression test is performed at room temperature in air. The load is applied on the test specimen in small steps of load 1g (4410 N). The data acquisition system is attached with the strain gauges, installed at the specified locations on the specimen, to attain the test data in the form of strains. The strain data has been further processed manually to get stress values using principal stresses formula [9].

7. Experimental Results and Discussion

1. The results of three strain gauges, Nos.1, 10 and 19, are not included in the study, as they are located in the low stress concentration areas and have small stress values, i.e. $\leq \pm$ 3.11 MPa. However, absolute error of the results (both FE and test) is also low for these strain gauges.
2. The value of the local stress obtained by the FE analysis at each strain gauge location is compared with the experimental result [3] obtained at the same location, as mentioned in table 2.

Table 2: FE and test results Comparison at load of 6g (26460 N).

Gauge No.	Stress (MPa)		% Error
	FE Analysis	Test	
2	-14.2	-12.1	14.7
3	-9.83	-9.92	-0.9
4	-22.2	-19.63	11.7
5	-21.8	-24.91	-14.2
6	-19.02	-22	-15.6
7	-25.84	-29.51	-14.1
8	-24.04	-22	8.5
9	-7.5	-8.6	-14.6
11	-18.38	-18.5	-0.6
12	-14.83	-14.4	2.9
13	-30.49	-30.2	0.9
14	-19.94	-16.8	15.7
15	***-37.18***	***-33.2***	***10.7***
16	-20.6	-17.43	15.5
17	-23.88	-21.8	8.7
18	-24.03	-23.32	3.0
20	-11.32	-10.6	6.4
21	-16.8	-18.81	-11.9
22	-26.65	-23	13.7

**Error= (Test-FE analysis)/Test×100*

3. It is clear from table 2, that the values of stresses obtained through FE analysis are comparable with the test values at most of the strain gauges locations. The errors between the two studies lie within the range of ±15.7%, which indicates the validity of the FE model.
4. Some dispersion in the experimental results mainly caused due to the allowance of the specimen over all height and thickness / flatness of the perforated plate. All strain gauges are pasted on the perforated plate which has too many flow holes due to the very limited available solid area it was very difficult to placed strain gauges there hence it may also cause some error.
5. The value of max. principal stress, -37.18 MPa, is obtained at strain gauge No. 15, at the same location of the FE result, i.e. -33.2 MPa (see Table 2). The max. principal stresses obtained through both studies are comparable and lie within the error of 10.7%.
6. The max. Seqv obtained by the FE analysis, 128 MPa, is obtained at the top surface of the perforated plate, near the edge of instrumentation tube flow hole. The test result is not available for the same location because pasting of the gauge at this location is not possible. Therefore, at this location the stress value determined by FE analysis cannot be compared with the test result. However, the max. Seqv, 128.9 MPa obtained by FE analysis is significantly less than the design

stress limit of the material, i.e., 205 MPa in case of SS 321 material, at room temperature.

8. Conclusions

The present study involved assessment of the structural integrity and determination of the stress concentration area of the bottom nozzle subassembly at load of 6g. The following conclusions have been drawn.

1. The max. stress values of both studies are in good agreement and significantly smaller than the limit of design stress of the bottom nozzle, thus bottom nozzle strength has safely fulfilled its mechanical design criterion at limiting load of 6g (26460 N).
2. The developed FE methodology can be utilized for evaluation of the designs changes in the bottom nozzle of CHASNUPP fuel assembly before conducting the confirmatory tests. Therefore, this analysis is useful for refining the safety and reliability of supplementary design modifications such as different material, minor changes in the geometry, etc.

References

[1] Waseem, N. Elahi, G. Murtaza and A.A. Siddiqui, "Structural integrity assessment and stress measurement of CHASNUPP-1 Fuel assembly skeleton", Int. J. Nucl. Eng. Des. vol. 266, pp. 55-62, 2014.

[2] Y. Zhang, et al. *Fuel Assembly Design Design Report*,SNERDI, China, 1994.

[3] SNERDI Tech. Doc., *Mechanical Strength and Calculation for Fuel Assembly*, Techanical Report, F3.2.1, China, 1994.

[4] *Specification for Stainless and Heat-Resisting Chromium-Nickel Steel Plate, Sheet, and Strip*, ASTM Standard A 167-82, 2013

[5] Waseem, N. Elahi, A.A. Siddiqui and G. Murtaza, "Fuel rod-to-support contact pressure and stress measurement for CHASNUPP-1(PWR) fuel", Int. J. Nucl. Eng. Des. vol. 241, pp. 32-38, 2011

[6] Waseem, N. Elahi, G. Murtaza and A.A. Siddiqui, "Structural integrity assessment and stress measurement of CHASNUPP-1 Fuel assembly", Int. J. Nucl. Eng. Des. vol. 280, pp. 130-136, 2014

[7] YU. Chen and YI. Jing, "Review and Prospect for 300 MWe fuel assembly design improvement in China, Proceedings of a technical meeting, Cadarache", IAEA-TECDOC-1454, France 22-26 November, 2004, pp. 179-187,

[8] *Practices for Force Verification of Testing Machines*, ASTM Standard E 0004-03, 2005.

[9] *Boiler and Pressure Vessel Code*, ASME Standard Section III, Division 1, Subsection NB, Article NB-3000, 2001.

The Nucleus ***60***, *No. 1 (2023) 51-55*

www.thenucleuspak.org.pk

The Nucleus
ISSN 0029-5698 (Print)
ISSN 2306-6539 (Online)

Value Addition in Gemstones by Nuclear Techniques

Waqar Ahmed Butt*, Fawad Mohyuddin

Pakistan Nuclear Society, Islamabad, Pakistan

ABSTRACT

Northern areas of Pakistan are rich in minerals and different types of precious/ semi-precious gemstones. One of these gemstones called topaz is quite abundant in Gilgit-Baltistan, Skardu and Kashmir regions. Although, topaz is a semi-precious stone but pink topaz from Mardan district in KPK province has a high worth in its natural form because it is rare in the world. In general, topaz is a colorless transparent stone, which is not very expensive. These semi-precious stones can be made precious by adding colors using different treatments like thermal heating, electron beam exposure, gamma rays or neutron irradiations. Except for electrons and neutrons, all other treatments give brown, golden or light blue colors, which are of low worth. The colors are usually not stable and fade away with the passage of time. About 30-40 times value can be added if the color is persistent dark blue. This deep blue color in topaz can be produced by neutron irradiation from a nuclear reactor. At present, for semi-precious stones, the world market is in the hands of blue topaz; typically named as Sky blue, Swiss blue and London blue. Countries like Indonesia, Thailand and US are already in this business and making significant profit. Pakistan Research Reactor (PARR-1) at the Pakistan Institute of Nuclear Science & technology (PINSTECH) has the capability to produce these desirable colors. Therefore, handsome revenue can be generated by utilizing this methodology. Apart from this, the other benefits are the development of a useful technology, collaboration between public and private sectors and application of nuclear techniques for peaceful purposes, which is one of the objectives of Pakistan Nuclear Society (PNS).

Keywords: *Topaz, color formation, research reactors, neutron irradiations, radioisotopes, elemental analysis*

1. Introduction

History reveals that different types of gemstones were regarded as a status symbol. Since ancient times, kings and queens used to wear gems embedded in gold for their grandeur and beauty. The royal families had a hobby to collect attractive gems like diamonds, ruby, sapphire, emerald, tourmaline, aquamarine and topaz etc. People attach particular stones with their good fortune and believe that the use of these stones have impact on their lives. Therefore, the business of precious stones has always been considered as profitable one. Various types of such precious and semi-precious stones are found in different areas of Pakistan mainly in the metamorphic rocks of mountainous regions Fig. 1. These are found in Northwest Frontier Province (Deer, Swat, Mansehra and Peshawar), Federally Administered Tribal Areas (Mohmand Agency, Bajaur Agency, Khyber Agency and Waziristan Agency), Northern Areas (Chilas, Gilgit, Mardan, Hunza, Shigar, Baltistan, Kashmol etc.) and in Balochistan Province (Kharan and Chaman) [1]. Some of these gemstones have inherent worth in their natural form while others can be made valuable by various color enhancement processes. Such gemstones are labeled as 'treated stones'. In general, the value of gemstones depends upon 4 Cs': color, clarity, cut and carat. The utmost important is of color, which can be induced by thermal heating, diffusion, coatings, bleaching and irradiation methods that include X-rays, gamma rays, electrons and neutrons. Except for neutrons, the induced colors are usually temporary. The research reactor at PINSTECH can serve this purpose, as it is a huge source of neutrons.

For this study, topaz was chosen due to the interest of gemstone dealers and exporters. This is mainly due to the big difference in price of natural and treated gemstones. The name

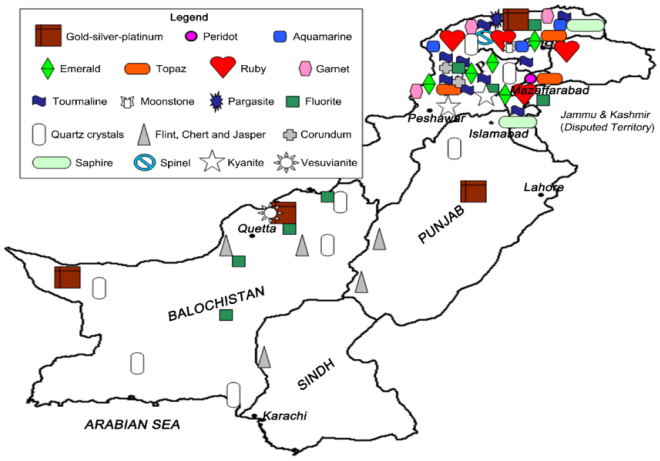

Fig. 1: Main areas of gemstones in Pakistan.

'topaz' is derived from the Greek Topázios (Topasos); old in the, which was famous for mining of yellow stone in ancient times. Alternately, it is believed that the topaz originates from Sanskrit word '*tapash*' due to the fire like appearance of golden topaz in sunshine. Worldwide, it is found in Afghanistan, Sri-Lanka, Czech Republic, Germany, Norway, Italy, Sweden, Japan, Brazil, United States, Mexico and Pakistan [2].

Topaz is an aluminum silicate with fluorine and hydroxyl ions having chemical formula $Al_2SiO_4(F,OH)_2$. Some general properties of topaz are given in Table-1 [3]. Both the main elements Al and Si do not cause induced activity problem but impurities with high capture cross sections may create problems when exposed to neutrons. Elemental analyses reveal that topaz from different mines may contain impurities like Mn, Sc, Co, Cs, Ta etc. Therefore, thermal neutrons are considered as undesirable as they activate metal impurities

*Corresponding author: waqaraaabutt@gmail.com

present inside the materials. To minimize their effect, strong absorbers like cadmium, indium and gadolinium is used to protect the material from thermal neutrons. Topaz changes its color due to formation of color centers (F-Centers) which are formed by bombardment with fast neutrons [4-8].

Table1: General Properties of Topaz

Chemical Formula:	$Al_2SiO_4(F,OH)_2$
Empirical Formula:	$Al_2(SiO_4)F_{1.1}(OH)_{0.9}$
Class	Silicates
Environment:	High temperature quartz veins and cavities in granites
Name Origin:	Named after its locality: Topasos Island in the Red Sea
Synonym:	Yellow stone

Most insulator crystals and pure alkali halide crystals are transparent to visible light. However, when irradiated, these crystals appear to be colored due to the selective absorption of some component of visible spectrum by certain imperfections, which are usually present in the crystal. Thus a color center is a lattice imperfection (or defect like vacancies) which absorbs visible light. The light of some specific wavelength gets absorb while the remaining part transmits through the material that causes the colored appearance. The transmitted beam received by our eyes contains only the remaining colors [9-16].

F-type color center formation is the reason of coloring in topaz. Fig. 2 is of a fluorite structure containing an 'F-center' where a fluorine ion has been replaced by an electron. The name F-center is from the German word for color, *farbe Farbenzenter'*, as crystals containing these point defects are highly colored. These defects have been investigated by various spectroscopic techniques. The F-centers are point defects and can be readily formed in alkaline halides with the help of ionizing radiation, such as a Tesla coil or X-ray source [17].

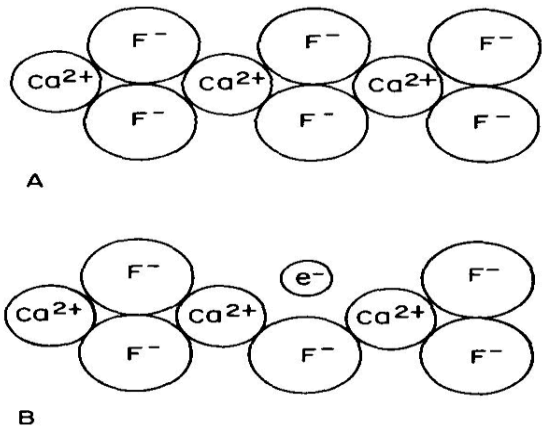

Fig. 2: Fluorite structure: (A) normal, (B) containing an 'F-center' where a fluorine ion is replaced by an electron.

2. Experimental

As pre-experimental arrangement, the surface of each stone was thoroughly washed in a standard decontamination soap solution, wiped with clean cloth and dried in air. First of all, raw topaz pieces were analyzed to see whether there was any radioactive element in the original material. For this purpose, gamma-ray spectroscopy system based on a high-purity germanium (HPGe) detector with associated electronics comprising of a Multichannel Analyzer was employed. The system was calibrated by using the standard Co-60 and Eu-152 sources from IAEA. The peak energies and the calibration spectrum of Eu-152 source is shown in Fig. 3.

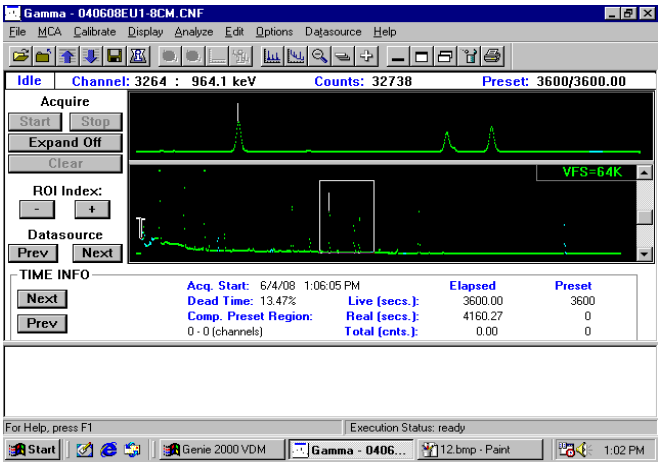

Fig. 3: Calibration of the detector using Eu-152.

The elemental analysis revealed that there was no radioactive impurity in any sample and its spectrum was the same as for background level of the laboratory where the analysis was performed Fig. 4.

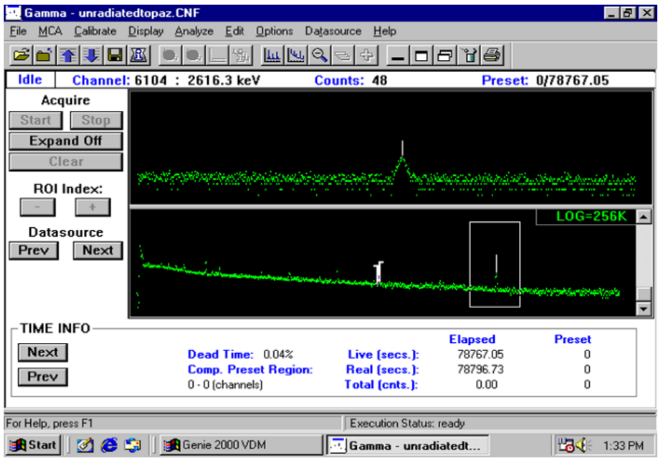

Fig. 4: The spectrum of raw topaz samples.

After that, a few pieces of topaz from Gilgit area, obtained with the courtesy of Gems and Gemology Institute, Peshawar were selected for irradiation inside the reactor core. For that initial attempt, two containers were used. A standard plastic (polyethylene) capsules for shorter time (less than one hour) used in pneumatic rabbit system of PARR-1 as shown in Fig. 5a and a high purity, reactor grade Al capsule for in-core irradiation as given in Fig. 5b.

Fig. 5a: Plastic capsule

Fig. 5b: Al capsule

A sheet of pure Cd (1mm thick) was placed inside the Al container to reduce the effect of thermal neutrons which were undesirable for this study. Similarly, the samples placed in the plastic container were wrapped with a thin sheet of Cd. The samples in plastic capsules were irradiated for 10 seconds and then 45 minutes whereas the samples in Al capsules were irradiated for 12 hours along with IAEA standard SL-1.

3. Results and Discussion

The main objective of this study is to analyze the changes that would occur in Pakistani topaz specifically from Gilgit area after irradiation with neutrons from PARR-1. These stones are originally transparent but can be colored with various treatments like electron beam heating, gamma radiations and neutron exposure. Prior to it, no work has been reported by utilizing neutrons. The study was carried out on topaz stones from different areas for different irradiation times.

3.1 Topaz irradiated for 10 sec

A few pieces of topaz stones (4-8 gm each) wrapped in 1 mm thick Cd sheet were put in plastic capsule and sent inside the reactor core through a pneumatic rabbit system. The neutron flux ~$5x10^{13}$ n/cm^2/sec turned colorless stones to brown. The overall doze on the lot was ~25 mSv. The plot of counts vs. energy is shown in Fig. 6. No residual activity was observed for irradiation of 10 seconds.

3.2 Topaz irradiated for 45 minutes

The same stones were reused in plastic capsule with Cd lining for 45 minutes. The neutron flux was the same. The sample kept in the pool for 2 days so as to reduce the induced activity. The capsule was opened in the hot cell by remote handling. It was found that there was not much activity in the stones (< 2 nCi/g). The color of all the samples changed to golden brown. The samples were taken to the analytical lab for elemental analysis. Negligible impurities were found in small concentrations. Fig. 7 is the plot of gamma ray spectra of topaz after irradiation for 45 minutes.

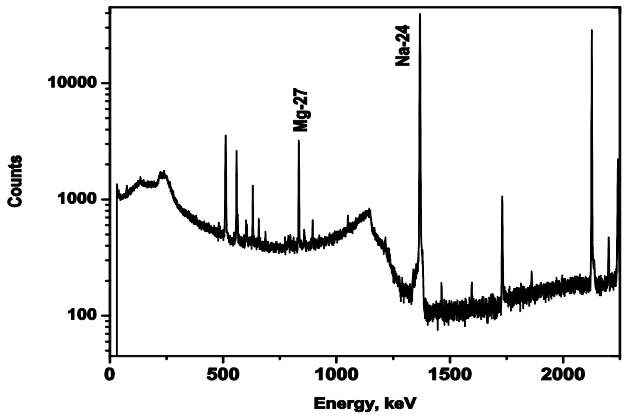

Fig. 6: Count verses energy plot for 10 sec.

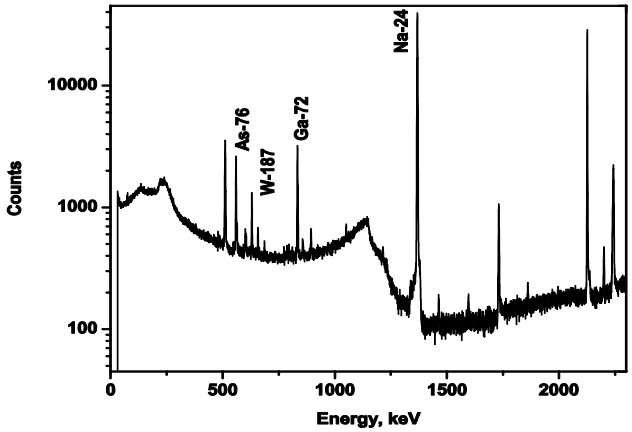

Fig. 7: Counts verses Energy plot for 45 min.

3.3 Topaz irradiated for 12 hours

Two pieces of topaz were packed in a standard Al capsule with Cd lining and sent for irradiation inside the core in a water-box channel where the neutron flux was quite high (~$2x10^{14}$ n/cm^2/sec). The samples were kept in the reactor pool for 2 days so that the induced activity went down. Capsule was cut in the hot cell by remote handling. It was found that there was not much activity in the stones. Some radioactive impurities (Cs-134, Ta-182 and Sb-124) were found in small concentration. Both the stones turned dark blue. The gamma ray spectrum and energy plot of topaz samples are presented in Fig. 8 and Fig. 9.

A detailed study on elemental analysis of topaz obtained from different places in the Northern areas of Pakistan was performed by Wasim et al [18]. They identified trace-level impurities of 22 elements after irradiation of topaz samples for different time intervals. Many of these were common impurities usually found in topaz depending upon the place from where these were obtained. Most of the impurities were the same as observed in this study. However, the focus was on long-live radioisotopes.

Ashbaugh [19] observed activity produced from the radionuclides of trace-element impurities such as Fe, Mn, Co, Zn, Sb, Ta, Cs, Sc and Tb. However, we did not find Mn, Co, Zn and Tb having longer half-lives.

A photograph of the stones irradiated for different times is given in Fig. 10. (Also provide photo of Topaz with no irradiation)

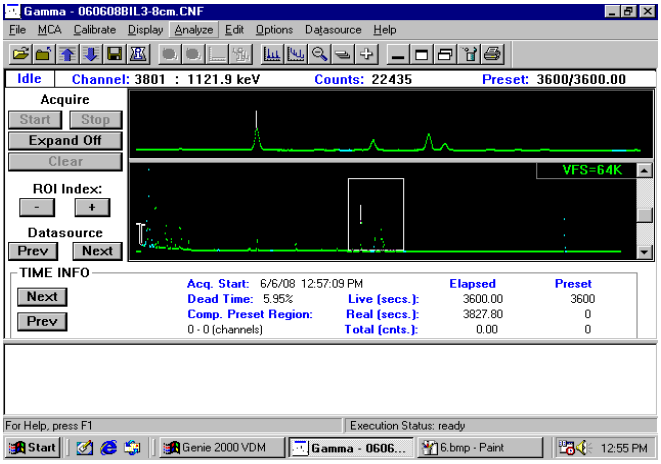

Fig. 8: The spectrum of topaz for 12 hours.

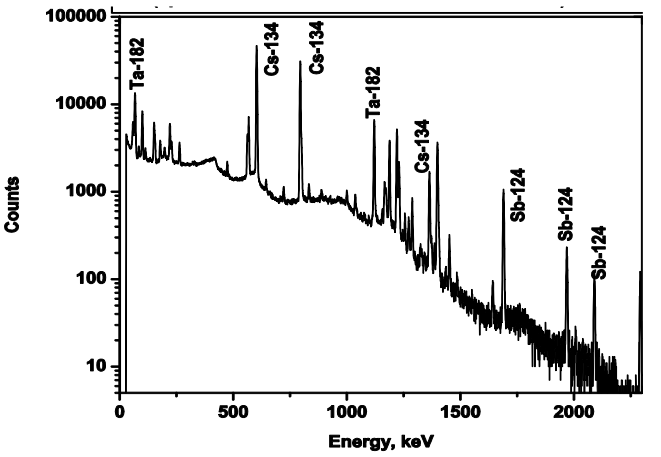

Fig.9: Counts verses Energy plot for 12 hours.

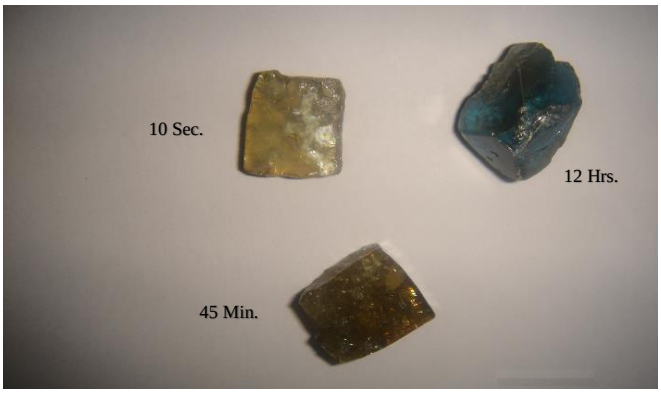

Fig. 10: Photograph of the stones for different irradiation times.

Table 2: Activity after 12 hrs irradiation

Radio-Isotopes	Half Half-life	Energy (keV)	Activity (Bq)
Sc-46	83.8 d	889	5.12E+03
Sb-124	60.2 d	1690	7.96E+05
Cs-134	2.06 y	603	3.72E+06
Ta-182	114.41 d	1120	1.49E+05

3.4 Irradiation of topaz in bulk

A visit to topaz mines was arranged with the logistic support from Pakistan Atomic Energy Commission (PAEC) and financial assistance from Pakistan Science Foundation (PSF). Hence, topaz stones in bulk quantity were purchased from the mining areas in Gilgit and Skardu. Actually, topaz is very similar to quartz and difficult to distinguish with naked eyes. Consequently, in the local markets it is sold mixed with quartz. To ensure its originality, the stones were purchased directly from the mines.

For large scale irradiations (material in kg), special containers of reactor grade pure aluminum sheets were designed and fabricated at the General Services Division (GSD) of PINSTECH. Pure cadmium sheet of 1 mm thickness was used as inside lining to minimize the effect of thermal neutrons. The container system called stringer is shown in Fig. 11. The material was then exposed to neutrons at a convenient position just outside the reactor core in high neutron flux. Generally, a high quality color enhancement in topaz occurs at a neutron fluence of 10^{17} n/cm^2, which can be achieved in 12-20 hours of reactor operation even if the fast flux is ~$2x10^{12}$ n/cm^2/sec.

Zhang, et al [20] observed that the color centers in topaz were produced after 12 hours of irradiation at 1.2×10^{19} neutrons/cm^2/sec. They irradiated the samples in a light water nuclear reactor at China Institute of Atomic Energy in Beijing. The samples were placed in cadmium-lined containers to reduce the amount of thermal neutrons caused by absorption and also to increase the amount of fast neutrons. They obtained deep blue color (London blue) in this process. Most of the samples could be handled after 95 days.

The gemstones irradiated in this process could be handled ideally after 3 months but to release in the market may take two years. This is because the dose level must be less than 2nCi/g (74Bq/g) according to the international regulations set by International Air Transportation Agency (IATA).

In the reactor run of 12 hours at 10MW, the stones were checked from a safe distance as the activity was much high and it was observed that the color of the stones was not dark blue. Apparently, it was deep sky blue with olive green shade. Therefore, the stones were kept inside the reactor pool at the specified position for the next reactor run after one week.

It is to mention that the PARR-1 reactor mainly operates for the production of radioisotopes for nuclear medical hospitals in

Fig. 11: Aluminum containers with Cd sheet inside.

the country and not exclusively for gemstones coloring purposes. However, after the 2nd reactor run of 12 hours at full power of 10 MW, all the stones turned dark blue. Since the residual activity was quite high, therefore, the material was kept inside the reactor pool for 3 months. After that the stringer containing topaz gemstones was shifted to the hot cell where the stones were poured into another container. Two representative samples were taken to the analytical lab where the elemental analysis was performed. It was found that the results were exactly the same as for the samples previously irradiated for 12 hours in Al capsule inside the reactor core. Therefore, the experimental study revealed that London blue topaz can be produced in bulk quantities by neutron irradiations of about 20 hours.

4. Conclusion

Pakistani topaz purchased from mining areas in Gilgit region was originally transparent and was not radioactive in raw form. After 10 seconds irradiation, its color changed to light brown and no radioactivity was found. Samples irradiated for 45 minutes changed color to golden brown and negligible activity was observed. The 12 hours irradiated samples turned dark blue. The elemental impurities like Ta-182, Cs-134, Sb-124 and Ag-110 were identified by using elemental analysis system based on high precision gamma ray spectroscopy system. Due to the longer half-lives of some of these radioisotopes, sufficient time was given to decrease residual activity below the prescribed limits. The activity was in the range of micro-curies. In the case of bulk irradiation, the activity was too high. After two reactor runs of weekly 12 hours operation, it was observed that about 20 hours of exposure with neutrons is required to change transparent topaz to dark blue. Due to the formation of long lived radioisotopes, the material in bulk quantity had to be kept inside the reactor pool for about 3 months and subsequent cooling of many months to attain the permissible limits for taking into the market. However, a huge amount of foreign exchange can be earned by export of these treated gemstones. This can be achieved by taking all the stake holders involved in this business on board.

References

[1] Pala International, "Pakistan's gemstones: An Overview", Live Oak Park Road, USA, 2008
URL:http://www.palagems.com/pakistanoverview.

[2] C.S. Hurlbut and C. Klein, "Manual of Mineralogy", John Wiley and Sons Ltd, 20th edition, ISBN 0-471-80580, 1985.

[3] Mineralogy Database, "Topaz mineral data", Themes Valley Minerals, Morocco, 1990 URL:http://www.webmineral.com/data/topaz.shtml

[4] W. Ying and G.Y. Bao, "Research on radiation-induced color change of white topaz", Radiation Physics and Chemistry, vol. 63, pp. 223-225, 2002.

[5] L. Pauling, "The crystal structure of topaz", Proceeding of the National Academy of Sciences, USA, vol.14, 1928.

[6] D.N. da Silva, K.J. Guedes, M.V.B. Pinheiro, J.M. Spaeth and K. Krambrock, "The microscopic structure of the oxygen–aluminium hole center in natural and neutron irradiated blue topaz", Physics and Chemistry of Minerals, vol.32, pp. 436-441, 2005.

[7] K. Krambrock, L.G.M. Ribeiro, M.V.B. Pinheiro, A.S. Leal, M.A. de Barros Correia Menezes and J.M. Spaeth, "Color centers in topaz: comparison between neutron and gamma irradiation", Phys. Chem. Minerals, vol. 34, pp. 437-444, 2007.

[8] T. Rauch and M. Würtenberger, "Method of coloring cut gemstones", US Patent, 7033640, 2006.

[9] K. Nassau, "The origins of color in minerals", American Mineralogist, vol. 63, pp. 219-229, 1978.

[10] K. Nassau, "The Physics and Chemistry of Color", Wiley, New York, 1983.

[11] K. Krambrock, M.V.B. Pinheiro, K.J. Guedes, S.M. Medeiros, S. Schweizer and J.M. Spaeth, "Physics and Chemistry of Minerals", vol. 31, pp. 168, 2004.

[12] M. A. Wahab, "Solid State Physics", 2nd Edition, Narosa Publishing House, India, 2005.

[13] A.S. Leal, K. Krambrock, L.G.M. Ribeiro, M.Â.B.C. Menezes, P. Vermaercke and L. Sneyers, "Study of neutron irradiation-induced colors in Brazilian topaz", Nuclear Instruments and Methods-A, vol. 580(1), pp. 423-426, 2007.

[14] S.O. Olabanji, O.A. Ige, C. Mazzoli, D. Ceccato, J.A. Akintunde, M. De Poli and G. Moschini, "Accelerator-based analytical technique in the evaluation of some Nigeria's natural minerals: Fluorite, tourmaline and topaz", Nuclear Instruments and Methods-B, vol. 240(1-2), pp. 350-355, 2005.

[15] K. Boonsook, W. Kaewwiset, P. Limsuwan and K. Naemchanthara, "Gamma ray evaluation of fast neutron irradiated on topaz from Sri Lanka by HPGe gamma ray spectrometry", J. Physics: Conference Series, Siam Physics Congress, vol. 901, 2017.

[16] A.M. Akhanov, M.T. Aitkulov, D.S. Sairanbayev, Sh.Kh. Gizatulin, N.K. Romanova, A.A. Shaimerdenov, Y.V. Chikhray, Zh. Ualzhanov and T.K. Zholdybayev, "Irradiation capsule design for neutron coloration of topaz in a WWR-K reactor", Applied Radiation and Isotopes, vol.190, pp. 110472, 2022.

[17] C.S. Hurlbut, and R.C. Kammerling, "Gemology", NY: John Wiley & Sons, Inc., 1991.

[18] M. Wasim, W. Zafar, M. Tufail, M. Arif, M. Daud and A. Ahmad, "Elemental analysis of topaz from northern areas of Pakistan and assessment of induced radioactivity level after neutron irradiation for color induction", J Radioanal Nucl Chem, vol. 287, pp.821–826, 2011.

[19] C.E. Ashbaugh, "Radioactive and radiation treated gemstones", Radioactivity & Radiochemistry, Vol. 2(1), pp. 42–57, 1991.

[20] J. Zhang, T. Lu, M. Wang and H. Chen, "The radioactive decay pattern of blue topaz treated by neutron irradiation", Gems & Gemology, vol. 47(4), pp. 302-307, 2011.

The Nucleus **60**, No. 1 (2023) 56-59

www.thenucleuspak.org.pk

The Nucleus
ISSN 0029-5698 (Print)
ISSN 2306-6539 (Online)

Quenching of Fluorescent ADS680HO molecule with Eco-Friendly Synthesized Silver Nanoparticles

Vadiraj B Tangod*

Department of Physics, Government First Grade College for Women's, Opposite to R N Shetty Stadium Office, Dharwad–580008. Karnataka, India

ABSTRACT

In this work, we have collected spectroscopic optical fluorescence and absorption spectra of the highly fluorescent laser dye molecule ADS680HO in different spectroscopic grade solvents with and without the amalgamation of eco-friendly synthesized silver nanoparticles (AgNP's), which resulted in the spectral intensities displaying quenching in the fluorescence and absorption intensities. It attributes the shape, dimension and bonding between the AgNP's and ADS680HO molecules, as well as the transfer of energy among the fluorescent probe and AgNP's. Fluorescence quenching of dye has innumerable uses for progress in cutting-edge bio-molecular labeling, fluorescence patterning and cancer treatment with chemotherapy.

Keywords: *SPR, RET, ADS680HO, absorption, fluorescence, quenching, AgNP's*

1. Introduction

This research paper explains a thorough understanding of the extremely fluorescent dye ADS680HO (C_{37} H_{39} N_2O_6Cl) of per chlorate series [1–7]. Spectroscopic studies of this molecule have sparked the curiosity to take the task in thorough understanding of the molecule. This aids to develop and tailor new types of molecules that can be used for specific applications, like [3] dye lasers, lithography, biosensors, microbiological schemes, dye based printing methods, molecular equipment, chemotherapy in the treatment of fatal diseases like cancer, extensive use in energy transformation phenomena, labeling proteins in bio-medical chemistry, to have comprehensive knowledge of fluorescence quenching., etc. By assuming extensive applications as an industrially important ADS680HO dye molecule, a complete understanding of its photo physical and behavioral nature inspires a complete, systematic report in this task.

In this communication, we report the quench of optical fluorescence along with the absorption spectra of ADS680HO dye molecule by naturally synthesized AgNP's. The quenching property of ADS680HO has immense industrial and medical applications, like chemotherapy to treat cancer. However, till now, no perfect and systematic study has been conducted by any investigator to explain the effects of absorption and fluorescence of this compound. Hence, it is our opportunity to disclose new exclusive, unique optical studies on fluorescence quenching with optical absorption studies of ADS680HO molecules and eco-friendly AgNP's.

Spectroscopic fluorescence and absorption spectra related to ADS680HO fluorescent molecules without and with AgNP's in different solvents are documented on the UV-VIS Spectra Suite Spectrometer with complete software (high-resolution model HR-4000 model, having resolution ±0.1nm). Various graphs are plotted on Origin software.

2. Investigation Section

2.1 Spectroscopic Measurements

Spectroscopic fluorescence and absorption spectra related to ADS680HO fluorescent molecules without and with AgNP's in different solvents are documented on the UV-VIS Spectra Suite Spectrometer with complete software (high-resolution model HR-4000 model, with resolution ± 0.1nm). Various graphs are plotted on Origin software.

2.2 Materials Used

American laser fluorescent ADS680HO dye was procured at ADS Source, Inc., and its structural and molecular formula is depicted in Fig. 1. Solvents are the alcohol series, acetonitrile, DMSO, ethyleacetate, toluene, glycerol, and benzene. Solvents are purchased from Sigma Aldrich and are of spectroscopic grade. Concentrations of the solution could be in the range of 10^{-5} mol/L. $AgNO_3$ salt is obtained from Himedia Laboratories Pvt. Ltd., India. All solution preparations are carried out using ultra-deionized water.

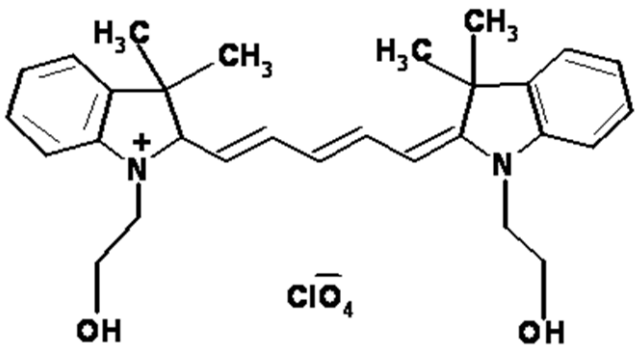

Fig. 1: Molecular Structure and IUPAC name of ADS680HO.

Molecular formula : C_{37} H_{39} N_2 O_6 Cl (commercial name ADS680HO)

IUPAC Name : 2-[5 -(1, 3-Dihydro-3, 3-dimethyl- (2- hydroxyethyl)-2H-benzindol-2-ylidene) -1, 3-pentadienyl]-3, 3-dimethyl-1-(2-hydroxyethyl)-3Hbenz[e] indolium perchlorate.

2.3 Green Nanotechnology: Preparation of Silver Nanoparticles (AgNP's) by Krishna Tulasi leaves

Fresh Krishna Tulasi (Ocimum Sanctum) plant leaves are washed thoroughly using deionized water. 40g of Ocimum sanctum leaves were thoroughly washed and boiled in 100 ml of distilled water to prepare the extraction. Further, the extract

*Corresponding author:*vadirajtangod@gmail.com*

was filtered and stored at 40 °C for future experimental work. This extract is used to reduce and stabilize the synthesis of silver nanoparticles. 1.5 ml of extract to 20 ml of silver nitrate ($AgNO_3$) (concentration of silver nitrate is 2 mM) solution on a magnetic stirrer container. The color turns yellow within 5–6 minutes. This color-changing property is an indication of the formation of silver nanoparticles. Here, Krishna Tulasi extract is composed of certain phytochemicals, namely: urosolic acid, euginal, eugenol,linalool, carvacrol, limatrol, caryophyllene, sitosterol, anthocyans methyl, and caricol. These phytochemicals are mainly responsible for the reduction of $AgNO_3$ salt to AgNP's. This chemical reduction reaction was carried out on a magnetic stirrer based hot plate at room temperature.

3. Surface Plasmon Resonance (SPR) of Eco-friendly synthesized silver nanoparticles

Nanoparticles have been specifically examined through Mie's scattering theory using Maxwell's electromagnetic equations regarding their dependence on the size of the particle and the surrounding medium. Mie's theory [8–13] is a Maxwell's electromagnetic explanation with mathematical calculations of the scattering of electromagnetic radiation by spherical nanoparticles. According to Mie's scattering theory, the particular size of the nanoparticles exposed by the particular wavelength results in a peak resonant wavelength. Two separate approaches based on particle size and target probe range can explain this. The first strategy is, limit of 2R << λ, (R is the radius of the nanoparticle and λ is the wavelength of incident electromagnetic radiation), where the electric dipole term oscillates maximum under the influence of exposed electromagnetic radiation, which is expressed expressively [8] as extinction cross-section (σ_{ext}), i.e., an explanation of the surface plasmon resonance (SPR) spectrum. Optical absorption spectrum is taken in the range of 325-575 nm region.

$$C_{ext} = \frac{24\,\pi\, R^3 \varepsilon_m^{\frac{3}{2}}}{\lambda} \frac{\varepsilon''}{(\varepsilon' + 2\varepsilon_m)^2 + \varepsilon''} \qquad (1)$$

ε′ real and ε″imaginary portions in the complex dielectric function ε_m $\left(\varepsilon_m = \varepsilon^{'} + i\varepsilon^{''}\right)$.

Second strategy is based on condition to SPR which is according to Maxwell's equation.

$$\varepsilon' = -2\,\varepsilon m \qquad (2)$$

In case of small AgNP's, dipole moment is experienced by an incident electric field which promotes the formation of surface polarization, i.e., charge, which predominantly affects the regaining of force by free electrons. The bottom line is that a higher wavelength of bulk metal absorption maintains a smaller surface plasmon band, thus, satisfying the equation-2.

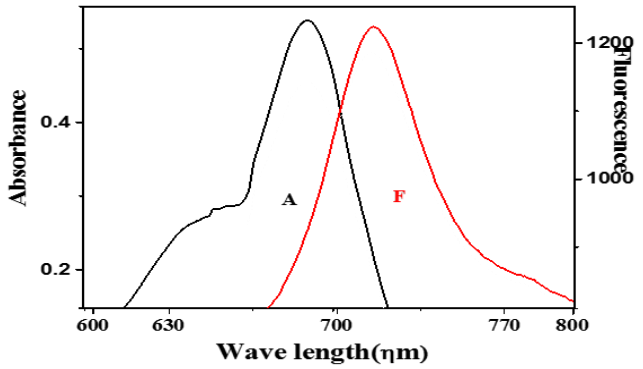

Fig. 2: Optical absorption and fluorescence spectra of ADS680HO in decanol solvent

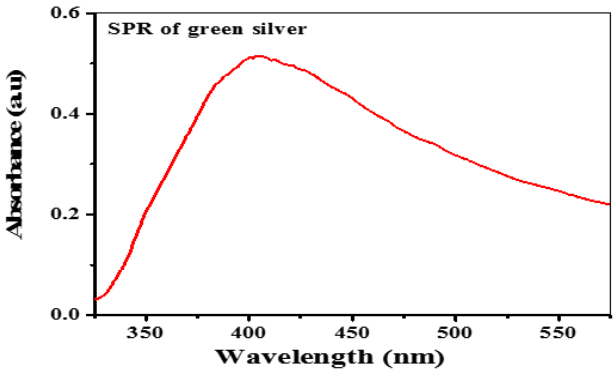

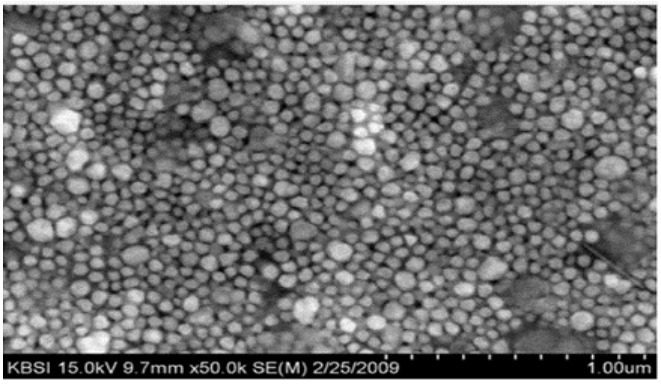

Fig. 3: SPR absorption spectra of eco-friendly synthesized nanoparticles of Silver. SEM (Scanning Electron Microscope) image.

4. Optical Fluorescence and Absorption Intensities Quenching of ADS680HO Laser Dye

This investigation reveals that fluorescence and absorption quenching were experientially noticed for ADS680HO laser dye in various alcohol solvents attached to AgNP's through hydrogen bonding. The emission and absorption spectra of ADS680HO before the influence of silver nanoparticles are shown in Fig. 2.

Typically, quenching in intensities of absorption and fluorescence is mainly attributed to energy rate transfer from probemolecules to AgNP's which is governed by [14] the following three factors [14]:

1. SPR band width
2. Peak position
3. Coulumbic interaction

Columbic interactions on energy transfer are due to the following two reasons:

1. Interaction among probe molecules with AgNP's it is subjected to densities of the charges.
2. Interaction between dipoles within the medium.

Charge density and dipole moment of a dye with AgNP's are related to energy transfer among dye molecules from the silver particle, which explains quenching of optical absorption in the ultra-violet region. This shows a band around 670–700 nm (ADS680HO), and is assigned π-π* transitions. This amalgamation of AgNP's and the chosen target dye molecule encourages strong quenching or enhancement [9–19] of fluorescence intensities, which is appreciably observed conditionally depending upon the nature and physical conditions of the target molecule.

Widening SPR describes the variety of molecules that are near AgNP's and the absorption / fluorescence intensity that may quench or enhance them. The width of the curve depends on the nature of the attaching molecules and is a function of the bonding between probe molecules and AgNP's. In our case, absorption and fluorescence quenching are noticed because of the close distance between AgNP's and ADS680HO. If fluorescent dye directly bonds to nanoparticles, it definitely reveals that fluorescence is completely and heavily quenched. Hence, in the present discussion, attachment is a little longer in range i.e bond length is larger, so intensity in quenching is rather low.

The size of nanoparticles affects the presence of the precise band of SPR in various alcoholic targeted solvents in conjugation with ADS680HO molecules was Examine Through the ultra-violet absorption spectrum at the range 300-600 nm Fig. 3. A series of alcohols are selected to definite reactions with alcoholic groups (–OH), nitrile, and chlorate groups in ADS680HO dye, which primes the patent properties of the silver and gold nanoparticle optical properties. If nanoparticle size becomes appreciably greater than the wavelength of the excitation (λ>> 2R), energy transfer can be estimated and confirmed with minor and extended regions of SPR. Silver nanoparticles and their spectroscopic properties are greatly prejudiced by respective their dimension, shapes, and nearby environmental conditions. The final thing to say is that resonant plasmon energy transfer is among tightly spaced nanoparticles, and the surrounding environment also matters.

The RET (Resonance Energy Transfer) model [9-19] was created on nonradiative decay, providing complete theoretic and thoughtful observations of quenching fluorescence behavior. These specific light interaction properties of metallic and dielectric molecules specifically investigated experimentally and also theoretically, are of prime interest in the current trend. If a particle is excited and oscillates with SPR in the presence of an incident electro-magnetic wavelength spectrum region, the excited system has an appreciably disturbing effect and a change in dipole moment, which shows the radiation response. Particularly, this optical radiation from dipole moments delivers a channel for the process of radiative decay. Instead, the Joule effect and surface plasmon absorption may cause non-radiative decay. The struggle between radiative and non-radiative decay energy transfer greatly affects the fluorescence emission spectra of the molecules located near the particles. Suppose non-radiative decay takes the major ruling effect, and fluorescence quenching phenomena happens. So, the variable distance behavior of the radiative and non-radiative rates explains quantum yield declines at a short distance from metal nanoparticles [5, 19-21].

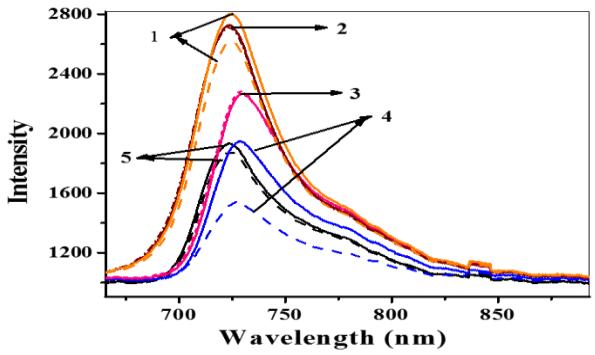

Fig. 4: Optical absorption spectra of Silver nanoparticles with (dotted)/ without (lined) in conjugation with ADS680HO along with solvents (1- methanol, 2-ethanol, 3-propanol, 4-butanol, 5-octanol).

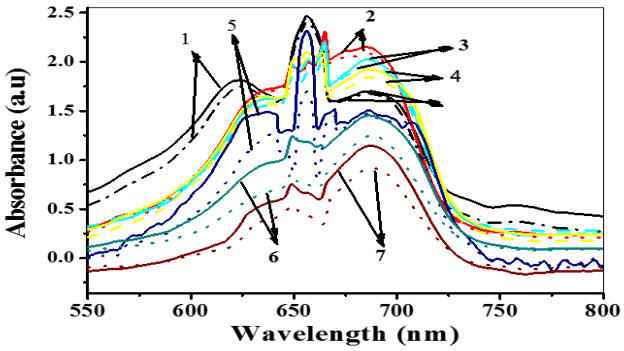

Fig. 5: Fluorescence image of silver nanoparticle with (dotted)/ without (lined) in conjugation with ADS680HO along with solvents (1-methanol, 2-ethanol, 3-octanol, 4-butanol, 5-ethanol, 6-decanol, 7-nonanol).

Our particular experimental quenching of fluorescence Fig. 4 is credited to RET from laser dye ADS680HO to eco-friendly synthesized nanoparticles. Particularly, this special non-radiative decay is assigned to the studies of the theory of Forster resonance energy transfer (FRET) [5, 22, 23]. A small amount of AgNP's is injected into ADS680HO dye solution in different alcohol solvents. Target dye molecules have a very high affinity to form complex clusters that surrounding's, which causes physical adsorption and results in optical quenching intensity. At higher concentrations of ADS680HO, large number of molecules adsorb on the AgNP's, improving the effectiveness of quenching. This quantum efficiency yield of AgNP's is given by FRET theory as below. Here Q is the quenching efficiency of quantum yield [5].

$$Q = \frac{\Gamma^R}{\Gamma^R + \Gamma^{NR}} \quad (3)$$

Γ^{NR}– non-radiative decay and Γ^R – radiative decay;

Presently, attachment of AgNP's to ADS680HO dye results in larger non-radiative decay and leads to quantum efficiency declination, Hence, it leads to fluorescence quenching. Fig. 4 and 5. Here, quenching is static and could also be attributed to an attachment of the dye with silver nanoparticles via complexes of the nanometal with –OH, nitrile, and chlorate groups Fig. 6.

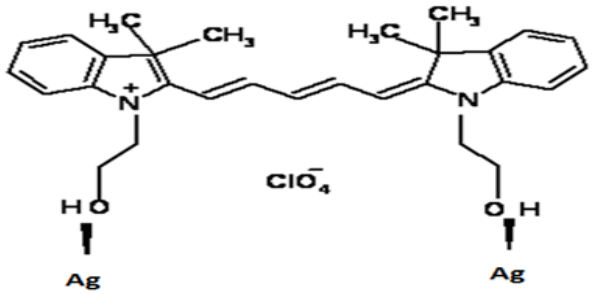

Fig. 6: Conjugation of AgNP's withADS680HO molecule.

5. Conclusions

Spectroscopic optical fluorescence and absorption spectra of ADS680HO molecule in various alcohol complexes with and without AgNP's show spectral intensities quenching. This is due to the probe's molecular dimension, its shape, coupling between the AgNP's and energy transfer between them. The intensity quenching property of fluorescence using AgNP's with ADS680HO leads to numerous and advanced usages, particularly fluorescence patterning, advanced in bio-molecular labelling, cancer chemotherapy treatment and many more.

References

[1] U.S. Raikar, V.B. Tangod, S.R. Mannopantar and B.M. Mastiholi, "Ground and excited state dipole moments of coumarin 337 laser dye", Optics Communications, vol 283. no 21, pp. 4289-4292, 2010.

[2] U.S. Raikar, V.B. Tangod, C.G. Renuka and B.M. Mastiholi, "Solvent effects and photophysical studies of ADS560EI laser dye", Afr. J. Pure Appl. Chem., vol. 4 no. 4, pp. 51, 2010.

[3] V.B. Tangod, P.U. Raikar, B.M. Mastiholi, S.G. Kulkarni and M.S. Jadhav, U.S. Raikar, "Photophysics studies of highly fluorescent ADS680HO laser dye conjugate with green silver nanoparticles", Optik – International Journal for Light and Electron Optics, vol. 127 no.2, pp. 677-685, 2016.

[4] U.S. Raikar, V.B. Tangod and B.M. Mastiholi, "Fluorescence quenching using plasmonic gold nanoparticles", Optics Communications., Vol. 284, no.19, pp. 4761-4765, 2011.

[5] V.B. Tangod, B.M. Mastiholi, M.G. Kotresh, P.B. Ganjihal, P. Raikar and U.S.Raikar, "Photo physical studies of silver nanoparticles on ADS740WS fluorescent dye", Proceedings of International Conference on Optical Engineering (ICOE), 2012.

[6] V.B. Tangod, P.U. Raikar, B.M. Mastiholi and U.S. Raikar, "Solvent polarity studies of highly fluorescent laser dye ADS740WS and its fluorescence quenching with silver nanoparticles", Canadian Journal of Physics., vol.92, no. 2, pp. 116-123. 2014

[7] B.M. Mastiholi, P.U. Raikar, V.B. Tangod, S.G. Kulkarni and U.S. Raikar, "Fluorescence Enhancement of C 314 Laser Dye Based on ICT between C 314 Laser Dye and Green Synthesized Gold Nanoparticles" IOSR Journal of Applied Physics (IOSR-JAP), vol. 6, no. 6 ver. III. pp. 43-47, Nov.-Dec. 2014.

[8] C.F. Bohren and D.F. Huffman, "Absorption and Scattering of Light by Small Particles", Wiley, New York. 1983.

[9] J. Perez-Juste, P. Mulvaney, L.M. Liz-Marzan, "Patterning and encryption using gold nanoparticles", International Journal of Nanotechnology., vol. 4, no. 3, pp. 215-225, 2007.

[10] I.I.S. Lim and C.-J. Zhong, "Molecularly-mediated assembly of gold nanoparticles", Gold Bulletin. vol. 40, no.1, pp.59-66, 2007.

[11] G. Zoriniants and W.L. Barnes, "Fluorescence enhancement through modified dye molecule absorption associated with the localized surface plasmon resonances of metallic dimmers", New J. Phys., vol. 10, pp. 105002, 2008.

[12] M. Eichelbaum, B.E. Schmidt and H.I. Rademann, "Three-photon-induced luminescence of gold nanoparticles embedded in and located on the surface of glassy nanolayers", Nanotechnology, vol.18, no.35 pp. 355702, 2008.

[13] B.M. Mastiholi, V.B. Tangod and U.S. Raikar, Optik, "Influence of metal nanoparticles on ADS560EI fluorescent laser dye", Int. J. Light Electron Opt., vol.124, no. 3, pp. 261-264, 2013.

[14] A. Kawski, P. Bojarski and B. Kuklinski, "Estimation of ground- and excited-state dipole moments of Nile Red dye from solvatochromic effect on absorption and fluorescence spectra", Chemical Physics Letters, vol. 463, pp. 410-412, 2008.

[15] A. Kawski, B. Kuklinski and P. Bojarski, "Photophysical properties and thermochromic shifts of electronic spectra of Nile Red in selected solvents. Excited states dipole moments", Chem. Phys., vol.359, no. 1-3, 58-63. 2009.

[16] M. Umadevi, N.A. Sridevi, A.S. Sharmila, B.J.M. Rajkumar, B. Mary, P.Vanelle, T. Terme and O. Khoumeri, "Influence of Silver Nanoparticles on 2,3-Bis(Chloromethyl)Anthracene-1,4,9,10-Tetraone", Journal of Fluorescence, vol. 20, no. 153-161, 2010.

[17] T. Forster, Zwischenmolekulare Energiewanderung und Fluoreszenz, "Zwischenmolekulare Energiewanderung und Fluoreszenz", Ann. Physik., vol. 2, pp.55, 1948.

[18] J. Zhu, J. Li, A. Wang, Y. Chen and J. Zhao, "Fluorescence Quenching of Alpha-Fetoprotein by Gold Nanoparticles: Effect of Dielectric Shell on Non-Radiative Decay", Nanoscale Res. Lett., vol.5, pp.1496, 2010.

[19] S.T. Dadami, S. Rayaprol, V. Sathe and B. Angadi, "Electric field induced structural, magnetic and ferroelectric properties of 0.6 $PbFe_{0.5}Nb_{0.5}O_3$-$0.4BiFeO_3$ multiferroic solid solution", Ceramics International, vol. 46, no.17, pp. 27595-27600, 2020.

[20] S.T. Dadami, I. Shivaraja, S.K. Deshpande, S Rayaprol and B Angadi, "$BiFeO_3$ induced enhancement in multiferroic properties of $PbFe_{0.5}Nb_{0.5}O_3$," Ceramics International, vol. 44, no.16, pp. 20449-20456, 2018.

[21] M.N. Taj, B.D. Prasad, R. Narapareddy, H. Nagabhushana, G Ramakrishna, B Mahesh and S.T. Dadami, "PANI-molybdate nanocomposites: Structural, morphological and dielectric properties for the effective electromagnetic interference (EMI) shielding applications in X-band", Applied Surface Science Advances, vol. 7, pp. 100203, 2022.

[22] H. Xu and K.S. Suslick, "Water-Soluble Fluorescent Silver Nanoclusters", Adv. Materials, vol.22, pp. 1078-1082, 2010.

[23] S. Mannopantara, H.H. Bendigeri, V.K. Kulkarni, V.S. Patil, D.H. Manjunatha and M.N. Kalas, "Preparation of colloidal Ag nanoparticles", Materials Today, vol. 60, pp. 1156-1159, 2022.

The Nucleus ***60****, No. 1 (2023) 60-63*

www.thenucleuspak.org.pk

The Nucleus
ISSN 0029-5698 (Print)
ISSN 2306-6539 (Online)

Thorium Based Indian Nuclear Program

Waqar Hussain[1], Khurram Maqsood Ahmed[2*], Adeela Azam[1], Sidra Rehman[1]

[1]*School of Politics and International Relations, Quaid-i-Azam University, Islamabad, Pakistan*

[2]*Department of International Relations, National Defence University, Islamabad, Pakistan*

ABSTRACT

India has the largest thorium reserves in the world. Normally, it is deposited in the rocks and can be extracted through specific processing, however, in India, it is available in pure and refined form. India has included utilization of Thorium as a major goal in its nuclear energy program because it has the large amount of thorium as compared to meager uranium reserves. Indian ambitious three stage nuclear program is aimed to fulfill its objective to achieve energy security whereas nearly 300 million of the population in India is estimated to be out of the national electricity grid. India is expanding its nuclear energy production to achieve the target of 63 GW into the total power share by 2032 and plans to further increase this share to 25% by 2050. However, the technology to use thorium as a fuel is quite complicated and no country has yet achieved this capability owing to the involvement of reprocessed nuclear fuel, which is quite hard to handle. While India is struggling to achieve a breakthrough in the development of technology to use thorium as blanket fuel for use in advanced reactor. The overall implications of such developments would result in the exponential increase in Indian fissile materials consequently jeopardizing the deterrence stability in South Asia. Once India is able to tap the weapon grade U-233 from thorium, then its fissile material stocks would increase exponentially resulting in exacerbating the Pakistani security dilemma vis-à-vis India.

Keywords: *Thorium, Indian Thorium Potential, Indian Three Stage Nuclear Program*

1. Introduction

In 1828, Jons Jacob Berzelius, a Swedish scientist, discovered Thorium [1]. It is naturally occurring element 3-4 times abundant than Uranium. It was named after "Thor". According to Norse (Scandinavian) mythology, 'Thor' was the god of war who is widely known as hammer-wielding god protecting the mankind. According to this mythology, Thorium is also attributed as "Asgard's Fire", Asgard being a small planetary body which is home of their gods [2].

Thorium is a radioactive material which occurs in nature; however, it cannot be readily used as a fuel. So to call it as "Thorium Fuel" is wrong because it is fertile material rather than a fissile material which itself cannot be used as a fuel but it can be de-generated or irradiated through certain process to convert it into uranium-233 which is fissile material and can be used as a powerful fuel. Due to its high radiation properties, Uranium-233 can be used in nuclear weapons. Although Thorium is found three times more as compared to uranium, yet it has never been used into reactors because it does not have the ability to start fission reaction. This aspect is associated with the proliferation-resistant trait of thorium as nuclear fuel.

The earliest reactor using thorium was introduced in United States in 1962[3]. However, the pace was slow because the focus was on Uranium based fuel and it was present in abundance in developed states. In 1996, International Atomic Energy Agency (IAEA) started a study to determine potential use of thorium as nuclear fuel. This was followed by USA's Shipping port Atomic Power Station project which was the first of a kind to breed thorium [4]. Currently, Norway is in test phase of two types of Thorium fuels since 2013 and is hoping to market it as soon as the regulatory formalities are met [5].

The top five countries with the most thorium reserves and the overall world reserves are shown in the table [Ref. 5]:

Table 1: Data showing top 5 countries with most thorium reserves and total reserves in the world

Country	Reserves in Kilo Tones
India	846
Brazil	632
Australia	595
USA	595
Egypt	380
World total	6,355

India has the largest known thorium reserves. It had envisioned its Thorium potential very early and had the three-stage program that would use thorium as fuel in the advanced reactors. India is pursuing its ambitious program but there are challenges of technological barriers and economic constraints. It is significant for India because it does not have large reserves of Uranium whereas it has huge Thorium reserves. India has been conducting research on utilizing Thorium for producing energy. For that purpose, it has developed a "Fast Breeder Test Reactor (FBTR)" and operating it for 27 years now for experimentation. However, still it is estimated that it would start production in 20 to 30 years from now [6].

It is hard to ascertain the financial benefits right now but if the technology matures, then it would be vital for ever growing energy requirements of India.

In order to dig into the issue, it is important to have an understanding of; (i) how thorium is used as a fuel, (ii) Indian thorium reserves and potential, (iii) Indian three stage nuclear

*Corresponding author:kma_sk@live.com

ambitions, (iv) thorium and issues of non-proliferation and (v) possible implication for Pakistan.

2. Thorium as Fuel

Thorium does not undergo fission automatically; therefore, it cannot be used directly in a reactor as a fuel. It is a fertile material which can absorb a neutron to make uranium-233 which is radioactive and produces fission. So, when we talk about Thorium as a fuel, it requires a certain fissile material that can be used as a 'driver' so that a chain reaction can start. There are two options for "fissile driver"; (i) to use Uranium-233 or Uranium-235 as drivers, or (iii) to use Plutonium-239 mix-oxide fuel [8]. However, all of these drivers cannot be readily supplied in a reactor because they are highly radioactive in this form and are very difficult to handle.

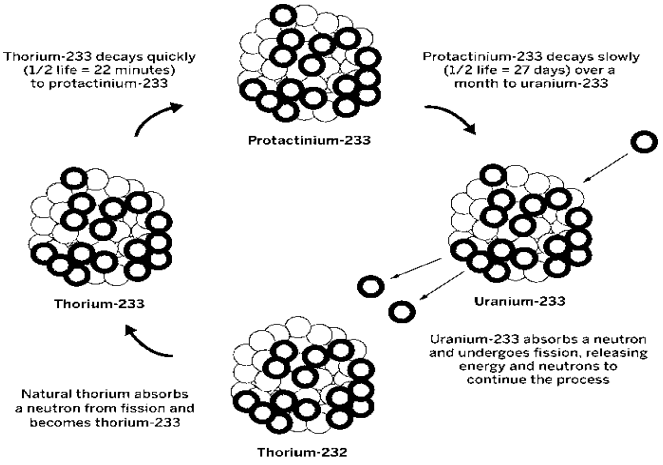

Fig. 1: Thorium energy cycle.

For the first option of using Thorium as fuel is through use of breeder reactor which can produce more U-233 than it consumes. Resultantly, this U-233 produced can be used as driver. But the breeder reactor requires good "neutron economy" i.e. the neutron loss during the reaction should be minimum possible to zero and all the neutrons are consumed. This can only be achieved in a slow neutron environment. With Uranium fuels having high speed neutrons, it becomes impossible to achieve slow neutron system which is ideal for thorium. The second option for the use of Thorium is to use it as "fertile matrix" in the form of "Mixed Thorium Plutonium Oxide (Th-Pu Mox)" wherein Plutonium serves as a "fissile driver".

The technology to use Thorium as a fuel is sophisticated but once developed; it is highly efficient as compared to the conventional reactors using Uranium as fuel. There are two types of fuel cycle of Thorium [7]:

2.1 Open Fuel Cycle

In this process Th-232 is irradiated by carrying out in-situ fission of U-233. During this process, U-233 is not separated from the product through chemical processing and the cycle remains open.

2.2 Closed Fuel Cycle

In this type of fuel cycle, U-233 is separated by chemically reprocessing Thorium. The resultant product U-233 is re-fabricated for further use as fuel in the reactor.

There are certain types of nuclear reactors in which Thorium can be used. According to World Nuclear Association (WNA), following reactors can utilize Thorium as fuel: "(i) The Pressurized Heavy Water Reactor (PHWRs), (ii) High Temperature Gas Cooled Reactors (HTRs), (iii) Pressurized Light Water Reactors (PWRs), (iv) Boiling Light Water Reactors (BWRs) and (v) Fast Neutron Reactors (FNRs)". In addition to that, there are further two types of reactors but they are still in conceptual phase. These include: "Molten Salt Reactors (MSRs)" and "Accelerator Driven Subcritical Reactors (ADSR)" [10].

3. Indian Thorium Reserves/Potential

The world's largest reserves of Thorium are found in India [8]. Coastal areas of Orissa sand complex, sands of Tamil Nadu (Manavalakkuricci), Kerala (Aluva and Chavara) are rich with monazite, ilmenite and garnet which are the sources of thorium. These reserves constitute 32 % of the world resources [9]. The following table shows the estimated thorium reserves in India according to "Atomic Minerals Directorate for Exploration and Research, India" [Ref.9]:

Table 2: Estimated Monazite reserves in India

State	Monazite (Kilo Tons)
Odhisa	2410
Andhra Pradesh	3720
Tamil Nadu	2460
Kerala	1900
West Bengal	1220
Jharkhand	220
Total	11930

According to Indian sources, these reserves are 11.94 million tones. These reserves can contribute to 360,000 tons of Thorium [10]. According to conservative calculations, 400,000 MW of electricity can be generated through these reserves in a year for about next 4 centuries.

4. Indian Three Stage Nuclear Program

Indian nuclear policy rests on the vision of Jawaharlal Nehru, the first Prime Minister of India, who laid the foundations of atomic research in India along with Dr. Homi Bhabha. The three stage program was proposed by Bhabha in November 1954. This proposal was well received by Nehru who supported it for the formal adoption by the government in 1958 [11].

The three stages include three steps for nuclear development.

First stage includes; installation and operation of "Pressurized Heavy Water Reactors (PHWRs) and light water reactors" to produce electricity as well as to produce plutonium from reprocessing of spent fuel.

In the second stage, India will develop Fast Breeder Reactors (FBRs) in which plutonium would be used to produce more and more U-233 from Thorium. In this process, a blanket of uranium and Thorium is used in the core to produce more uranium and plutonium than it was fed in the system.

At the final stage, Advanced Heavy Water reactors will be developed to use thorium plutonium fuel in order to produce U-233 which in turn is used as fuel for reactors. During the process of thorium fission, about 66% power is produced [12].

In all of these stages, used fuel needs to be reprocessed to recover fissile materials for recycling.

5. Thorium Based Program

India has become the first country to experiment utilization of Thorium in the breeder reactor [13]. For the last 27 years, India is working on operationalizing fast reactors of 500 MWe using Sodium as coolant. This type of fast reactors would produce the required amount of plutonium and uranium which will be used by the third stage advanced reactors. However, experts say that it would take India another 20 to 30 years for maturation of technology let alone its operationalization and benefitting from it [14].

6. Prototype Fast Breeder Reactor (PFBR) and KAMINI

India is still working on development of its first Prototype Fast Breeder Reactor (PFBR). The objective of fast reactor is to generate fissile material for utilizing Thorium. This is done by using fertile material like U-238 or Th-232 and bombarding them with neutrons. The sodium cooled PFBR does not use thorium; rather it uses U-238. There are several technological challenges attached to fast reactors. These challenges include: (i) the problem of corrosion of pipes and steel vessels, (ii) production of high amount of radiation and (iii) the fuel cycle is costlier because of involvement of automated cycles like re-fabrication, reprocessing and chemical separation of used fuel. These challenges have been a major hurdle in any breakthrough in the FBR technology.

The "**KAMINI** (Kalpakkam Mini reactor)" is located in Kalpakam at Indira Gandhi Center for Atomic Research. It is a research reactor that became critical in 1996 and has the capacity to produce 30 KW of energy. It was one of a kind reactor particularly contrived to use Thorium as fuel. It is the only reactor in the world to have Thorium-plutonium blanket [15]. It is not only a fast breeder reactor but the output of plutonium breed has dual use: (1), for use in the next reactor; and (2), for use on a nuclear-tipped inter-continental missile.

Conditioned to materialization, the concept of using thorium as a fuel is wrought with complications. Theoretical explanation of thorium as nuclear fuel suggests that there are two complications in using thorium in a FBR [16]; (i) it requires a huge amount of plutonium to initiate the FBR containing thorium blanket. India does not have the indigenous uranium which can be reprocessed to get the plutonium. However, the Indo-US nuclear deal allows India to get uranium from other countries [17]; and (ii) to avoid creation of U-232 which is a highly radiotoxic material.

Under the process, the concept of fertile to fissile conversion of Thorium is used to get the U-233 which is capable of fission in nuclear reactor. Thorium-232 is natural raw material which is used to create uranium-233 which is done by bombarding it with neutrons. This can be done by putting thorium inside the reactor in the form of blanket over the plutonium fuel.

Thorium-232 transmutes into protactinium-233 upon absorption of neutron. Spontaneously, protactinium transmutes into uranium-233 which is highly radioactive and can be readily used in a nuclear weapon. The explosive power of uranium-233 is more as compared to uranium-235 so there is no need to enrich it and it is quite different from plutonium because it can be simply employed in a gun-type bomb like the one dropped on Hiroshima and does not require implosion like that of a plutonium based nuclear weapon.

Along with Uranium-233, there is also uranium-232 isotopes are produced which are highly undesirable because it produces burst of gamma radiations that damages the electronic equipment [18]. Alternatively, to avoid this problem, protactinium can be removed chemically from the reactor and wait until it is converted into uranium 233. This is a recipe for making any type of nuclear weapon. Development of such a capability would result in multiplying the Indian capability to produce U-233 which equivalent to HEU.

7. Thorium and issues of non-proliferation

While one narrative goes on that, Thorium, also called the "other" nuclear fuel, is considered to bring revolution in the nuclear industry which would have the traits of being environment friendly, economical and nuclear proliferation resistant. However, the counter narrative also exists that nothing related to nuclear can be risk free.

It is claimed that Thorium is the most suitable fuel for future nuclear reactors. But in an article of the journal, *Nature* of Dec 2012, the scholars are of the view that it is not as advantageous as being portrayed. The researchers consisting of Dr Stephen F. Ashley and Dr. Geoffrey T. Parks from the University of Cambridge; Professor William J. Nuttall from The Open University; Professor Colin Boxall from Lancaster University; Professor Robin W. Grimes from Imperial College London have highlighted that Thorium decays in four stages: to start with, thorium-232 breaks into thorium-233 which is unstable and converts into protactinium within 22 minutes. Then after 27 days it decays into uranium-233 which has the capability to undergo fission reaction.

There is a chance of proliferation during the chemical separation of protactinium-233 which is then transmuted into uranium-233 [19]. These chemical processes are not much complicated and it can be done by using chemical lab equipment with complete secrecy.

Importantly, the authors have pointed out that from total of 1.6 tons of Thorium, nearly 8kg uranium-233 can be separated which is enough for one nuclear weapon. More strikingly, it can be done "in less than a year [Ref.19]." Considering that, one can

imagine the potential of India in terms of fissile material stocks using Thorium.

Furthermore, the smuggling and illegal mining of thorium has been reported in India. Several news reports have highlighted a major scam of 2.1 million ton of Monazite that has been disappearing from Indian shores. This amount is equal to 19.5 kilo tons of thorium [20]. Furthermore, it was allowed by the Indian Government.

8. Implications for Pakistan

For Pakistan it can cause two kinds of implications: one, the FBR is out of safeguards and India can divert excessive plutonium to its nuclear program at will; and second, if thorium fuel cycle gets operationalized, then it would provide India with abundant stock of U-233. These implications will further reinforce the fissile material quandary of Pakistan [21].

In this scenario, policy options for Pakistan in terms of matching the fissile material stocks become increasingly limited owing to its limited uranium reserves. However, Pakistan should continue to bring innovations in its arsenal and steadily increase its fissile material stockpiles in order to maintain the full spectrum deterrence. In addition to that Pakistan should continue to voice its principled stance regarding FMCT and condemn the discrimination at all levels.

9. Conclusion

India has embarked on a journey to exploit its thorium reserves for energy generation using a modern, indigenous designed and locally produced fast breeder reactors for more than 20 years. However, this Indian dream is decades away from becoming true as according to R. Rajaraman, Professor of Theoretical Physics, Jawaharlal University, Delhi, it would take 20 to 30 years for the Thorium based nuclear reactors to be functional.

Considering the huge Thorium reserves Indian dream of Thorium energy is practically possible. It would not only cater for the energy needs of India but it would also enable it to be less dependent on other countries for the uranium based nuclear fuel as it does not have sufficient indigenous reserves of Uranium.

Strategically, if India is able to mature its technology for utilizing Thorium, it would bring anxiety for Pakistan because it would give two pronged advantage to India in terms of increasing its nuclear stockpile. One that it would enable India to reserve its indigenous Uranium for military purposes; and second that with further technological innovation, India may be able to chemically extract U-233 from the reactor process. However, this is highly difficult and involves sophisticated technology.

References

[1] Royal Society of Chemistry. *Thorium* [Online]. Available: http://www.rsc.org/periodic-table/element/90/thorium. [Accessed: 06 May. 2022].

[2] The Economist. (2014, April 12) *Asgard's Fire* [Online] Available: https://www.economist.com/science-and-technology/2014/04/12/asgards-fire. [Accessed: 15 May. 2022].

[3] M. Kazimi, "Thorium Fuel for Nuclear Energy", *American Scientist*, vol. 95, no. 5, pp: 408, October, 2009.

[4] Presentation Ceremony, "Shippingport Atomic Power Station: A Historic Engineering Landmark Achieved", May 20, 1980. [Online]. Available:http://files.asme.org/ASMEORG/Communities/History/Landmarks/5643.pdf. [Accessed: 25 May. 2022].

[5] World Nuclear Association. *Thorium*, [Online] Available: http://www.world-nuclear.org/information-library/current-and-future-generation/thorium.aspx. [Accessed: 28 May. 2022].

[6] A. Lele, (2018, Feb) "India's Thorium Dream is True, Critical for Growth of the Technology", *Sputnik News*. [Online] Available: https://sputniknews.com/analysis/201802261061995444-indias-thorium-draem/. [Accessed: 01 June. 2022].

[7] International Atomic Energy Agency (2005), "Thorium Fuel Cycle: Potential Benefits and Challenges", IAEA-TECDOC-1450. [Online] Available:https://www.pub.iaea.org/MTCD/publications/PDF/TE_1450_web.pdf. [Accessed: 06 June. 2022].

[8] World Nuclear Association. *Thorium.* [Online] Available: http://www.world-nuclear.org/information-library/current-and-future-generation/thorium.aspx. [Accessed: 06 June. 2022].

[9] M. Dabas, (2017, Feb) "India has World's Largest Thorium Reserves, so Why Can't We Use it as a Source of Clean Energy?", *The India Times*, [Online]. Available:https://www.indiatimes.com/news/india-has-world-s-largest-thorium-reserves-so-why-can-t-we-use-it-as-a-source-of-clean-energy-272058.html. [Accessed: 12 June. 2022].

Source: Atomic Minerals Directorate for Exploration and Research, India. [Online]. Available: www.amd.gov.in/. [Accessed: 16 June. 2022].

Bhaba Atomic Research Center (BARC) "Anu Shakti: Atomic Energy in India", [Online]. Available: http://www.barc.gov.in/about/anushakti_sne.html. [Accessed: 18 June. 2022].

[10] A.K. Chaturvedi, "Nuclear Energy in India's Energy Security Matrix: An Appraisal," VIJ Books in association with *Rajiv Gandhi Institute of Petroleum*, Delhi, India, pp. 100-101. 2014

[11] Ibid.

[12] R. Rajaraman, (2018, Feb) "India's Thorium Dream is True, Critical for Growth of the Technology", *Sputnik News*, [Online]. Available: https://sputniknews.com/analysis/201802261061995444-indias-thorium-draem/. [Accessed: 19 June. 2022].

[13] Kalpakam Mini Reactor (KAMINI), *Nuclear Threat Initiative*. [Online] Available: http://www.nti.org/learn/facilities/852/. [Accessed: 20 June. 2022].

[14] IAEA TECDOC-1155, (2000) "Thorium Based Fuel Options for the Generation of Electricity: Developments in the 1990s", [Online] Available:https://www.pub.iaea.org/MTCD/publications/PDF/te_1155_prn.pdf. [Accessed: 21 June. 2022].

[15] Amitai Etzioni, (2015, Feb) "The Darker Side of US-India Nuclear Deal", *The Diplomat*, [Online]. Available: https://thediplomat.com/2015/02/the-darker-side-of-the-u-s-india-nuclear-deal/. [Accessed: 21 June. 2022].

[16] World Nuclear Association, (2021) *Thorium* [Online]. Available: http://www.world-nuclear.org/information-library/current-and-future-generation/thorium.aspx. [Accessed: 22 June. 2022].

[17] Stephen F. Ashley, Geoffrey T. Parks, William J. Nuttall, Colin Boxall & Robin W. Grimes, (2012, Dec) "Nuclear Energy: Thorium Fuel has Risks", *Nature*, No. 492: 31-33. [Online]. Available: https://www.nature.com/articles/492031a. [Accessed: 23 June. 2022].

[18] Jaideep Prabhu, (2014, Apr) "What Happened to the Rs. 60 Lakh Crore Thorium Scam", *Daily News and Analysis*. [Online]. Available: http://www.dnaindia.com/analysis/standpoint-what-happened-to-the-rs-60-lakh-crore-thorium-scam-1982959. [Accessed: 27 June. 2022].

[19] Adrian Levy, (2015, Dec) "India is Building a Top-Secret Nuclear City to Produce Nuclear Weapons, Experts Say", *Foreign Policy*. [Online]. Available:https://foreignpolicy.com/2015/12/16/india_nuclear_city_top_secret_china_pakistan_barc/. [Accessed: 30 June. 2022].

The Nucleus ***60****, No. 1 (2023) 64-70*

www.thenucleuspak.org.pk

The Nucleus
ISSN 0029-5698 (Print)
ISSN 2306-6539 (Online)

Continuous Heating and Cyclic Heating for Composite Materials Containing PA2200 and Ceramic Additives (Al_2O_3, MgO and Nanoclay) Monitoring System

Meraj Danish

Department of Mechanical Engineering, Maharshi University of Information Technology, Lucknow, India

ABSTRACT

In this harsh competition, additive manufacturing (AM) is an incredible breakthrough for aerospace, automobile and tooling industries. It can transform a computer-aided-design (CAD) into 3D component without tools or human intervention. Selective Laser Sintering (SLS) is an AM technique that utilizes high power laser to sinter tiny particles of a polymer powder into a solid object based on 3D model data. This work focuses on improving material optimization for the SLS process and establishing the best fabrication settings for developing products with superior attributes. By combining a commercially-available SLS materials like: PA2200 (polyamide) with ceramic additives (e.g., Al_2O_3, MgO and Nanoclay), new composite materials have been produced. It is shown that these composite materials are capable to produce sintered specimens that have superior mechanical and flammability properties than that of pure PA2200.

Keywords: *Selective Laser Sintering, Polyamide, Mechanical Properties, Flammability*

1. Introduction

Selective Laser Sintering (SLS) is an (AM) technology that can produce complex component geometry directly from 3D CAD software [1]. SLS builds parts from powder. Sintered components are produced when an infrared (IR) laser beam's heat overcomes the surface tension of particles, fusing them together [2, 3]. Two feed cartridges distribute powder over the construction area with a roller so that the next layer may be applied. This continuous until the part is produced. Through the use of a low melting point temperature binder, the SLS method is being employed to synthesize a variety of materials with varied properties as well as triturated substance to generate a geometrically precise sintered object. According to Madea and Childs, the SLS process has the capacity to adapt to a variety of materials [4]. SLS is among the most crucial prototype methods. To evade probable fire of the powder quantifiable particles, the entire polymer processing method is carried out in a heated hollow filled with inert fume. The powder layer is scanned and heated by the laser beam's thermal energy, causing shared sintering of the physical particles. The stage is dropped for the width of one coat, allowing a fresh powder layer to be laid. The new layer is perused, modified to the next higher cross-section, and adhered to the old one. SLS made prototypes are increasingly being employed as functioning parts with good mechanical qualities. The precision of the CAD prototypical, the technique of sheet cutting, machine determination, ray balance, coating width, material reduction, optical maser speediness, laser control, energy compactness, working improper temperature and hatching coldness are all elements that influence this need. Thus, AM refers to the layer-by-layer fabrication of three-dimensional physical models directly from CAD without any cutters, tools of fixtures specific to the object geometry [5, 6]. Objects of any kind of geometric (direct assemblies, conformal, custom, complex) or material (any variety–poly/metal/ceramic, non-equilibrium, gradient–mono/composite/gradient, porous/lattice, soft/hard) intricacy can be produced. Federico Lupone [2], utilized information from a 3D model, the SLS process melts just the areas of a polymer powder bed that are needed to create a final product. Then, a layer-by-layer method is used to acquire the complicated geometric components.

Khalid Mutashar Abed [3] reported that SLS may be used with a broad variety of materials, giving researchers a new avenue to explore in the field of AM or Solid Freeform Fabrication (SFF). In order to improve the quality and mechanical qualities of the components mentioned, various studies have been conducted using SLS technique on materials such as polymer metal composite ceramics and sand.

According to Lu Pan [4], selective laser melting (SLM) has emerged as a leading technology for metal AM. SLM is used to create 3D pieces in order to establish corrections between mechanical qualities, microstructure, and process parameters. SLM process's success in reducing grain size, and its mechanical qualities.

Both SLS and SLM, is a powder–based additive manufacturing process that allows the production of functional 3D parts directly from a CAD–model. During the process, successive layers of metal powder particles are molten and consolidated on the top of each other by the energy of a high intensity laser beam. Consequently, almost fully dense parts without need for any post–processing other than surface finishing are produced. Customized medical parts, tooling inserts with inserts with conformal cooling channels and functional components with high geometrical complexity are good examples to reveal the scope of the application areas of this process [7, 8]. SLS automatically fuses powdered industrial materials together using a high-powdered laser, SLM fuses powdered materials together by heating them until they reach a melting point.

Fig. 1 shows a schematic example of SLS system. Commercial machines differ for example in the way the powder is deposited (roller or scraper), the atmosphere, and in the type of laser they use (Fiber, CO_2, or Nd: YAG laser).

*Corresponding author: mech.mdmdanish@gmail.com

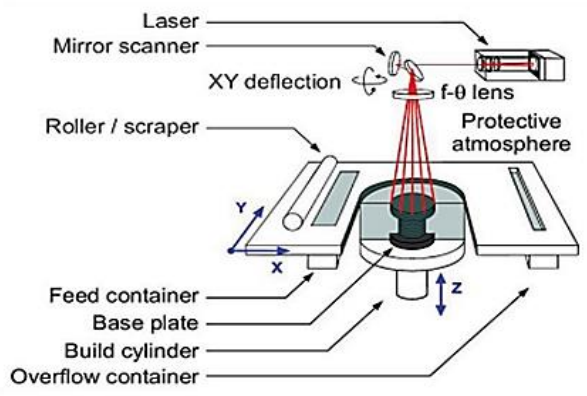

Fig. 1: A schematic view of the SLS/SLM process

Laser processing of materials is generally accompanied with high cooling rates due to the short interaction time and high thermal gradients. The high cooling rates during SLS/SLM may result in the formation of non-equilibrium phases, quasi-crystalline phases and new crystal phases with extended composite ranges. Finer structures may be observed in the microstructure at sufficiently high cooling rates compared to the conventional manufacturing methods. Moreover, during the SLS/SLM process, gas bubbles and oxide inclusions can become entrapped in the material during solidification due to various causes such as decrease in the solubility of the dissolved elements in the melt pool during cooling and solidification, chemical reaction or trapped gas. Therefore, the mechanical and material properties obtained after SLM may be different than the properties of materials produced by conventional production techniques [9].

2. Materials and Methods

2.1 Materials in SLS

SLS can process almost any substance as long as it's in dry powder and the powder particles ignite or sinter when heated. The bulk of materials falls within this category. Powder particles with limited fusing or sintering abilities can be laser sintered by adding a substitute binder material (typically a polymer) to the basic powder. Once the entire piece has been sintered, the sacrificial binder may be removed depending on the "green" area (in which the metal particles are bounded together by polymer–polymer bonds) in a thermal furnace. The green part is usually porous, has low mechanical properties and need to be post–processed. The use of a sacrificial binder allows for the expansion of the pellet of laser sinterable materials. Laser sintering stands out among fast prototyping processes with its extensive material compatibility, surpassing other sinterable materials and techniques. It enables rapid production and processing of a wide range of materials, making it a versatile and efficient method for fast prototyping applications, however, the range of materials (powders) that can be laser sintering without a fatal binder is rather extensive [10]. In SLS, polymer dry powders are the initial and are yet the most extensively used product.

Parts made from amorphous polymers, such as polycarbonate (PC) powders, provide excellent dimensional precision, feature determination, and shallow quality (contingent on the ounce size). They are, however, partly cemented. As a result, these components are only suitable for situations where part strength and longevity are not required. SLS masters are commonly used in the production of silicone rubber and cast epoxy moulds.

Semi-crystalline polymers, such as nylons (polyamide (PA)), can be sintered to generate completely dense components with mechanical properties equivalent to injection moulded ones. The total shrinkage of these semi – crystalline polymers throughout the SLS process is around 4%, hindering the manufacture of accurate components. The mechanical properties of these nylon – based components make them perfect for high – strength functional prototypes [11]. Even though amorphous powders may still generate higher resolutions and smoother surfaces, new nylon powder grades (such as Duraform PA12) provide resolution and surface roughness that is comparable to PC, making PA ideal for casting silicone rubber and epoxy moulds respectively.

2.2 Working Principle of Additive Manufacturing

In contrast to subtractive manufacturing methods, additive manufacturing is described by ASTM F2792 – 12A as "the process of combining materials to produce items from 3-D model data, generally layer upon layer" [12]. To further understand how the AM process works, the product's CAD model is originally developed in modelling software with the help of the product's requirements. After CAD model is created, it is sectioned along parallel planes that have the same width as the individual layers. The resulting slices have sharp, squared – off edges, much like the staircase effect. These once 3D models are now reduced to the smaller 2D slices. It seems like a difficult 3D issue has been simplified into a set of 2D planes. The geometric 3D model is tiled into a compact 2D file called an STL file before being sent out. Tessellation is the process of approximating the surfaces of a CAD model with a grid of triangles, with each triangle's surface normal and vertex coordinates being recorded.

2.3 Methodology

Sample of composite materials containing PA2200 and one of three ceramic additives (Al_2O_3, MgO and Nanoclay) were heated in an oven simulating the SLS process under conditions designed to mimic those of the SLS process, the oven was kept at a specific temperature (211^0C) for a range of times, and the powders were kept from oxidizing (yellowing) by a constant supply of nitrogen. Because the powder in the left and right cartridges can only be exposed to a maximum of 100^0C during SLS process, and the powder in the bed section can only be subjected to a maximum of 180^0C, samples of the composite materials were heated to both of these temperatures. Composite material samples were stored at room temperature and then in the refrigerator for 25, 50, 75, and 100 hours. There are two ways to heat samples of shaped composite materials, (i) continuous heating and (ii) cyclic heating. The first (continuous heating method is used to

simulate the SLS process for a single build, while the second (cyclic heating) method simulates the SLS process for multiple builds by removing the composite materials samples from the oven, allowing them to cool to room temperature, and then re–heating them. The impact of time and temperature on the powder characteristics was investigated by testing and analyzing sample composite materials with a particle size of 75 to 100 µm, in its natural state, the material is semi–crystalline. The flammability grade value with respect to Nanoclay wt.% in PA2200 shown in Table 1.

For constructing components in SLS process, we often utilize a blend of compliance with the specifications. To obtain a good surface smoothness the procedure parameters employed for outline contact include lower laser control and skimming speed compared to shading exposure. It will deform if not allowed to cool in a controlled atmosphere for an extended period of time due to the outer environment's quick cooling. The component acquires large pressures as it cools fast. As a result, the part is permitted to cool for 4–5 hours inside the platform. Specification for constructing components, we often utilize a blend of new powder and previously used but unsintered powder.

Table 1 Flammability grade value with respect to nanoclay wt% in PA2200

Sr. No	Wt.% Nanoclay	Flammability Grade	Remark 1	Remark 2	Remark 3
1	0	V_2	Flame restated in 30 second after either application of test flame.	Time may not exceed 250 seconds for the ten flame applications for each set of 5 specimens.	The specimens can drip flaming particles.
2	5	V_2	Flame restated in 30 second after either application of test flame.	Time may not exceed 250 seconds for the ten flame applications for each set of 5 specimens.	The specimens can drip flaming particles.
3	10	V_2	Flame restated in 30 second after either application of test flame.	Time may not exceed 250 seconds for the ten flame applications for each set of 5 specimens.	The specimens can drip flaming particles.
4	15	V_1	Flame retards in 30 seconds after either application of test flame.	Time may not exceed 250 seconds for the ten flame applications for each set of 5 specimens.	The specimens may not drip flaming particles.

2.4 Details of material

Figure 2 is made from Polyamide Duraform powder. The previously used powder has qualities that differ from virgin powder after going through a heating cycle. The material utilized had been renewed, and the mixing ratio was 70% used powder and 30% virgin powder [13]. Because using more fresh powder causes the product to curl, only 30% fresh powder may be utilized to make components.

2.5 SLS test parts layout

These five pieces are manufactured at a process station (Vanguard HS) in this SLS setup, as depicted (Figure 2–Figure 6). As illustrated, the pieces are placed in the construction. The central part is exactly in the middle of the construct, with the other parts at similar distances from the center, i.e., the origin of additional parts is 35 mm out from the shape's center. It was known quality, based on sintering presentation involvement, that pieces were put in the same plane/build sinter with minimum delay. As a result, additional tests, i.e., the fabrication of other pieces throughout a similar variety of parameters as the rectangular blocks, are carried out to give samples for the various measurements.

The percentage by weight of fillers in PA2200 corresponds to the flammability grade rating shown in Table 2. The composite materials were heated at 100^0C and 180^0C for 25, 50, 75 and 100 hours to determine the best values for the process parameters. DSC analysis was performed on the heat – treated samples (ISO 11357–6, 2008). The DSC curve shows that the glass transition, recrystallization, and melting point of PA2200 are hardly impacted by loading with different concentrations of three different additives (Al_2O_3, MgO and Nanoclay) (see Figure 2, Figure 3, Figure 4, Figure 5, Figure 6). The following figures shows the connection between T_g, T_c and T_m of composite materials as determined by analyzing the DSC data for the materials. Graph 1 displays the effects of temperature and time on the glass transition, transition temperature, and transition temperature of Silane–Montmorillonite (SMMT) Nanoclay/PA2200 composite, Graph 2 displays the effect of temperature and time on T_g of SMMT Nanoclay/PA2200 composite, Graph 3 displays the effect of temperature and time on Tc of SMMT Nanoclay/PA2200 composite, Graph 310 displays the effect of temperature and time on Tm of SMMT Nanoclay/PA. Theoretically, it has been postulated that the molecular weight is a common factor impacting T_g, T_c and T_m of the composite material. An increase in molecular weight is held accountable for an increase in T_g and T_m of the composite material, while a decrease in T_c of the composite material is held accountable. Furthermore, crystalline index (CI) is a key factor in obtaining a high – quality SLS sintered component [14]. By factoring in the percentage by weight of polymer in the composite, the crystalline index (CI) was determined using Equation;

$$\mathrm{CI} = \frac{\Delta \mathrm{H_m}}{\Delta \mathrm{H_f}(1-\mathrm{f})} \times 100$$

"Where $\Delta \mathrm{H_f}$ is melting enthalpy for a theoretically 100 percent crystalline PA2200, which is 209.2 J/g and f is the mass fraction of the filler. The peak melting temperature Tm, peak crystalline temperature Tc, melting enthalpy $\Delta \mathrm{H_m}$ and crystalline enthalpy $\Delta \mathrm{H_c}$ were extracted from the DSC curves. The CI% value is calculated for PA2200 and mentioned composite materials using the equation. Melt Flow Index (MFI) is a crucial metric for gauging the quality of SLS fabricated components.

3. Measurements

3.1 Dimensional Accuracy

As illustrated in Figure 7 and Table 2, the dimensional accuracy of SLS specimens is indicated by error S_1. For each worth, three capacities are taken and the normal value is obtained. The dimensional error S_1 represents the part's dimensional correctness and is defined as:

$$S_1 = \left[\frac{A_1 - A_0}{A_0}\right] \times 100$$

Where A_0 is the computer – generated design size and A_1 is the actual size unrushed using a vernier caliper. At this point in the sintering process, the material dimensions are stable. The sintering process has two stages, the first of which is the formation of the neck, and the second of which is the completion of the sintering process. The early sintering, stage so often occurs during heating and is characterized by the rapid expansion of the interparticle neck. As the neck grows, sinter mass is transferred along with it. There is no shrinking at this stage because the sinter mass does not lose porosity throughout this process.

3.2 Melt Flow Index (MFI)

Manually calculating the MFI from the known sample to Mass and measurement time yields values expressed in g/10 min; The formula used to determine MFI is

$$\mathrm{MFI}(T,m) = \frac{600m}{t}$$

MFI is significant in the combination of Nanoclay and PA2200 materials as it evaluates their flowability and processability, ensuring efficient and consistent SLS outcomes.

3.3 Melting Temperature (T_m)

The melting temperature is reached when the polymers have accumulated enough thermal energy to begin chain motion freely enough to behave like a viscous liquid. The temperature has a significant effect on the viscosity of the molten polymer. Even more, when the temperature rises, the polymer's viscosity drops automatically:

$$\eta_0 = A\exp^{(\Delta E/RT)}$$

3.4 Mechanical Properties

Mechanical Properties of specimens studied under ambient conditions: include tensile strength, elongation at break, and density. As illustrated specimens were examined using universal testing equipment.

4. Results and Discussion

4.1 Results

To enhance the flame retardant and mechanical properties of the sintered specimen and lower the cost of the Polyamide 12 through the addition of ceramic additives, a new composite material has been developed from ceramic additives (Al_2O_3, MgO and Nanoclay) separately with Polyamide 12 (PA2200) (Al_2O_3, MgO and Nanoclay).

For the purpose of controlling SLS parameters and obtaining consistent quality of fabricated SLS specimens, the thermal properties of composite materials of ceramic additives (Al_2O_3, MgO and Nanoclay) filler and Polyamide 12 of the virgin powder have been studied at various filler percentages (ranging from 0% to 15% by weight).

In an effort to cut down on production time and material waste, researchers have investigated the feasibility of using a technique called pressure less casting to create specimens with qualities comparable to those of SLS components.

It is planned to implement a mechanism for adjusting the percentage of ceramic additions (Al_2O_3, MgO and Nanoclay) filler in Polyamide 12. The use of virgin powder in the SLS system and the creation of a mechanism for regulating the quantity of virgin powder to be added to use powder have both been explored. Powder fitness and mechanical characteristics may be accurately predicted using the melt flow index (MFI), as shown by the correlation between the two [15, 16].

Additionally, a summary of the materials used in the SLS process is provided, and a methodology is developed for selecting the material to be used in the part fabrication on the SLS process based on the properties requirement of application for a fluorescent lamp holder product, by way of the value engineering method. For appropriate material selection and the manufacturing of high – quality components using the SLS process, the method shown in this demonstration has been demonstrated to be effective. The addition of Al_2O_3, MgO and Nanoclay in polyamide 12 (PA12) can have various effects. Al_2O_3 and MgO can enhance the mechanical properties, such as strength and stiffness, while Nanoclay can improve thermal stability and barrier properties. These additives can enhance the overall performance and functionality of PA12–based materials.

4.2 Mechanical Properties

Table 3 lists the mechanical characteristics of the polyamide SLS sample. The tensile strength and extension at the disruption of these SLS samples are both quite low, according to estimated values. The fundamental reason for this is that these components have a low thickness and a large number of voids. Furthermore, the influence of layout on mechanical properties on various portions shows that mechanical characteristics decline as we advance down the Y-axis.

Figures 8 shows pictures of several samples collected using a metallurgical microscope. We can see that the powder particles are not tightly packed, and we can still clearly distinguish between them. Only adjacent particles link together, resulting in distinct pores in the components, which are visible from the sintered part/engulfed air bubble. These are feasible as a result of the evaluation of gases during the solidification process. Which leads to a reduction in the mechanical characteristics of certain sections.

4.3 Melt Flow Index

Metal Flow Index is a crucial metric for gauging the quality of SLS–fabricated components and determining whether to re–inject virgin powder with proper amount of reclaim (Chow and Ishak Mohd 2007). To find best settings for the SLS process, it is helpful to have a firm grasp of the thermal characteristics of composite material made up of PA12 plus one or more additives (Al_2O_3, MgO and Nanoclay). In addition, the thermal and physical characteristics of both sintered and unsintered powder are investigated in order to provide a system for regulating SLS parameters and ultimately for achieving reliable, high–quality SLS specimens throughout the fabrication process. Exposure of the unsintered powder to high temperatures and long heating durations are the most influential elements in the ageing or degradation of composite material of three distinct additions (Al_2O_3, MgO and Nanoclay) with PA12 [17]. Graph 1 displays the melt flow index of the SMMT Nanoclay/PA2200 composite, Graph 2 displays that of the Aluminum Oxide / PA2200 composite, and Graph 3 displays that of the Magnesium Oxide / PA2200 composite. When comparing the effects of MFI on materials heated to 100^0C for 0 – 100 hours against 180^0C for 0 – 100 hours, the former has a smaller impact. At 180^0C and during the first 25 hours, the MFI decreases the most, and the competition for the same temperature and time period causes the viscosity to rise quickly.

Table 2. Dimensional accuracy of SLS parts

Sr. No.	Measurements		A_0	S_1 % of Part 1	S_1 % of Part 2	S_1 % of Part 3	S_1 % of Part 4	S_1 % of Part 5
1	Length of side	X	30	0.25	0.264	0.258	0.254	0.265
		Y	30	0.26	0.263	0.257	0.261	0.264
2	Width of rib	X	1	0.12	0.18	0.09	0.07	0.19
		Y	1	0.12	0.19	0.06	-0.03	0.19
3	Thickness	Z	3.75	0.33	0.333	0.333	0.336	0.370
4	Circle at center	R_1	1.5	0.073	-0.04	0.113	0.133	-0.14
		R_2	1.5	0.086	-0.033	-0.02	0.186	-0.03
		R_3	1.5	0.060	-0.006	0.106	0.146	0.12
5	Thickness of base	Z	1.25	0.416	0.448	0.464	0.456	0.528
6	Average	S%		0.138	0.156	0.170	0.192	0.185

Table 3. Mechanical Properties of SLS Parts

Sr. No.	Measurements	Values of Part 1	Values of Part 2	Values of Part 3	Values of Part 4	Values of Part 5
1	Tensile Strength (MPa)	47.49	47.48	47.48	47.48	47.45
2	Elongation at break (%)	17.3	17.2	17.2	17.0	17.1
3	Density (gm/cc)	0.960	0.958	0.558	0.57	0.595

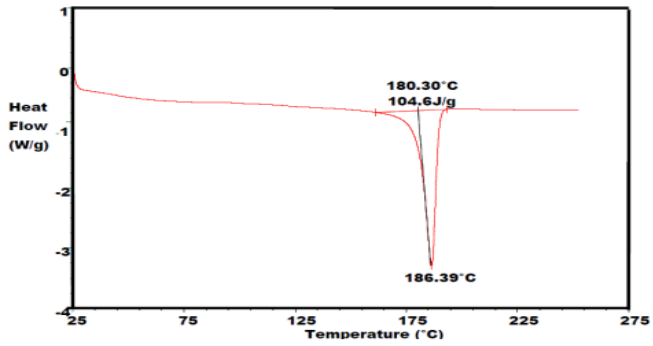

Figure 2: DSC of PA2200 (Non – heat treated)

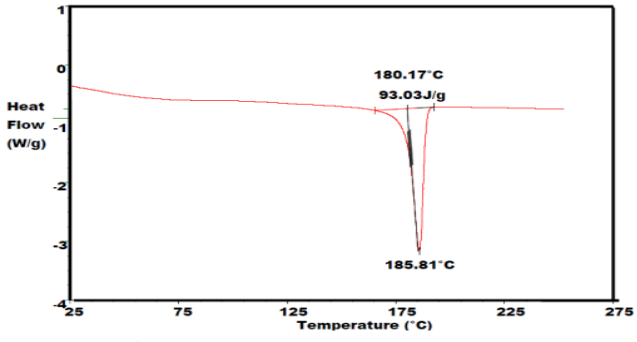

Figure 3: DSC of SMMT Nanoclay 5 wt.% / PA2200 composite (Non – heat treated)

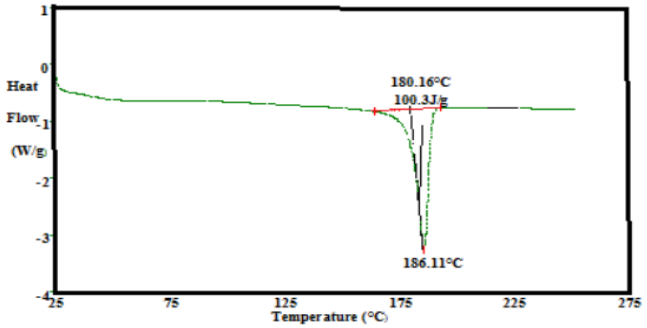

Figure 4: DSC of Aluminum Oxide 5 wt.% / PA2200 composite (Non – heat treated)

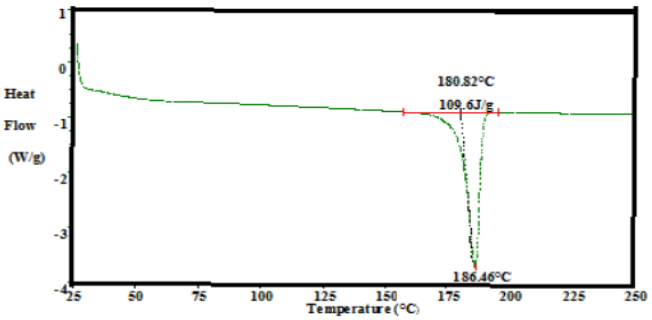

Figure 5: DSC of Aluminum Oxide 10 wt.% / PA2200 composite (Non – heat treated)

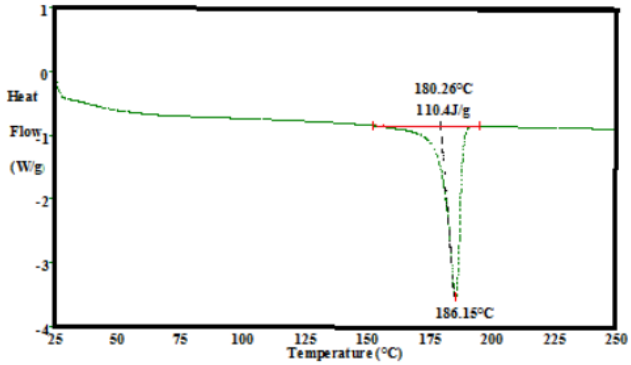

Figure 6: DSC of Magnesium Oxide 5 wt.% / PA2200 composite (Non–heat treated)

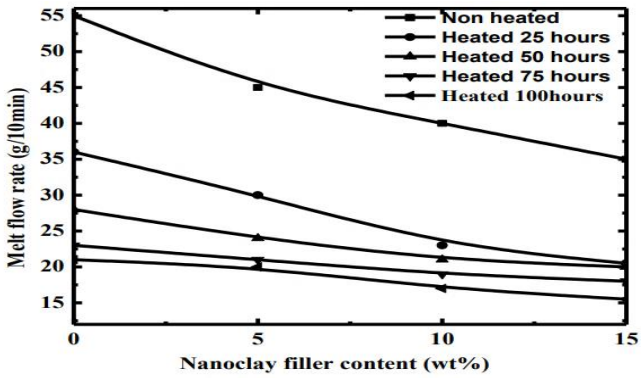

Graph 1: Melt Flow Index of SMMT Nanoclay/PA2200 composite

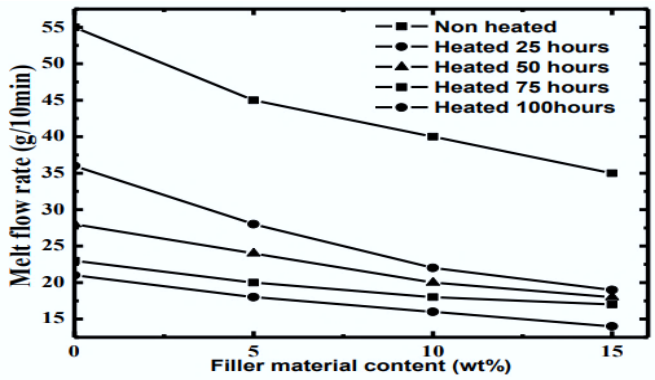

Graph 2: Melt Flow Index of Aluminum Oxide / PA2200 composite

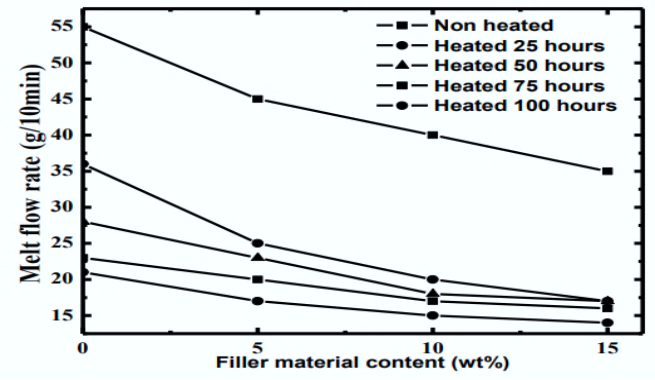

Graph 3: Melt Flow Index of Magnesium Oxide / PA2200 composite

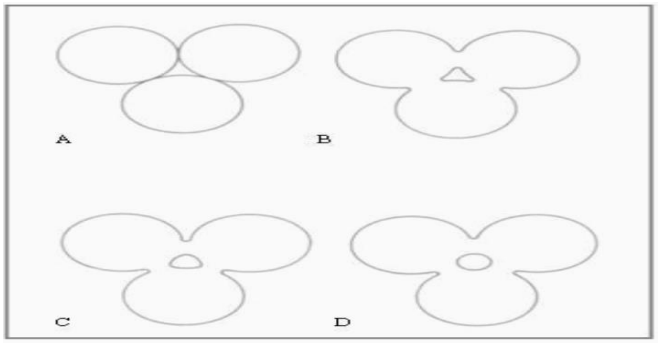

Figure 7: Three sphere sintering model (A) Original Point Contacts (B) Neck Growth (C) Pore Rounding

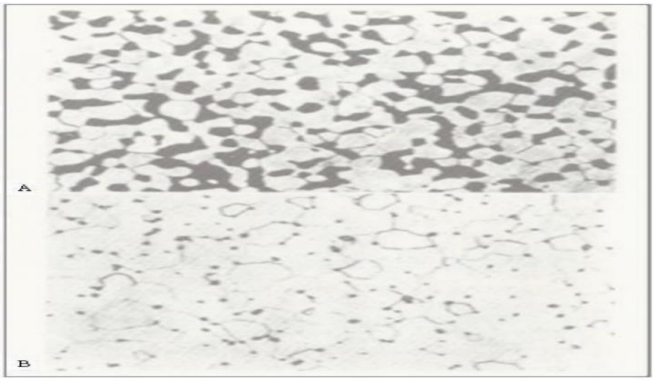

Figure 8: Photo micrographic illustration of change from interconnected to isolated porosity (A) Early phase with interconnected porosity (B) Later Phase with closed porosity

5. Conclusion

The fields in which additive manufacturing is used are expanding. Particularly relevant to the SLS technique. Improvements in the utilized material are necessary for the SLS method to become competitive and a good option for innovative applications (i.e., quick production). The goal of this study is to reduce the price of Polyamide 12 and significantly enhance the quality of SLS fabricated parts by first optimizing the selection of existing materials based on the properties required by applications, and then improving the properties of SLS materials by combining ceramic additive (Al_2O_3, MgO and Nanoclay) with Polyamide 12 to form a new composite material (Al_2O_3, MgO and Nanoclay).

Reference

[1] M. Siming, S. Zhongxia, A. Shang, P. Zhang, C. Tang, Y. Huang, C.L.A Leung, P.D. Lee, X. Zhang, and X. Wang, "Additive manufacturing enabled synergetic strengthening of bimodal reinforcing particles for aluminum matrix composites," Additive Manufacturing Journal, vol. 70, no. 3, pp. 103–117, May 2023.

[2] F. Lupone, E. Padovano, F. Casamento, and C. Badini, "Process phenomena and material properties in selective laser sintering of polymers," Materials Journal, vol. 15, no. 1, pp. 1–37, Dec 2021.

[3] K.M. Abed, "Investigation of properties of selective laser sintering of titanium alloy composite," Journal of Mechanical Engineering Research and Development, vol. 44, no. 9, pp. 34–44, May 2021.

[4] P. Lu, Z.C. Lin, W. Liang, L. Tong, and L.X. Cheng, "Research on mechanical properties and microstructure by selective laser melting of 316L stainless steel," Mater. Res. Express, vol. 6, no. 12, pp. 60–80, April 2020.

[5] N.A. Hamzah, N.A.A Razak, M.S. Karim, and H. Gholizadeh, "A review of history of CAD/CAM system application in the production of

transtibial prosthetic socket in developing countries (from 1980 to 2019)," Proceedings of the Institution of Mechanical Engineers, Part H: Journal of Engineering in Medicine, vol. 235, no. 12, pp. 1359–1374, July 2021.

[6] T. Kozior, C. Dopke, N. Grimmelsmann, I.J. Junger, and A. Ehrmann, "Influence of fabric pretreatment on adhesion of three-dimensional printed material on textile substrates," Advances in Mechanical Engineering, vol. 10, no. 2, pp. 1–8, Aug 2018.

[7] J. Bochnia, and S. Blasiak, "Fractional relaxation model of materials obtained with selective laser sintering technology," Rapid Prototyping Journal, vol. 25, no. 1, pp. 76–86, Jan 2019.

[8] S. Fafenrot, N. Grimmelsmann, M. Wortmann, and A. Ehrmann, "Three -dimensional (3D) printing of polymer-metal hybrid materials by fused deposition modeling," Materials Journal, vol. 10, no. 10, pp. 209–219, Oct 2017.

[9] T. Kozior, and C. Kundera, "Evaluation of the influence of parameters of FDM technology on the selected mechanical properties of models," Procedia Engineering, vol. 192, no. 7, pp. 463–468, June 2017.

[10] S. Adamczak, P. Zmarzly, T. Kozior, and D. Gogolewski, "Assessment of roundness and waviness deviations of elements produced by selective laser sintering technology," 23rd International Conference Engineering Mechanics, pp. 70–73, May 2017.

[11] E.O. Olakanmi, R.F. Cochrane, and K.W. Dalgarno, "A review on selective laser sintering/melting (SLS/SLM) of aluminum alloy powders: Processing, microstructure, and properties," Progress in Materials Science, vol. 74, pp. 401–477, Oct 2015.

[12] C. Kundera, and T. Kozior, "Mechanical properties of models prepared by SLS technology," AIP Conference Proceedings, vol. 17, no. 2, pp. 1–12, Oct 2018.

[13] A. Verma, S. Tyagi, and K. Yang, "Modeling and optimization of the direct metal laser sintering process," Springer's International Journal of Advanced Manufacturing Technology, vol. 77, no. 7, pp. 847–860, Oct 2014.

[14] C. Kundera, and T. Kozior, "Elastic bellows prepared by selective laser sintering," Applied Mechanics and Materials, vol. 630, no. 17, pp. 318–325, Sep 2014.

[15] G.V. Salmoria, J.L. Leite, L.F. Vieria, A.T.N. Pires, and C.R.M. Roesler, "Mechanical properties of PA6/PA12 blend specimens prepared by selective laser sintering," Polymer Testing, vol. 31, no. 3, pp. 411–416, May 2012.

[16] K.A. Ghany, and S.F. Moustafa, "Comparison between the products of four rpm systems for metals," Rapid Prototyping Journal, vol. 12, no. 2, pp. 86–94, Mar 2006.

[17] M. Badrossamay, and T.H.C. Childs, "Further studies in Selective Laser melting of Stainless and Tool Steel Powders," International Journal of Machine Tools and Manufacture, vol. 47, no. 5, pp. 779–784, April 2007.

The Nucleus ***60****, No. 1 (2023) 71-77*

www.thenucleuspak.org.pk

The Nucleus
ISSN 0029-5698 (Print)
ISSN 2306-6539 (Online)

Amkhoi Geopark: Geotourism and Socio-economic Development of the Rural Areas of Chaupahari Forest and Adjoining Area, Birbhum, West Bengal, India

Bikas Saha

Department of Geology, Durgapur Government College, J.N. Avenue, Durgapur, West Bengal, India.

ABSTRACT

Tourism that encourages or intensify the distinctive geological character of a place is called as geotourism. Interpretation, promotion and preservation of geological characters are the main focuses of the geotourism. Different abiotic ingredients, biotic components and cultures are involved in geotourism and as a result, this tourism redecorates its busyness. Geotourism represents the upgradation and shielding of the geoheritage sites by education and interpretation. This new form of tourism is environmentally futuristic. By popularizing tourist places into geosites, geotourism protects the geopark with the understanding of geologists. India is rich in georesources and geosites. It shows variety and uniqueness in terms of geological characteristics, types of rocks, fossils and landscapes but little attention has been given while acknowledging the geoparks and geoheritage sites. Geological sites with tourism potential and recreational potential will play important roles in socio-economic development. Angiosperm wood fossils have been discovered in the year 2006 from a tribal village, named Amkhoi, near Chaupahari forest, Illambazar of Birbhum district. After the inauguration of a fossil park here in Amkhoi in the year 2018, its success encourages its extension and further planning for geotourism. The Wood Fossil Park at Amkhoi attempts to integrate economic benefits for the local community by imparting education and awareness on the geo-site and hence is a good stride for attaining sustainability perspectives.

Keywords: *Geopark; Geotourism, Socioeconomic Activity, Geo-conservation, Amkhoi Wood Fossil Park, Sustainable Tourism, Chaupahari Forest*

1. Introduction

In the recent past, Prof. Thomas A Hose of department of Earth Science of the Bristol University invented the term "*geotourism*". It was first coined in 1995. Hose defined geotourism as *"to ensure the value and social preservation of geological and geomorphological sites and their materials and to provide interpretative facilities and services for the use of students, tourists and other casual recreationalists"*. Interpretation, promotion and preservation are the main focuses of geotourism. As per Dowling and Newsome (2010) [1], it is an arrangement of tourism of natural areas where landscape and geology are the centre of attention. As time goes by geotourism and its definition evolved in 2012, an updated version of the definition of geotourism states that "geotourism is the providing of informative and service facilities for geosites and geomorphosites and their surrounding topography together through their allied in-situ and ex-situ artefacts, to build of constituency for their conservation by making appreciation, learning and research for current and future generations".

Due to the involvement of different abiotic ingredients, biotic components and culture, geotourism redecorates its busyness. Geotourism represents the upgradation and shielding of the geoheritage sites by education and interpretation. It is appearing as a new form of tourism which is environmentally futuristic. By popularizing tourist places into geosites, geotourism protects the geopark with the understanding of geologists.

The word 'fossil' is Latin word 'fossilis', which means something obtained from digging. Fossils, the paleontological treasures, are preserved remains, impression or trace of organism that existed in past geological ages [2, 3]. They are generally found in sedimentary rocks. Fossilization is the process by which the remains of an organism gradually transformed into fossil. Fossils are the data sources on paleo-environmental history. Fossils are the non-renewable earth heritages. They are imparting scientific knowledge on the climate of the past, past depositional environment of sediments, past geographical conditions, relative age determinations and past ecology [4]. Regarding the tourism potentiality of the fossil park, there are some research gaps that exist. This study aims to highlight the tourism potential in the youngest wood fossil park in India located at Amkhoi in West Bengal.

By involving many geologists, proprietors, social workers, tourism contributors, local people and private-public bodies, UNESCO started the concept of geoheritage park in the year 2001. By 2004, this beginning was converted into a program known as UNESCO Global Geoparks Network (GGN). Within the 44 member-country of UNESCO Global Geoparks Network (GGN), there are 161 UNESCO Global Geoparks. As a result of UNESCO initiative, newer and newer geosites are discovered worldwide due to the spreading appreciation of different processes of the earth as well as field surveying [5].

Fossil parks are distributed all over the world and they are acknowledged as the seeds of modern geotourism. Some of these fossil parks are achieving UNESCO's world heritage sites title such as Australian Fossil Mammal Sites (Riversleigh/Naracoorte), Australia; Joggins Fossil Cliffs, Canada; Dinosaur Provincial Park, Canada; Chengjiang Fossil Site, China and Messel Pit Fossil Site, Germany. With their exceptional heritage and scientific values, these fossil parks have been complemented by UNESCO with its recognition under the Global GeoPark Network. For geotourism promotion and geoheritage conservation, these Global GeoPark Networks can play crucial roles [6]. There are numerous geoparks across the world which are primarily

*Corresponding author: sahabikas@gmail.com

based on fossils only. Geological Reserve of Haute Provence (France), Petrified Forest of Lesvos (Greece), Nature Park Terra Vita European Geopark (Germany), Abberley and Malvern Hills (UK), Geopark Schwabian Alb (Germany), Hateg Country Dinosaur Geopark (Romania) and Forest Fawr Geopark, Wales (UK) are among the popular geoparks where fossils are the main attraction [7].

India is rich in georesources and geosites but tiny consciousness has been rewarded while acknowledging the geoparks and geoheritage sites. From Archean to the Recent age, India shows variety and uniqueness in terms of geological characteristics, types of rocks, fossils and landscapes. But there are no ceremoniously accepted geoparks in India. Even, none of the geological sites have ever been nominated for World Heritage recognition. Geotourism is still at its juvenile stage in India despite the positive efforts of the Geological Survey of India which recognized 34 geological sites as National Geological Monuments for visitors among which there are seven fossil parks namely Siwalik Fossil Park, Himachal Pradesh; Marine Gondwana Fossil Park, Chhattisgarh; National Fossil Wood Park, Thiruvakkarai, Tamil Nadu; National Fossil Wood Park, Sathanur, Tamil Nadu; Akal Wood Fossil Park, Rajasthan; Jhamarkotra Stromatolite Park, Rajasthan; and Bhojunda Stromatolite Park, Rajasthan. Apart from these, there are several fossil parks scattered in the different parts of the country viz, Indroda Dinosaur and Fossil Park, Gujarat; Dinosaur National Park Bagh, Madhya Pradesh; Mandla Plant Fossil Park, Madhya Pradesh; Ghugha National Fossil Park, Madhya Pradesh; Salkhan Fossil Park, Uttar Pradesh; Wadadham Fossil Park, Maharashtra; Dinosaur Fossil Park, Balasinor, Gujarat; Kutch Fossil Park, Gujarat; and Amkhoi Wood Fossil Park, West Bengal which could be classified based on four main fossil groups – Invertebrate fossil, vertebrate fossil, wood fossil and stromatolite fossil (Fig. 1) [2, 8]. There are only 3 – 4 wood fossil parks in India. One of them is the Amkhoi. Therefore, we ought to preserve the park for its uniqueness.

For the purpose of conservation of geosites, many researchers in India are trying to identify contemporary geoparks. Some researchers are trying to show the geotourism potential of Arunachal Pradesh. Ahluwalia [9] has focused on the geoheritage sites, geodiversity and eventuality of geoparks of India. Geotourism in the Kutch region of Gujarat is in the developing stage. Tirupati Eparchaean Unconformity is a notified National Geo-Heritage Monument situated at Namalagundu of Andhra Pradesh [10].

Succession with Fossils	Type of Fossil	Age	Place	Reference
Tipam and Dupitila Groups of Assam	Wood Fossils	Middle–Late Miocene	Dhemaji and Lakhimpur districts of Assam	[11]
Barmer Hill Formation	wood-boring trace fossil Asthenopodichnium	Palaeocene	Barmer Basin on Lunu village on the Barmer– Bishala road	[12]
James Ross Island, Antarctic Peninsula	Fossil wood of the Winteraceae	Upper Cretaceous	James Ross Island, Antarctic Peninsula	[13]
Mcrae Formation, South-Central New Mexico, USA	Angiosperm Wood Fossil	Late Cretaceous	South-Central New Mexico, USA	[14]

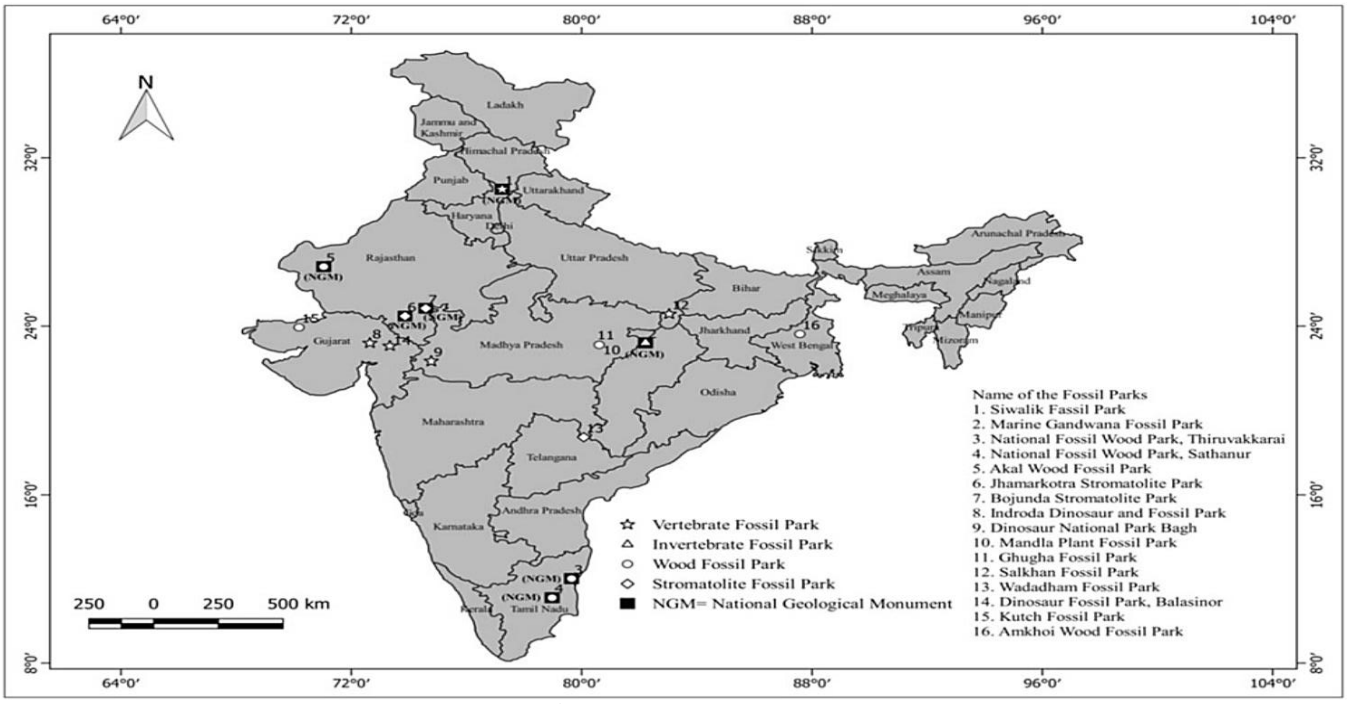

Fig. 1: Map of India showing National Geological Monuments [2, 8].

For socio-economic development, geological sites with tourism potential and recreational potential are playing important roles. Apart from promoting and conserving geoheritage sites, potent conversion of principles of geotourism outstandingly provides in the development of tourism as well as add economic value surrounding the geoheritage sites [15]. At present, geotourism is a new gesture to increase the bits of knowledge of tourists. And these knowledges are not only about a natural resource but also about the local culture and their preservation processes. In respect of commercial development in most of the countries, geotourism is still at an early stage. And in the development of geotourism of any geosites, geoparks are the pioneer. To explore different ingenious strategies and geomarketing, the involvement of local communities is very compelling. Moreover, to promote the socio-economic conditions of the local people and to increase the knowledge of geology among local bodies, we should set up geoparks. The flow of money is always towards geoparks side when tourists move to geoparks and tourists also exporting some agricultural products, local products and some cottage industry products with them. Geoparks have to support the establishment of local crafts and replicas, as well as support local products. Thus, visitors to geoparks can actually take with them, together with emotions and knowledge, manufactured goods.

About 18% of the world's population, i.e., nearly about 1.3 billion people are living in India. Among these 1.3 billion, 65% of the population are living in rural areas [16]. So, for socio-economic development of the rural areas of India, geotourism sites in the rural area will play an important role. To convert any geoheritage sites to geopark, the collaborative endeavour is needed. Through recognizing, declaring, promoting, preserving and branding, partners of the collaborative venture will help to promote the geoheritage site to geopark. Moreover, to establish geopark, we can use India's vast geodiversity and extraordinary scenic beauty. Here in this article, we are presenting Amkhoi village as new possibility in terms of new geopark namely Amkhoi Wood Fossil park.

2. Study Area and Geology

Amkhoi fossil park, located at Chaupahari forest of Illambazar Forest range, Birbhum, is contemplated as one of the great geological treasures. Presence of the huge number of wood fossils demonstrated by a million years old sunken forests.

Amkhoi is that type of small village situated in the west side of West Bengal in the Chaupahari Forest near Illambazar where wood fossil has been discovered. Amkhoi Wood Fossil Park (23°37′25″ N, 87°34′56″ E) is situated about 20 kilometres from Bolpur town in Birbhum (Fig. 2) [3]. The park is about 10 hectares in size and is spread over villages like Amkhoi, Jambuni etc in the forest of Chaupahari at Illambazar. The park is maintained by the caretaker recruited by Forest Department, Govt. of West Bengal.

In the eastern part of the Indian subcontinent, the Bengal basin has been evolved. Towards west and north, this basin is bounded by Indian Shield and towards east, by Indo – Burman Ranges. Pericratonic Bengal, sedimentary basin deposited along the east coast margin of India [17]. It consists of easterly dipping shelf in the western and south western part of Bengal basin [18]. The famous Rarh Bengal is consisting of the Western lateritic part of West Bengal [19, 20].

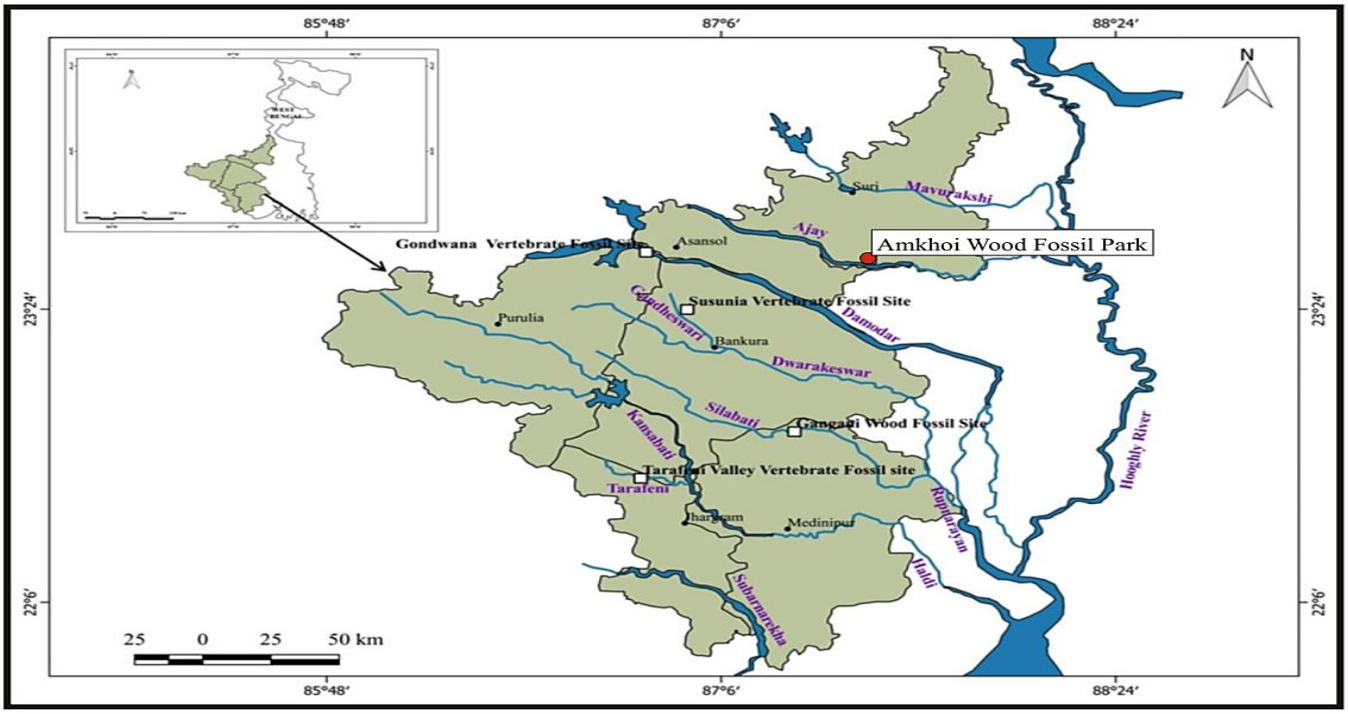

Fig. 2: Location map for Amkhoi Fossil Park (After Chakrabarty & Mandal, 2019) [3]

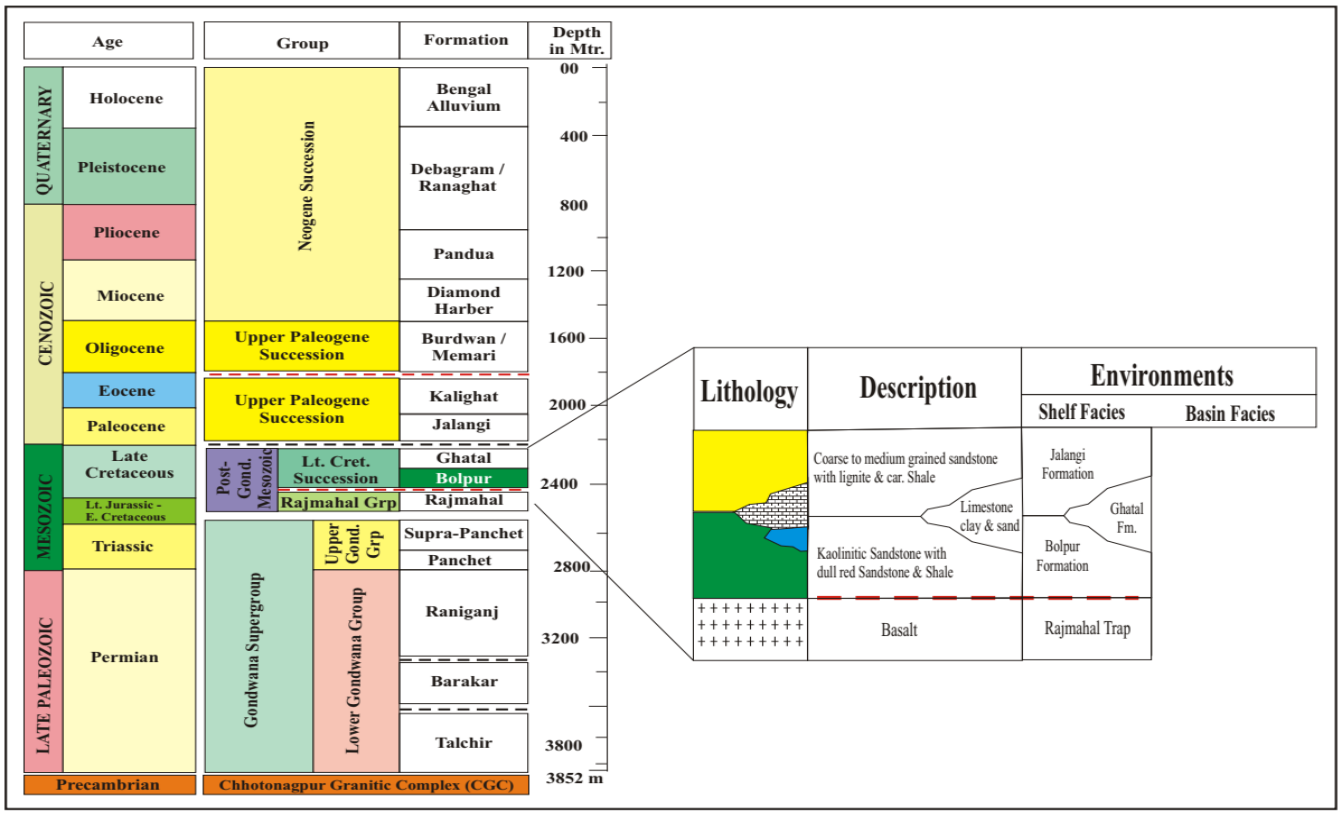

Fig. 3: Wood fossils of Amkhoi preserve in the Late Tertiary sedimentary succession of Bolpur Formation (After 2 & 23]

Geometry-wise Bengal basin is asymmetric with thinner, softly plunging sediment cover in both the western and northern parts of the basin [21, 22]. Sediment continues to accumulate in a basin-ward direction. Stratigraphy, sedimentation, tectonics and history of basin evolution in the different parts of the basin, over the entire belt show considerable heterogeneity.

Particularly, the stratigraphy in the different parts of the basin differs and as a result, the basin reflects contrasts both in pattern and history of deposition in the discrete basin [23].

These wood fossils of Amkhoi were preserved in the Late Cretaceous sedimentary succession, i.e., in Bolpur formation, uncovered in several individual patches in and around the western part of Bengal Basin (Fig. 3) [23]. These wood fossils were discovered at Amkhoi during the digging of a pond. Concrete walls have been made around that pond (Fig. 4). Lithostratigraphically, these fossils are found in the cobble and pebble conglomerate strata.

3. Discussion

India is an exceptional country due to its fascinating geological history and it is transparent in its huge number of breathtaking and absorbing geological features dotted all over the subcontinent. Geological Survey of India (GSI) recognized some of these geological heritages as 'National Geological Monuments' (Fig. 1) [2 & 23]. GSI recognized these Monuments from the huge varieties of geosites like EcoGeo Monuments, Fossil Park, Geological Marvels, Rock Monuments, Stratigraphy Monuments, Stromatolite Park, Wood Fossil Park, present across the sub-continent.

Fig. 4: Petrified wood or Wood Fossils discovered during digging of this pond at Amkhoi village during 2006.

Dating back to the early Permian onwards, as India was a part of Gondwana Land, India has a very rich deposit of fossil flora. Wood fossils and vertebrate fossils are also available across the parts of West Bengal [2].

The trees have been transformed into wood fossils during Late Miocene period here at Amkhoi. They have uprooted from the uphills of Rajmahal hills and Chotonagpur plateau

due to force majeure and transported by intermittent floods and later on, under suitable conditions, they became petrified.

It is assumed that the trees were transported to the lower catchment of the drainage basin by intermittent floods after uprooted by natural calamities in the upper catchment area. Later on, these uprooted from upper catchments, and transported to the lower catchment's trees became petrified (Fig. 5). Depending upon the terrain characteristics, two major types of wood fossils generated – (i) silicified and (ii) calcified. But most of them transformed into silicified wood fossils (Fig. 6).

Fig. 5: Growth Rings is visible within the wood fossils of Amkhoi Fossil Park (Black Arrows).

Fig. 6: Silicified (white arrow) as well as Chartified (black arrow) Wood Fossil preserved in the area.

Amkhoi geoparks is now in the juvenile stage in terms of geotourism. During 2019, on an average, 300 to 350 persons per week used to visit Amkhoi geoparks. Now the number has increased significantly. Amkhoi geoparks are snuggled in the lap of a thick, dry, deciduous forest, namely Chaupahari Forest. The park is situated in the Amkhoi village within Chaupahari Forest, covering an area of about 10 hectares. The forest of Chaupahari consists of Mahua (Madhuca longifolia), along with some other flora which helps the indigenous people to live their life including honey from the forest (Fig. 7).

Fig. 7: Floral assemblages of present Chaupahari Forest of Illambazar Forest Range, which are the supply line of different natural, forest products for the indigenous people of Amkhoi as well as Chupahari Forest.

The fossil park is in the developing stage, still now, with the help of some group of local villagers. They are guarding their natural treasure by turning the king system. These local people also help the visitors with their quarries. Still, the fossils hunters and antiquethieves are robbing these treasure land and selling these valuable fossils online for millions of dollars. But later on, when the local villagers realized the value of those natural treasures, they are taking care of the park. Local women set up a cafeteria, the sales centre here in the geopark. Due to the increasing number of visitors to geoparks, sell of different types of products also increasing day by day. Before starting the Amkhoi geoparks, villagers used to sell very few local, indigenous products like hand-held fans, Sital Pati Mat made of Date, Palm leaves, different sized containers made of bamboo, Mahua oil and Mahua fruits, and different drawing with natural colour. Even the indigenous people of Amkhoi and adjoining areas are using the natural colour extracted from the wood fossil (Fig. 8 & 9) to paint their houses (Fig. 10). So as a result, the villagers are noticing a slow but steady progress in their life and livelihood. Economically these villagers are more sound than pre-geopark times. Some resorts are constructed after the fossil park opened to the general public. Local people were talking about the economic developments of the area after the opening of the park. Indigenous people especially male persons were mostly addicted to country liquor. As a result, both the economy and their means of survival were unhealthy. But it has reduced remarkably since the establishment of the fossil park. So geotourism definitely improves the socio-economic conditions of the indigenous people of the Amkhoi village as well as the adjoining areas.

In the last two decades, globalization and the influence of the people of the west bring huge advancements in the thinking of the Indian people, thanks to the digital age and the

Fig. 8: Aesthetically pleasing, soft lustre and hues of different colours present within Petrified Wood.

Fig. 9: Hollow space (marked by white arrow), which was pocket of natural colour within the Wood Fossil.

Fig. 10: Indigenous people of Amkhoi and adjoining areas are using the natural colour extracted from the wood fossil to paint their houses.

recently launched Digital India programme. People have started to explore nature with their increasing economic affordability. People are taking an interest towards weekend outings and with increasing inclination towards weekend outings.

At present, both the local public as well as the decision-makers in India are not realizing the importance of geoheritage sites properly. With the physical development of land surface and interventions for creating new landscapes, the landscape creating the menaces to geosites is growing day by day. INTACH (2016) [25] yielded a draft resolution as "The National Geological sites (conservation, protection and maintenance) Act. 2013" for adaptation to Govt. of India but is still to be made a law.

4. Conclusion

Indian sub-continent is enriched with extraordinary and rich geo-wealth. These multitudinous, elegant features, landforms and landscape of India bear huge knowledge-based, ethnic and societal desirability.

There are only seven heritage sites from India included in the list of World Heritage Sites in the last three decades. In UNESCO's list of Global Geoparks Network (GGN), not a single geoparks from India will pop up [26].

Due to the socio-economic development of certain sectors of tourists, their behaviour as well as purchase habit has changed across the country. Therefore, some other forms of tourism like ecotourism, geo-tourism, agro-tourism, wildlife tourism, rural tourism, geo-ecotourism are explored by the government. By recognizing geotourism potential, the tourism potency of West Bengal will reinforce. By developing geotourism through pragmatic analysis and by applying geospatial techniques, geotourism will flourish more and the state will unearth more scope for its people. Hence geotourism will bring economic growth to the state.

Conservation of the paleontological resource is the primary aim of establishing any fossil park. Hence, to conserve this Amkhoi park, the authority should educate the local people as well as the visitors about these fossils and promote geotourism for the sustainable socio-economic development of the local community. As the Amkhoi wood fossil park is new, it can offer new employment opportunities as well as new economic activities to benefit the local people [26].

If local communities share fairly in the benefits that come out from geotourism opportunities, then only any geotourism venture should only be considered successful.

Declaration of Competing Interest

The authors declare that they have no known competing financial interests or personal relationships that could have appeared to influence the work reported in this paper.

Acknowledgements

The author acknowledges Mr. Ramprasad Bauri, Caretaker of the Amkhoi geopark, for providing various

information about Amkhoi geopark and adjoining areas. The author express gratitude to Durgapur Govt. College for infrastructural facilities. This research did not receive any kind of grant from any funding agencies.

References

[1] D. Newsome and R.K. Dowling, "Geotourism: The tourism of geology and landscape", Oxford: Goodfellow Publishers, 2010.

[2] R. Mandal and P. Chakrabarty, "Tourism Potentials of Fossil Parks as Geoheritage Sites: A Study in Western and South Western Region of West Bengal, India" In: Jana, N.C. et al. (eds.), Livelihood Enhancement through Agriculture, Tourism and Health, Advances in Geographical and Environmental Sciences, pp. 247–260, 2022. https://doi.org/10.1007/978-981-16-7310-8_13

[3] P. Chakrabarty and R. Mandal, "Geotourism development for fossil conservation: a study in amkhoi fossil park of west bengal in india", GeoJournal of Tourism and Geosites, vol. 27, no. 4, pp. 1418–1428, 2019. https://doi.org/10.30892/gtg.27425-444

[4] R.S. Dietz, T.L. Pewl and M. Woodhoush, Petrified wood (Araucarioxylon Arizonicum): proposed as Arizona's state fossil. J Arizona-Nevada Acad Sci, vol. 22, no. 2, pp. 110, 1987.

[5] P.E. Migon and P. Migon, "Promoting and interpreting geoheritage at the local level – bottom-up approach in the land of extinct volcanoes, Sudetes, SW Poland", Geoheritage, vol. 11, pp. 1227–1236, 2019. https://doi.org/10.1007/s12371-019-00357-2

[6] G. Császár, M. Kázmér, B. Erdei and I. Magyar, A possible Late Miocene fossil forest PaleoPark in Hungary. Notebooks on Geology-Book 2009/03 (CG2009_B03), 2009, Chapter 11:130.

[7] S. Turner, Promoting UNESCO Global Geoparks for sustainable development in the Australian-Pacific region. Alcheringa, Special Issue 1, 351–365, 2006. https://doi.org/10.1080/031155 10609506872

[8] Geological Survey of India (2017). https://bhukosh.gsi.gov.in/Bhukosh/Geotourism.html

[9] A.D. Ahluwalia, "Indian geoheritage, geodiversity: Geosites and geoparks", Current Science, vol. 91, no. 10, pp. 1307, 2006.

[10] P.R.C. Phani, "Geological excursion to Eparchaean unconformity at Namalagundu, Anantapur District, Andhra Pradesh, India", e-Journal Earth Science India, pp. 1–8, 2016. https://www.researchgate.net/publication/297546285.

[11] R.C. Mehrotra, S.K. Bera, S.K. Basumatary and G. Srivastava, Study of fossil wood from the Middle–Late Miocene sediments of Dhemaji and Lakhimpur districts of Assam, India and its palaeoecological and palaeophytogeographical implications, J. Earth Syst. Sci., vol. 120, no. 4, pp. 681–701, 2011.

[12] S.C. Mathur, N.S. Shekhawat, S.L. Nama, C.P. Khichi, A. Soni, S. Mathur and V.S. Parihar, The wood-boring trace fossil Asthenopodichnium from Palaeocene sediments of the Barmer Hill Formation, western Rajasthan, India, Current Science, vol. 114, no. 7, 2018. doi: 10.18520/cs/v114/i07/1540-1544

[13] Poole and J.E. Francis, The First Record of Fossil Wood of Winteraceae from the Upper Cretaceous of Antarctica, Annals of Botany 85, pp. 307–315, 2000. doi:10.1006/anbo.1999.1049.

[14] E. Estrada-Ruiz, H.I. Martínez-Cabrera, SRS Cevallos-Ferriz, "Fossil woods from the Olmos Formation (late Campanianearly Maastrichtian), Coahuila, Mexico," Am J Bot, vol. 97, pp. 1179 – 1194, 2010.

[15] R.K. Dowling, "Geotourism's global growth", Geoheritage, vol. 3, no. 1, pp. 1–13, 2011.

[16] B.C. Prabhakar and K.N. Radhika, "Recognizing New Geoheritage Sites in Karnataka, India", Geoheritage, vol. 14, no. 3, 2022. https://doi.org/10.1007/s12371-021-00626-z

[17] B. Prasad and B.S. Pundir, "Gondwana biostratigraphy and geology of West Bengal Basin and its correlation with adjoining Gondwana basins of India and western Bangladesh", J. Earth Syst. Sci., vol. 129, no. 22, 2020. 22 https://doi.org/10.1007/s12040-019-1287-2

[18] A.B. Roy and A. Chatterjee, "Tectonic framework and evolutionary history of the Bengal Basin in the Indian subcontinent", Current Science, vol. 109, no.2, pp. 271–279.

[19] S. Sengupta, "Geological framework of the Bhagirathi-Hooghly Basin", In: Bagchi K (ed) The Bhagirathi-Hooghly Basin, Proceedings of Interdisciplinary Symposium, University of Calcutta (Kolkata), pp. 3–8, 1972.

[20] K. Bagchi and K.N. Mukherjee, "Diagnostic Survey of Rarh Bengal (Part II)", University of Calcutta, Calcutta, 1983.

[21] Uddin and N. Lundberg, "Miocene sedimentation and subsidence during continent–continent collision, Bengal basin, Bangladesh", Sediment. Geol., vol. 164, pp. 131–146, 2004.

[22] J.R. Curray, F.J. Emmel and D.G. Moore, "The Bengal Fan: Morphology, Geometry, Stratigraphy, history and processes", Mar. Pet. Geol, vol. 19, pp. 1191–1223, 1993.

[23] U. Ganguli, "A new lithostratigraphic unit at the Western fringe of West Bengal India", India J Geol., vol. 67, no. 4, pp. 282–288, 1995.

[24] Geological Survey of India (2017). https://bhukosh.gsi.gov.in/Bhukosh/Geotourism.html

[25] INTACH (Indian National Trust for Art and Cultural Heritage: Natural Heritage Division) (2016) A monograph on national geoheritage monuments of India Web. http://naturalheritage.intach.orguploads 2017/11.

[26] UNESCO (2020) International Geoscience and Geoparks Programme (IGGP) UNESCO Earth Sciences Web: http://www.unesco.org/new/en/naturalsciences/environment/earth-sciences/international-geoscience-and-geoparks-programme/. Accessed 20 Oct 2020.

The Nucleus ***60***, *No. 1 (2023) 78-85*

www.thenucleuspak.org.pk

The Nucleus

ISSN 0029-5698 (Print)
ISSN 2306-6539 (Online)

Insight into the Local Atomic Structure Order and Luminescence of Rare Earths

Latif Ullah Khan[1,2*], Zahid Ullah Khan[2,3], Muhammad Abdullah Umer[4]

[1]*Synchrotron-light for Experimental Science and Applications in the Middle East (SESAME) P.O. Box 7, Allan 19252, Jordan*

[2]*Department of Fundamental Chemistry, Institute of Chemistry, University of São Paulo (USP), Zip Code 05508-000, São Paulo-SP, Brazil*

[3]*Department of Biochemistry, Institute of Chemistry, University of São Paulo (USP), Zip Code 05508-000, São Paulo-SP, Brazil*

[4]*Department of Physics, National Central University, Taoyuan City, 320 Taiwan, ROC*

ABSTRACT

The rare earth (III) complexes are remarkable photoemitters in visible to near-infrared spectral region, manifesting wide photonic applications in organic light-emitting diodes (OLEDs), telecommunications, optical lasers, display devices, optical quantum memories and medical diagnostics. In order to get detailed insight into the photo-physical characteristics of the luminescent rare earth complexes, it is very important to probe the local chemical environment/electronic structure of the trivalent rare earth ion sites. The X-ray absorption fine structure spectroscopy (XAFS) is very efficient to probe the RE^{3+} ions from oxidation state/electronic structure in the X-ray absorption near edge spectroscopy (XANES) range to the local atomic structure order around the photoabsorber in extended region (EXAFS). In this work, we explored the electronic and local atomic structure of the typical RE^{3+} β-diketonate complexes, $[Eu(TTA)_3(H_2O)_2]$ and $[Gd(TTA)_3(H_2O)_2]$, TTA: 3-thenoyltrifluoroacetonate by XANES, EXAFS fit and continuous Cauchy wavelet transform (CCWT) analyses. The optical properties are discussed based on the local structural evidences of RE^{3+} site obtained from the quantitative analysis of the XAFS data. The visualization of visible emission under irradiation with hard X-ray beam demonstrated that the $[Eu(TTA)_3(H_2O)_2]$ complex can be an efficient new generation X-ray organic scintillator.

Keywords: *Rare Earth Complexes, EXAFS, CCWT, Optical Spectroscopy*

1. Introduction

The rare earth (RE) materials have demonstrated wide applications in science and technology [1], for instance light emitting diodes (LEDs), display technology [2], laser technology [3], luminescence sensors [4], renewable energy/solar cells [5], optical fibers [3], optical thermometry [4] and biosensors/fluorescence probes for bioimaging [6]. The rare earths are comprised of seventeen elements, containing La, Ce, Pr, Nd, Pm, Sm, Eu, Gd, Tb, Dy, Ho, Er, Tm Yb, Lu, Sc and Y. Among them, both the yttrium (Y) and scandium (Sc) belong to the *d*-block and are usually occurred in the same ore deposits as the lanthanides (*f*-block) and manifested the similar chemical properties. Therefore, these two elements are also included in the rare earths [7, 8]. It is noteworthy that the rare earth elements are usually occurred as traces in the mostly geological environments/ores. However, they are not exceptionally in very low concentration, when compared to many other elements [7]. Therefore, despite their name, the rare earth elements (exception of the radioactive promethium) are relatively abundant in Earth's natural resources.

The rare earth ions materials display efficient emission from UV-visible to near-infrared spectral regions, due to the 4f-4f intraconfigurational energy level structure [1], displaying longer luminescence lifetimes, larger stokes/anti-stocks shifts and high quantum yield [8]. In downconversion mechanism the RE^{3+} compounds absorb the high energy photons (UV, X-ray), undergoing energy transfer between the sensitizer and emitter rare earth ions and follow the cascade downconversion pathways in the 4f-4f intraconfigurational energy levels to emit the visible photons (stock shift). Whereas, in upconversion mechanism, these materials upconvert the low energy near infrared laser stimulation to higher energy visible emission (anti-stock shift) [1,2]. Among the trivalent rare earth ions phosphors, Eu^{3+}, Tb^{3+}, Sm^{3+} and Tm^{3+} emit red, green, orange and blue light, respectively, whereas, the Gd^{3+} manifest emission in the UV region [9]. The Yb^{3+}, Nd^{3+} and Er^{3+} display near-infrared luminescence. Though, the 4f-4f intraconfigurational transitions of lanthanides are parity-forbidden according to the selection rules (Laporte rule). Thus, the RE^{3+} ions exhibit low molar absorption cross-sections ($\alpha_{abs} < 4\times10^{-20}$ cm^2) [10].

However, for the RE^{3+} coordination complexes, the organic ligands of larger absorption cross-sections can indirectly excite the rare earth ions *via* an intramolecular energy transfer mechanism, involving transfer of energy from the triplet state of the ligand to the emitting energy level of the metal center (*antenna effect*) [1]. Thus, in present situation, the Laporte's rule is slightly relaxed for the 4f-4f intraconfigurational transitions due to the mixing of opposite parity electronic configurations [11, 12] produced by odd components of a non-centrosymmetric ligand field. Fundamentally, if the RE^{3+} complex is irradiated with the UV source, the coordinated ligand molecule undergoes excitation to its excited state, thereby transferring energy non-radiatively to the excited energy levels of RE^{3+} ion (emission center) [1, 8, 13], which follows non-radiative path to the emitting level and decay radiatively to the ground energy levels, generating characteristic narrow emission lines of the RE^{3+} ion. For, instance the europium (III) β-diketonates are important class of compounds in coordination chemistry, showing strong red luminescence (visible spectral region) from narrow emission lines, arising from the $^5D_0 \rightarrow {}^7F_J$ (J = 0−4) intraconfigurational transitions of the Eu^{3+} ion [11]. The Gd (III) complexes have been studied as remarkable T_1 contrast agents for the MRI

*Corresponding author: latifullah.khan@sesame.org.jo

imaging, owning to the paramagnetic Gd^{3+} ion. In addition, the Eu^{3+} and Gd^{3+} β-diketonates complexes have been used in organic light emitting diodes (OLEDs) [14].

X-ray Absorption Fine Structure (XAFS) is a highly sensitive and element specific [15] technique that probe efficiently the metal ion, to gain understanding on the oxidation state/electronic structure in near edge region (XANES) and the local atomic structure order till few angstroms in extended region (EXAFS) [15, 16]. Athena form Demeter package [17] is widely used software among the literature reported XAFS techniques for processing the measured X-ray absorption spectroscopy data. The OCEAN code [18], FDMNES code [19] and Xspectra quantum espresso [20] are usually used for the near-edge region (XANES) fitting analyses. However, most common quantitative analyses software's packages of extended region (EXAFS) include Artemis from Demeter [17], GNXAS [21], Larch (X-ray larch) [22] and reverse Monte-Carlo (RMC) method [15,23]. The modern data science machine-learning/deep neural network (DNN), for instance PyFitIt packages [24] have been implied to simulate the XANES/EXAFS of the metals [25]. In the present work, the local atomic structure of the Gd^{3+} and Eu^{3+} complexes were probed by the EXAFS fit analysis, using Artemis from the Demeter package. The photoluminescence properties of these RE^{3+} complexes are discussed based on the derived local atomic structure/RE^{3+} site from the quantitative analyses of their EXAFS data.

2. Materials and Methods

RE^{3+} (RE = Eu, Gd) complexes were gently provided by the research group of Prof. Hermi F. Brito, laboratory of *f*-block elements, Institute of Chemistry, University of São Paulo (USP), Brazil and their synthesis is already reported by this research group [13]. The emission spectra of these complexes were measured using a HORIBA Jobin-Yvon Fluorolog®-3 Spectrofluorometer, equipped with an excitation monochromator and a Czerny-Turner iHR320 monochromator for emission. The Spectrofluorometer contains a 450 W Xenon short-arc-lamp, as an excitation source, and the emission data were acquired with a Synapse® CCD detector (1024x512 pixels resolution).

X-ray absorption fine structure data were measured on the BM-08 XAFS/XRF beamline [26], of the Synchrotron-light for Experimental Science and Applications in the Middle East (SESAME), operating at 2.5 GeV in "decay" mode and 300 mA maximum electron current. The three ionization chambers for measuring the beam intensity were filled with optimum mixtures of He/N_2 gases at a total pressure of 1.0 bar. The XAFS data of Eu L_3-edge (6977 eV) and Gd L_3-edge (7243 eV) were measured in transmission mode at room temperature, using a double-crystal Si (111) monochromator, and signals acquired at ionization chambers were subsequently amplified by Stanford picoammeters and digitalized by a voltage to frequency converter before being finally read by the counters at the PXI-NI. The pellets of samples (13 mm diameter) were prepared by applying pressure (less than 2 tons) on the homogeneous mixture of the calculated quantity of finely ground sample and polyvinylpyrrolidone (PVP) powder. The sample quantity for the pellets was obtained from calculation according to their input formulae in XAFS mass software, giving the absorption coefficient (μ_t) ~ 1.5 above the Eu/Gd L_3-edges.

3. Results and Discussion

3.1. Probing Local Atomic Structure Order of Rare Earths

The key knowledge on the local structure/chemical environment of the trivalent rare-earth complexes is important to describe their optical properties. The RE^{3+} complexes demonstrate usually higher coordination numbers and ionic bonding characters (metal-ligand bond). The Eu^{3+} and Gd^{3+} *β*-diketonates exhibit eight-coordination number with tetrakis and tris geometries of chemical formulae, $[RE(\beta\text{-diketonate})_4]^-$ and $[RE(\beta\text{-diketonate})_3(\text{unidentate})_2]$, respectively. Nevertheless, the RE^{3+} *β*-diketonates are usually reported in literature as polyhedrons of Monoclinic (P21/c space group) or Triclinic ($P\bar{1}$ space group) systems [27,28]. Therefore, crystal structure refinement by EXAFS fit analyses can provide an effective approach to probe the local atomic structure order of RE^{3+} complexes and thereby get insight into their luminescence properties.

3.1.1. XANES Study

The normalized Eu L_3-absorption edge XANES spectrum of the Eu^{3+} *β*-diketonate manifested the high intensity white line peak at ~6983 eV, from the $^2p_{3/2}$ initial state to 5d final state electronic transition of the trivalent europium ion (Fig. 1a). The reported literature reveals that the total area under a white line peak for the Eu L_3-edge spectrum can be correspondes to the number of empty 5d states [29]. Accordingly, about similar white line peak area was observed for the Eu^{3+} *β*-diketonate as that of the $EuCl_3{\cdot}6H_2O$, suggesting a similar electronic configuration and consequent empty 5d levels (Fig.1a). The Gd L_3-edge XANES spectrum of the Gd^{3+} *β*-diketonate complex $[Gd(TTA)_3(H_2O)_2]$ manifested prominent white line peak at 7249 eV from the $^2p_{3/2}$ initial state to 5d final state transition, representing the Gd in +3 oxidation state, which was found similar to that of the reference Gd_2O_3 [30] (Fig.1b). However, the establishment of association between the prominent features of the XANES and the corresponding configuration of the RE^{3+} ion in local chemical environment is not very simple. Thus, quantitative analysis of the near edge region is highly demanded recently, accordingly, Khan and coworkers [15] have demonstrated the quantitative analysis of the L_3-edge XANES of rare earth complexes, using PyFitIt machine learning approach.

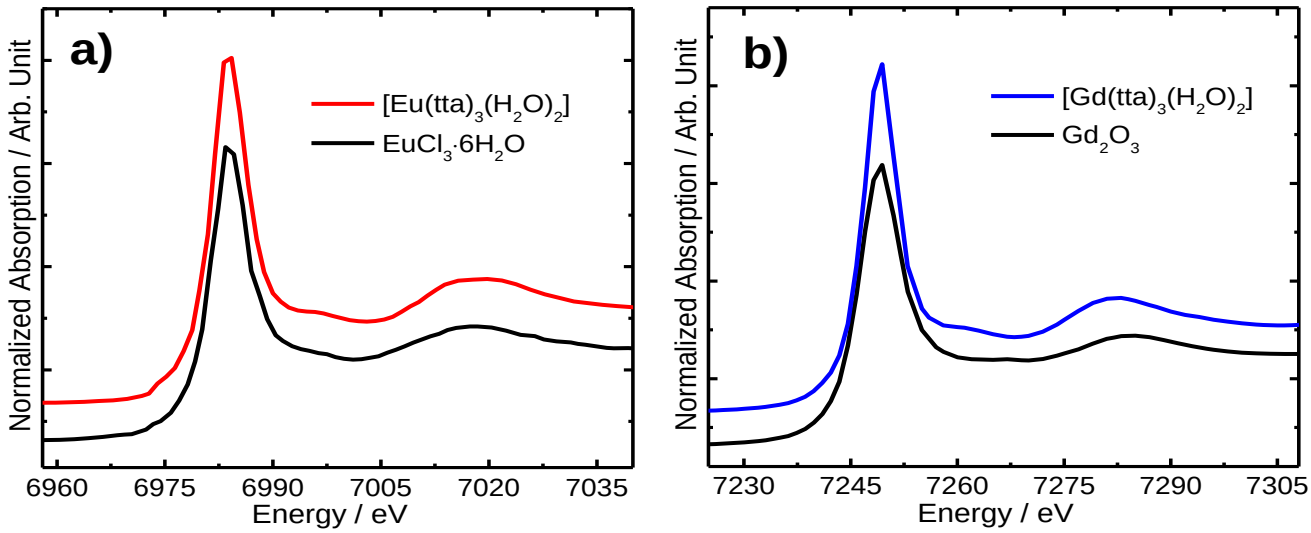

Fig. 1: Normalized Eu (6977 eV) and Gd (7243 eV) L_3-edges XANES spectra of the luminescent $[Eu(TTA)_3(H_2O)_2]$ (a) and $[Gd(TTA)_3(H_2O)_2]$ (b) complexes, respectively, TTA: 3-thenoyltrifluoroacetonate.

3.1.2. EXAFS Study

The quantitative analysis of the extended X-ray absorption fine structure (EXAFS) data of Eu^{3+} and Gd^{3+} β-diketonate complexes is very crucial for probing the local atomic structure order at the Eu^{3+} and Gd^{3+} sites that can guide to gain better knowledge on their optical properties. Accordingly, quantitative nonlinear best fits to the experimental EXAFS data $[\chi(k)]$ of these complexes were accomplished, using Artemis software from the Demeter package [17]. The preprocessing of the experimental XAFS data, including background subtraction, spectrum alignment and normalization was performed in Athena from the Demeter package, which is prerequisite for the quantitative EXAFS data analysis. The background Rbkg of 1 Å was set for the EXAFS fit of both Eu and Gd L3-edges. Artemis software is implemented the FEFF8-lite code that calculates efficiently the values of the effective scattering amplitude (Fi(k)), effective scattering phase shift ($\phi_i(k)$) and mean free path of the photoelectron (λ) (standard EXAFS Equation 1) [31], form the input data of corresponding crystallography crystal structure.

$$\chi(k) \approx \sum_i \left(\frac{(N_i S_0^2) F_i(k)}{k R_i^2} \sin\left(2kR_i + \phi_i(k)\right) \exp(-2\sigma_i^2 k^2) \exp\left(-\frac{2R_i}{\lambda(k)}\right) \right) \quad (1)$$

where, S_0^2 is the passive electron reduction factor, N_i is the degeneracy of path, R_i is the average distance between the central photoabsorber and the neighboring atoms, $F_i(k)$ is the effective scattering amplitude, σ_i^2 is the Debye-Waller factor, representing mean square relative displacement (MSRD) along the equilibrium path length, $\phi_i(k)$ is the effective scattering phase shift, including contributions from the central atom and all scattering atoms and λ is the mean free path of the photoelectron. In the present work, we used the crystal structure of a = 10.311 Å, b = 11.835 Å and c = 14.257 Å lattice parameters and P $\bar{1}$(2) space group, belonging to the triclinic system [27], in order to calculate the effective backscattering amplitude and phase shift (EXAFS Equation 1). Accordingly, the FEFF8-lite code implemented in Artemis was employed to generate various scattering paths [32] from the corresponding crystal structures for both the RE^{3+} complexes.

The experimental EXAFS data were quantitatively analyzed by performing nonlinear best fit in R-space from 1.2 to 2.6 Å interval for the $[Eu(TTA)_3(H_2O)_2]$ and 1–2.56 Å range for the $[Gd(TTA)_3(H_2O)_2]$, selecting the Hanning window in the *k* ranges of 2.5-10.5 $Å^{-1}$ and 3-10.4 $Å^{-1}$ for the $[Eu(TTA)_3(H_2O)_2]$ and $[Gd(TTA)_3(H_2O)_2]$ complexes, respectively. In this fitting procedure, all the oxygen single scattering paths, making octa-coordination geometry around the rare earth site were included in the theoretical EXAFS model. The S_0^2 and energy shift (ΔE_0) were set similar for all the scattering paths during fit. The interatomic distances (*R*) and Deby Waller factor σ^2 were refined relatively to get the best fit outcome. The Eu (6977 eV) and Gd (7243 eV) L_3-edges k^3-weighted EXAFS signals of the $[Eu(TTA)_3(H_2O)_2]$ and $[Gd(TTA)_3(H_2O)_2]$ complexes were found quite identical to each other, demonstrating the similar local atomic structure for both the rare earth complexes (Fig. 2). Moreover, the Fourier transform (FT) of the Eu L_3-edge $\chi(k)$ exhibited the first high intensity peak from the Eu–O bonds pairs, representing the octa-coordination geometry around the Eu^{3+} ion site for the Eu^{3+} complex (Fig. 2a). Theoretically, the eight neighboring oxygen atoms present in the first three single scattering paths (2.2–2.5 Å), constituting the octa-coordination geometry for the $[Eu(TTA)_3(H_2O)_2]$ complex (Table 1) were observed from the best fit result.

Similarly, Fourier transform (FT) of the Gd L_3-edge EXAFS data (Fig. 2b) also manifested a first high intensity peak related to the Gd-O for the $[Gd(TTA)_3(H_2O)_2]$ complex. The octahedral geometry comprised of the eight oxygen neighboring atoms was also validated by the quantitative

EXAFS fitting result for the $[Gd(TTA)_3(H_2O)_2]$ complex. It is noteworthy that the Eu-O bond distances (Table 1) were found somewhat larger than the Gd-O ones, attributing to the higher atomic radius of Eu^{3+} (1.066 Å) then the Gd^{3+} (1.053 Å) ion. Nevertheless, the quantitative EXAFS fit result indicated the existence of square anti-prism local structure for both the $[Eu(TTA)_3(H_2O)_2]$ and $[Gd(TTA)_3(H_2O)_2]$ complexes.

The continuous Cauchy wavelet transform (CCWT) [33] was employed to further explore the EXAFS data of the $[Eu(TTA)_3(H_2O)_2]$ and $[Gd(TTA)_3(H_2O)_2]$ complexes (Fig. 3), using a code developed in high programing language MATLAB R2020a. The CCWT modulus is efficiently demonstrated the coordination shells composed of the neighboring backscatterers around the photoabsorber, as RGB colored maps in the 2D CCWT image [15], concurrently, this solved the input EXAFS data into corresponding two-dimensional *k* and *R* spaces. The X-ray absorption fine structure's literature studies revealed that the lower atomic number atoms, such as O are more effectively backscattered at lower *k* values [15].

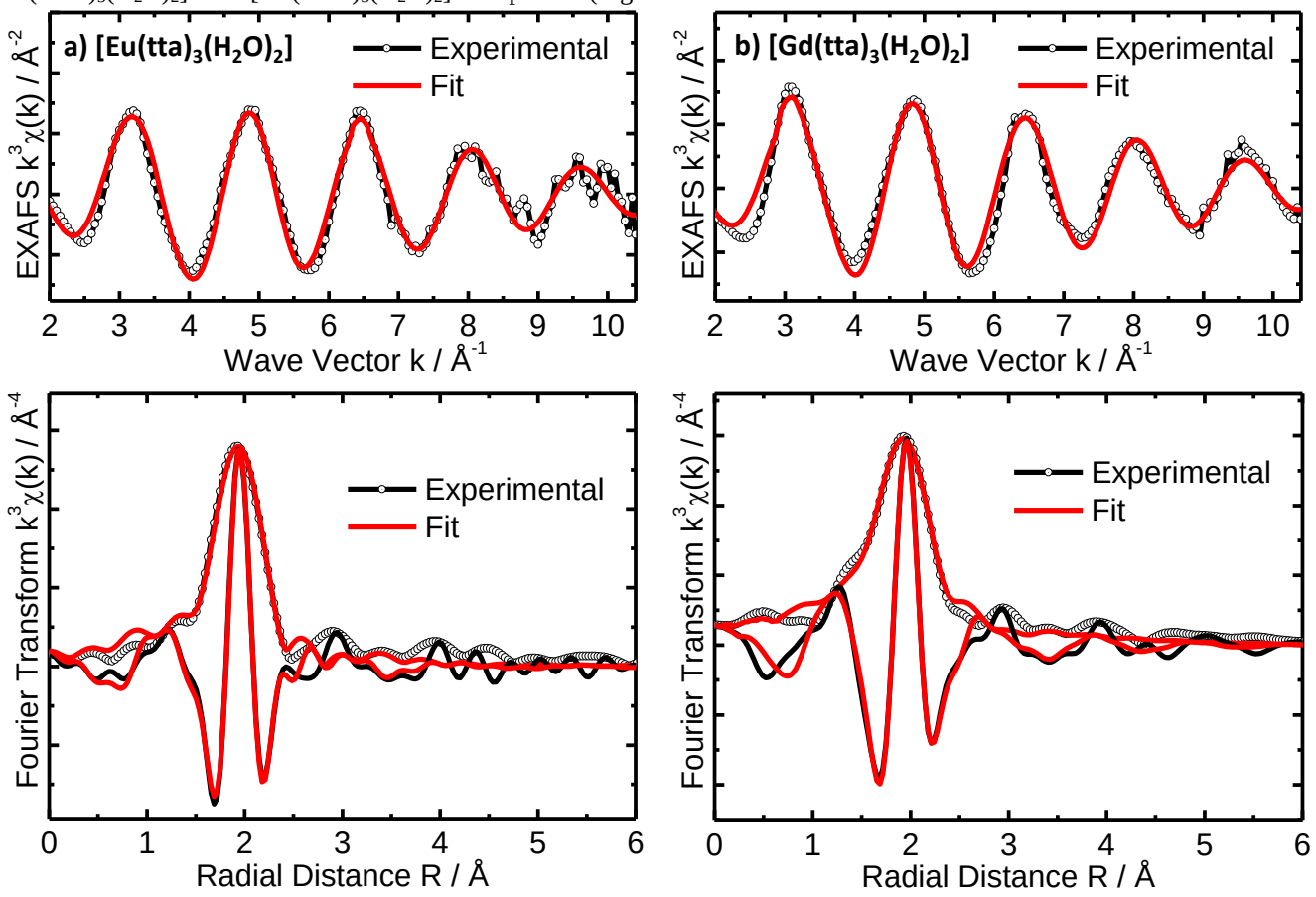

Fig. 2: Experimental k^3-weighted EXAFS signals (top) and their respective Fourier transforms (bottom) with best fits at the Eu (6977 eV) and Gd (7243 eV) L_3-edges for the $[Eu(TTA)_3(H_2O)_2]$ (a) and $[Gd(TTA)_3(H_2O)_2]$ (b) complexes, respectively, showing both the amplitudes and the real parts of the Fourier transforms of the data and the fits.

Table 1: Derived EXAFS fitting parameters, including N_{degen}: degeneracy of the path, R: mean coordination shell radii, σ^2: mean square relative displacements (MSRDs) or Debye–Waller factor, S_0^2: passive electron reduction factor E_0: photoelectron energy and R_{factor}: goodness of the fit for the $[Eu(TTA)_3(H_2O)_2]$and $[Gd(TTA)_3(H_2O)_2]$ complexes.

Complex	Bond	N_{degen}	R(Å)	σ^2(Å^2)	S_0^2	E_0 (eV)	R_{factor}
$[Eu(TTA)_3(H_2O)_2]$	Eu-O_1	1	2.287±0.07	0.0135±0.0036	1.0	10	0.0055
	Eu-O_2	3	2.434±0.017	0.0060±0.0023	1.0	10	0.0055
	Eu-O_3	4	2.500±0.012	0.0060±0.0023	1.0	10	0.0055
$[Gd(TTA)_3(H_2O)_2]$	Gd-O_1	1	2.247±0.018	0.0116±0.0031	1.0	7.7	0.0036
	Gd-O_2	3	2.354±0.012	0.0042±0.0020	1.0	7.7	0.0036
	Gd-O_3	4	2.467±0.009	0.0043±0.0025	1.0	7.7	0.0036

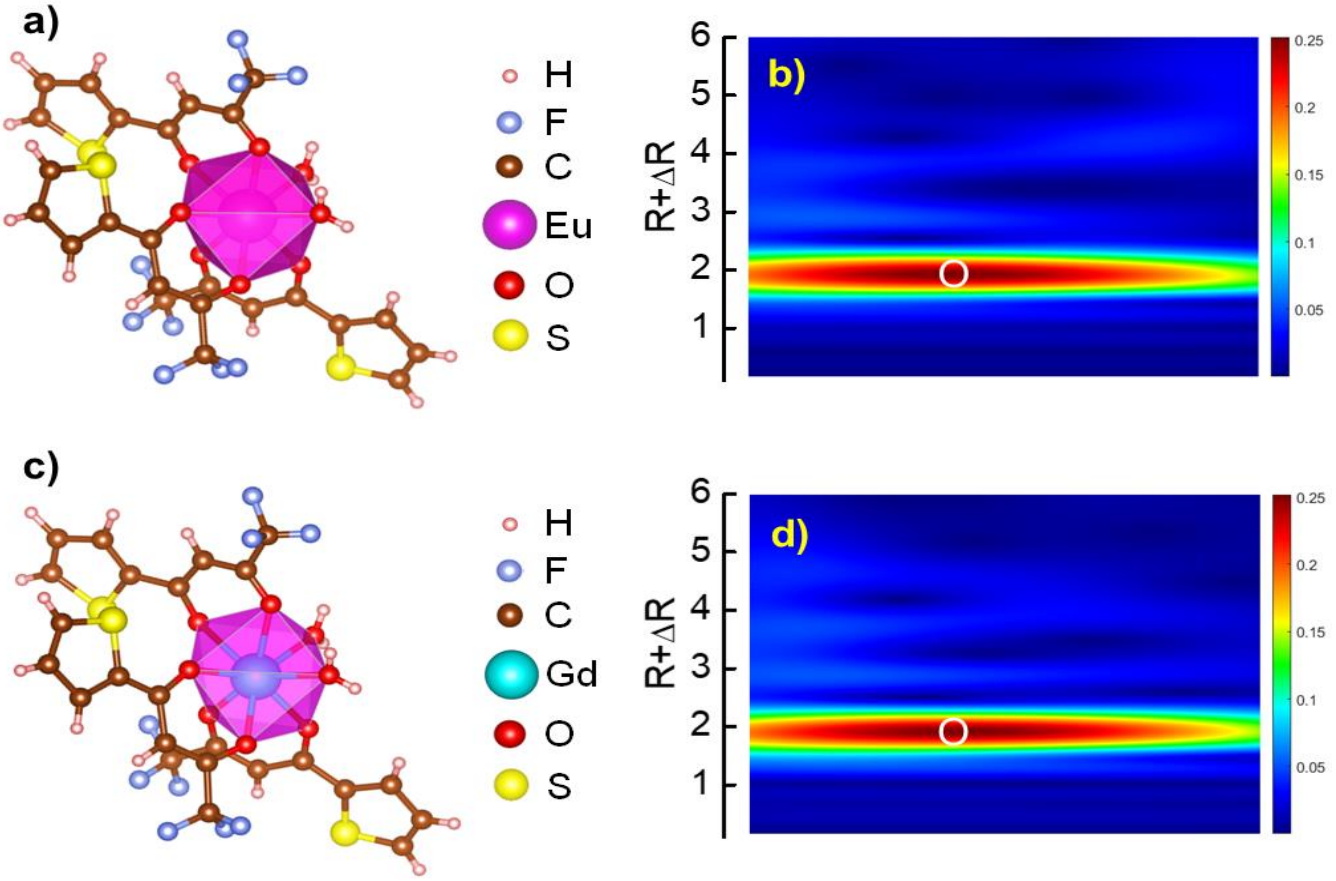

Fig. 3: The three-dimensional structures and Continuous Cauchy wavelet transform (CCWT) analyses for the $[Eu(TTA)_3(H_2O)_2]$ (a,b) and $[Gd(TTA)_3(H_2O)_2]$ (c,d) complexes. Two-dimensional CCWT images yielded from the experimental EXAFS data of both the compounds, visualizing the O backscatterer as a dark-red color map.

Whereas, the high atomic numbers atoms are considered highly effective backscatterers at higher k values. Because, the effective scattering amplitude ($F_i(k)$) of the neighboring atoms around photoabsorber (EXAFS Equation) are considerably contributed to the changes in amplitude of the normalized XAFS data. This parameter is efficiently associated with the number of repulsive electrons in the electronic clouds of the neighboring backscatterers. It is noteworthy that the CCWT modulus effectively showed the coordination geometry, represented by O backscatterers (octa-coordination) around Eu^{3+} and Gd^{3+} ions as a dark-red color map in 2D image (Fig. 3b,d), suggesting a square antiprismatic three-dimensional local structure (Fig. 3a,c) for both the $[Eu(TTA)_3(H_2O)_2]$ and $[Gd(TTA)_3(H_2O)_2]$ complexes, corroborated by quantitative EXAFS fit.

3.2. Optical Properties

The emission spectrum of the $[Gd(tta)_3(H_2O)_2]$ complex (Fig. 4a) showed the phosphorescence from the T_1 state of the 3-thenoyltrifluoroacetonate (tta) ligand. It is noteworthy that the first excited state ($^6P_{7/2}$) of Gd^{3+} ion is located at 32000 cm^{-1} energies, quite higher than the T_1 state of the β-diketonate ligands. Thus, it cannot accept energy from the lower-lying excited state of tta ligand through intramolecular ligand-to-metal energy transfer mechanism [11]. Therefore, the emission lines from the 4f-4f intraconfigurational transitions were not observed in the emission spectrum of the $[Gd(TTA)_3(H_2O)_2]$, measured at 77 K temperature. The emission spectrum of the $[Eu(TTA)_3(H_2O)_2]$ complex (Fig. 4b) was recorded at room temperature in the 570–720 nm wavelength range, monitoring excitation at the $S_0 \rightarrow S_n$ intra-ligand transition of the TTA ligand. This spectrum displayed characteristics emission lines attributed to the $^5D_0 \rightarrow {}^7F_J$ transitions (where J = 0−4) of the Eu^{3+} ion with the dominant $^5D_0 \rightarrow {}^7F_2$ hypersensitive transition. It is noteworthy that the the relative intensities of the narrow emission lines from the Eu^{3+} $^5D_0 \rightarrow {}^7F_{0\text{-}4}$ transitions can efficiently probe the local chemical environment and symmetry site around the Eu^{3+} site in their complexes [34]. There are several notable features, associated with 4f-4f intraconfigurational transition of the Eu^{3+} ion. The $^5D_0 \rightarrow {}^7F_0$ is a forced electric dipole (FED) transition, occurring *via* dynamic coupling (DC) mechanism and it borrows intensity mainly from $^5D_0 \rightarrow {}^7F_2$ transition through the *J*-mixing effect, when it is allowed by symmetry. Therefore, this transition can only be observed in the emission spectrum of the compounds, whereas, the Eu^{3+} ion occupies C_n, C_{nv} and C_s symmetry sites [34]. The $^5D_0 \rightarrow {}^7F_1$ is an allowed and pure magnetic dipole transition that does not affect by the ligand field effect, furthermore, its intensity is

largely independent of the chemical environment around the Eu^{3+} and mainly depends on the refractive index of the crystal. Therefore, it displays almost constant intensity for all the trivalent europium ions compounds. The $^5D_0 \rightarrow {}^7F_2$ is a FED and DC hypersensitive transition, its intensity is strongly affetced by the chemical environment, mainly small angular changes in the local coordination geometry [11,35]. Additionaly, $^5D_0 \rightarrow {}^7F_4$ FED transition is also the most sensitive to lanthanide-ligating atom bond distances.

It is noteworthy that the appearance of the $^5D_0 \rightarrow {}^7F_0$ transition and considerable intensity of the $^5D_0 \rightarrow {}^7F_2$ transition in the emission spectrum (Fig. 4b) of the $[Eu(TTA)_3(H_2O)_2]$ complex manifested low symmetry site (triclinic system) for the Eu^{3+} ion, as demonstrated by the quantitative EXAFS fit analysis. The photoluminescence data of the $[Eu(TTA)_3(H_2O)_2]$ complex also demonstrated that luminescence sensitization path is mainly occurred through the energy transfer from the first T_1 excited state of the TTA ligand to the $^5D_1$ excited level of the Eu^{3+} ion (Fig. 4c). It is worthful to mention that the $[Eu(TTA)_3(H_2O)_2]$ complex displayed the red emission color under UV irradiation lamp at 365 nm wavelength. Whereas, prominent visible emission was also observed under irradiation with X-ray beam at 7300 eV energy above the Eu L_3-edge (Fig. 4d). The photograph was captured with CMOS camera focused on the sample at the end station of BM-08 XAFS/XRF beamline, SESAME light source. This finding demonstrated that the $[Eu(TTA)_3(H_2O)_2]$ complex can be an efficient new generation hard X-ray organic scintillator.

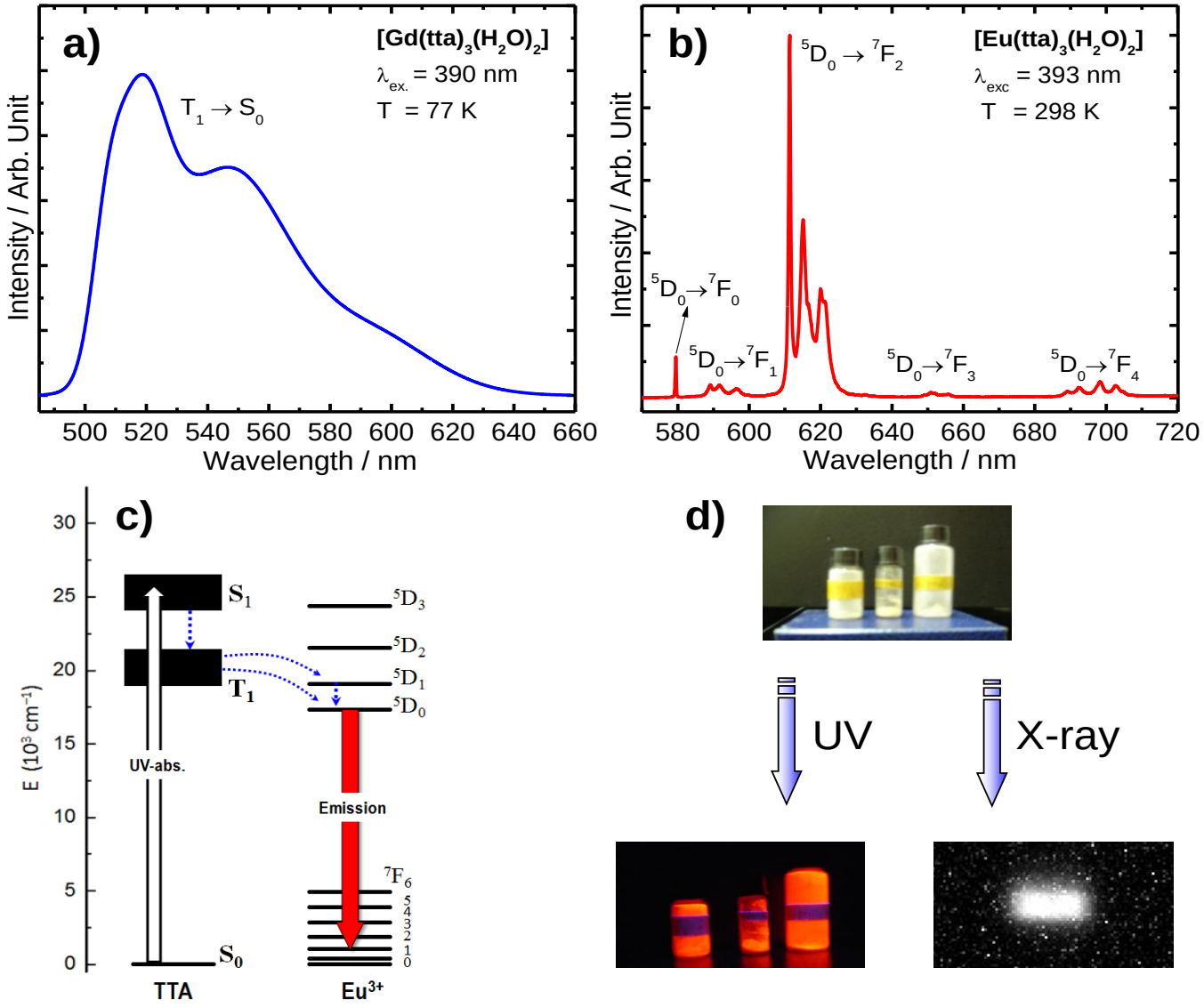

Fig. 4: Emission spectra of the $[Gd(TTA)_3(H_2O)_2]$ (a), $[Eu(TTA)_3(H_2O)_2]$ (b) complexes recorded in solid state at 298 K and 77 K temperatures, respectively. Partial energy level diagram (c) of the $[Eu(TTA)_3(H_2O)_2]$. The dashed arrows represent non-radiative decays, the red color arrow corresponds to the radiative decay of the Eu^{3+} ion, most probably intramolecular energy transfer processes from the TTA to Eu^{3+} ion. Photographs of $[Eu(TTA)_3(H_2O)_2]$ (d) taken with a digital camera displaying the prominent emission color under UV irradiation lamp at 365 nm wavelength and hard X-ray beam at 7300 eV energy.

4. Conclusions

The electronic and local atomic structure of the luminescent RE^{3+} β-diketonate complexes (RE = Eu, Gd) were probed by exploring the X-ray absorption near edge region (XANES) and quantitatively analyzing the experimental extended region *via* EXAFS fit and continuous Cauchy wavelet transform (CCWT) analyses. This result demonstrated that the octa-coordination of oxygen backscatterers around the RE^{3+} ion in square anti-prism geometry (Triclinic system) for both the $[Eu(TTA)_3(H_2O)_2]$ and $[Gd(TTA)_3(H_2O)_2]$ complexes. The photoluminescence properties revealed that the presence of the $^5D_0 \rightarrow {}^7F_0$ forced electric dipole (FED) transition and considerable intensity of the $^5D_0 \rightarrow {}^7F_2$ FED hypersensitive transition in the emission spectrum of the $[Eu(TTA)_3(H_2O)_2]$ complex demonstrated low symmetry site (triclinic system) for the Eu^{3+} ion, corroborating the quantitative EXAFS analyses.

Acknowledgement

The authors acknowledge the financial support by the Pakistan Nuclear Society (PNS), Pakistan and Royal Society of Chemistry Inclusion and Diversity Fund (RSC). Z.U. Khan is grateful to Fundação de Amparo à Pesquisa do Estado de São Paulo (FAPESP), the Postdoc research grant (No. 2021/00356-6). We thank Prof. Hermi F. Brito, laboratory of *f*-block elements, Institute of Chemistry, University of São Paulo (USP), Brazil for providing the rare earth complexes. We also acknowledge Dr. Tariq Bhatti, PAEC Pakistan for correction and technical writing of the manuscript. We extend our gratitude to the BM-08 XAFS/XRF Beamline of SESAME synchrotron light source for XAFS data measurements.

References

[1] J.C.G. Bünzli, "On the design of highly luminescent lanthanide complexes," Coordination Chemistry Reviews, vol. 293-294, pp. 19-47, June, 2015.

[2] M. Pan, W.M. Liao, S.Y. Yin, S.S. Sun, and C.Y. Su, "Single-phase white-light-emitting and photoluminescent color-tuning coordination assemblies," Chemical Reviews, vol. 118, no. 18, pp. 8889-8935, Sep. 2018.

[3] K. Kuriki, Y. Koike, and Y. Okamoto, "Plastic optical fiber lasers and amplifiers containing lanthanide complexes," Chemical Reviews, vol. 102, no. 6, May, 2002.

[4] J.F.C.B. Ramalho, L.D. Carlos, P.S. André, and R.A.S. Ferreira, "mOptical sensing for the internet of things: A smartphone-controlled platform for temperature monitoring," Advance Photonics Research vol. 2, no. 6, pp. 2000211, June, 2021.

[5] V. Kumar, O.M. Ntwaeaborwa, T. Soga, V. Dutta, and H.C. Swart, "Rare earth doped zinc oxide nanophosphor powder: A future material for solid state lighting and solar cells," ACS Photonics, vol. 4, no. 11, Oct., 2017.

[6] Z.U. Khan, M.K. Uchiyama, L.U. Khan, and K. Araki, "Wide visible-range activatable fluorescence ZnSe:Eu^{3+}/Mn^{2+}@ZnS quantum dots: local atomic structure order and application as a nanoprobe for bioimaging," Journal of Material Chemistry B, vol. 10, no. 2, pp. 247-261, Jan., 2022.

[7] D.A. Atwood, The Rare Earth Elements: Fundamentals and Applications. Hoboken, NJ, USA: John Wiley & Sons, Inc., 2005.

[8] G.F. de Sa´, O.L. Malta, C. de Mello Donega´, A.M. Simas, R.L. Longo, P.A. Santa-Cruz, E.F. da Silva Jr., "Spectroscopic properties and design of highly luminescent lanthanide coordination complexes," Coordination Chemistry Reviews, vol. 196, pp. 165-195, 2000.

[9] K. Binnemans, "Lanthanide-Based Luminescent Hybrid Materials," Chemical Reviews, vol. 109, no. 9, pp. 4283-4374, Sep. 2009.

[10] D. Manzani, K. Nigoghossian, M.F. Iastrensk, G.R. Coelho, M.V. dos Santos, L.J.Q. Maia, S.J.L. Ribeiro, and M.G. Segatelli, "Luminescent silicone materials containing Eu^{3+}-complexes for photonic applications," Journal of Material Chemistry C, vol. 6, no. 30, July, 2018.

[11] L.U. Khan, H.F. Brito, J. Hölsä, K.R. Pirota, D. Muraca, M.C.F.C. Felinto, E.E.S. Teotonio, and O.L. Malta, "Red-green emitting and superparamagnetic nanomarkers containing Fe_3O_4 functionalized with calixarene and rare earth complexes," Inorganic Chemistry, vol. 53, no. 24, pp. 12902-12910, Dec., 2014.

[12] R.T. Moura, A.N.C. Neto, R.L. Longo, and O.L. Malta, "On the calculation and interpretation of covalency in the intensity parameters of 4f-4f transitions in Eu^{3+} complexes based on the chemical bond overlap polarizability," Journal of Luminescence, vol. 170, part 2, pp. 420-430, Feb., 2016.

[13] L. Blois, A.N.C. Neto, O.L. Malta, and H.F. Brito, "The role of the Eu^{3+} $^7F_1$ level in the direct sensitization of the $^5D_0$ emitting level through intramolecular energy transfer," Journal of Luminescence, vol. 247, Article No. 118862, July, 2022.

[14] J. Fang, H. You, J. Chen, J. Lin, and D. Ma, "Memory devices based on lanthanide (Sm^{3+}, Eu^{3+}, Gd^{3+}) complexes," Inorganic Chemistry, vol. 45, no. 9, pp. 3701-3704, May, 2006.

[15] L. U. Khan, Z. U. Khan, L. Blois, L. Tabassam, H. F. Brito and S. J. A. Figueroa, "A Strategy to Probe the Local Atomic Structure of Luminescent Rare Earth Complexes by XANES Simulation Using Machine Learning Based PyFitIt Approach" Inorganic Chemistry, vol. 62, no. 6, 2738–2750, Jan. 2023.

[16] J. Terry, M.L. Lau, J. Sun, C. Xu, B. Hendricks, J. Kise, M. Lnu, S. Bagade, S. Shah, P. Makhijani, A. Karantha, T. Boltz, M. Oellien, M. Adas, S. Argamon, M. Long, and D.P. Guillen, "Analysis of extended X-ray absorption fine structure (EXAFS) data using artificial intelligence techniques," Applied Surface Science, vol. 547, Article No. 149059, May, 2021.

[17] B. Ravel, and M. Newville, "ATHENA, ARTEMIS, HEPHAESTUS: data analysis for X-ray absorption spectroscopy using IFEFFIT," Journal of Synchrotron Radiation, vol. 12, part. 4, pp. 537-541, July, 2005.

[18] C. Vorwerk, B. Aurich, C. Cocchi, and C. Draxl, "Bethe-Salpeter equation for absorption and scattering spectroscopy: Implementation in the exciting code," Electronic Structure, vol. 1, no. 3, Article No. 037001 Aug., 2019.

[19] O. Bunău and Y. Joly, "Self-consistent aspects of X-ray absorption calculations," Journal of Physics: Condensed Matter, vol. 21, no. 34, Article No. 345501, Aug., 2009.

[20] P. Giannozzi, S. Baroni, N. Bonini, M. Calandra, R. Car, C. Cavazzoni, D. Ceresoli, G.L. Chiarotti, M. Cococcioni, I. Dabo, "QUANTUM ESPRESSO: A modular and open-source software project for quantum simulations of materials," Journal of Physics Condensed Matter, vol. 21, no. 39, Article No. 395502, Sep., 2009.

[21] K. Hatada, F. Iesari, L. Properzi, M. Minicucci, and A. di Cicco, "New graphical user interface for EXAFS analysis with the GNXAS suite of programs," Journal of Physics: Conference Series, 712, Article No. 012002, 2016.

[22] M. Newville, "Larch: An analysis package for XAFS and related spectroscopies," Journal of Physics: Conference Series, 430, Article No. 012007, 2013.

[23] R. L. McGreevy, and L. Pusztai, "Reverse Monte Carlo Simulation: A new technique for the determination of disordered structures," Molecular Simulation, vol. 1, no. 6, pp. 359-367, Dec. 1988.

[24] A. Martini, S.A. Guda, A.A. Guda, G. Smolentsev, A. Algasov, O. Usoltsev, M.A. Soldatov, A. Bugaev, Yu. Rusalev, C. Lamberti, A.V. Soldatov, "PyFitit: The software for quantitative analysis of XANES spectra using machine-learning algorithms," Computer Physics Communications, vol. 250, Article No. 107064, Nov. 2020.

[25] J. Timoshenko, C.J. Wrasman, M. Luneau, T. Shirman, M. Cargnello, S.R. Bare, J. Aizenberg, C.M. Friend, and A.I. Frenke, "Probing atomic distributions in mono- and bimetallic nanoparticles by supervised machine learning," Nano Letter, vol. 19, no. 1, pp. 520-529, Dec., 2019.

[26] M. Harfouche, M. Abdellatief, Y. Momani, A. Abbadi, M. Al Najdawi, M. Al Zoubi, B. Aljamal, S. Matalgah, L. U. Khan, A. Lausi, and G. Paolucci, "Emergence of the first XAFS/XRF beamline in the Middle East: providing studies of elements and their atomic/electronic structure in pluridisciplinary research fields," Journal of Synchrotron Radiation, vol. 29, part, 4, pp. 1107-1113, July, 2022.

[27] V. Vallet, A. Fischer, Z. Szabó, and I. Grenthe, "The structure and bonding of Y, Eu, U, Am and Cm complexes as studied by quantum chemical methods and X-ray crystallography," Dalton Transactions, vol. 39, issue, 33, pp. 7666-7672, July, 2010.

[28] N. Hasan, and K. Iftikhar, "Synthesis, crystal structure and photoluminescence studies of [Eu(dbm)$_3$(impy)] and its polymer-based hybrid film," New Journal of Chemistry, vol. 43, issue, 6, pp. 2479-2489, Jan., 2019.

[29] C.F. Bueno, A.Y. Ramos, A. Bailly, E. Mossang, and L.V.A. Scalvi, "X-ray absorption spectroscopy and Eu^{3+}-emission characteristics in GaAs/SnO_2 heterostructure," SN Applied Sciences, vol. 2, Article No. 1579, Aug., 2020.

[30] H. Asakura, S. Hosokawa, K. Teramura, and T. Tanaka, "Local structure and L_1 - and L_3-Edge X-ray absorption near edge structures of middle lanthanoid elements (Eu, Gd, Tb, and Dy) in their complex oxides," Inorganic Chemistry, vol. 60, issue, 13, pp. 9359-9367, Jul. 2021.

[31] L.U. Khan, N. Jabeen, I. Jabbar, S. Jamil, A. Kanwal, Z. Akhter, M. Usman, M.Z. Abid, and M. Harfouche, "Investigating local structure of ion-implanted (Ni^{2+}) and thermally annealed rock salt CoO film by EXAFS simulation using evolutionary algorithm," ACS Applied Energy Materials, vol. 4, no. 3, pp. 2049-2055, Feb., 2021.

[32] S.D. Kelly, K.M. Kemner, J.B. Fein, D.A. Fowle, M.I. Boyanov, B.A. Bunker, and N. Yee, "X-ray absorption fine structure determination of pH-dependent U-bacterial cell wall interactions," Geochimica Cosmochimica Acta, vol. 66, no. 22, pp. 3855-3871, Nov., 2002.

[33] M. Muñoz, P. Argoul, and F. Farges, "Continuous Cauchy wavelet transform analyses of EXAFS spectra: A qualitative approach," American Mineralogist, vol. 88, no. 4, pp. 694-700, Apr. 2003.

[34] K. Binnemans, "Interpretation of europium (III) spectra," Coordination Chemistry Reviews, vol. 295, pp. 1-45, July, 2015.

[35] L.U. Khan, L.F.M. Zambon, J.L. Santos, R.V. Rodrigues, L.S. Costa, D. Muraca, K.R. Pirota, M.C.F.C. Felinto, O.L. Malta, and H.F. Brito, "Red-emitting magnetic nanocomposites assembled from Ag-decorated Fe_3O_4@SiO_2 and Y_2O_3:Eu^{3+}: Impact of iron-oxide/silver nanoparticles on Eu^{3+} emission," Chemistry Select, vol. 3, no. 4, pp. 1157-1167, Jan., 2018.

The Nucleus ***60****, No. 1 (2023) 86-97*

www.thenucleuspak.org.pk

The Nucleus
ISSN 0029-5698 (Print)
ISSN 2306-6539 (Online)

Role of In-Service Inspections in Nuclear Power Plants (NPPs)

Mahmood Khan[1,2*], Muhammad Umer Farooq Awan[1,3], Khurram Lal[1], Muhammad Gulab[1], Shabbir Ahmed[1], Zaheer Ahmed[1]

[1]*National Centre for Non-Destructive Testing (NCNDT), Islamabad, Pakistan*

[2]*Institute of Space Technology (IST), Islamabad Pakistan*

[3]*Pakistan Institute of Engineering and Applied Sciences (PIEAS), Islamabad, Pakistan*

ABSTRACT

The National Centre for Non-destructive Testing (NCNDT) since its inception in 1995 has been providing Pre-Service Inspections (PSI) and In-Service Inspections (ISI) services to the nuclear power plants (NPPs) in the country. In Pakistan, a total of six NPPs are operational with a cumulative capacity of 3620 MWe. All the efforts are made to ensure the safe and reliable operation of NPPs and the provision of an uninterrupted supply of electricity to improve the life of the common man. While extreme care is taken during the design, construction and commissioning of the structures, systems and components, a constant health monitoring system has to be ensured throughout the life (i.e., 40-50 years) of NPPs in accordance with the design parameters. The plant-specific codes & standards explain the ISI methods and acceptance criteria for critical life-limiting components, pressure boundary components and welds etc. Recently remotely controlled, advanced mechanized inspection systems for the inspection of reactor pressure vessels (RPV) and steam generators (SGs) have been procured. These systems are being used during the re-fueling outages (RFOs) of NPPs. Different conventional and non-conventional NDT methods were used for inspection. The components where unacceptable indications are revealed by ISI are repaired, replaced, or isolated. The baseline data generated during PSI is used for the comparison and surveillance. The observations made during ISI are subjected to thorough review and analysis by qualified experts to obtain assurance that unacceptable degradation in component quality is not occurring and it remains fit for service.

Keywords: *PSI: Pre-Service Inspection, In-Service Inspection, NPP: Nuclear Power Plant, NCNDT: National Centre for Non-Destructive Testing, NDT: Non-Destructive Testing*

1. Overview of Nuclear Power Plants (NPPs) in the World

Our world's temperatures are rising due to human activities and now this climate change is threatening every aspect of human life. Fossil fuels are the major contributor (approximately 75 %) to the emissions of these greenhouse gases responsible for climate change [1]. Drastic reduction of the greenhouse gas emissions is unavoidable whereas the energy access and economic opportunity for billions of people is expanding simultaneously.

The world is looking for clean energy [2]. Climate change, energy storage and variable energy output are some of the challenges faced for the long-term use of renewable resources (solar, wind etc.) [3]. Nuclear power plants are promising solution as they provide carbon-free energy [4]. These plants have the lowest carbon footprint and are reliable and cost-effective [5]. Nuclear energy requires less fuel (0.5 kg of nuclear fuel produces the same energy as 1000 tons of coal), can provide an interrupted supply of power for a longer time and is a plausible solution to meet the increasing energy demand [6]. Around 10 % of the world's electric power is generated by a total of 442 nuclear power reactors that are operational worldwide whereas around 52 nuclear power plants are under construction [7, 8]. Consequently, the value of operating NPPs has increased and NPP life management, especially service life extension has become a worldwide issue.

The goal of this paper is to place non-destructive evaluation (NDE) in the context of NPP life management and life extension and to show its increasing role in ensuring plant long-term operation. The part of the NCNDT in the PSI & ISI of NPPs in Pakistan and recent advancements in the development of indigenous mechanized inspections are also discussed.

2. Nuclear Power Plants in Pakistan

There are seven NPPs in Pakistan with a total capacity of 3620 MWe. Of these seven NPPs, six are operational and are pressurized water reactors (PWRs) whereas the remaining is a pressurized heavy water reactor (PHWR) and is permanently shut down. The oldest nuclear power plant K-1, the only PHWR, started its operation in 1971. It is a CANDU type reactor which had a capacity of 137 MWe. After completing 50 years of successful and safe operation it was permanently shut down in 2021.

Four of the six operational plants are 300 MWe two-loop PWR reactors based on CNP-300 and are called C series reactors namely C-1, C-2, C-3 and C-4. These are situated in Mianwali and started operation in 2000, 2011, 2016 and 2017.

Fig. 1: Aerial view of Nuclear Power Plants in Mianwali

*Corresponding author:mahmoodkhan77@gmail.com

Table 1: Specifications of NPPs in Pakistan

Sr. No.	Characteristic	K-1	C-1	C-2	C-3	C-4	K-2	K-3
1.	Plant Type	CANDU (PHWR)	PWR	PWR	PWR	PWR	PWR	PWR
2.	Power Output	137s MWe	325 MWe	325 MWe	340 MWe	340 MWe	1100 MWe	1100 MWe
3.	Year of Operation	1971	2000	2011	2016	2017	2021	2022
4.	No. of Loops	2	2	2	2	2	3	3
5.	Codes and Standards for In-Service Inspections	ASME BPVC (Section XI)	ASME BPVC (Section XI)	ASME BPVC (Section XI)	ASME BPVC (Section XI)	ASME BPVC (Section XI)	RSE-M	RSE-M
6.	Fuel	Natural Uranium	LEU (Low Enriched Uranium)	LEU	LEU	LEU	LEU	LEU
7.	Status	Permanently Shutdown	Operational	Operational	Operational	Operational	Operational	Operational
8.	Location	Karachi	Mianwali	Mianwali	Mianwali	Mianwali	Karachi	Karachi

The other two reactors namely K-2 and K-3 are situated in Karachi and are Generation III 1000 MWe, three-loop PWR reactors which became operational in 2021 and 2022. These are based on the French codes RCC-M, RSE-M etc. Table 1 shows the major specifications of the NPPs of Pakistan for comparison.

3. Role of Non-Destructive Testing (NDT) in Nuclear Power Plants

3.1 Key Components of a Nuclear Power Plant (PWR)

NPPs involve the conversion of heat generated by nuclear fission into electrical energy. Nuclear fission occurs in the reactor pressure vessel (RPV) where the fuel is placed in fuel assemblies. The melting of fuel is to be avoided and its cooling is done through highly pressurized water (called primary coolant). Several radiations including neutrons, gamma radiations, alpha and beta particles are produced in the RPV. These radiations can lead to the embrittlement of the material which can cause the failure of the material. Boric acid is added to the water for fine control of the reactivity. Different gasses are also produced in the reactions and the chemistry of the coolant is to be controlled to avoid corrosion effects (oxygen, hydrogen etc.). For coarse control of the reactivity, control rods are used which are made of a material having a higher neutron absorption coefficient (silver-indium-cadmium control rods are used in Westinghouse design-based PWR NPPs). Different penetrations for instrumentation (neutron flux, temperature, pressure measurements etc.) thimbles are also present in the RPV. It is made up of carbon steel with an internal cladding of stainless steel.

The coolant from the RPV gets heated and is taken to the steam generator (SG) where it is passed through several U-tubes and returned to the RPV. Outside these U tubes, feedwater passes (which is at lower pressure) and gets converted to steam which is then taken to the turbine where it expands and rotates the turbine and electricity is generated. The U tubes are made up of Inconel (Nickel based alloy) and are thousands in numbers. This is an interface of the primary coolant with the feedwater. If the tubes get damaged due to corrosion or foreign material the primary coolant may be released into the feedwater and the radiation will be leaked. This can cause radiation exposure to the workers and the public. The number of steam generators equals the number of loops of PWR.

Pressurizer (PRZ) controls the pressure of the primary coolant during the power surges. It is a vessel having electric heaters at the bottom and a spray line at the top. It contains a water steam interface (water at the bottom and steam at the top) and their conversion, either way, controls the surges. It is also made up of carbon steel internally cladded with stainless steel. There is only one pressurizer in the primary coolant system. The primary coolant is circulated between the aforementioned equipment with the help of a reactor coolant pump (RCP). The RCP is equipped with a casing enclosed with an impeller and linked to the motor through a shaft and different seals are present to avoid leakages. The RCP is also provided with a flywheel to provide inertia to the pump in case of power loss to prevail cooling of the primary coolant. There is an RCP in each loop of the primary coolant system. This equipment is placed inside a containment to prevent the leakage of radiation to the environment in any unfortunate accident.

There are other supporting systems along with this main primary coolant system which are divided into different classes called Safety Class 1, 2 and 3 and non-safety class depending upon the consequences, in case they fail, on the safety of NPPs. The safety of NPPs is much more important than that of conventional power plants due to radiation safety concerns. The melting of the fuel is to be avoided to keep the fission reaction under control. With the advancement, several passive safety systems have been added to the reactor design to ensure the safe operation of NPPs.

3.2 Non-Destructive Testing

NPPs have different phases during their lifetime namely: design, manufacturing, installation, commissioning, operation and de-commissioning. During the design phase according to relevant codes and standards, NDT methods are specified for ensuring quality control during the manufacturing and as a damage assessment tool during the

installation and operation phases. The basic goal is to find the discontinuities and defects in the material which can lead to the failure of the material. The sizes of these defects are to be measured and characterized. The specific sections of codes are referred to for the NDT methods employed for the PSI during installation and ISI during re-fueling outages (RFO). Inspections are made during the manufacturing and based on accept reject criteria repairs are made if necessary. Hence, during manufacturing using NDE methods quality is ensured. Afterwards, during installation inspections PSI is performed to provide baseline data for comparison during the inspections in ISI of NPPs.

RFOs are carried out once every 14-18 months depending upon the design to replace the depleted fuel from the peripheries with fresh fuel and the core is rearranged to attain uniform neutron flux during operation. During these outages along with the fuel replacement, several inspections (ISI) are carried out as per codes and standards for ageing assessment of components/equipment and different piping for life assessment and ageing management. In ISI, service defects are expected to appear and are targeted for detection and characterization. The service defects include fatigue cracks, corrosion, stress-corrosion cracking, flow accelerated corrosion, radiation embrittlement, erosion, wear etc. NPPs are an uninterrupted source of clean power and are often operated as base-load power plants. So, efforts are made to enhance their life and keep them operating based on the assessment made during these inspections. Hence these inspections are of utmost importance.

Different NDT methods are used for inspections based on the application including: visual testing (VT), radiographic testing (RT), ultrasonic testing (UT), eddy current testing (ET), magnetic particle testing (MT), dye-penetrant testing (PT), acoustic emission (AE). UT and RT are used for volumetric examinations whereas VT, PT, MT & ET are used for surface examinations. Also, ET is used mainly for the inspections of tubes in steam generators, condensers and heat exchangers. Highly skilled and qualified manpower equipped with specified reliable inspection equipment is required for these inspections. Procedures are developed and planning is done by the trained engineers to perform these inspections reliably and safely as health safety due to the radiation environment is of concern. Manual inspections are performed which rely heavily on the competency of the person performing them. These inspections do not require installations and hence are versatile and adaptable to sudden changes. Semi-mechanized and mechanized inspections are also performed to reduce operator-based errors and reliable data acquisition is performed but requires excessive installation and exceptionally trained and experienced manpower for understanding, successful execution and interpretation [9]. Before the inspections are performed, following points are needed to be known and are mentioned in the plant-specific codes and standards:

1. Type of expected flaw.
2. The frequency of inspections depends upon the nature of the component, the more critical the component the more frequent the inspections.
3. The method to be used for the detection of an expected flaw depends upon codes/standards, the PSI/ISI program and the nature of the defect (surface, internal).
4. Preparation of components including insulation to be removed, arrangement of scaffolding and planning of jobs in as low as reasonably achievable (ALARA) radiation level.
5. Qualification requirements of procedure, equipment or inspector, on open or blind samples as per codes and standards.

Based on the ISI assessment of the life of NPP is made and decision on the extension in the operation of the plant is made. Along with NDE different surveillance capsules are placed inside the RPV (of the same material as of RPV) for destructive testing. These include specimens of different testing including: toughness and fatigue to assess the effect of radiation embrittlement. Before the operation of NPP, testing is performed on unirradiated material for baseline data and subsequently, the samples are withdrawn during each RFO for the life assessment and condition monitoring. These all measures are taken to extend and ensure the safe operation of NPPs and are indicative of strict safety regulations imposed on NPPs.

4. National Centre of Non-Destructive Testing

NCNDT was established in 1995 with the mandate to provide quality NDT training and services to the industrial sector of the country. NCNDT is providing training and certification in different NDT techniques as discussed in previous section namely: UT, RT, ET, VT, MT and PT. NCNDT has trained 7517 personnel through 446 courses in conventional and advanced NDT techniques. Qualified and experienced personnel are also providing services in the NDT techniques to the national industry. The number of the qualified manpower in different techniques is shown in Figure 2.

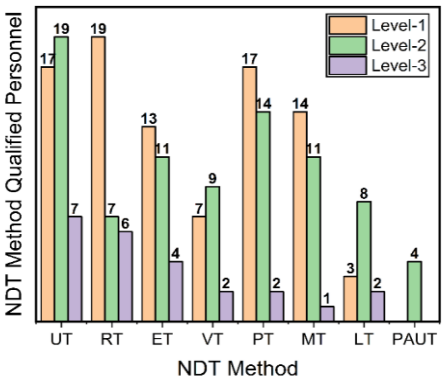

Fig. 2: Number of NDT Qualified Manpower

NCNDT is extensively involved in the PSI before operation and ISI of NPPs during their schedule re-fueling outages and is discussed in detail in next section. Equipment calibration services and third-party inspection and evaluation

services are also being provided. Services related to mechanical testing (creep, fatigue, tensile testing, impact testing, hardness analysis), metallographic testing and material characterization are also available. These facilities are also being used to provide failure and life assessment analysis.

Recently, services of lifting equipment inspection and concrete testing have also been started. NCNDT is carrying out international collaboration with International Atomic Energy Agency (IAEA) for enhancement of its capabilities. NCNDT is accredited with ISO-17024 and ISO-17020 from Pakistan National Accreditation Council (PNAC). Cooperation with universities is also being carried out for research and development and several students are facilitated for their internship programs.

5. Role of NCNDT in NPPs

NCNDT has been involved in the inspections carried out in the NPPs in Pakistan. Starting from the In-Service Inspection of conventional island components of C-1 in 2001. NCNDT started inspecting welds of piping and Class 1, 2 and 3 components in 2010. Meanwhile, NCNDT has participated in and performed inspection of welds of piping in the Pre-Service Inspections of C-3, C-4, K-2 and K-3. Radiographic inspection of the welds of the steam generator using an indigenously developed source positioning tool has been performed for C series NPPs. In 2017 mechanized inspection of the steam generator was performed and in 2023 mechanized inspection of the reactor pressure vessel is going to be performed using specialized mechanized equipment.

Overall NCNDT has participated in:

1. 15 RFOs of C-1
2. 09 RFOs of C-2
3. 04 RFOs of C-3
4. 04 RFOs of C-4
5. 01 RFO of K-2
6. 01 RFO of K-3

Table 2: Inspections Performed by NCNDT

Sr. No.	Inspection	Started In	Details
1.	Inspection of piping of non-nuclear safety class	2004	This includes PT, MT, UT and RT of the welds.
2.	Inspection of piping welds of safety class 3	2006	This includes PT, MT, UT and RT of the welds.
3.	Inspection of piping welds of safety class 2	2006/2008	This includes PT, MT, UT and RT of the welds of various auxiliary and safety systems.
4.	Inspection of piping welds of safety class 1	2010	This includes VT, PT, UT and RT of the: Primary coolant piping Valves in the primary system Auxiliary piping in the main primary system Secondary side of steam generator Main steam system (MSS) valve components MSS piping
5.	Inspection of tubes of condenser, heat exchangers, generator, air coolers	2002	This includes the eddy current (ET) inspections of the tubes.
6.	Inspection of reactor coolant pump welds	2008	This includes the UT of nozzles to safe end and safe end to main coolant piping welds.
		To be performed in 2023	The RT of the nozzles to safe end and safe end to piping welds using specialized source positioning tools for K-2 and K-3.
7.	Inspection of pressurizer welds		This includes the UT of pressurizer welds.
		To be performed in 2023	This includes RT of upper head to nozzles and manhole welds, surge nozzle to bottom head and upper head to shell circumferential welds to be performed using specialized source positioning tools for K-2/K-3.
			This includes the RT of nozzles to safe end dissimilar welds
8.	Inspection of steam generator welds	2016	This includes the RT of steam generator primary nozzles to safe end and safe end to piping welds using specialized source positioning tool for C-series.
		To be performed in 2023	This includes the RT of steam generator primary nozzles to safe end and safe end to piping welds using specialized source positioning tools of K-2/K-3.
9.	Inspection of the RPV closure head	2018	This includes the VT of the closure head cladding.
10.	Mechanized inspection of steam generator	2017	This includes the mechanized eddy current inspection of the SG tubes.
11.	Mechanized inspection of reactor pressure vessel	To be performed in 2023/2024	This includes the UT, RT of the RPV welds, CCTV inspection of the RPV cladding in the most irradiated area, UT and ET of RPV closure head studs and ligaments and control rod drive mechanism omega welds.

NCNDT has also provided NDE inspection services in NPPs as a subcontractor of China Nuclear Operations Ltd. (CNPO), China during PSI and first ISI of C-3 and C-4 and during the PSI of K-2 & K-3. Fig. 3 shows the major milestones of inspections performed by NCNDT in chronological order.

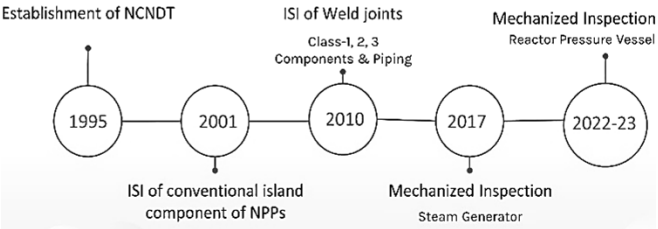

Fig. 3: Inspections Performed by NCNDT in NPPs

Table 2 shows the details of inspections performed by NCNDT.

6. Inspections in Nuclear Island

In this section, inspections of the critical components performed on the nuclear island are discussed.

6.1 Reactor Pressure Vessel

The reactor pressure vessel is made from fine-grained ferritic steel (ASME SA 508, 16MnD5 RCC-M). The material has excellent weldability and high toughness [10]. It has a height of approximately 40 ft. It is internally lined with austenitic steel cladding typically around 3-10mm. The RPV has inlet and outlet nozzles depending upon a number of loops/steam generators. The RPV has a closure head through which control rods are inserted and vents are present. It is made up of shells (3 in Westinghouse-based design) welded together and a hemisphere at the bottom. A flange is welded at the top of the upper shell for the closure head to be bolted to the vessel [11]. Several welds are present and are discussed in section 6.1.3. The RPV contains highly pressurized water at a high temperature. The core is present in the RPV and is situated at the centre of the containment. The water is highly radioactive as it is heated through nuclear fission. A typical PWR Westinghouse-based RPV is shown in Fig. 4.

The inspections of RPV are performed underwater during the RFO and hence the reactor internals must be removed prior to the inspections. Specialized mechanized/robotic equipment has been developed by different NDT companies to perform the inspections. For these inspections several techniques are required including [12]:

1. Visual and Eddy current testing as surface examination.
2. Ultrasonic testing and radiographic testing as volumetric examination.

In the past such examinations were performed manually usually from the outside of RPV whereas now advanced automated technology is available to perform the examinations from the inside of RPV which includes:

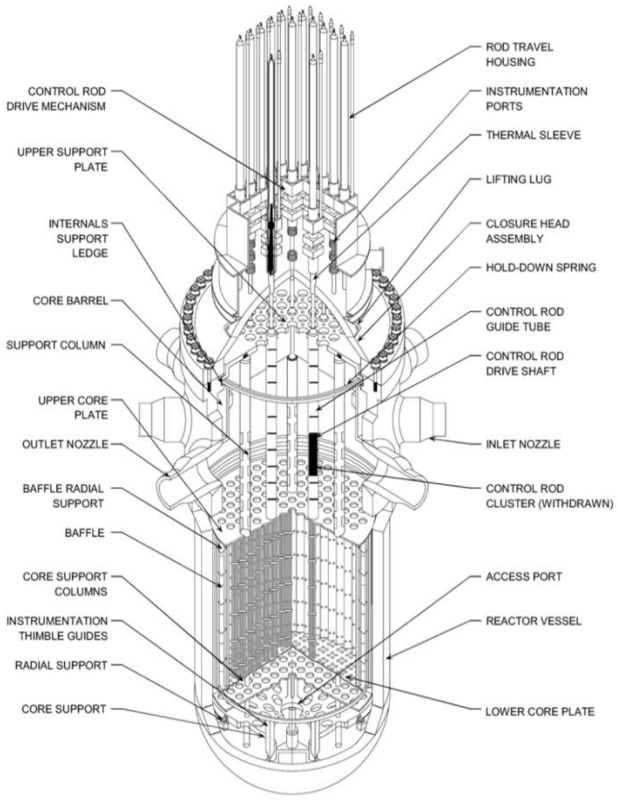

Fig. 4: A typical PWR RPV [13]

1. Automated ultrasonic examination with conventional UT probes.
2. Automated ultrasonic examination with phased arrays UT (PAUT) probes.
3. Automated ultrasonic examination with conventional and phased arrays UT probes.

In the early nineties, companies implemented the NDT technique for automated remote testing of reactor pressure vessel welds from inside with conventional UT technique and recently PAUT technique has been implemented and qualified.

6.1.1 Objectives of RPV-ISI

The following are the main objectives of the In-service inspections of RPV:

1. To perform RPV examination according to the relevant standards (e.g., ASME Code Sec. XI, RSE-M).
2. To examine RPV welds and other critical areas (core region, distribution ring, core barrel support lugs, baffle to former bolts) based on current knowledge, experience from similar examination programs, in-depth design information and good engineering practice.
3. Evaluate the integrity of the reactor pressure vessel.

6.1.2 RPV Degradation Mechanism

The inspection of RPV is critical due to the action of the following degrading mechanisms [14-18]:

1. Radiation embrittlement causes a significant decrease in the ductility of a material, which decreases the fracture toughness. It occurs mostly in the active height of the fuel assemblies i.e., in the intermediate and lower shell of RPV and slightly above and below it. It affects the region where the end-of-life fluence (time integrated neutron flux) is around 10^{21} n/m^2.
2. Thermal ageing also causes a decrease in ductility by the embrittlement due to copper precipitation etc.
3. Temper embrittlement due to the impurity of phosphorus concentration which causes phosphorous segregation-induced weakening of grain boundaries.
4. Fatigue which is caused by the transients. These transients fluctuate the temperature and pressure to another set of loadings (cyclic loading) which initiates and propagates the cracks due to vibrations etc.
5. Corrosion of different types including:
   a. Intergranular attack (IGA), stress corrosion cracking (SCC), flow assisted corrosion crack.
   b. Corrosion of welds.
   c. General corrosion and pitting.
   d. Corrosion due to boric acid.
6. Wear (maintenance operations, opening and closing of the RPV)

6.1.3 RPV Weldments

As explained previously RPV comprises of shells and a hemispherical bottom head. The upper shell has a flange for the closure head placement. The performance of the RPV weldments (both base metal and HAZ) is critical to the safe and efficient operation of the nuclear reactor. Weldments have a different microstructure than the base metal, they are more susceptible to failure and their inspections are more important. Certain RPV weld regions are vulnerable to stress corrosion cracking and other environmental degradation.

1. Cracking and erosion in connection welds.
2. Nozzle cracking in dissimilar metal welds.
3. RPV structural integrity is highly dependent on welding residual stress profiles (stress distributions in the region of the weld).

Major welds of RPV include:

1. Longitudinal shell welds
2. Circumferential welds (shell to shell, shell to bottom head)
3. Nozzles to shell welds
4. Dissimilar nozzle to safe end weld

Along with the inspections of these welds (which are carried out by UT, except nozzle to safe end weld carried out by both UT and RT), an inspection of the cladding in the most irradiated area (as explained before) is carried out by VT, ET and UT for detection of surface and subsurface cracks. Inspection using UT, ET and VT is performed for RPV studs, nuts, threads, ligaments and washers in the flange. VT of the closure head cladding is also performed as required by the codes and standards.

6.1.4 325 MWe NPP – ASME

A typical 325 MWe Westinghouse PWR RPV with its weldment and inspection to be performed is shown in Fig. 5. The inspection of Westinghouse-based RPV is executed on ASME B&PV Code Section XI.

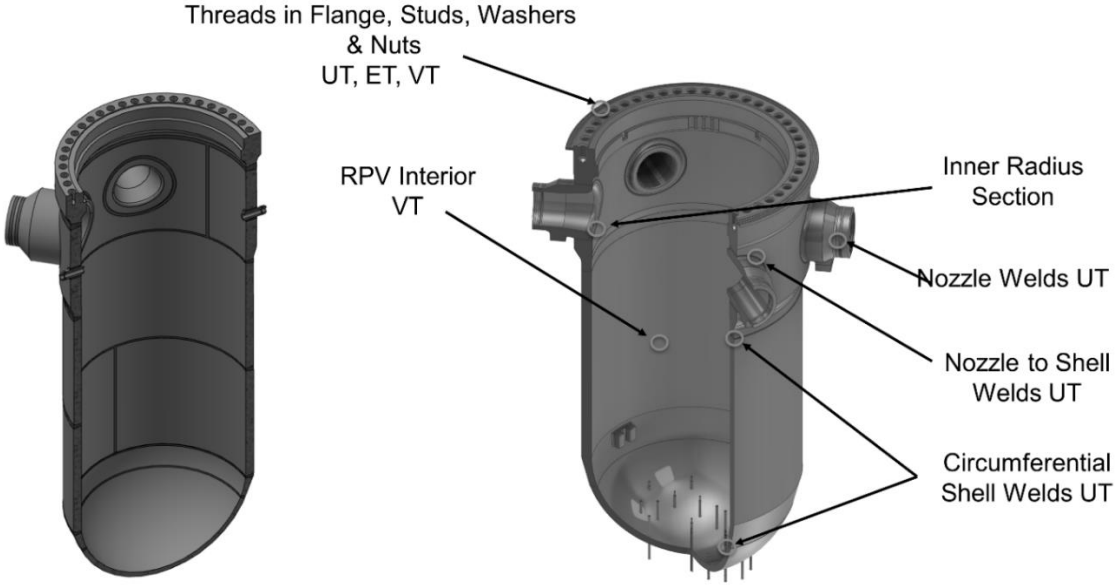

Fig. 5: A typical 325 MWe RPV

6.1.5 1000 MWe NPP – RSE-M

A typical 1000 MWe French code RCC-M PWR RPV with its weldment and inspection to be performed is shown in Fig. 6. The inspection of such RPV is based on the RSE-M code.

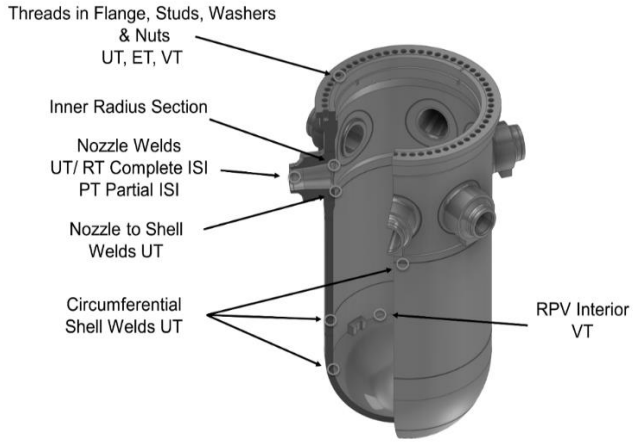

Fig. 6: A typical 1000 MWe PWR RPV

6.1.6 RPV Inspections

Specialized automated inspection systems for RPV have been developed by different NDT companies which is adjustable to different RPV designs (for different diameter and depth). The system constitutes a manipulator which provides 6 or 7 degrees of freedom (DOF) and is connected to the mainframe of the equipment. The system is placed on the RPV flange using the polar crane and RPV guiding studs. It is aligned to the RPV at 0° keyway. It is submersible up to 30 meters. The components are designed to be radiation resistant. The system is remotely operated from the distance. The system has different end effectors to carry out the inspections and are connected to the manipulator depending upon the required inspection. The end effectors include:

1. Nozzle inner radius end effector for ultrasonic testing of nozzle to safe end welds, nozzle inside surface and nozzle inner radius area.
2. Shell end effector for ultrasonic testing of shell welds and lower head weld.
3. Tangential end effector for ultrasonic testing of nozzle to shell welds.
4. RT end effector to place the gamma radiation source at the welds center and to displace the water from surroundings for the radiographic testing of nozzle to safe end welds and safe end to primary coolant piping welds for 1000 MWe NPPs.

These end effectors are remotely interchanged from the refueling bridge via remote docking system (RDS) to Manipulator placed at the RPV flange during the inspections and are maneuvered during the inspections. The system is linked with data acquisition and data analysis systems, which can be performed remotely. These systems complete the inspections in a shorter period to reduce the refueling outage time.

6.2 Steam Generator

Steam Generator (SG) is a U-tube heat exchanger in which pressurized primary coolant from RPV passes through the tubes and boils the feedwater on the outside of the tubes. It has approximately 60 ft in height and is the biggest component of NPP. The tubes are thin and are made up of inconel (nickel-based alloy) 600 which has been replaced by inconel 690 and 800 due to its better corrosion resistance. Thousands of such tubes are present in the steam generator which pass through a tube sheet at the bottom and U bend is at the top. At the bottom of the steam generator manholes are provided along with the primary coolant inlet and outlet nozzles. The details of such tubes for a typical 325 Mwe and 1000 MWe PWR reactor are shown in Table 3.

Table 3: Tube Parameters of Typical 325 and 1000 MWe Steam Generator

Steam generator tubes parameters	K-series PWR Reactor	C-series PWR Reactors
Material	Inconel 690	Inconel 800
Tubes quantity	5835	2977
OD (outer diameter)	17.48mm	22.00mm
Wall thickness	Row1-2, 1.04mm	1.2
	Row3-112, 1.02mm	1.2
Straight tube length	9600mm-9772.49mm	7035 mm (avg)
Shortest tube length	19459.34mm	19233 mm
U-bend tube radius of row 1	82.55mm	62 mm
U-bend tube radius of row 112	1520mm	1364 mm

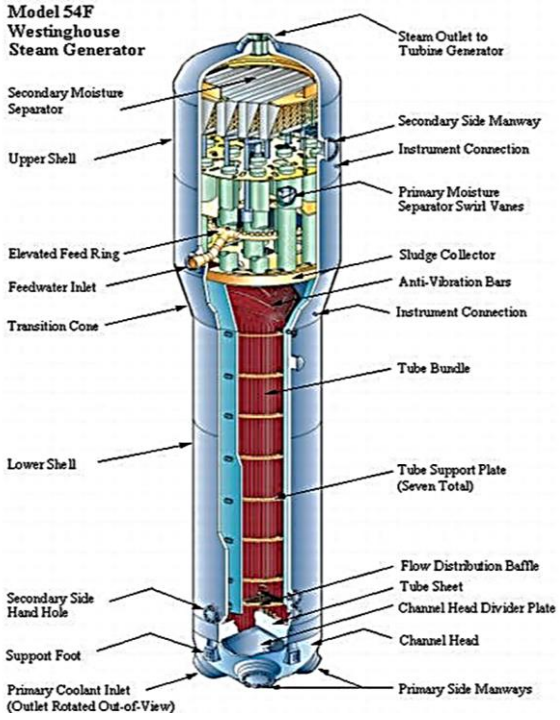

Fig. 7: A Typical Westinghouse Steam Generator [19]

The secondary side of a typical SG includes the "J" rings through which feed water enters the SG, passes through the annulus and then at the shell side around the tubes where steam is produced. It then passes from the top region where chevron-type and swirling vane-type moisture separators are present and reduces the moisture of the steam (minimum 99.75%) to avoid degradation of turbine blades. The steam then leaves the SG through different safety valves to the turbine. A typical SG is shown in Fig. 7.

6.2.1 Objectives of SG ISI

SG tubes not only transfer the heat between primary and secondary systems but also act as a physical boundary between radioactive and non-radioactive coolants. If one or multiple tubes puncture/burst due to a routine ageing process (highly unlikely) or any sudden unforeseen event (due to different degrading mechanisms as discussed in 5.2.2) then both closed loops primary and secondary loops will be mixed and radiation will start to spread and contaminate the secondary side equipment. This spread of radiation will not only disrupt the normal operation of NPPs by damaging the equipment but also be hazardous to the environment and plant personnel. The sudden burst of the steam line will lead to the depressurization of the secondary side. This will produce excessive pressure difference and can cause the rupture of a large number of tubes. The rupture of tubes will depressurize the primary system which can cause loss of coolant accident (LOCA) and subsequently melting of the core [20].

To avoid this gradual or sudden failure of this boundary regular inspections of SG tubes are performed using Eddy Current Testing (ET) technique. Whereas the Nozzles welds with the safe end are inspected through Radiographic Testing (RT) technique.

6.2.2 Steam generator degradation mechanisms

Corrosion is one of the major degrading mechanisms of SG. The chemistry of feedwater is very important and is needed to be controlled to avoid ageing. When steam is formed if there are any impurities present, these will be left behind and get accumulated. These accumulated impurities initiate the corrosion phenomenon. The corrosive products are also produced from the flow accelerated corrosion in the wet steam areas and from the general corrosion of the carbon steel [21]. Different degradation mechanisms occur in the SG as discussed below [22-25].

1. Localized corrosion causes the pitting of tubes both on tube sheets and tubes and is very dangerous.
2. Primary water stress corrosion cracking (PWSCC) under constant (in Heat Affected Zone) and increasing stress (in case of rupture), is observed more frequently in the upper region of the U-bend and is initiated from the inside radius or in crevice regions.
3. Outer diameter stress corrosion cracking and intergranular attack cause circumferential or axial cracks. These occur at the tube-to-tube sheet crevices, tube support plate and free span.
4. Thinning due to accumulation of sludge on tube sheet. The sludge prevents the contact of coolant with the surface increasing its temperature. Wetting and drying alternating regions are formed at which the corrosion is maximum.
5. Denting due to compressive force applied by magnetite accumulated in the gap between intermediate support plate and tubes from accelerated corrosion of carbon steel.
6. Fretting wear occurs due to the vibrations produced as the fluid bends and exerts stresses on the tubes. Cracks and thinning of tubes occur due to these vibrations. These occur at the contact points of anti-vibration bars and tubes etc.
7. High cycle fatigue due to high-stress levels and flow-induced vibrations. It occurs at the upper support plate if tubes are clamped.
8. Foreign material intrusions FMI (any material that is not part of the system or component as designed like bolts, broken parts, debris etc.) if not carefully traced and removed during the refueling outages may get stuck at the tube bundle [26]. Relative motion between these loose parts and the tube bundle results in wear, thinning or rupture of the tubes.
9. Wastage occurs due to the phosphate chemistry. It occurs at the tube sheet crevices, sludge pile, support plates and anti-vibration bars and general thinning is produced.

6.2.3 Steam Generator Weldments

Typical welds in a steam generator are shown in Fig. 8.

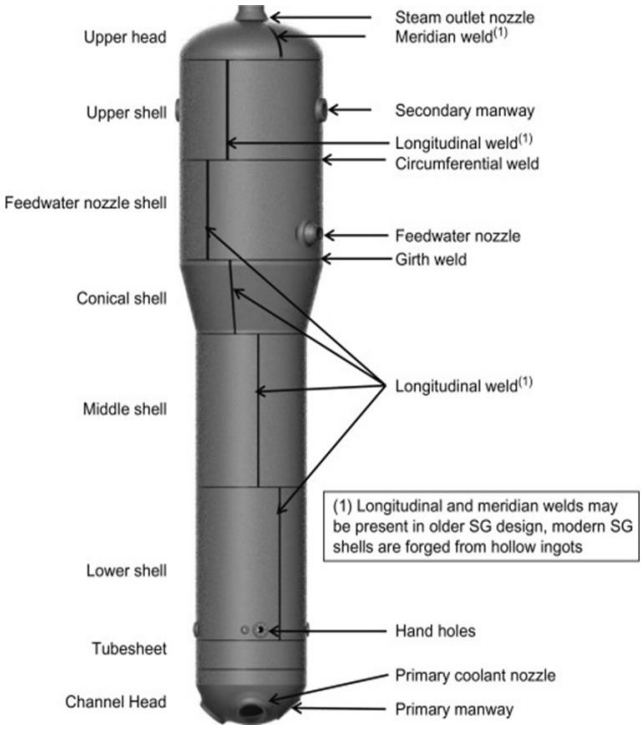

Fig. 8: SG Weldments [27]

6.2.4 Steam Generator Inspections

Different examinations are performed during the ISI as per applicable codes and standards. Some of these include Eddy

current examination of steam generator tubes and radiographic examination of primary inlet and outlet nozzles to safe end and safe end to piping welds.

6.2.4.1 Eddy Current Testing of Steam Generator Tubes

Specialized equipment is used for Eddy current examination of tubes in which a push-pull mechanism is used for the insertion and retrieval of the probe in the tubes. Through the signal analysis defects are recognized and sized by comparison from calibration samples with known defects and a decision on the plugging of the tubes is made based on the applicable codes and standards. The system of ET examination of steam generates tubes includes [28]:

1. Manipulator/robot for probe positioning
2. Eddy current instrument
3. Eddy current probe
4. Calibration standard
5. Pushers for transporting the probe
6. Remote control and communication transmission equipment
7. Computers for data acquisition and analysis
8. Video surveillance system

A typical ET examination system of tubes is shown in Fig. 9.

Fig. 9: Typical ET SG Tubes Inspection System

6.2.4.2 Radiographic Inspection of Primary Nozzles Welds

The radiographic examination of the primary nozzles' welds is performed through specialized designed tools. The mounting plate of the tool is installed on the manhole whereas it has a pipe along with a centering mechanism to place the gamma-ray source at the centre of the weld for panoramic exposure.

6.3 Pressurizer

It is a cylindrical vessel of approximately 50 ft in height and has hemispherical heads at the top and bottom. The material is carbon steel (18MND5/16MND5) internally lined with stainless steel. A large number of electric heaters are placed at the bottom of the pressurizer (PRZ). It has saturated water (heated through heaters) at the bottom and saturated steam at the top. There is a surge nozzle at the bottom of PRZ which links it with the primary coolant system. Normally the water comprises 50/60% volume of PRZ. It controls the pressure of the primary coolant in case of transients through the action of heaters and sprays line. Different safety nozzles are present at the top head along with the spray nozzle and manhole. Different instrumentation penetrations are also provided to measure the temperatures and water level etc. [27]. A typical PRZ is shown in Fig. 10.

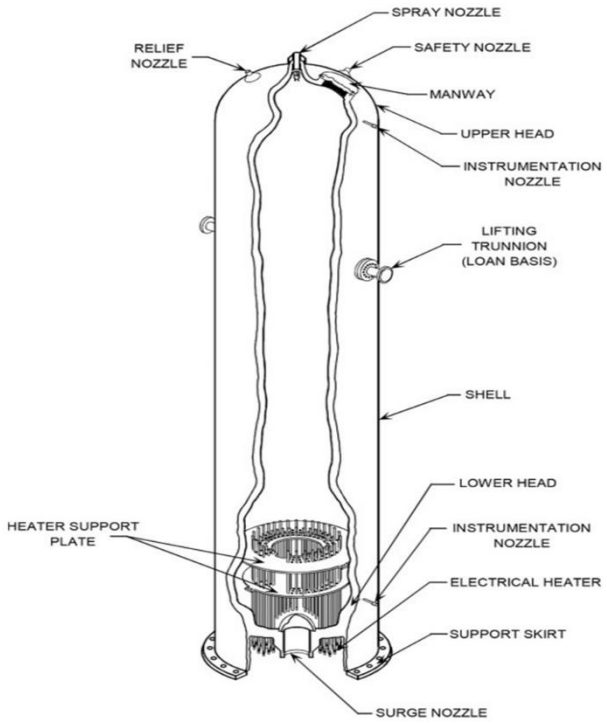

Fig. 10: A typical Pressurizer [29]

In the case where the primary coolant temperature decreases the water somehow contracts and flows from PRZ into the primary coolant system. This is called an out-surge. This decreases the water level which results in expanding the steam hence pressure in the pressurizer decreases. Resultantly, the electric heaters are actuated to boil more water into the steam to increase the pressure and restore the conditions. Contrarily, when the temperature of the primary coolant increases the water flows into the pressurizer and compresses the steam in PRZ hence increasing its pressure. This is called an in-surge. The spray line is actuated when pressure decreases below a set point and relatively cold water from RCP is sprayed in the PRZ. This results in the condensation of steam at the top and allows the coolant to expand and restore normal conditions. Automatic pressure relief valves are present to depressurize the system in case of the pressure gets to such a value that cannot be controlled through heaters or spray. If the pressure gets beyond the control of pressure relief systems (i.e. heaters, spray or safety valves) the reactor gets tripped automatically [30].

6.3.1 Objectives of Pressurizer In-Service Inspection

As explained before the pressurizer maintains the pressure of the primary coolant. Different safety systems are provided with the pressurizer to safely operate the nuclear power plant. Defects in heaters may lead to their ineffective working and if large number of heaters get damaged then this can become a serious issue. Therefore, tracking, maintenance and replacement (if required) of the malfunctioning heaters is to be performed to maintain the pressure of the system. Different components of the pressurizer are subjected to inspections including the heaters, nozzles welds, circumferential welds, cladding etc.

6.3.2 Pressurizer Degradation Mechanisms

Different degradation mechanisms of pressurizer components include [31-34]:

1. Low cycle thermal fatigue in vessels, nozzles and heaters.
2. Flow-induced vibrations.
3. Boric acid corrosion through coolant leakage from electric heater sheath and instrumentation penetrations.
4. Primary water stress corrosion cracking (PWSCC) in the vessel.
5. Thermal embrittlement in spray heads.
6. Electrical ageing (burnout) for heaters.
7. Thermal stratification in the surge nozzle. This occurs when two fluids of different temperatures meet. This occurs for fluid flowing with low velocity. This results in the application of different loads on the nozzle and piping due to temperature differences.
8. Thermal stripping of the surge nozzle due to temperature variation at the interface causes high cycle fatigue cracks.
9. Thermal cycling in the surge nozzle occurs due to transients and the interaction of turbulence in the fluid with the stratified fluid. This also causes fatigue cracks. The damage is maximum when the velocity is small with a large temperature difference. The potential for the maximum damage is during the heat-up and cooldown of the reactor.

6.3.3 Pressurizer Weldments

Pressurizer welds include circumferential shell welds, shell to upper and lower head welds, spray line and safety valve nozzles to upper head welds, surge nozzle to bottom head welds, dissimilar nozzles to safe end welds and manhole to upper head welds etc.

6.3.4 Pressurizer Inspections

According to RSE-M (French code for in-service inspection of mechanical components), radiographic examinations of nozzles to head, upper shell to head weld, manhole to upper head and nozzles to safe end dissimilar welds are to be performed. Visual examination of the internal surface of the pressurizer and acoustic examination of heaters is to be performed. Ultrasonic examination of the lower head to shell weld is to be performed.

The radiographic examinations of upper head to shell, upper head to nozzles and manhole, surge nozzle to bottom head, the source is to be placed inside and complete examination can be performed in a single exposure. Specialized source positioning tools have been developed by inspection companies for this purpose. Tools are installed at the manhole and provide a pathway for the source guide tube to pass through it. For the upper head to shell and upper head to nozzles welds tool of hook shape is used and the source is placed at the centre of the weld for the former and the centre of the upper head for the latter. Whereas for the lower head to surge nozzle a sophisticated tool, in the shape of a hanging umbrella, is used which is lowered in the PRZ using steel rope to the lower support plate of heaters. The centering is ensured by acquiring support from the shell. Panoramic exposure for all the welds is taken. The positioning tools are shown in Fig. 11. The dissimilar welds are exposed by using a double wall single image both on and off-axis for weld and buttering examination [35].

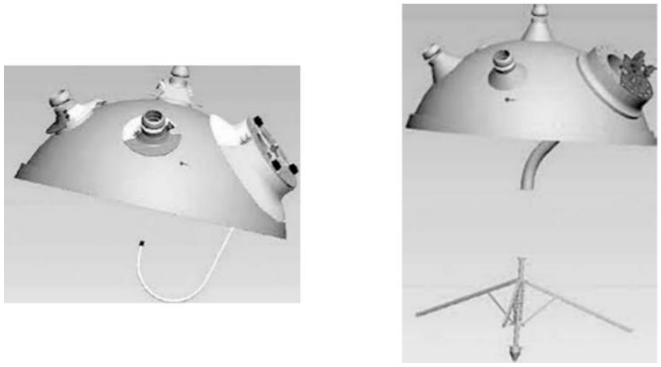

Fig. 11: Radiographic Examination Tools for RT [35]

6.4 Reactor Coolant Pump

In each loop of PWR, a Reactor Coolant Pump (RCP) is present to circulate the primary coolant. It is a single-stage centrifugal pump. The height of a typical RCP is around 30 ft. The suction is vertical with a horizontal discharge. It has a carbon steel casing internally lined with stainless steel provided with inlet and outlet nozzles. The casing encloses the impeller which is connected to the motor via a shaft. A flywheel is provided to keep the water flowing in case of power loss and to avoid any accident such as a core meltdown. As the primary coolant is radioactive hence leakages from the pump are to be avoided. Three seals are provided to the shaft to avoid leakages. Water at a higher pressure is inserted in the RCP to cool the seals and bearings and this also stops the primary coolant from leaking out.

6.4.1 Reactor Coolant Pump Degradation Mechanisms

The degradation mechanisms of RCP include [36]:

1. Fatigue due to transients and shaft vibrations. Thermal stresses and alternating bending stresses can also initiate fatigue cracks.
2. Stress corrosion cracking in the pump casing.

3. High cycle fatigue for pump shaft.
4. Corrosion for pump studs.
5. Foreign material intrusion induced damages.

6.4.2 Reactor Coolant Pump Weldments

RCP weldments include the inlet and outlet nozzles to safe end welds and safe end-to-piping welds.

6.4.3 Reactor Coolant Pump Inspections

Radiographic examination for casing welds is performed using specialized source positioning tools. The tools are fixed at the casing flange and they provide a guiding path to the source through a pipe. The source is placed at the centre of the weld and off-axis position (for buttering examination as per the standard requirement if any) for panoramic exposures. Visual examination of the casing's internal surface is also to be performed.

6.5 Safety Class Piping Welds

The primary coolant piping is made up of austenitic stainless steel. Ultrasonic testing and dye penetrant testing are performed for piping welds as per codes and standard requirements. The main degradation mechanism for the piping is fatigue (due to pressure shocks, thermal fatigue and excessive vibrations), thermal ageing, primary water stress corrosion cracking, boric acid corrosion, thermal stratifications and atmospheric corrosion [37, 38].

6.6 Non-nuclear Safety Class Components and Piping

NCNDT has been performing inspection activities of equipment and piping in the conventional island since RFO-1 of C-1. The key components include: the main steam turbine (HP/LP turbines), steam condensers, moisture separator reheaters, lube oil coolers, HP/LP heaters, exciter/generator air coolers, cross-over piping, governing valves and generators etc.

7. Conclusion

This paper discusses the non-destructive examinations performed during the In-Service Inspections of nuclear power plants with a brief introduction to NPPs in Pakistan, NCNDT and the history of NCNDT in NDT examinations. The examinations have been thoughtfully decided and recommended in the plant codes and standards with the intervals. The NDT examinations have been thoughtfully decided and recommended in the relevant plant codes and standards with their respective intervals in which they must be performed repeatedly for condition assessment. The results of these examinations are compared with baseline (PSI) data and analysis is performed for the life assessment based on the defects' sizes and their growth.

References

[1] D.J. Wuebbles and A.K. Jain, "Concerns about climate change and the role of fossil fuel use," *Fuel Processing Technology*, vol. 71, no. 1, pp. 99-119, 2001.

[2] P.A. Owusu and S. Asumadu-Sarkodie, "A review of renewable energy sources, sustainability issues and climate change mitigation," *Cogent Engineering*, vol. 3, no. 1, p. 1167990, 2016.

[3] T. Trainer, "Some problems in storing renewable energy," *Energy Policy*, vol. 110, pp. 386-393, 2017.

[4] I.C. Change, "Mitigation of climate change," *Contribution of working group III to the fifth assessment report of the intergovernmental panel on climate change*, vol. 1454, p. 147, 2014.

[5] E. AKYÜZ, "Advantages and disadvantages of nuclear energy in Turkey: Public perception," *Eurasian Journal of Environmental Research*, vol. 1, no. 1, pp. 1-11, 2017.

[6] D. Basu and V. Miroshnik, "Advantages of Nuclear Power,", pp. 7-21, 2019.

[7] *Nuclear Power Reactors in the World*. Vienna: International Atomic Energy Agency, 2021.

[8] D.S. Siqueira, J. de Almeida Meystre, M.Q. Hilário, D.H.D. Rocha, G.J. Menon, and R.J. da Silva, "Current perspectives on nuclear energy as a global climate change mitigation option," *Mitigation and Adaptation Strategies for Global Change*, vol. 24, no. 5, pp. 749-777, 2019.

[9] J. Enkvist, A. Edland, and O. Svenson, "Human factors aspects of non-destructive testing in the nuclear power context A review of research in the field," Sweden 1104-1374, 1999, Available: http://inis.iaea.org/search/search.aspx?orig_q=RN:30026316.

[10] J.H. Kim, "Reactor nozzle inspection based on the laser-guided mobile robot," *International Journal of Advanced Robotic Systems*, vol. 15, no. 1, p. 1729881417748443, 2018.

[11] *Assessment and Management of Ageing of Major Nuclear Power Plant Components Important to Safety: PWR Vessel Internals*. Vienna: International Atomic Energy Agency, 2007.

[12] J. Freixa, "SBLOCA with Boron Dilution in Pressuirzed Water Reactors, Impact to the Operation and Safety," 2007.

[13] Y. Bouveret, M. Algarotti, L. Hernandez, J.P. Landez, and M. Lutsen, "PWR reactor vessel in-service inspection according to RSEM," in *Proc. ECNDT*, 2006.

[14] *Integrity of Reactor Pressure Vessels in Nuclear Power Plants: Assessment of Irradiation Embrittlement Effects in Reactor Pressure Vessel Steels*. Vienna: INTERNATIONAL ATOMIC ENERGY AGENCY, 2009.

[15] W. Corwin, R. Nanstad, D. Alexander, R. Stoller, J. Wang, and G. Odette, "Thermal embrittlement of reactor vessel steels," Oak Ridge National Lab.1995.

[16] A. Sarkar, B.K. Kumawat, and J.K. Chakravartty, "Low cycle fatigue behavior of a ferritic reactor pressure vessel steel," *Journal of Nuclear Materials*, vol. 462, pp. 273-279, 2015.

[17] J. Congleton, T. Shoji, and R.N. Parkins, "The stress corrosion cracking of reactor pressure vessel steel in high temperature water," *Corrosion Science*, vol. 25, no. 8, pp. 633-650, 1985.

[18] J. Park, O. Chopra, K. Natesan, W. Shack, and W. Cullen Jr, "Boric acid corrosion of light water reactor pressure vessel materials," in *Proceedings of the 12th International Conference on Environmental Degradation of Materials in Nuclear Power System-Water Reactors*, pp. 459-468, 2005.

[19] S. Šadek and D. Grgić, "Operation and Performance Analysis of Steam Generators in Nuclear Power Plants," in *Heat Exchangers-Advanced Features and Applications*: IntechOpen, 2017.

[20] P. MacDonald, V. Shah, L. Ward, and P. Ellison, "Steam generator tube failures," Nuclear Regulatory Commission, 1996.

[21] K. Kang and L. Kupca, "Assessment and Management of Ageing of Major Nuclear Power Plant Components Important to Safety: Steam Generators," Tech. Rep. TECDOC-1668, IAEA1999.

[22] S.J. Green and J.P.N. Paine, "Materials Performance in Nuclear Pressurized Water Reactor Steam Generators," *Nuclear Technology*, vol. 55, no. 1, pp. 10-29, 1981.

[23] P. Berge and J.R. Donati, "Materials Requirements for Pressurized Water Reactor Steam Generator Tubing," *Nuclear Technology*, vol. 55, no. 1, pp. 88-104, 1981.

[24] L. Obrutsky, J. Renaud, and R. Lakhan, "Overview of steam generator tube-inspection technology," *CINDE Journal*, vol. 35, no. 2, pp. 5-8,10-13, 2014.

[25] S. Mahey, "Flow-Induced Vibrations of foreign objects inside steam generator's tube bundle," University of Waterloo, 2017.

[26] D. Urjan, "Foreign Material Exclusion Program at CNE Cernavoda Nuclear Generating Station," 2008.

[27] T. Sollier, "15-Nuclear steam generator inspection and testing," in *Steam Generators for Nuclear Power Plants*, J. Riznic, Ed.: Woodhead Publishing, pp. 471-493, 2017.

[28] S.Y. Ismail and S. Lee, "A Review of APR 1400 Steam Generators Tube Degradation and State-of-The-Art Inspection Techniques."

[29] T.W. Kerlin and B.R. Upadhyaya, "Chapter 10 - Reactor thermal-hydraulics," in *Dynamics and Control of Nuclear Reactors*, T. W. Kerlin and B.R. Upadhyaya, Eds.: Academic Press, pp. 111-127, 2019.

[30] N.R. Commission, "Pressurized Water Reactor (PWR) Systems," *Reactor Concepts Manual, US NRC Technical Training Center*, vol. 603.

[31] T.J. Katona, "19-Plant life management (PLiM) practices for water-cooled water-moderated nuclear reactors (WWERs)," in *Understanding and Mitigating Ageing in Nuclear Power Plants*, P. G. Tipping, Ed.: Woodhead Publishing, pp. 633-705, 2010.

[32] Y. Jeong and S. Hwang, "Materials management strategies for pressurized water reactors (PWRs)," in Materials Ageing and Degradation in Light Water Reactors: Elsevier, 2013, pp. 315-334.

[33] M. Hrazsky and M. Mikus, "Nuclear Power Plant Mechanical Components Ageing Management Programs in Slovakia," 2007.

[34] H. Sohn, J.Y. Yang, H.S. Lee, and B.J. Park, "20 - Sensing solutions for assessing and monitoring of nuclear power plants (NPPs)," in *Sensor Technologies for Civil Infrastructures*, vol. 56, M. L. Wang, J. P. Lynch, and H. Sohn, Eds.: Woodhead Publishing, pp. 605-637, 2014.

[35] J. Hao, D. Deng, J. Wang, S. Wang, and X. Hua, "Radiography Inspection Technology of CPR1000 Nuclear Power Unit Pressurizer," in *Energy Materials 2014*, Cham, Springer International Publishing, pp. 539-544, 2016.

[36] V. N. Shah, A.G. Ware, D. A. Conley, P. E. Macdonald, and J. J. Burns, "Aging assessment of PWR surge and spray lines and LWR coolant pumps," *Nuclear Engineering and Design*, vol. 118, no. 3, pp. 329-342, 1990.

[37] B. Liang, G. Li, and G. Wang, "Periodic remaining life evaluation program of PWR pressurizer surge line accounting for thermal stratification effect," 2007.

[38] A. Ballesteros, R. Sanda, M. Peinador, B. Zerger, P. Negri, and R. Wenke, "Analysis of events related to cracks and leaks in the reactor coolant pressure boundary," *Nuclear Engineering and Design*, vol. 275, pp. 163-167, 2014.

The Nucleus ***60****, No. 1 (2023) 98-107*

www.thenucleuspak.org.pk

The Nucleus
ISSN 0029-5698 (Print)
ISSN 2306-6539 (Online)

Organophosphate Pesticides Use and Contamination in Groundwater of Pakistan: A Review

Mamoona Sadia[1], Muhammad Mohsin[2], Muhammad Sami Ur Rehman[3], Zafar Iqbal[4], Abdur Rehman[5*], Nargis Naheed[6]

[1]*Department of Environmental Science, Govt. College University, Faisalabad, Pakistan*

[2]*Department of Geography, Govt. Sadiq Egerton Graduate College, Bahawalpur, Pakistan*

[3]*Department of Geography, Govt. College (Boys), Khayaban-e-sir Syed, Rawalpindi, Pakistan*

[4]*Department of Geography, Govt. Gradate College, Jhang, Pakistan*

[5]*Department of Earth Sciences, University of Sargodha, Pakistan*

[6]*Department of Zoology, Wildlife and Fisheries, University of Agriculture, Faisalabad, Pakistan.*

ABSTRACT

Water pollution and contamination is a grave risk to the human as well as environment in Pakistan augmented by the disposal of industrial waste, fertilizers and pesticides into the water sources. The objective of this review paper is to sum-up the use and evaluating the studies of organophosphate pesticides contamination in groundwater of Pakistan. This review paper also pinpoints the detrimental effects of these pesticides on to the human health and environment. It also considers the present state of familiarity to fix the future action plan in research on pesticides in Pakistan. It is manifested that pesticides have a long history of use against insects and other pests. Pesticides are used to enhance agricultural productivity as well as for indoor applications, however, their side effects include damaging the useful insects, wildlife losses, ruins the crops and food chain and health danger to the human and animals etc. It is also evident that in Pakistan, the groundwater is being contaminated at higher levels with the excessive use of pesticides especially organophosphates. It is also noted that a little work has been done on residues analyses of these organophosphates in groundwater of Pakistan especially in Punjab province. Therefore, in order to make sustainable use of pesticides and decrease their harmful impacts, the strong implementation of legislation is required and the utilization of pesticides should be reduced. Furthermore, favoring the biological control and integrated pest management (IPM) should be the main focus of the quarters concerned.

Keywords: *Organophosphate Pesticides, Groundwater, Environment, Human Health, Pakistan*

1. Introduction

Pesticides are referred to as chemicals to control and regulate a diversity of pests that can destroy crops and livestock and lessen the productivity of farmlands. Organophosphates (OP) are a set of pesticides compounds including some of the highly poisonous chemicals employed in agriculture. Organophosphate poisonousness is because of the capacity of the chemicals to constrain an enzyme, acetylcholinesterase (Figure 2) at cholinergic junctions of the nervous system [1]. Water pollution and contamination are amongst the important issues in Pakistan caused by poor monitoring and management of drinking water quality. Many of the parameters of potable water quality agreed by the WHO are often violated in many developing countries like Pakistan etc. [2-4]. Additionally, the drinking water sources are being contaminated with the disposal of industrial waste, fertilizers and pesticides into the water sources throughout the country [5]. Applications of pesticides are the major contributing aspects to the decline of quality of water [6]. The pesticides are the chemical compounds that are utilized to switch, destroy, alleviate, prevent, or resist many insects, rodents, wild plants, fungi or other organisms that can impends human health and the area's economy [7]. The pesticides are used to protect crop, preserve food, materials and protect from vector-borne diseases (malaria, dengue, leishmaniasis and Japanese encephalitis) which executes up to one million children each year. Pesticides save energy and labor, and increase crop production in agriculture [8]. The increasing intensification of agricultural practices in developing countries (e.g. Pakistan) enhances the occurrence and risk of pest attacks [9].

Pesticides are toxic by design, their manner of action is by marking systems or enzymes in the pests which may be alike or very same to systems or enzymes in humans and thus, they put dangers to the environment and the health of humans. Mishandlings and over use of pesticides cause deposition of pesticides to inner part of vegetable, soil and water in the residual form [10, 11]. The objective of this review paper is to sum-up the use and evaluating the studies of organophosphate pesticides contamination in groundwater of Pakistan. It also pinpoints the detrimental effects of these pesticides on to the human health and environment. Further, this paper also considered the present status of pesticide knowledge in Pakistan to formulate and direct the future action plan in pesticide research.

2. Pesticides Consumption in Pakistan

Agriculture is the largest sector of Pakistani's economy with 21% contribution to GDP and employing about 44% of the workforce [12]. Agrochemicals use in Pakistan had come into practice in the year of 1954 with the volume of 254 metric tons. For meeting its domestic needs, Pakistan has extremely trusted on imported pesticides and insecticides. By the mid-1960s, Pakistan made great progress in domestic pesticides manufacturing by founding two manufacturing units viz. DDT-Nowshera and BHC and DDT-Kala Shah Kaku and pesticides consumption has reached over 7,000 tons per annum [13]. During 1970s, no further progress have been made and these plants became out of dated and were shut downs. Later on about 20 formulation plants were installed in Pakistan, the pesticide manufacturing, importing, selling, and

*Corresponding author: abdurrehmanuospk@gmail.com

monitoring rules and regulations were quantified according to the Agricultural Pesticide Ordinance 1971 and Agriculture Pesticide Rules 1973 [14, 15]. By the installation of pesticides plants, the level of consumption of pesticides was increased to 16,226 metric tons in 1980s. In 1989, the pesticides distribution and sale were transferred to the private sector from the public sector, which carried out a five-fold surge in the consumption of pesticide in one year and has increased by 1,169% during the last 20 years [16, 17]. During the financial year of 2019-20, Pakistan has imported the pesticides of the worth of 220 million US dollars that increased to 484 million US dollars in financial year of 2021-22 [18, 19].

Empirical analysis of pesticide import trend and marketing price index showed that the total expense on the buying of pesticides is increasing annually in Pakistan. Local companies offered incentive schemes and great profit margins of up to 30% to the brokers to fetch full share of market as compared to the transnationals of up to 15% in Pakistan [20]. Among the top active transnationals' of pesticide trade in Pakistan were Bayers, Burma Shell, Ciba-Giegy, FMC, Dow Chemicals, ICI, Hoechest, Sandoz and Pacific. Now at present time, over 108 types of insecticides, 39 types of weedicides, 30 types of fungicides, 6 types of rodenticides and 5 types of acaricides are being utilized in Pakistan. Among the province wise share of pesticide market, the Punjab is on top with 90% share, Sindh for 8% and both KPK and Balochistan hold 2% respectively [21]. In the Punjab province, before 1983 to 1997 only 5-10% of the crop cultivating area has been handled with pesticides which are now enhanced to 100% [17].

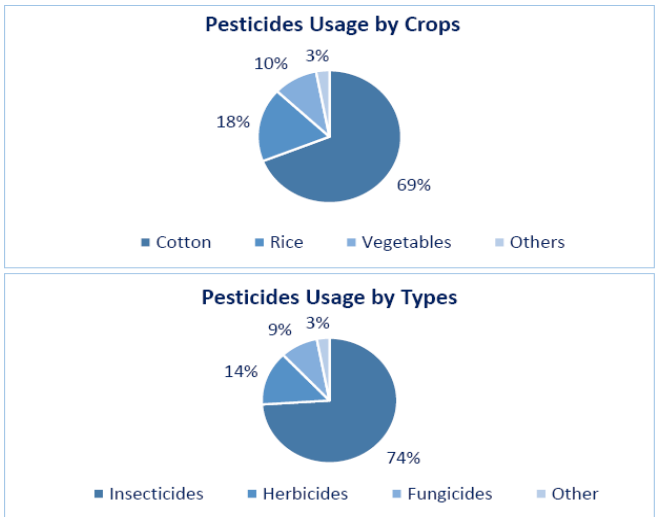

Fig. 1: Pesticides Usage by Crops and Types in Pakistan [19]

In Pakistan, the usage of pesticides is ever increasing to control pests and for better output of agricultural crops [22]. A study conducted at Multan shows that the highest share of cultivators (79.4%) dependent on the pesticides for management of pests [23]. Presently, there are about 170 registered pesticide products and 272 registered importers of these pesticides in the country that are being regulated by the Department of Plant Protection (Ministry of National Food Security and Research). Majority of the pesticides are utilized in cotton crop which are chiefly insecticides (Figure 1) [19].

3. Organophosphate Pesticide in Pakistan

Organophosphate (OP) chemicals are the organic compounds of phosphoric acid derived that are most commonly used as pesticides and nerve agents with highly poisonous nature [24]. They also used in cropping areas and having massive efficiency, wide coverage of numerous species and low diligence. Moreover, the OP pesticides and nerve agents have a mutual mechanism of work [25, 73]. In Pakistan, OPs and CMs (Carbamates) are used because of their availability and rapid decay in the environment instead of organochlorine (OC) pesticides [26, 27]. Tetraethyl pyrophosphate was the first OP synthesized in 1854. During the years of 1934-1944, a German chemist named Gerhard Schrader and his coworkers synthesized about 2,000 OP compounds at I.G. Farben industries including parathion (as a pesticide) and sarin, soman and tabun, as chemical warfare nerve agents [28]. Today, more than 100 kinds of OP pesticides are available in the market for the check of numerous pests and insects, each having different toxicity levels and a variety of pest control applications including insecticides, nematicides, acaricides, and fungicides [29, 30]. Nowadays, OP pesticides are extensively manufactured and utilized in Pakistan. A survey of Southern parts of Punjab, Pakistan, was conducted to evaluate the extent of wide-ranging used pesticides and demonstrated that many OP pesticides were used in different districts of Pakistan, i.e. Layyah, Muzaffargarh, Multan, Khanewal and Faisalabad [31]. Among Organophosphorus pesticides, Malathion, Profenofos, Chlorpyrifos and Triazophos were extensively used and the top ten insecticides in Pakistan [32]. Sale of endosulfan, chlorpyrifose, profenophose and monocrotophos was 117.9, 44.9, 36.7 and 22.3 metric tons respectively [33]. These pesticides are used to control bollworms, aphids, fruit borers, red spiders, cutworms and leaf hoppers on a wide range of crops such as wheat, cotton, maize, cereals, fruits and vegetables. These are generally efficient in the control of plant roundworms [34, 35].

4. Fate of Organophosphate Pesticides

The knowledge on chemical, physical and biological processes that governs the transportation, distribution and fate of pesticides and their transformation products in the groundwater is important to assess the pesticides residues. Pesticide contamination in the groundwater is due the certain reasons like occurrence and distribution in relation to their use. In the environment, these OP chemicals do not persist however; their larger usage and decaying rates can cause these compounds to deposit in soils, and from where they ultimately enter into groundwater and rivers [36]. The pesticide contamination in groundwater may be from non-point sources and from point sources [37]. Like the Diazinon, an OP, often exists in point sources (e.g. wastewater treatment plant effluents) and non-point sources (e.g. storm water runoff) in

agricultural and urban areas and is extremely toxic [38]. In last few years, attention of political, public and scientific concerns have shifted toward non-point sources. Groundwater contamination from nonpoint sources (NPSs) is a bigger environmental concern because non-point sources are comparatively not easy to recognize [39]. Furthermore, the use of agricultural pesticides is one of the key problems in urban and rural cultivated areas, with the dispersion of common pollutants through polluted air, water and other physical ways [40]. It is observed that hydrophobicity and persistence are two key properties of the pesticides. If these are water solvable or have fewer octanol–water partition co-efficient and low soil half-life then the contamination of groundwater will be higher [41, 42, 17]. Also, the rate of pesticides degradation is affected by soil type, pH, soil moisture, organic contents and the concentration of pesticides in the soil. However, the mobility of pesticides and their transfer to water bodies depend on total organic contents in soil, pesticide half-life, soil texture, depth to water table, mechanisms and kinetics of sorption and desorption from soil particles [43]. Sandy loam soil facilitates the mobility of pesticides and they may get distributed in the soil up to a depth of 35 cm [44]. Especially, the main concerns are the timings and application amounts, and the usage of larger quantities of these pesticides during irrigation to crops rainfall aids the chemicals to reach groundwater [45]. Therefore, the organophosphates (OPs) are more readily infiltrated in the groundwater as compared to other types of pesticide [46].

5. Pesticide Contamination of Groundwater in Pakistan

The extensive pesticides use has regulated the pests in Pakistan, but it has originating many environmental issues same as other developing countries. It is estimated that annually, over half million people in Pakistan are unluckily suffered from pesticides and other agro-compounds [47]. Pesticide contamination of groundwater is an extensive pollution problem. As a consequence of widespread and repeated use, pesticide residues have been detected in high concentrations in groundwater serving as drinking water resources. Pesticide concentration may cross the limits in drinking water ($0.1 \mu g L^{-1}$) for individual pesticides [48]. Ali and Jabbar [49] carried out a research in Faisalabad (Punjab, Pakistan) and disclosed that the groundwater fetched from a depth of 30 to 40 feet is polluted with remains of pesticide namely cyalothrin (traces to 0.0002 ppm), monocrotophos (0.04-0.06 ppm) and endrin (0.0001-0.0002 ppm). In some areas of Sindh and Punjab, groundwater has been established toxic and is continuously being polluted due to excessive use of pesticides [50].The residues of pesticides are found in shallow drinking water wells of Punjab close to the areas where a large amount of pesticides are being used [51]. In addition, a fish slaying tragedy in the Rawal Lake was become a headline news in Pakistan and at international level. The said lake supplies the drinking water to a population of 1.5 million of Rawalpindi City. Numerous research institutions reported high elevated percentage of pyrethroids pesticide in this lake [52]. Similar investigation of pesticide contamination in groundwater was conducted in the tobacco growing area of Mardan (KPK) where methyl parathion, chlorpyrifos, endosulfan and profenophos were found. The water table of this area was 3.6 to 5 feet [53]. In Pakistan, it is reported in a study that out of 107 collected samples of groundwater, 31 were contaminated with pesticides and were exceeding the safe potable water limit as per the WHO and FAO [5]. This influence the groundwater utilized as potable water by the human and marks them susceptible to the detrimental effects of these pesticides [55]. Ahad et al., [51] reported that diazinon, methyl parathion, fenitrothion, endosulfan and azinophos methyl with residual level of 0.003, 0.01,0.00,0.13 and 0.001ug/L respectively in cotton-growing area of Multan with water table of 5.0 to 18 feet.

In continuation with the above facts of the studies, the pesticides pollution of groundwater in four concentrated districts of cotton growing had also been elevated. Water samples were collected from wells in the areas of Dera Ghazi Khan, Bahawalnagar, Rajanpur and Muzaffargarh, districts of Punjab. The pesticides which are mostly applied in these districts were analyzed. The percentage of detection of endosulfan, methyl parathion and monocrotophos was 8%, 5.4% and 35.1% in July; 24.3%, 8% and N.D. (not detected) respectively in October [41]. A bulk of pesticides with 5,000 and 3,000 tons are distributed in the Punjab and Sindh provinces respectively. In addition, 46,500 liters of liquid pesticides and 366 tons of solid were used in Karachi, the biggest city of Pakistan and a major share of these pesticides has seeped down to groundwater and polluted it. Moreover, it was found that about 70 tons of pesticides were vanished because of low quality packing material and caused groundwater contamination in Sahiwal [56]. Furthermore, WWF-Pakistan [57] revealed that about 3,800 tons of expired pesticides could not be abolished in Pakistan because of lack of budget and necessary technology. As well as a considerable amount of outdate pesticides and obsolete were testified in majority of the districts of Punjab province, which in result, mounting the risk of environmental degradation.

6. Pesticides Exposure and Poisoning

The consumption and varieties of pesticides have been enhancing significantly as crop production and population numbers are geared up. In this regard, pesticide mishandling turns into more serious and this has outcome in great environmental pollution and danger for human health. It is established that consumption patterns of pesticides has passed notable variations since 1960s. In 1962, the American biologist Rachal Carson was amongst the first to mention the problems associated with the overuse of the pesticides in her seminal book ‘Silent Spring’. This publication raised the huge concerns about the influences of the pesticides on the human health and environment [45]. The excessive pesticide use is dangerous for not only environment but also for human health [58, 59]. Likewise, contamination of water bodies and deaths due to pesticides has been serious in past years [60]. Policy formulators, farmers and other shareholders should be search for devices to evaluate the dangers of pesticide for minimizing

pesticide effects on human health and surrounding ecosystem. In this regard, the new decision support system of Pesticide Use Risk Evaluation (PURE) developed by California Environmental Protection Agency (CEPA) is being used to evaluate specific pesticide risks to soil and groundwater. In PURE, the risk score is calculated by the corresponding share of the Predicted Environmental Concentrations (PEC) to the poisonous score for chosen endpoint organisms. The risk scores in PURE is ranging between 0-100, (where 0 represents negligible risk while 100 for the highest risk) [61].

Pesticides are used to slay the certain organisms on crops, houses, gardens and parasites in medicines but low awareness caused environmental and health risks. Therefore, the pesticides are being extensively abused in the farms in Pakistan. In a study, it is found that very few (less than 2%) farm participants were aware the names of the pesticides they were utilizing and one-third of the workers were not aware the pesticides to be used in crops. Few workers (29%) used protective clothing and majority of the participants (96%) had contributed in immixing pesticides together before use. A considerable number of participants (18%) had no information about the health related risks of pesticides. It is noted that at least one pesticide metabolite was found in every field worker. Hence, pesticide contamination is not source-dependent but hostile in human metabolism system [62]. The pesticides, particularly organophosphate (OP) pesticides like chlorpyrifos, have been often utilized for excessive time to maintain product quality, protect agricultural crops from various pests and to increase yield. Lappharat et al. [63] evaluated the dermal exposure to chlorpyrifos in rice farmers. The concentrations of chlorpyrifos were higher and ranging 526.34 ± 478.84 mg/kg in males than the females (500.75 ± 595.15 mg/kg). Average daily intake collected from seven study sites on male and female farmers were as 31.72 × 10(-4), 193.32 × 10(-4), 5.38 × 10(-4), 190.48 × 10(-4), 170.47 × 10(-4), 465.91 × 10(-4) and 43.04 × 10(-4) mg/kg/day respectively. The mean hazard quotient (HQ) and 95th percentile level was noticed to be higher than permissible limit of HQ>1. Especially the paddy farmers in paddy fields were at great danger for antagonistic health effects due to constant dermal exposure to chlorpyrifos. Shakerkhatibi et al. [64] assessed the contamination of pesticides in rural groundwater of northwest Iran. The pesticides residual of the 78 collected water samples was found 26.9% of the total samples with accumulations of over 0.5 μg/L and amongst diazinon, profenofos and malathion were traced as the most recurrently detected pesticides with the determined accumulations of 0.614, 0.542 and 0.456 μg/L respectively.

However, the bioavailability of pesticides in humans can become severe dysfunctions, metabolic and even absolute disease states. A study showed that pesticide spray-workers (n=140) and controls (n=110) have the substantial impact on serum enzyme point ($p<0.001$) by analytical means. Monocrotophos was the major cholinesterase inhibitor among all the pesticides used there. The finding of deposit absorptions in blood serum samples of spray-workers for monocrotophos was determined as 0.005 mg/kg body weight [65]. The notable rise in enzyme level of glutamate oxaloacetate transaminase (GOT), alkaline phosphatase (ALP) and glutamate pyruvate transaminase (GPT) was also reported in farm-station workers, Gadap, Karachi due to the diazinon and monocrotophos [66]. The dolphin (*Platanista gangetica minor*) found in Indus River (Pakistan) is one of the world's highly threatened cetacean mammals. The largest population of this dolphin is found between Sukkur and Guddu barrages, officially declared as the Reserve of Indus dolphin. The habitat of this species is compact to one fifth of its historic distribution range. The major threat to the Indus dolphin is water contamination due to usage of toxic pesticides to exploit fish catch [67, 68]. The toxicity of pesticides has the potential to enter in aquatic system and the possible consequences of pesticide bioaccumulation of the food chain. The organophosphates were also detected in Rawal and Simly lakes [69]. Therefore, because of the extensive applications of pesticides, there has been a turn in the new algal biocoenosis that subsidize to water blooms [70].

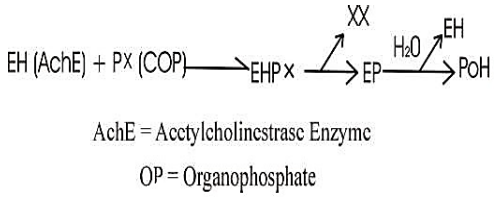

Fig. 2: Organophosphates binding to the enzyme acetylcholinesterase [24]

Diazinon, a poisonous OP, prevents the enzyme acetylcholinesterase, which hydrolyzes the neurotransmitter acetylcholine and driven to a suite of intermediary syndromes (Figure 2) including respirational, myocardial and neuromuscular transmission impairment [71]. Further, it also causes diarrhea, generalized weakness, depression, abnormal posturing and anorexia [72, 73]. Acetylcholinesterase (AChE) has an ability to measure the inhibitory strength of certain nerve agents and may offer an early estimation on the toxic level. A wide range of nerve agents are there having more strength of *k*i values (Table 1) than many pesticides except few ones. For instance, chlorpyrifos-oxon, a vigorous substance of pesticide chlorpyrifos is much stronger than tabun, a nerve agent [74]. These values give the information of early raw approximation of the potential in vitro poisonousness. Nevertheless, different intervening factors are considered vital for the determination of real in vitro poisonousness of OPs i.e. volatility, biological and chemical steadiness, lipophilicity and the way of contact [75, 76].

Deviations in metabolism among species and exposed levels have a fundamental part in diazinon's bioaccumulation among various organisms in a wide variety of efficiencies and concentrating ratios [83]. In Pakistan, malathion is one of the greatly used pesticides in agriculture. The recurrence exposure to malathion at the groundwater pollution degrees exerts unsympathetic effects on the hepatic drug-metabolizing system. Malathion exposure affects the body or weight of

Table 1. In vitro potential strength of selected OPs (pesticides, nerve agents) toward human Acetylcholinesterase.

OP	*k*i	OP	*k*i
Fenamiphos	0.002	TEPP	59.7
Propophos	0.03	Methylsarin	105
Tetrachlorvinphos	0.03	Dimethyl-VE	125
Methamidophos	0.05	Leptophos	134
Monocrotophos	0.06	Tabun	182
Trichlorfon	0.07	Dimethyl-VX	222
Dicrotophos	0.15	Chlorpyrifos-oxon	269
Omethoat	0.16	Ethylsarin	327
Ethoprophos	0.23	Diisopropyl-VE	368
Heptenophos	1.38	Naled	377
Bromfenvinphos	1.43	Sarin	398
Chlorfenvinphos	1.72	VE	433
Pirimiphos-methyl-oxon	2.81	Diethyl-VX	551
Dichlorvos	3.55	VX	1150
Profenofos	4.08	n-Propylsarin	1260
Malaoxon	4.74	Soman	1930
Mevinphos	6.64	n-Butylsarin	2790
N-Diethyltabun	7.77	Chinese VX	3210
Dimethyl-amiton	8.57	neo-Pentylsarin	3240
Paraoxon-methyl	11.3	Cyclosarin	4390
N-n-Propyltabun	11.8	Russian VX	4580
Amiton	18.9	sec-Pentylsarin	4870
Diisopropyl-amiton	27.4	iso-Butylsarin	5330
O-Methyltabun	32.1	iso-Pentylsarin	5460
Paraoxon-ethyl	33.0	n-Pentylsarin	9500

Source: [77, 78, 79, 80, 81, 82]

Note: ki is the bi-molecular inhibition rate constant assumed as 105 M^{-1} min^{-1}

liver and the different biochemical parameters [84]. However, the adverse impacts of malathion on the health of human and ecosystem are of mounting apprehension. The narrative malathion haptens are synthesized to develop an enzyme linked immunosorbent assay (ELISA) screening method and this ELISA is utilized to assess malathion in the samples of groundwater and surface water. On this basis, the satisfactory results were obtained by the GC-MS reference method for malathion environmental monitoring in natural waters [85]. Likewise, methyl parathion, ethyl parathion were also found to be acutely toxic [86]. Similarly, profenofos, a type of organophosphate is a potential acetylcholinesterase inhibitor [87]. Generally, the organophosphates impede acetylcholinesterase in the nervous system of pests and are splits into six sub-types as; phosphates, phosphorothioates, phosphorodithioates, phosphorothiolates, phosphonates and phosphoramidates (Figure 3) [24]. The toxicity and metabolism levels of OPs are depends on the structural variations of these compounds. For instance, the pesticides i.e. paration, diazinon and malathion [88].

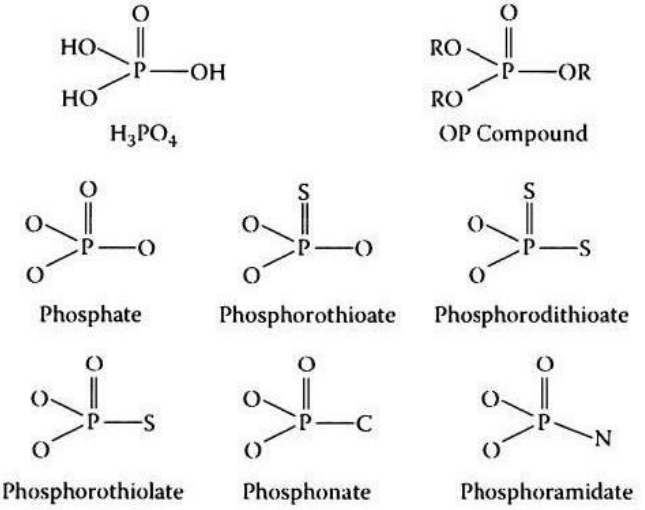

Fig. 3: The structure of Organophosphates by chemical arrangement [24]

Endocrine glands have unique importance in human body as they accomplish certain tasks and characteristics but they disrupted by many chemical compounds [89]. Endocrine disrupting chemicals (EDCs) are chemicals that change the humans' usual working of the endocrine system. Pesticides are the compounds that have been recognized as endocrine disruptors [90]. The extreme contact to regular and synthetic environmental compounds and poisons can have negative impacts on the endocrine system and reproductive health [91]. An assessment of susceptibility to a composite mix-up of pesticides resulted in a substantial rise of DNA decay in farmers, who were persistently disclosed to pesticides in crop fields. The Leukocytes exposed to pesticides from 47 agriculture workers were assessed with comet assay. The significant variation ($P<0.001$) in DNA decay of disclosed individuals (14.80 ± 3.04µm) was noticed when compared with control group (6.54 ± 1.73µm) in cotton grown areas of Pakistan [92].

Pesticides have negative impact on environment and human health. Intensive pesticide use in Bolivia has reported increasing problems of acute pesticide poisonings and chronic effects like neurological problems, cancers, teratogenicity, sterility and environmental pollutions [93]. Apart, the excessive misuse and overuse of pesticides by naive growers enhanced the health and environmental danger particularly in the vital cotton growing districts of Pakistan [94]. In Pakistan, cotton picking is mainly accomplished by women who are at a great risk to pesticide remains due to their low fiscal freedom and wide use of pesticides during the picking season [95].

Table 2. Brief of the physicochemical properties and phase of the intoxication of Organophosphates.

Pesticides	Physical and Chemical Properties	Exposition	Toxicokinetics	Toxicodynamics	Signs and Symptoms	Treatment
Organophosphorus	Organic compounds containing phosphorus. The properties vary with the size and structure. In general are more soluble in organic solvents	Skin, conjunctiva, gastrointestinal tract and lungs	Rapidly absorbed and metabolized by P450 isozymes in oxom form, more toxic than the parent compounds	Covalent bonds with the serine residue in the active site of acetyl cholinesterase (reversibly or irreversibly)	Muscarinic syndrome and nicotine syndrome, resulting of excess acetylcholine in the synaptic cleft	Maintenance of vital functions and cholinesterase levels. It is important to avoid the use of parasympathomimetic agents

Source: [88, 102, 103, 104, 105, 106]

Abbas et al. [96] published findings from their investigation in Bahawalnagar, Sahiwal and Vehari districts of Punjab that most of the women respondents (91.3%) were unaware of the health risks of the pesticides. Therefore, the peripheral blood was collected from 69 unexposed females and 69 cotton pickers and employed to evaluate the impact of pesticide vulnerability on inherited decay as well as on serum cholinesterase and hepatic enzymes. Rates of alkaline aspartate, aminotransferase and phosphatase were higher; the levels of serum cholinesterase were lower in the vulnerable workers as compared with the control group (P<0.001). The vulnerable group shown greatly enhanced occurrences of total number of micronuclei in binucleated lymphocytes was (16.51 ± 4.27 vs. 5.86 ± 3.09, P<0.001 and binucleated cells with micronuclei were (12.72 ± 3.48 vs. 4.35 ± 2.44, P<0.001) in comparison with the control group [97]. Similar study was done in Multan district of Punjab and Khairpur district of Sindh and found impact of pesticides on reproductive hormones (LH and FSH) of females [98, 99]. A broad range of terrestrial and aqua ecosystems have been long known as polluted with OP pesticides. These pesticides have great mammalian poisonousness and it is absolutely vital to eliminate them from the environment. About 200,000 metric tons of nerve agents have to be cracked worldwide due to this group of pesticide [100]. However, specific OPs such as triorthocresyl phosphate inhibits neurotoxic esterase and results in a delayed type of axonal pathology. Hexane pathology has been found in screen printers and these circumstances highlighted the demand for improved precautionary and work-related measures [101]. The selected physiochemical properties and intoxication of organophosphates is summarized in table 2.

7. Pesticide Management and Control

Information concerning mobility of pesticide is vital for the estimation of pesticide management practices. In recent times, there has been a great rise in the use of pesticide for numerous purposes like: to control plant insects, weeds and other plant disease [107]. However, in spite of their effectiveness, it is estimated that just 0.1% of OPs are reached their wished goal [108]. But still the population is threatening by the nerve agents and OP pesticides and their treatment is a continuing challenge for medical field [74]. Thus, lysimetric studies have been undertaken to expand evaluation schemes to save groundwater from deleterious impacts reasoned by the use of pesticide. By using lysimetric studies, particular observing tasks and deterrence ways for the safety of waters can be examined. The obtained findings can offer to the local agencies and the decision makers with recognition of a device for delimitating hazard areas. Pesticide remnants form found at the bottom of lysimeters were 1.52 > 2.1 > 2.74 m which could be a sign of an 'Index of Risk' for groundwater contamination [109]. A recent study detected the chief pesticide groups' chemical residues of OPs, i.e. profenofos, chlorpyrifos and triazophos in collected water samples of 15 districts of the Punjab province, where the maximum concentration in water sources of core areas during winters exhibited by profenofos at 5,665 ng L^{-1} [110]. Notwithstanding, the continued efforts made on national and international level to ban greatly noxious OP pesticides self-poisoning with pesticides residues remains a key medical issue particularly in developing countries, initiating over 100,000 causalities every year [111]. Therefore, the Integrated Pest Management (IPM) suggests different pest control ways to minimize the artificial pesticide application [112]. Pesticides are vital element of an IPM that plays a key role in rising agrarian production. Biopesticides are safer alternatives to conventional pesticides. The synthetic insecticides (imidacloprid, endosulfan and profenofos) and biopesticides (spinosad and biosal) were analyzed and measured their half-lives. The average half-life of biopesticides, was 3.47 and 1.66 days for spinosad and biosal respectively whereas, conventional pesticides were persistent with average half-life of 3.14, 2.57 and 2.11 days for endosulfan, imidacloprid, and profenofos respectively [113]. Bioremediation can propose a competent and cheap way for sanitization of contaminated ecosystems and obliteration of nerve agents. The first microorganism identified that could damage OP chemicals was *Flavobacterium sp*. Since, a number of bacterial and fungal species were isolated and cultured which can damage a variety of OP chemicals in liquid cultures [114]. The agriculture ministries of less developed countries must focus on the enhanced and monitored use of OP compounds as pesticides. They should also encouraged growers to utilize natural pesticides and organic agriculture rather than compound pesticides [1]. It is also necessary to educate the public about the various forms of natural pest control and select unbleached paper products like paper (for office or home use), coffee filters, toilet tissues and napkins [91].

8. Conclusion

Pesticides are widely used since long ago against insects and other pests in Pakistan. Pesticides especially the OPs are used to enhance agricultural productivity are inevitable in agriculture and other uses but they are proven to be highly toxic and harmful for wildlife, positive insects, remnants in crops and food chain. They are also posing risk to human health, animals and surrounding environment due to fatal chemicals and toxins. It is therefore, strong implementation of legislation is required and the usage of pesticides should be minimizing and strongly dispirited. While the focus should be on biological controlling measures usage and encouraging the IPM. It is also evident that the groundwater resources in Pakistan have been contaminated particularly with OPs pesticides. A little work has been done on residues analyses of these pesticides in groundwater of Pakistan exclusively in Punjab Province. Therefore, this study will be supportive for future research and policy formulation regarding to monitor the nature and adverse impacts of these pesticides in groundwater, on humans health and environment.

Reference

[1] M. Kazemi, A.M. Tahmasbi, R. Valizadeh, A.A. Naserian and A. Soni, "Organophosphate pesticides: A general review", Agricultural Science Research Journals, vol. 2, p. 512-522, 2012.

[2] M. Mohsin, S. Safdar, F. Asghar, and F. Jamal, "Assessment of Drinking Water Quality and its Impact on Residents Health in Bahawalpur City", International Journal of Humanities and Social Science, 3(15), p. 114-128, 2013.

[3] M. Mohsin, S. Safdar, M. Nasar-u-Minallah and A. Rehman, "Monitoring of physiochemical quality of drinking water in selected areas of Bahawalpur City, Pakistan", Journal of Biodiversity and Environmental Sciences, vol. 14(6), p. 186-196, 2019.

[4] N.N. Riaz, F. Rehman, S. Hussain, S.A. Ahmad, "Quality Assessment of Drinking Water in Vehari District of Punjab, Pakistan", International Journal of Economic and Environmental Geology, vol. 12(2), p. 21-26, 2021.

[5] M.K. Daud, M. Nafees, S. Ali, M. Rizwan, R.A. Bajwa, M.B. Shakoor, M.U. Arshad, S.A.S. Chatha, F. Deeba, W. Murad, I. Malook and S.J. Zhu, "Drinking water quality status and contamination in Pakistan", BioMed Research International, Article ID 7908183, p. 1-18, 2017.

[6] A. Azizullah, M.N.K. Khattak, P. Richter and D.P. Hader, "Water pollution in Pakistan and its impact on public health: A review", Environment International, vol. 37, p. 479-497, 2011.

[7] C. Dolan and B. Mannan, "Pesticide Use and Wildlife", The University of Arizona Cooperative Extension, College of Agriculture and Life Sciences, The University of Arizona, Tucson, Arizona 85721, October, 2009, Available from: www.cals.arizona.edu/pubs/natresources/az1481i.pdf (29 July, 2010).

[8] K. Loague, D.L. Corwin and G.E. Brown, "Groundwater vulnerability to pesticides: An overview of approaches and methods of evaluation", John Wiley and Sons: New York, USA, 2005.

[9] J.S. Bernal and R.F. Medina, "Agriculture sows pests: how crop domestication, host shifts, and agricultural intensification can create insect pests from herbivores", Current Opinion in Insect Science, vol. 26, p. 76-81, 2018.

[10] B. Kumari, R. Kumar, V.K. Madan, R. Singh, J. Singh and T.S. Kathpal, "Magnitude of Pesticidal Contamination in Winter Vegetables from Hisar, Haryana", Environmental Monitoring and Assessment, vol. 87, p. 311-318, 2003.

[11] A. Quintero, M.J. Caselles, G. Ettiene, N.G. de Colmenares, T. Ramirez and D. Medina, "Monitoring of organophosphorus pesticide residues in vegetables of agricultural area in Venezuela", Bulletin of Environmental Contamination and Toxicology,vol. 81, p. 393-396, 2008.

[12] GOP, "Economic Survey of Pakistan 2017-18", Ministry of Finance, Government of Pakistan (GOP); Islamabad, Pakistan, 2018.

[13] Paktech, "Present status of pesticide industry", 2004, Available from: http://www.paktechsearch.com/Problemsolution.asp (29 September, 2006).

[14] Saarcnet, "Strong agricultural base justifies an agrochemical", 2001, Available online: www.saarcnet.org/saarcnetorg/saarc_summit/Pakistan/agrochemicals.htm (29 June, 2002).

[15] R.B. Mazari, "Country report on international code of conduct on the distribution and use of pesticides", Department of Plant Protection, Ministry of Food, Agriculture and Livestock, Government of Pakistan, 2005.

[16] H. Shahid, "Pakistan's use of pesticides increased 1,169% in 20 years: FAO Daily Times", 2003, Available from: http://www.dailytimes.com.pk/default.asp?page=story_15-1-2003_pg5_6 (01 January, 2003).

[17] M.I. Tariq, "Leaching and degradation of cotton pesticides on different soil series of cotton growing areas of Punjab, Pakistan in Lysimeters", Ph.D. Thesis, University of the Punjab, Lahore, Pakistan, 2005.

[18] GOP, "Economic Survey of Pakistan 2018-19", Finance Division, Government of Pakistan, Islamabad. 2019. Available from: http://www.irispunjab.gov.pk/Economic%20SurveyNews/Economic%20Survey%202018-19.pdf (29 May 2022).

[19] PACRA, "Pesticides Sector Study", The Pakistan Credit Rating Agency Limited, February 2022.

[20] A.A. Khooharo, R.A. Memon and M.U. Mallah, "An empirical analysis of pesticide marketing in Pakistan", Pakistan Economic and Social Review, vol. 46, p. 57-74, 2008.

[21] A.M. Khan, "Pakistan agricultural pesticides association", 2000, Available from: http://www.cpp.org.pk/Assoc/associations.html (19 January, 2003).

[22] C.A. Damalas and M. Khan, "RETRACTED: pesticide use in vegetable crops in Pakistan: insights through an ordered probit model", Crop Protection, vol. 99, p. 5964, 2017.

[23] F.Z.A. Khan, S.A. Manzoor, H.T. Gul, M. Ali, M.A. Bashir, M. Akmal, M. Haseeb, M.U. Imran, M. Taqi, S.A. Manzoor, M. Lukac and S.V. Joseph, "Drivers of farmers' intention to adopt integrated pest management: a case study of vegetable farmers in Pakistan", Ecosphere, vol. 12(10), p. 3812, 2021b.

[24] S.A. Shad, "Insecticides and their Applications", First Edition, Higher Education Commission – Pakistan, 2018.

[25] A.G. Canlı, B. Sürücü, H.I. Ulusoy, E. Yılmaz, A. Kabir and M. Locatelli, "Analytical Methodology for Trace Determination of Propoxur and Fenitrothion Pesticide Residues by Decanoic Acid Modified Magnetic Nanoparticles", Molecules, vol. 24, p. 4621, 2019.

[26] A.V. Jain and C.G. Ramesh, "Analysis of Organophosphate and Carbamate Pesticides and Anticholinesterase Therapeutic Agents, Toxicology of Organophosphate and Carbamate Compounds", Academic Press: Burlington, p. 681-701, 2006.

[27] P. Wang, S. Jiang, D. Liu, H. Zhang and Z. Zhou, "Enantiomeric Resolution of Chiral Pesticides High-Performance Liquid Chromatography", Journal of Agriculture and Food Chemistry, vol. 54, p. 1577-1583, 2006.

[28] K. Soltaninejad and S. Shadnia, "History of the Use and Epidemiology of Organophosphorus Poisoning (Ch. 2)", In: M. Balali-Mood, M. Abdollahi (Eds.), Basic and Clinical Toxicology of Organophosphorus Compounds, London, Springer-Verlag, pp. 25-43, 2014.

[29] M. Balali-Mood and H.R. Saber, "Recent advances in the treatment of organophosphorous poisonings", Iranian Journal of Medical Sciences, vol. 37(2), p. 74-91, 2012.

[30] S.M. Nurulain, "Different approaches to acute organophosphorus poison treatment", Journal of Pakistan Medical Association, vol. 62(7), p. 712-717, 2012.

[31] S.A. Baig, N.A. Akhter, M. Ashfaq, and M.R. Asi, "Determination of the Organophosphorus Pesticide in Vegetables by High-Performance Liquid Chromatography", American-Eurasian Journal of Agricultural & Environmental Sciences, vol. 6(5), p. 513-519, 2009.

[32] I.A. Chaudhry, "Pesticides production can avert agro-chemicals shortage", 2004, Available from: http://www.pakissan.com/english/news/newsDetail.php?newsid=99 (29 July, 2006).

[33] M. Saleem, and M. Arshad, Environmental hazards of pesticides, 2005, Available from: http://www.pakissan.com/english/issues/environmental.hazards.of.pesticides.shtml (26 August, 2006).

[34] S. Rani, V.K. Madan and T.S. Kathpal, "Persistence and Dissipation Behavior of Triazophos in Canal Water under Indian Climatic Conditions", Ecotoxicology and Environmental Safety, vol. 50(1), p. 82-84, 2001.

[35] R.E. Mauldin, T.M. Primus, T.A. Buettgenbach and J.J. Johnston, "A simple HPLC method for the determination of chlorpyrifos in black oil sunflower seeds", Journal of Liquid Chromatography and Related Technology, vol. 29, p. 339-348, 2006.

[36] M. Sirotkina, I. Lyagin and E. Efremenko, "Hydrolysis of organophosphorus pesticides in soil: New opportunities with ecocompatible immobilized His6-OPH", International Biodeterioration & Biodegradation, vol. 68, p. 18-23, 2012.

[37] J.E. Barbash and E.A. Resek, "Pesticides in ground water: Distributions, trends, and governing factors", Ann Arbor Press: Chelsea, p. 588, 1996.

[38] H. Durmaz, Y. Sevgiler and N. Üner, "Tissue-speciWc antioxidative and neurotoxic responses to diazinon in Oreochromis niloticus", Pesticide Biochemistry and Physiology, vol. 84, p. 215-226, 2006.

[39] J.L. Domagalski and N.M. Dubrovsky, "Monocrotophos chemical and physical properties: A Review", Contamination and Toxicology, vol. 39, p. 12, 1994.

[40] I. Werner, F.G. Zalom, M.N. Oliver, L.A. Deanovic, T.S. Kimball and J.D. Henderson et al., "Toxicity of storm-water runoff after dormant spray application in a French prune orchard, Glenn County, California, USA: temporal patterns and the effect of ground covers", Environmental Toxicology and Chemistry, vol. 23, p. 2719-2726, 2004.

[41] M.I. Tariq, S. Afzal and I. Hussain, "Pesticides in shallow watertable areas of Bahawalnagar, Muzafargarh, D. G. Khan and Rajan Pur Districts of Punjab, Pakistan", Environment International, vol. 30, p. 471-479, 2004a.

[42] M.I. Tariq, S. Afzal and I. Hussain, "Adsorption of pesticides by salorthids and camborthids of Punjab, Pakistan", Toxicological & Environmental Chemistry, vol. 86(4), p. 247-64, 2004b.

[43] T.B. Moorman, K. Jayachandran and A. Reungsang, "Adsorption and desorption of atrazine in soils and subsurface sediments", Soil Science, vol. 166, p. 921-929, 2001.

[44] M. Rani, S. Saini and B. Kumari, "Leaching behaviour of chlorpyriphos and cypermethrin in sandy loam soil", Environmental Monitoring and Assessment, vol. 186, p. 175-182, 2014.

[45] M.F.F. Bernardes, M. Pazin, L.C. Pereira and D.J. Dorta, "Impact of Pesticides on Environmental and Human Health", In: A. C. Andreazza and G. Scola (Eds.). Toxicology Studies - Cells, Drugs and Environment, doi: 10.5772/5971, 2015.

[46] D.K. Stepien, J. Regnery, C. Merz and W. Puttmann, "Behavior of organophosphates and hydrophilic ethers during bank filtration and their potential application as organic tracers. A field study from the Oderbruch, Germany", Science of Total Environment, vol. 460, p. 150-9, 2013.

[47] M.I. Khan, M.A. Shoukat, S.A. Cheema, H.N. Arif, N.K. Niazi, M. Azam, S. Bashir, I. Ashraf and R. Qadri, "Use, Contamination and Exposure of Pesticides in Pakistan: A Review", Pakistan Journal of Agricultural Sciences, vol. 57(1), p. 131-149, 2020.

[48] E. Gozdereliler, "Groundwater bacteria: Diversity, activity and physiology of pesticide degradation at low concentrations", Ph.D. Thesis, Department of Environmental Engineering, Technical University, Denmark, 2012.

[49] M. Ali and A. Jabbar, "Effect of pesticides and fertilizers on shallow groundwater Quality. Final technical report (Jan. 1990–Sep. 1991)", Pakistan Council of Research in Water Resources (PCRWR), Government of Pakistan, Islamabad, 1992.

[50] M.I. Tariq, S. Afzal, I. Hussain and N. Sultana, "Pesticides exposure in Pakistan: A review", Environment International, vol. 33, p. 1107-1122, 2007.

[51] K. Ahad, Y. Hayat, I. Ahmad and M.H. Soomro, "Capillary chromatographic determination of pesticides residues in groundwater of Multan Division", The Nucleus, vol. 38, p. 145-149, 2001.

[52] A. Ahad, A. Mohammad, F. Mehboob, A. Sattar and I. Ahmad, "Pesticide residues in Rawal Lake, Islamabad, Pakistan", Bulletin of Environmental Contamination and Toxicology, vol. 76(3), p. 463-470, 2006.

[53] K. Ahad, T. Anwar, I. Ahmad, A. Mohammad, S. Tahir, S. Aziz and U.K. Baloch, "Determination of insecticide residues in groundwater of Mardan Division, NWFP, Pakistan: A case study", Water SA, vol. 26(3), p. 409-412, 2000.

[54] M. Ali and A. Jabbar, "Effect of pesticides and fertilizers on shallow groundwater Quality", Final technical report (Jan. 1990 to Sep. 1991). Pakistan Council of Research in Water Resources (PCRWR); Government of Pakistan, Islamabad, Pakistan, 1992.

[55] A. Waseem, H. Ullah, M. Rauf and I. Ahmad, "Distribution of natural uranium in surface and groundwater resources: A review", Critical Reviews in Environmental Science and Technology, vol. 45, p. 2391-2423, 2016.

[56] JICA, Country profile on environment: Pakistan, 1999, Japan International Corporation Agency, Available from: http://www.jica.go.jp/english/global/env/profiles/e99pak.pdf (10 January, 2003).

[57] WWF-Pakistan, "Pollution issues: Chemical fertilizers & pesticides", 2000, Available from: http://www.wwfpak.org/pollutionissues.htm (11 December, 2002).

[58] F.Z.A. Khan, S.A. Manzoor, M. Akmal, M.U. Imran, M. Taqi, S.A. Manzoor, M. Lukac, H.T. Gul and S. Joseph, "Modelling pesticide use intention in Pakistani farmers using expanded versions of the theory of planned behavior", Human and Ecological Risk Assessment: An International Journal, vol. 27, p. 687-707, 2021a.

[59] E. Lavison Sasso, R. Cattaneo, T. Rosso Storck, M.M. Spanamberg, V.A. Sant and B. Clasen, "Occupational exposure of rural workers to pesticides in a vegetable-producing region in Brazil", Environmental Science and Pollution Research, vol. 28, p. 25758-25769, 2021.

[60] W.J. Zhang, F.B. Jiang and J.F. Ou, "Global pesticide consumption and pollution: With China as a focus", Proceedings of the International Academy of Ecology and Environmental Sciences, vol. 1(2), 125-144, 2011

[61] Y. Zhan and M. Zhang, "Pure: A web-based decision support system to evaluate pesticide environmental risk for sustainable pest management practices in California", Ecotoxicology and Environmental Safety, vol. 82, p. 104-113, 2012.

[62] B. Shomar, K. Al-Saad and J. Nriagu, "Mishandling and exposure of farm workers in Qatar to organophosphate pesticides", Environmental Research, vol. 133, 312-20, 2014.

[63] S. Lappharat, W. Siriwong, N. Taneepanichskul, M. Borjan, M.H. Perez, and M. Robson, "Health risk assessment related to dermal exposure of chlorpyrifos: A case study of rice growing farmers in Nakhon Nayok Province, Central Thailand", Journal of Agromedicine, vol. 19, p. 294-302, 2014.

[64] M. Shakerkhatibi, M. Mosaferi, M. J. Asghari, E. Lotfi and M. Belvasi, "Pesticides Residue in Drinking Groundwater Resources of Rural Areas in the Northwest of Iran", Health Promotion Perspectives, vol. 4(2), p. 195-205, 2014.

[65] S.M. Soomro, G.M. Seehar, M.I. Bhanger and N.A. Channa, "Pesticides in the blood samples of spray-workers at agriculture environment: The toxicological evaluation", Pakistan Journal of Analytical and Environmental Chemistry, vol. 9, p. 32-37, 2008.

[66] M.A. Azmi, S.N.H. Naqvi, M.A. Azmi and M. Aslam, "Effect of pesticide residues on health and different enzyme levels in the blood of farm workers from Gadap (rural area) Karachi—Pakistan", Chemosphere, vol. 64(10), p. 1739-44, 2006.

[67] U. Waqas, M. I. Malik and L. A. Khokhar, "Conservation of Indus River Dolphin (Platanista gangetica minor) in the Indus River system,

Pakistan: An overview", Record of Zoology Survey of Pakistan, vol. 21: 82-85, 2012.

[68] T.A. Saqib, S.N. Naqvi, P.A. Siddiqui and M.A. Azmi, "Detection of pesticide residues in muscles, liver and fat of 3 species of Labeo found in Kalri and Haleji lakes", Journal of Environmental Biology, vol. 26, p. 433-8, 2005.

[69] S. Iram, I. Ahmad, K. Ahad, A. Muhammad and S. Anjum, "Analysis of pesticides residues of Rawal and Simly lakes", Pakistan Journal of Botany, vol. 41, p. 1981-1987, 2009.

[70] P. Roman, D. Cardona, L. Sempere and F. Carvajal, "Microbiota and organophosphates", Neurotoxicology, 75, p. 200-208, 2019.

[71] D.C. Smegal, "Human health risk assessment chlorpyrifos", US Environmental Protection Agency, Office of Prevention, Pesticides and Toxic Substances, Office of Pesticide Programs, Health Effects Division, US Government Printing Office: Washington, DC, USA, p. 1-131 2000.

[72] D.J. Larkin and R.S. Tjeerdema, "Fate and effects of diazinon", Reviews of Environmental Contamination and Toxicology, vol. 166, p. 49-82, 2000.

[73] US EPA, "Risks of diazinon use to the federally listed California red legged frog (Rana aurora draytonii) ", Environmental Fate and Effects Division, Office of Pesticide Programs, Washington, DC, USA, 2007.

[74] F. Worek,·H. Thiermann and T. Wille, "Organophosphorus compounds and oximes: a critical review", Archives of Toxicology, vol. 94, p. 2275-2292, 2020.

[75] H. Rice, "Toxicology of organophosphorus nerve agents", In: F. Worek, J. Jenner, H. Thiermann (Eds.) Chemical warfare toxicology. Royal Society of Chemistry, Cambridge, UK, p. 81-116, 2016.

[76] R.A. Young and A. Watson, "Organophosphate nerve agents", p. 97-126, 2020.

[77] N. Aurbek, N.M. Herkert, M. Koller, H. Thiermann and F. Worek, "Kinetic analysis of interactions of different sarin and tabun analogues with human acetylcholinesterase and oximes: Is there a structure-activity relationship?", Chemico Biological Interactions, vol. 187, p. 215-219, 2010.

[78] N. Aurbek, H. Thiermann, L. Szinicz, P. Eyer and F. Worek, "Analysis of inhibition, reactivation and aging kinetics of highly toxic organophosphorus compounds with human and pig acetylcholinesterase", Toxicology, vol. 224, p. 91-99, 2006.

[79] F. Worek, N. Aurbek, M. Koller, C. Becker, P. Eyer and H. Thiermann, "Kinetic analysis of reactivation and aging of human acetylcholinesterase inhibited by different phosphoramidates", Biochemical Pharmacology, vol. 73, p. 1807-1817, 2007a.

[80] A. Bartling, F. Worek, L. Szinicz and H. Thiermann, "Enzyme-kinetic investigation of different sarin analogues reacting with human acetylcholinesterase and butyrylcholinesterase", Toxicology, vol. 233, p. 166-172, 2007.

[81] F. Worek, N.M. Herkert, M. Koller, N. Aurbek and H. Thiermann, "Interaction of pentylsarin analogues with human acetylcholinesterase: a kinetic study", Toxicology Letters, vol. 187, p. 119-123, 2009.

[82] F. Worek, H. Thiermann, L. Szinicz and P. Eyer, "Kinetic analysis of interactions between human acetylcholinesterase, structurally different organophosphorus compounds and oximes", Biochemical Pharmacology, vol. 68, p. 2237-2248, 2004.

[83] V. Aggarwal, X. Deng, A. Tuli and K. S. Goh, "Diazinon-chemistry and environmental fate: A California perspective", Reviews of Environmental Contamination and Toxicology, vol. 223, p. 107-140, 2013.

[84] S.B. Naraharisetti, M. Aggarwal, S.N. Sarkar and J.K. Malik, "Concurrent subacute exposure to arsenic through drinking water and malathion via diet in male rats: effects on hepatic drug-metabolizing enzymes", Archives of Toxicology, vol. 82, p. 543-551, 2008.

[85] E.M. Brun, M. Garces-Garcia, M.J. Banuls, J.A. Gabaldon, R. Puchades and A. Maquieira, "Evaluation of a novel malathion immunoassay for groundwater and surface water analysis", Environmental Science and Technology, vol. 39, p. 2786-2794. 2005.

[86] A.S. Fjordboge, A. Baun, T. Vastrup and P. Kjeldsen, "Zero valent iron reduces toxicity and concentrations of organophosphate pesticides in contaminated groundwater", Chemosphere, vol. 90, p. 627-633, 2013.

[87] M. Ismail, R. Ali, T. Ali, U. Waheed and Q.M. Khan, "Evaluation of the acute toxicity of profenofos and its effects on the behavioral pattern of fingerling common carp (Cyprinus Carpio L., 1758)", Bulletin of Environmental Contamination and Toxicology, vol. 82, p. 569-573, 2009.

[88] M.J. Ellenhorn and D.G. Barceloux, "Medical Toxicology. Diagnosis and Treatment of Human Poisoning", Elsevier (Ed.), New York, p. 1512, 1988.

[89] Y. Khan, H. Ullah, M. Bibi and P. Zur, "Chemicals that Disrupt the Endocrine System and their Effects on Human Health", Journal of Endocrinology, vol. 6(1), p. 000179, 2022.

[90] W. Mnif, A.I.H. Hassine, A. Bouaziz, A. Bartegi, O. Thomas and B. Roig, "Effect of endocrine disruptor pesticides: A review", International Journal of Environmental Research and Public Health, vol. 8(6), p. 2265-2303, 2011.

[91] M.A. Ashraf and M. Wilson. "Endocrine Disrupting Chemicals: Sources, Effects and Treatments", Acta Chemica Malaysia, vol. 3(2), p. 39-47, 2019.

[92] J.A. Bhalli, T. Ali, M.R. Asi, Z.M. Khalid, M. Ceppi and Q.M. Khan, "DNA damage in Pakistani agricultural workers exposed to mixture of pesticides", Environmental and Molecular Mutagenesis, vol. 50, p. 37-45, 2009.

[93] M.D.E. Jors, "Acute pesticide poisonings among small-scale farmers in La Paz County Bolivia", Master's Thesis. Department of International Health, Institute of Public Health, University of Copenhagen, Denmark, 2004.

[94] A.A. Khooharo, "A Study of Public and Private Sector Pesticide Extension and Marketing Services for Cotton Crop", Ph.D. Thesis, Department of Agricultural Education, Extension & Short Courses, Faculty of Agricultural Social Sciences, Sindh Agriculture University, Tando Jam, Pakistan, 2008.

[95] K. Bakhsh, N. Ahmad, M.A. Kamran, S. Hassan, Q. Abbas, R. Saeed and M.S. Hashmi, "Occupational hazards and health cost of women cotton pickers in Pakistani Punjab", BMC Public Health, vol. 16, p. 961, 2016.

[96] M. Abbas, I. Mehmood, A. Bashir, M.A. Mehmood and S. Hassan, "Women Cotton Pickers' Perceptions about Health Hazards due to Pesticide use in Irrigated Punjab", Pakistan Journal of Agricultural Research, vol. 28(1), p. 76-84, 2015.

[97] T. Ali, J.A. Bhalli, S.M. Rana and Q.M. Khan, "Cytogenetic damage in female Pakistani agricultural workers exposed to pesticides", Environmental and Molecular Mutagenesis, vol. 49, p. 374-380, 2008.

[98] R. Ahmad, M.K. Baloach, A. Ahmad, R. Rauf, H. Siddiqui and M.Y. Khokar, "Evaluation of toxicity due to commercial pesticides in female workers", Pakistan Journal of Medical Sciences, vol. 20, p. 392-296, 2004.

[99] S. Rizwan, I. Ahmad, M. Ashraf, S. Aziz, T. Yasmine and A. Sattar, "Advance effect of pesticides on reproduction hormones of women cotton pickers", Pakistan Journal of Biological Sciences, vol. 8, p. 1588-91, 2005.

[100] B.K. Singh and A. Walker, "Microbial degradation of organophosphorus compounds", FEMS Microbiology Review, vol. 30, p. 428-471, 2006.

[101] U. K. Misra and J. Kalita, "Toxic neuropathies", Neurology India, vol. 57, p. 697-705, 2009.

[102] D.B. Barr and L.L. Needham, "Analytical methods for biological monitoring of exposure to pesticides: a review", Journal of Chromatography. B, vol. 778, p. 5-29, 2002.

[103] L.G. Costa, "Toxic Effects of Pesticides", In: C. D. Klaassen (Ed.), Cassarett and Doull's Toxicology, The Basic Science of Poisons (7th Ed.), McGraw-Hill, New York, USA, p. 883-930, 2008.

[104] B.P. Paudyal. "Organophosphorus poisoning", Journal of Nepal Medical Association, vol. 47(172), p. 251-258, 2008.

[105] H. Thiermann, F. Worek and K. Kehe, "Limitations and challenges in treatment of acute chemical warfare agent poisoning", Chemico Biological Interactions, vol. 206(3), p. 435-43, 2013.

[106] M.A. Gallo and N.J. Lawryk, "Organophosphorus pesticides", In: W. J. Hayes Jr. and E. R. Laws Jr. (Eds.), Handbook of Pesticide Toxicology, San Diego: Academic Press, 2, p. 917-1123, 1991.

[107] S. Batool, A. Amer, Q.S. Rana and R.R. Javed, "Effects of Pesticides: A Review", International Journal of Agriculture & Sustainable Development, vol. 4(2), p. 74-84, 2022.

[108] J. Neylon, J.N. Fuller, C. van der Poel, J.E. Church and S. Dworkin, "Organophosphate Insecticide Toxicity in Neural Development, Cognition, Behaviour and Degeneration: Insights from Zebrafish", Journal of Developmental Biology, vol. 10, p. 49, 2022.

[109] M.I. Tariq, S. Afzal and F. Shahzad, "Fate of carbosulfan and monocrotophos in sandy loam soils of Pakistan under field conditions at different watertable depths", Journal of Environmental Monitoring, vol. 12, p. 1119-1125, 2010.

[110] Z. Javaid, Ghazala, M. Ibrahim, A. Mahmood and A.A. Bajwa, "Pesticide Contamination of Potable Water and its Correlation with Water Quality in Different Regions of Punjab, Pakistan", Water, vol. 15, p. 543, 2023.

[111] E.J. Mew, P. Padmanathan, F. Konradsen, M. Eddleston, S.S. Chang, M. R. Phillips and D. Gunnell, "The global burden of fatal self-poisoning with pesticides 2006–15: Systematic review", Journal of Affective Disorders, vol. 219, p. 93-104, 2017.

[112] J. Pretty and Z.P. Bharucha, "Integrated pest management for sustainable intensification of agriculture in Asia and Africa", Insects, 6, p. 152182, 2015.

[113] M.F. Akbar, M.A. Haq, F. Parveen, N.Yasmin and S.A. Sayeed, "Determination of synthetic and bio-insecticides residues during aphid (Myzus persicae (sulzer) control on cabbage crop through high performance liquid chromatography", Pakistan Entomology, vol. 32, p. 155, 2010.

[114] H.B. Shafiq, M. Ajaz and S.A. Rasool, "Bacterial and toxic pollutants in lakes of river Indus", Pakistan Journal of Botany, vol. 43, 1765-1772, 2011.

The Nucleus **60**, No. 1 (2023) 108-111

www.thenucleuspak.org.pk

The Nucleus
ISSN 0029-5698 (Print)
ISSN 2306-6539 (Online)

A Comprehensive Review of the Impact of Thermal Radiations on Energy Exchange Systems

Muhammad Ashraf

Department of Mathematics, Faculty of Science, University of Sargodha, Sargodha, Pakistan

ABSTRACT

Radiations or electromagnetic rays have a significant role in energy emission from nuclear explosions as well as energy transmission in furnaces and combustion chambers. The radiations are considered in computing thermal influence in devices such as a rocket nozzle, nuclear power plants for space applications, or a gaseous-core nuclear rocket. Energy is transferred between separated elements without a medium in case of radiations or electromagnetic rays. The structure, surface quality, temperature and wavelength of the rotation angle at which radiation is emitted or absorbed by the surface and the spectral distribution of the radiation encountered on the surface are only a few of the variables that affect the radiative behavior. In some important situation, heat is transferred within the solid media or highly viscous media is considered so that convection in the medium is not important. The combined radiation-conduction is important in glassy materials and can be used as a coating to protect the interior of a body from high external temperature. Also, the radiation-conduction process plays a crucial role in controlling how hot or cold the ablating layer is. In these circumstances, the temperature distribution has an impact on how the ablating substance will melt, soften or evaporate. The main novelty of the current work is to highlight the important aspects of thermal radiation effects on heat transfer mechanism and to focus on recent developments in this field.

Keywords: *Thermal Radiation, Radiation-conduction Parameter, Radiative Heat Flux, Temperature Field*

Classical and Recent Efforts

Present study comprises on two parts that is (i) classical and (ii) recent knowledge of the different aspects of the radiation-conduction heat transfer processes. Special emphasizes is given to the proper usage and determination of radiation-conduction parameter effects on the behavior of heat transfer mechanism which exists in literature. Furthermore, the connection between radiation and the other heat transport modes is discussed with the reference of previous published classical and recent literature. In order to obtain solutions for radiation-conduction energy in an emitting and absorbed medium, the energy equation for two dimensional boundary layer flows by following [6] is of the form:

$$\frac{\partial T}{\partial t} = \nabla \cdot (k\nabla T - q_r) \tag{1}$$

where q_r is the radiative heat flux and can be used to describe the space between two dark panels [6].

$$q_r = -\frac{4\sigma}{3\alpha_R}\frac{\partial T^4}{\partial y} \tag{2}$$

There are two zones that make up the temperature field. As the area typically has a low thickness, it may be assumed that it is optically thin and that radiation will travel through it without being attenuated. The reader interested in this topic is referred to study [6] for further information. Our main focus on current study is to review the influence of radiation-conduction parameter on thermal boundary layer and heat transfer processes. The detail of literature review targeted the above issue is given in below paragraphs.

The injection of absorbing particles is useful to shield the surface of thermal radiation beam if the injection rate is relatively high [1]. In addition to the radiative heat index $Rd \gg 1$, the heat flux in the inner zone of a thick boundary layer cannot be accurately anticipated using the thicker assumption alone. In comparison to the case where there is no radiation, the presence of radiation tends to diminish enthalpy rates, their inclinations and a thickening of the heat flow separation [3]. The choice of appropriate range of the parameters involved in the flow model and due to the effect of the absorbing radiation at the entrance of the pipe increases the heat transfer rate [4]. For controlled tests of transmitting heat radiation in absorbing and emitting substances, glass is a valuable medium [5]. Because radiant emission is temperature-dependent and thermal radiation is crucial for applications involving the rate of heat and mass transfer [6]. Radiation cannot be disregarded in the prediction of heat exchange because its features rely on the spectral absorption coefficient, index of refraction, thickness, boundary conditions and temperature field [7-8]. In reference [9], the author highlighted the usefulness of a formulation of the radiant energy exchange equation in terms of dimensionless variables for the case in which heat generation rates of the cylinder are known and the temperature are sought. According to Gilpin et al. [10], melting occurs on lakes and streams as a result of assimilation of radiant energy in ice. Since gas absorbs energy, the radiation intensity in wavelength intervals in actual medium drops across the beam path [11].

In each of the three convectional processes, the dimensionless local shear stress and local rate of heat transmission are decreased as the thermal radiation parameter is increased [12]. It has been shown that [13], the whole heat transmission in the packed bed under the stated operational circumstances is found to be mostly unaffected by thermal radiation and intra particle conduction. The radiative dispersion hypothesis for radiation heat transfer is the most preferred method [14]. In the presence of thermal radiation, local friction factor is decreased and local Nusselt quantity is increased [15].

*Corresponding author: muhammad.ashraf@uos.edu.pk

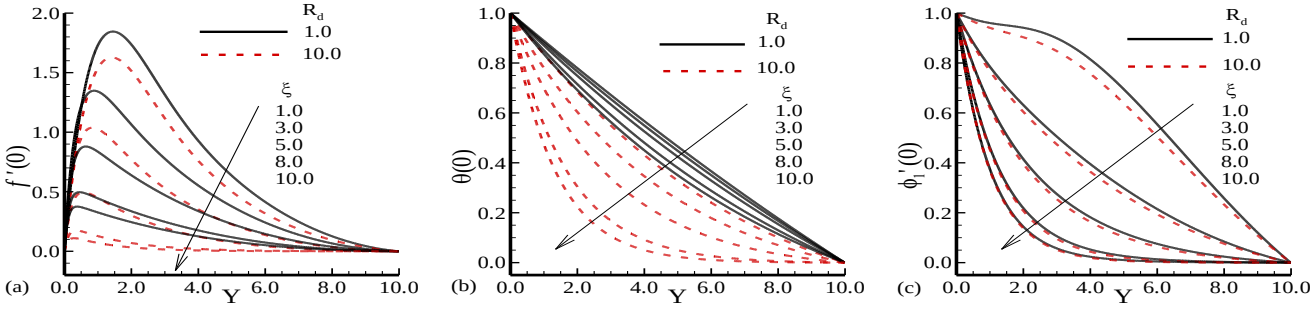

Fig. 1: Highlights the velocity profile, temperature distribution and magnetic flux along permeable surface for different values R_d in the presence of aligned magnetic field.

Molla et al. [16] claimed that local Nusselt quantity and the average heat transmission rate is improved when the quantities of radiation/conduction parameter and surface heating parameter along vertical wavy surface are increased. The local velocity, temperature field and magnetic field transversal component all decline when the radiation-conduction index rises [17]. Furthermore, they concluded that for increasing values of radiation parameter the Nusselt number is increased and the obtained results with the help of finite difference method are given in Table 1.

Table 1: Computational data for local Nu_x along the surface distance ξ for two values of radiation parameter R_d by keeping other parameters constant in the flow model under the influence of aligned magnetic field.

ξ	$R_d = 1.0$	$R_d = 10.0$
0.05	0.29162	0.34621
0.1	0.29321	0.34935
0.4	0.30251	0.36789
0.8	0.31429	0.39189
1.0	0.31992	0.40360
4.0	0.39612	0.57401
8.0	0.50613	0.83791
10.0	0.56757	0.98672

Molla et al [18] showed that the shearing force and rate of heat transport are provided as a function of coefficient of skin friction, local mean and Nusselt factor for a wide range of radiation/conduction characteristics. In the presence of thermal radiation, the detail of velocity profile, temperature distribution and current density along a magnetized porous surface has been demonstrated [19]. The obtained numerical results are presented in Fig. 1(a)-(c). It is shown that, along a porous surface the velocity profile, temperature distribution and magnetic flux are decreased for increasing values of radiation parameter R_d.

The optical and thermal properties of real ceramic foam at high temperature were taken into account both theoretically and experimentally [20].

Radiant heat flux can account for more than one-third of the total thermal gradient in highly porous transparent plastic or polyethylene microspheres. By carefully balancing porosity, one can drastically lower the equivalent conductivity of polymeric foam [21]. The increase of thermal radiation restraints the convective heat transfer and overall heat transfer uniformly [22]. In systems with significant thermal loads, the water jacket acts as a heat shield between hot and cool regions [23]. The non-stationary temperature regime scenario with quick heating and cooling stages, the thickness temperature distribution cannot be predicted by the ETC model with absolute error less than 502013100k [24]. The behavior of thermal radiation in coiled curved pipe for the different ranges of involved parameter is predicted in our previous work [25]. The appearance of metal in functionally graded thermal barrier coating; degraded the insulation performance [26]. In order to control heat radiation, the idea of photon chemical potential is crucial [27]. For increasing values of radiation parameter u and θ are enhanced and ϕ shows the opposite behavior [28]. They obtained the numerical results around different positions of the sphere as given in Fig. 2(a)-(c).

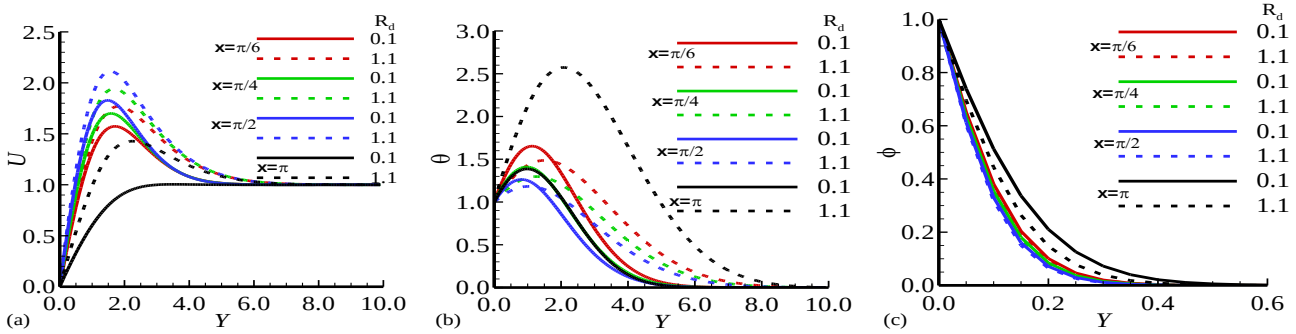

Fig. 2: Highlights the velocity profile(u), temperature distribution (θ) and mass concentration (ϕ) against normal distance Y around the solid sphere for various values of R_d in the presence of aligned magnetic field.

Table 2: Highlight the slopes of dimensionless velocity (u), dimensionless temperature (θ) and mass concentration (ϕ) around different locations of a solid sphere in the presence of aligned magnetic field.

X	$\frac{\partial u}{\partial y}$		$\frac{\partial \theta}{\partial y}$		$\frac{\partial \phi}{\partial y}$	
	R_d=0.1	R_d=1.1	R_d=0.1	R_d=1.1	R_d=0.1	R_d=1.1
$\frac{\pi}{6}$	2.03983	2.12816	0.94670	0.57034	0.37895	0.44799
$\frac{\pi}{4}$	2.47647	2.61447	0.70285	0.42245	0.52161	0.59891
$\frac{\pi}{2}$	2.94238	3.13261	0.53525	0.31783	0.64543	0.72913
π	0.57847	1.26779	-0.41769	1.25722	-1.40916	0.02432

Further, they also concluded the slopes of velocity, temperature and mass concentration for different values of radiation parameter as given in Table 2. It is also shown that the behavior of above said quantities is different at different position.

In associated conductive/radiative heat transfer, the impact of radiant heat grows significantly and contributes for >75% of the heat transmission [29]. The understanding of radiative distribution function characteristics gives a model for the commercial assessment of radiative heat transport in a specific dense system [30].

Conclusion

In current review, we have offered a unified perspective on classical and recent trends towards physical significances of the heat transport consequences of radiant heat on energy exchange systems.

We have summarized the following conclusions:

- All the three modes of the convective heat transfer experience a reduction in locally thermal transport rate and local shear force in the presence of thermal radiation.
- The radiant heat and intraparticle conduction do not play a significant role in the packed bed under specified operating conditions.
- In case of thermal boundary layer, the enthalpy gets lower when radiant energy is contained in the layers.
- Radiative distributive function characteristics provide a reference for industrial analysis and radiative heat transfer in dense particular system.
- The inclusion of thermal radiation or radiative heat flux in diffusion energy equation yields that heat transfer average and local Nusselt number is increased for the increasing values of radiative parameter and surface heating parameter.
- In systems with significant thermal loads, the water jacket acts as a heat shield between hot and cool regions.
- Thus, this review will be useful for the researchers to understand how the classical ideas can tune the current issues raised in energy exchange system?

References

[1] C.A. Fritsch, R.J. Grosh and M.W. Wildin, "Radiative heat transfer through an absorbing boundarylayer," J. Heat Transfer, Vol. 88, no. 3, pp. 296-304, 1966.

[2] J.L. Novotny and K.T. Yang, "The interaction of thermal radiation in optically thick boundary layers," J. Heat Transfer, Vol. 89, no. 4, pp. 309-312, 1967.

[3] J. Shawrtz, "Radiation coupled viscous flows," Int. J. Heat and Mass Transfer, Vol. 11, no. 4, pp. 689-697, 1968.

[4] B.L. Pearce and A.F. Emery, "Heat transfer by thermal radiation and laminar forced convection to an abosorbing fluid in the entery region of a pipe," J. Heat Transfer, Vol. 92, no. 2, pp. 221-230, 1970.

[5] N.D. Eryou and L.R. Glicksman, "An experimental and analytical study of radiative and conductive heat transfer in molten glass," J. Heat Transfer, Vol. 94, no. 2, pp. 224-230, 1972.

[6] R. Siegel and J.R. Howell, "Thermal radiation heat transfer," NY: McGraw-Hill, 1972.

[7] E.E. Anderson, R. Viskanata and W.H. Stevenson, "Heat transfer through semitransparent solids," J. Heat Transfer, Vol. 95, no. 2, pp. 179-186, 1973.

[8] R. Viskanata and E.E. Anderson, "Heat transfer in semitransparent solids, in Thomas F. Irvine, Jr., and James P. Hartnett (eds.)," Advances in Heat Transfer, Vol. 11, pp. 317-441, 1975.

[9] R.L. Cox, "Radiative heat transfer in arrays of parallel cylinders," Ph.D thesis Tennessee University, Knoxville, 1976.

[10] R.R. Gilpin, R.B. Robertson and B. Singh, "Radiative heating in ice," J. Heat Transfer, Vol. 99, pp. 227-232, 1977.

[11] H.A. Vercammen and G.F. Forment, " An improved zone method using Monte Carlo Techniques for the simulation radiation in industrial furnaces," Int. Journal of Heat and Mass Transfer, Vol. 23, no. 3, pp. 329-337, 1980.

[12] M.A. Hossain and H.S. Takhar, "Radiation effects on mixed convection along a vertical plate with uniform surface temperature," Heat and Mass Transfer, Vol. 31, pp. 243-248, 1996.

[13] A.A. Jalalzadeh-Azar, W.G. Steele and G.A. Adebiyi, "Heat Transfer in a High-Temperature Packed Bed Thermal Energy Storage System-Roles of radiation and intraparticle conduction," Journal of Energy Resource Technology, Vol. 118, no. 1, pp. 5057, 1996.

[14] Vadim A. Petrov, "Combined radiation and conduction heat transfer in high temperature fiber thermal radiation," International Journal of Heat and Mass Transfer, Vol. 40, no. 9, pp. 2241-2247, 1997.

[15] K.A. Yih, "Effect of radiation on natural convection about truncated cone," Int. J. Thermal Science, Vol. 42, no. 23, pp. 4299-4305, 1999.

[16] M.M. Molla and M.A. Hossain, "Radiation effect on mixed convection laminar flow along a vertical wavy surface," Int. J. of Thermal Science, Vol. 46, no. 9, pp. 926-935, 2007.

[17] M. Ashraf, S. Asghar and M.A. Hossain, Thermal radiation effects on hydromantic mixed convection flow along a magnetized vertical porous plate. Mathematical Problems in Engineering, vol. 2010, article ID 686596, 30 pages, 2010.

[18] M.M. Molla, M.A. Hossain and S. Siddiqa, "Radiation effect on free convection laminar flow from an isothermal sphere," Chemical Engineering Communucations, Vol. 198, no. 12, pp. 1483-1496, 2011.

[19] M. Ashraf, S. Asghar and M.A. Hossain, Computational study of the combined effects of conduction radiation and hydro magnetic on natural convection flow past a magnetized permeable plate. Appl. Math. Mech. (English Edition), 33(6), 731-750, 2012.

[20] R. Coquard, D. Rochais and D. Baillis, "Conductive and radiative heat transfer in ceamic and metal foams at finite temperature," Fire Technology, Vol. 48, pp. 699-732, 2012.

[21] P. Ferlk, R. Pokorney and J. Kosek, "Multiphase approach to couple conduction-radiation heat transfer in reconstructed polymeric foams," International Journal of Thermal Sciences, Vol. 83, pp.68-79, 2014.

[22] G. Yang and J.Y. Wu, "Effects of natural convection, wall thermal conduction, and thermal radiation on heat transfer uniformity at a heated plate located at the bottom of a three-dimensional rectangular enclosure," Numerical Heat Transfer, Part A: Applications, Vol. 69, no. 6, pp. 589-606, 2016.

[23] R. Kantor, "Modeling of a coupled radiation-conduction heat transfer through a heat shield in vacuum thermal isolation applications," Procedia Engineering, Vol. 157, pp. 271-278, 2016.

[24] R.A. Mironov, M.O. Zabezhailov, V.V. Cherepanov, M.Yu. Rusin, "T ransienradiative-conductive heat transfer modeling in constructional semitransparent silica ceramics, International Journal of Heat and Mass Transfer," Vol. 127, pp. 1230-1238, 2018.

[25] M. Ashraf, R. Yasmeen and M. Ahmad "Thermal radiation mixed convection boundary layer flow in tightly coiled curved pipe for large value of Richardson number,". Thermal Science: Vol. 22, No1A, pp. 147-156, 2018.

[26] W.A. Ge, C.Y. Zhao and B.X. Wang, "Thermal radiation and conduction in functionally graded thermal barrier coatings. Part II: Experimental thermal conductivities and heat transfer modeling," International Journal of Heat and Mass Transfer, Vol. 134, pp. 166-174, 2019.

[27] Li, Y., Li, W., Han, T. *et al*., "Transforming heat transfer with thermal metamaterials and devices". Nat Rev Mater Vol. 6, pp. 488–507, 2021.

[28] A. Abbas, M. Ashraf and A. Jawad "Chamkha, Combined effects of thermal radiation and thermophoretic motion on mixed convection boundary layer flow," Journal of Alexandria Engineering, Vol. 60, pp. 3243-3252, 2021.

[29] Chao Fan, Xin-Lin Xia, Wei Du, Chuang Sun, Yang Li, "Numerical investigations of the coupled conductive-radiative heat transfer in alumina ceramics," Heat and Mass Transfer, Vol. 135, 106097, 2022.

[30] B. Liu, J. Zhao, L. Liu and A.V. Gusarov, "Analytical relation of radiation distribution function in random particulate systems," Heat and Mass Transfer, Vol. 141, 106555, 2023.

Information for Authors

Submission: Manuscripts [in Word (.doc, .docx, .rtf)] should be submitted by one of the authors of the manuscript through the online submission system at www.thencleuspak.org.pk after registration of corresponding author. If for some technical reason on-line submission is not possible, then write an email describing the problem along with your phone no. at editorinchief@thenucleuspak.org.pk

Terms of Submission: Each submission to The Nucleus implies that the manuscript presents the results of original scientific research and has not been published nor has been submitted for publication elsewhere. The article is written in clear and Standard English. The reported research meets all applicable ethical standards and research integrity. The submitted manuscripts is screened for plagiarism during the editorial process.

Units of Measurement: should be presented simply and concisely using System International (SI) units.

Article Structure

Subdivision - numbered sections: The article should be divided into clearly defined and numbered sections. Subsections should be numbered 1.1 (then 1.1.1, 1.1.2, ...), 1.2, etc. (the abstract is not included in section numbering). Any subsection may be given a brief heading. Each heading should appear on its own separate line.

Title: should be concise and informative. Avoid abbreviations and formulae where possible.

Author names and affiliations: Provide complete name of all the authors, their affiliation, complete postal addresses, contact numbers and e-mail addresses. Present the authors' affiliation addresses below the names. Indicate all affiliations with a lower-case superscript letter immediately after the author's name. Clearly indicate the corresponding author by superscript*. Further when manuscript is under review process, as per policy of the journal, author cannot be addeded, deleted and sequence of author can't be altered.

Keywords: Provide a maximum of 6 keywords, These keywords will be used for indexing purposes.

Introduction Section: States the objectives of the work and provides an adequate background, avoiding a detailed literature survey or a summary of the results.

Experimental Section: should contain sufficient detail to allow the work to be reproduced. Methods already published should be indicated by a reference, only relevant modifications should be described.

***Theory/calculation S**ection:* Should extend, not repeat, the background to the article already dealt with in the Introduction and lay the foundation for further work. In contrast, a Calculation section represents a practical development from a theoretical basis.

Results and Discussion: should provide the significance of the results of the work. A combined Results and Discussion section is often appropriate. Avoid extensive citations and discussion of published literature.

Conclusions: It should be presented in a short Conclusions section.

Acknowledgments: (if any) should be included at the very end of the paper before the references and may include supporting grants, presentations, and so forth.

References: We follow IEEE style for citations of references. Must be numbered consecutively and citations of references in text should be identified using numbers in square brackets (e.g., as discussed by Smith [9]; as discussed elsewhere [9, 10]). Reference to a publication:

[Ref number] Author's initials. Author's Surname, "Title of article," Title of journal abbreviated in Italics, vol. number, issue number, page numbers, Abbreviated Month Year.

[4] K.A. Nelson, R.J. Davis, D.R. Lutz, and W. Smith, "Optical generation of tunable ultrasonic waves," Journal of Applied Physics, vol. 53, no. 2, pp. 1144-1149, Feb., 2002.

For more details please see the link IEEE style for citations of different materials

Figures and Tables: Include all figures and tables in the word file of the manuscript. Figures and tables should not be submitted in separate files. If the article is accepted, authors may be asked to provide the source files of the figures. All figures should be cited in the paper in a consecutive order. In all figures, remove all unnecessary boxes, lines, marks. The resolution of all the figures must be at least 300 dpi. Tables should be cited consecutively in the text. Every table must have a descriptive title and if numerical measurements are given, the units should be included in the column heading. Vertical rules should not be used.

The Nucleus

An Open Access International Scientific Journal

ISSN : 0029-5698 (Print)
EISSN : 2306-6539 (Online)

Recognized by HEC in 'Y' Category

Call for Papers

Why Publish in The Nucleus?

- One of the Oldest Scientific Journals in Pakistan
- Regularly Published since 1964
- Published Both Electronically & in Paper Format
- Multidisciplinary
  - Natural Sciences
  - Applied Sciences
  - Engineering & Technology
  - Management Sciences
- Open Access
- Peer Reviewed*
- No Publication Charges
- High Visibility
- Electronic Submission
- Rapid On-line Publication (within three months)

Abstracted and Indexed in:

- Chemical Abstracts
- Biological Abstracts
- INIS Atom Index
- Bibliography of Agriculture (USA)
- The Institute of Electrical Engineers Publications
- Virology Abstracts (England)
- Pakistan Science Abstracts

For Further Information

Editorial Office The Nucleus
PINSTECH, 45650 Nilore
Islamabad. Pakistan
For Online
http://www.thenucleuspak.org.pk
E-mail
editorialoffice@thenucleuspak.org.pk

Why Perish when you can Publish in The Nucleus?

*Potential Reviewers are Invited to Submit their CV's Through E-mail